博士論文

Degradation of stress-strain properties of sand in undrained torsional shear tests

(非排水中空ねじりせん断試験による砂の強度・変形特性の損傷に関する研究)

by

Muhammad UMAR
(ムハマッド ウマル)

A Thesis
Submitted in Partial Fulfilment of the
Requirements for the Degree of
Doctor of Engineering

Department of Civil Engineering
The University of Tokyo

August 2019

Dedication

I dedicate this thesis to my parents for nursing me with affections and love. Thanks for your support and love in making this milestone possible for me.

ABSTRACT

In this study, undrained behavior of saturated Toyoura sand is invested up to the extremely large shear strain. Five series of test was conducted on saturated Toyoura sand by pluviation were performed in a modified torsional shear apparatus capable of achieving double amplitude shear strain (γ_{DA}) exceeding 100% under quasi simple shear condition.

In the first series, the undrained monotonic test was conducted from a relative density of 19% to 72%. A series of the monotonic result showed that with the increase in the relative density, shear strength a quasi-steady-state (QSS), undrained peak strength and residual strength (ultimate steady-state (USS)) increased. However relative density below 23% neither the QSS or USS was observed, and sandy specimen developed extremely large deformation after exceeding the transient peak. The shear strength was recovered after exceeding shear strain of 60% in Dr <23%.

The second series of the test included a multistage, by repeated cyclic loading desired amplitude of damage, the strain was achieved, following an undrained monotonic loading until extremely large shear strain. In the series of multistage stage test, cyclic loading to reach the desired damage strain, followed by an undrained monotonic loading exceeding single amplitude shear strain of 50% showed a continues degradation of shear strength at peak undrained strength irrespective of density state, cyclic stress ratio and confining pressure. At large shear strain, non-uniform deformation became significant along the specimen length.

In the third series of test, the specimen was subjected to the drained initial static shear to simulate slope condition in reversal and non-reversal stress condition. Following that after achieving the desired damage strain, the loading mode was changed to monotonic without

opening the drainage valve and continued until extremely large strain. Peak undrained strength degraded irrespective of the amplitude of initial static shear.

In the fourth series in which the specimen was reconsolidated after achieving desired damage strain showed different characteristic in the effective stress path, with the virgin specimen, however, they reached same undrained peak strength and residual strength.

In the fifth series of test, non-uniformities observed in the specimen was investigated by 3D digital image analysis by VIC 3D. To accurately capture the surface deformation, the undrained monotonic, and a cyclic test followed by monotonic static loading under non-reversal conditions showed the progressive development of shear band(s) and consequently the development of non-uniformities in the specimen. 3D Digital image analysis using VIC 3D captured the progressive development of the shear band and boundary was identified between a uniform and non-uniform deformation. Residual strength in undrained loading is defined on the basis of the comparison of DIC and experimental test results.

From all the series of the test on the saturated Toyoura sand in undrained condition, strength degraded as a result of the formation of the shear band. Strength degradation solemnly depends on the amplitude of damage strain and independent of the cyclic stress or a combination of static shear and cyclic shear.

Two degradation correlation is developed based on the initiation and full formation of the shear band under undrained conditions i-e limiting undrained strength and residual strength.

Modified Newmark stability analysis of Fujimana Dam stability analysis was performed by incorporation the degradation correlations of Toyoura sand. Estimated settlement increased from 0.15m to 2.3m provides a better collapse explanation of Fujinuma Dam.

ACKNOWLEDGMENT

TABLE OF CONTENTS

CHAPTER 1: Introduction and literature review

CHAPTER 2: Material, apparatus, and test procedure

CHAPTER 3: Characterization of undrained monotonic behavior under extremely large strain

CHAPTER 4: Influence of damage strain on undrained static shear strength

CHAPTER 5: Strain localization influence on undrained strength

CHAPTER 6: 3D image analysis to capture strain localization

CHAPTER 7: Fujinuma dam stability analysis by Newmark-D

CHAPTER 8: Conclusions and recommendations

LIST OF FIGURES

CHAPTER 1

CHAPTER 2

CHAPTER 3

CHAPTER 4

CHAPTER 5

CHAPTER 6

CHAPTER 7

LIST OF TABLES

CHAPTER 1

Introduction and literature review

CHAPTER 1: Introduction and literature review

TABLE OF FIGURES

CHAPTER 1: Introduction and literature review

1.1   Introduction

Seismic disasters have left bitter experiences hitting the inhabited area resulting in the severe damages to earth structures such as during the Niigata 1964 and 1983 Nihonkai-Chubu earthquakes, Japan. In 1971, the San Fernando earth-dam collapsed during a powerful earthquake that hit Southern California, USA (Seed et al. 1975).

More recently, during the 2011 Canterbury Earthquake Sequence (New Zealand) and 2011 Off the Pacific Coast of Tohoku Earthquake (Japan), 2016 Kumamoto earthquake, resulted in the collapse of earth-fill dams, liquefaction induced lateral spreading, landslides, embankments, retaining wall, lifelines facilities and river levees (Hamada et al. 1994, Cubrinovski et al. 2011, Kiyota et al. 2011, Tatsuoka et al. 2017, Chiaro et al. 2015, Chiaro et al. 2017).

After the Great East Japan Earthquake, damage survey report was compiled by Joint editorial committees to summarize the number of damages to earth structures (Great East Japan Earthquake disaster (2015)). In addition to the damages, the committee collected the information about design practice effective at the time of the earthquake.

From the last two decades, significant advancements and improvements have been made to build seismic resilient earth structures. However, still, significant losses were reported following a seismic event. That fact can be explained by either the earth structures have not been carefully designed, or construction quality remained poor or as structures transmit the load to the ground, and any problem in the assessment of ground resistant against seismic event will be reflected in the superstructures. Ground response to earthquake load is complicated based on assumptions or lack of the research gap or contrary to actual and assumed behavior, which is also reflected in the superstructure damages.

During seismic shaking, ground deformation, which in some scenario becomes significantly large to cause damage to structures. The phenomena that induce substantial deformation in the ground is term as "Liquefaction," and it resulted in the catastrophic failures in the past.

Liquefaction is a phenomenon "when a fully saturated granular material is subjected to seismic loading, result in the generation of excess pore water pressure, which consequently reduces the effective stress and ultimately reaching zero."

Liquefaction is used to describe a phenomenon of loss of stiffness and strength in saturated cohesionless soil. It is essential to distinguish between the soil behavior 1) flow failure or true liquefaction 2) progressive failure or cyclic mobility.

1.2   Flow failure or true liquefaction

In loose saturated cohesionless granular material that is mostly suspectable to flow failure, mainly due to low undrained strength. Once the cyclic stress induced by the earthquake exceeds undrained soil strength, it resulted in the flow of the soil mass. Flow failure in a gentle slope (inclination < 5°) triggered by small to a large seismic event.

1.3   Progressive failure or cyclic mobility

Progressive failure is the progressive reduction in the stiffness as a consequence of the generation of excess pore water generation by the earthquake loading. Soil recovers its strength by repeated cyclic loading as a result of cyclic mobility.

1.4   Case histories for liquefaction flow failure

1.4.1   The collapse of San Fernando dam - 1971

In 1971, as a result of the san Fernando earthquake, the upstream slope of San Fernando dam was collapsed. It was constructed by hydraulic filling, mixing the material with the water and transporting and compacting. Figure 1.1 shows the dam before the collapse, whereas Figure 1.2 and Figure 1.3 shows the conditions after the earthquake. Steep slide head scarp as can be seen in Figure 1.2 and remained freeboard in Figure 1.3.

The dam was constructed by sandy material, and under the static condition, the factor of safety against instability was more than 2. Following its collapse, several investigative studies conducted by Seed et al. (1975), Lee et al. (1975), Seed et al. (1975) to find the reason of collapse. The main conclusion from their finding was that, the dam fill was in loose state, and is subjected to liquefaction as the result of earthquake shaking.

Figure 1.1: The San Fernando dam (pic courtesy to H.B Seed)

Figure 1.2: Upstream face of the dam after drawing down the reservoir
(Pic courtesy to H.B Seed)

Figure 1.3: Slide head scarp general view (Photo courtesy Duncan)

Samples collected from the collapsed dam site, and undrained shear strength was measured by Seed et al. 1988. The undrained shear strength measured was corrected for various parameter such as sample disturbance, earthquake consolidation. The average value interpreted for sand sample (fines content <22%) was sufficient to maintain stability by the earthquake (Bayme and Beaty 2000). Strength loss maybe occurred after the earthquake shaking, due to possible pore pressure redistribution.

1.4.2 The collapse of Fujinuma Dam -2011

Fujinuma reservoir was located on the right branch of upper sunoko river in Fukushima. It had a main and auxiliary dam. These dams were constructed in 1937, and the main dam was an earth-fill dam having a height of 18.5m and crest length of 133.2. Whereas, the auxiliary dam was also earthen filled having a height of 10.5m and crest length of 72.5m.

These dams (main and auxiliary) were collapsed during the 2011 Tohoku Earthquake having a magnitude of 9.0 (Figure 1.6). Eight (8) people died as a result of the collapse and several houses inundated by the discharge of water. Similar to San Fernando dam, Fujinuam dam under static loading had a factor of safety of more than 2.0 (Duttine et al. 2015a and b).

The main dam collapsed as reported by Tanaka et al. (2012, 2016) mainly due to poorly compacted dam fills top, middle and bottom as suggested by field investigation the degree of compaction of top fill was 87%, middle 81%, and bottom 90%(Figure 1.5).

Top-fill sandy soil was highly liquefiable in loose and saturated and undrained strength significantly degradation of undrained strength during an earthquake.

Figure 1.4: View of the main Fujinuma dam before collapse (Tanaka et al. 2012)
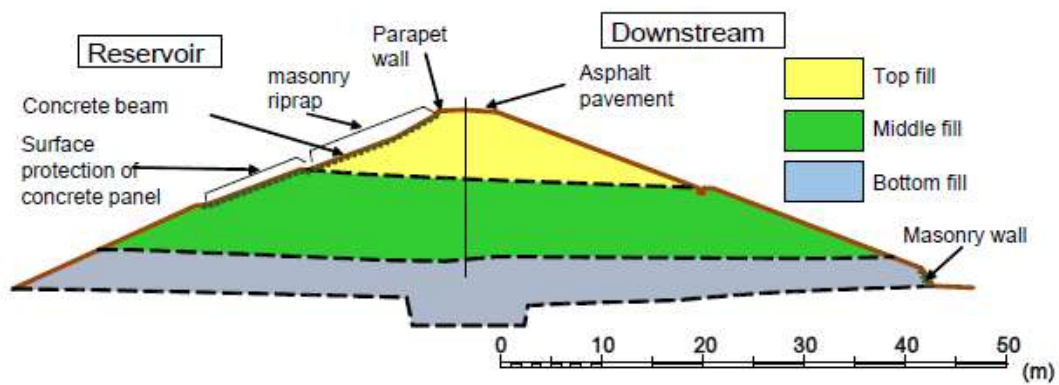
Figure 1.5: Typical cross-section of the main dam before collapse (Tanaka et al. (2012))

Figure 1.6: Breaching of Main Fujinuma Dam (Courtesy of Fukushima Pref.)

1.5　　　Undrained behavior of soil

The collapse of the earthen dam considered safe during an event of earthquake compels to revisit the behavior of sandy soils under undrained shearing and review our existing design methodologies and assumptions.

Granular materials consist of three-phase system i-e soil solids, voids filled with water and air. Granular material behavior is highly dependent on water filled in voids and air. As air is more compressible than water and has the tendency to migrate into the soil skeleton, therefore it controls how the granular material is going to behave in case of a seismic event.

In Japan, around 200,000 small and medium irrigation dams are present, mainly consist of sandy material constructed in a layered manner, similar to the Fujinuma dam. Sandy soil is more vulnerable to liquefaction and loss of strength during a seismic event. Therefore the current study is emphasizing on these types of soils.

1.6　　　Definition of undrained shear strength under monotonic loading

In the laboratory, the undrained monotonic test has been used to evaluate flow deformation of sand. Castro (1969) in his extensive experimental study showed that, when loose saturated sand sheared in undrained conditions in triaxial compression, the specimen reached a unique stress condition at large deformation, irrespective of initial stress condition but mainly dependent on the initial density. Poulous (1981) called this state a steady-state, the state of soil at which the soil continues to deform a constant state of effective stress and at a constant void ratio. Latter Pooroonshasb (1989) and Pooroonshasb and Consoli (1991) renamed the steady sate to ultimate steady-state. The shear strength at ultimate state has been considered as the undrained shear strength of the material.

The term critical state and steady-state are analogous to each other, referring to the same state of deformation in soils (deformation at constant volume, constant shear stress, and constant effective stress). These two states have been already investigated to be as same by various

researchers i-e Been et al. (1991), Verdugo and Ishihara (1996), Riemer and Seed (1997). Figure 1.7 shows a typical behavior in term of effective stress path and stress-strain of clean sand. Monotonically loaded saturated clean sand exhibit an undrained instability state (UIS) consequently reaching a state of Quasi steady state (QSS). Quasi-steady state (QSS) is defined as at state at which the shear stress reaches a local minimum in undrained shearing (Alarcon-Guzman et al. 1988).

Previous studies showed QSS a distinct state which does not coincide with the phase transformation state (PTS). However, the undrained shear strength is almost identical at QSS and PTS. If the undrained shearing results in the steady-state after exceeding the ultimate instability line (UIS) for loose sand, this shear strength is taken as the undrained strength and respectively used in the design.

Studies have been conducted on the effect of density on the ultimate steady-state (Verdugo and Ishihara (1996), Murthy et al. 2007), using triaxial compression apparatus. For very loose sand, they showed after exceeding the UIS, soil reached the ultimate steady-state. They generally showed a relationship between void ratio and shear strength at PTS but unable to establish a relationship of undrained strength at USS and void ratio for sandy material. The primary reason is attributed as in a triaxial compression test, as the confining pressure is not so high, sandy specimen tends to dilate at substantially large deformation and observed resistance at the USS becomes considerably high. Murthy et al. (2007) conducted a forty-six (46) undrained monotonic triaxial compression test. During their test, initially, specimen contacted followed by dilation. This dilation behavior continued until the end of their test. They were unable to reach the USS in the undrained monotonic test for the clean sand.

During earthquake ground experience simple shear loading contradictory to applied triaxial compression loading as recognized by Vaid et al. (1990) and Vaid (1990) showed the mode of loading played a significant role in determining the behavior and simple shear devices can

replicate behavior closer to the field in element testing in the laboratory.
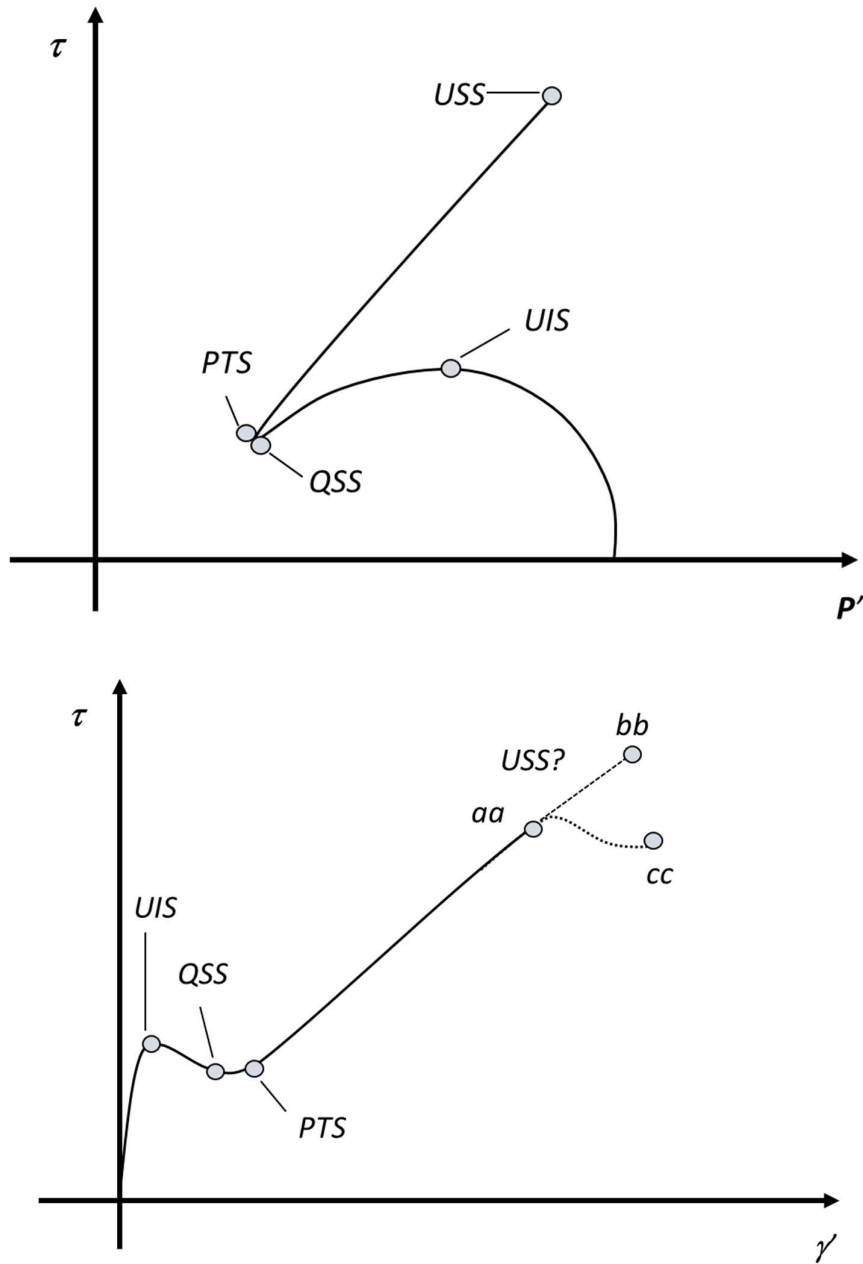
Figure 1.7: Characteristic states of undrained behavior of clean sand for medium dense and dense sand: ultimate critical sate (USS), Phase transformation state (PTS), Quasi steady-state (QSS), undrained Instability state (UIS)

Recently, simple shear loading devices using hollow cylindrical torsional shear showed that

anisotropic characteristics of the soil dilatancy could affect the undrained response of sandy material (Nakata et al. 1998, Yoshimine et al. 1996, Yoshimine et al. 1998, Yamamuro et al. 1998 and Geogiannnou et al. 2008).

A question arises if shearing results in QSS and then USS following strain hardening, which state should be used to define undrained strength for the design purpose. Importantly, how the soil is going to behave, reaching and exceeding USS. Either it will continue to harden (Figure 1.7, aa-bb) or strain-softening leading followed by residual state (Figure 1.7 aa-cc).

As the author investigated, there exists not a single study that reported the ultimate steady state for clean sand, in addition no correlation exists between the undrained peak resistance at ultimate steady-state under triaxial compression test or torsional simple shear test under low confining pressure.

1.7   Definition of post liquefaction undrained static shear strength

In the last decade significant effort has been made to study and understand the triggering mechanism of liquefaction undrained behavior of sandy materials leading to liquefaction (Iwasaki et al. 1986, Mohamad et al. 1986, Bouckovalas et al. 2003, Sivathayalon et al. 2004 Kamata et al. 2009 and Wang et al. 2017).

Most of the previous research emphasized on the liquefaction susceptibility of different granular materials. Only a limited number of studies investigated the post liquefaction response of sandy material. Vaid and Thomas (1995) conducted an extensive series of test on a Fraser sand using triaxial apparatus by liquefying a specimen by repeated cyclic loading followed by undrained monotonic loading without opening the drainage valve. They investigated the effect of relative densities and confining pressure on the post liquefaction undrained static strength with increasing amplitude of double amplitude axial strain. They concluded that the liquefied specimen showed nearly zero stiffness up to the level of strain during monotonic loading

followed by abrupt recovery of soil stiffness and shear stress with the increase in the axial strain. No residual strength was apparent, regardless of the initial density state. The consistent findings were reported by Kiku & Tsujini (1996), i-e liquefied specimen recovered its stiffness and strength upon monotonic shearing.

Sivathayalan & Vaid (2004) investigated the post liquefaction undrained monotonic behavior of a frozen reconstituted sample of alluvial sand. They characterize the post liquefaction behavior into three (3) phase during undrained monotonic loading (Figure 1.8). During phase 1, specimen exhibited nearly zero stiffness and strength. In phase 2, the specimen continues to recover its stiffness and strength over the considerable amplitude of axial strain. During the final phase, the specimen showed constant stiffness as well as increases in the strength. They summarized that the liquefied sand showed a strain hardening owing to the ability of liquefied soil to dilate on shearing.
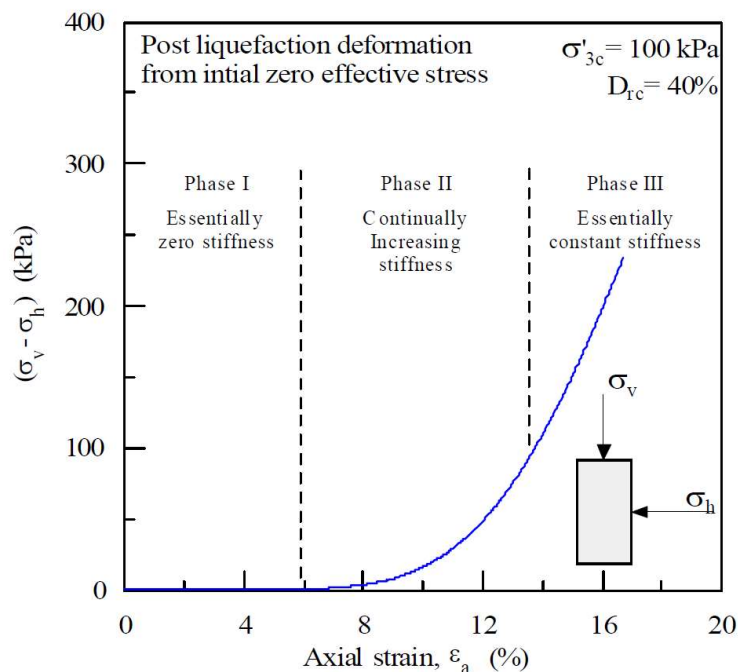
Figure 1.8: Post liquefaction undrained monotonic stress-strain behavior of reconstituted Fraser river sand (after Sivathayalan and Vaid (2004))

Whereas the strength is taken at a specific strain level to be incorporated in the analysis of

saturated earth structures. Figure 1.9 shows the post liquefaction comparison of measured and assumed in the analysis. It is evident that this approach overestimates the post liquefaction shear strength and consequently lead to an unrealistic prediction of a factor of safety.
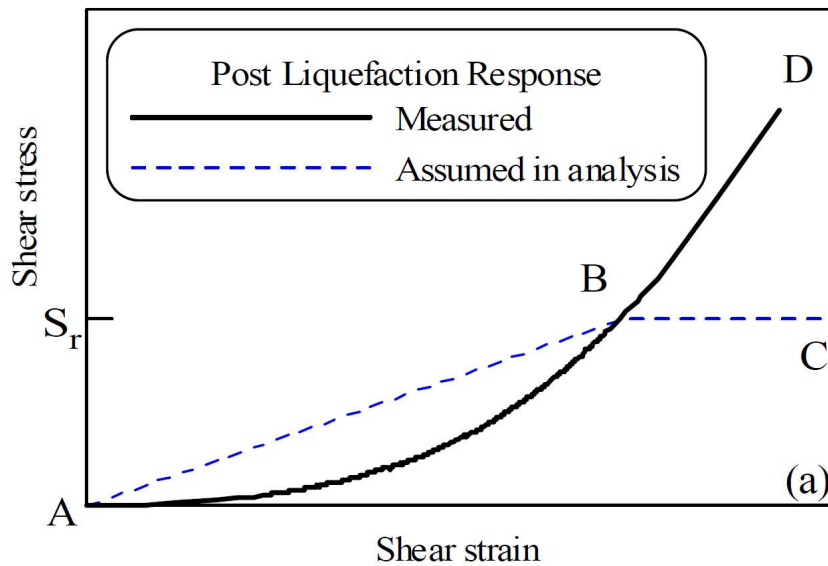
Figure 1.9: Assumed and measured post liquefaction undrained monotonic stress-strain behavior of reconstituted Fraser river sand (after Sivathayalan and Vaid (2004))

The post liquefaction strain hardening behavior was validated by Shamoto et al. 1996 (Figure 1.10) by using a torsional simple shear device. The specimen was sheared monotonically with a varying shear strain amplitude before loading monotonically without opening the drainage. He concluded that the shear stress and strain relations are nearly parallel to each other. However, the shear strain values at the same shear stress level are different, whereas their effective stress paths almost coincide with each other. Consistent with the finding of Vaid and Thomas (1995) residual state was not reached regardless of strain history.
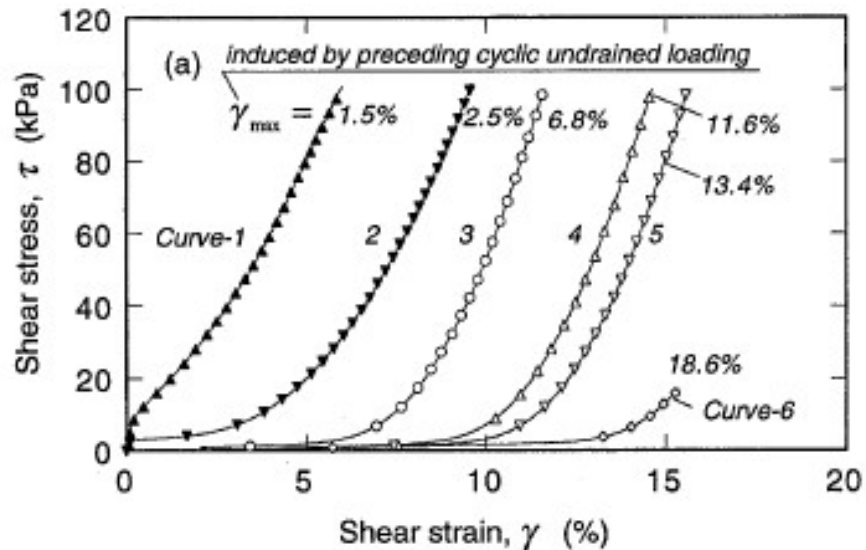
Figure 1.10: Post liquefaction stress behavior of Toyoura sand with a varying amplitude of shear strain history (after Shamoto et al. (1997))

Kokusho et al. (2004) using triaxial apparatus investigated the particle size effect on post liquefaction undrained monotonic behavior. He concluded that well-graded soils tend to dilate more predominant than exhibited by poorly graded sols.

A subsequent study conducted by Sitharam et al. (2009) showed that the post liquefaction undrained monotonic behavior was affected by applied axial strain to cause liquefaction. The undrained monotonic behavior of liquefied and non-liquefied samples is shown in Figure 1.11, by Dash (2016). The result showed that the two samples of Toyoura sand with identical initial relative density consolidated at the same mean effective stress but subjected to different loading paths. Dash (2016) concluded that stiffness and strength are comparable before and after liquefaction.
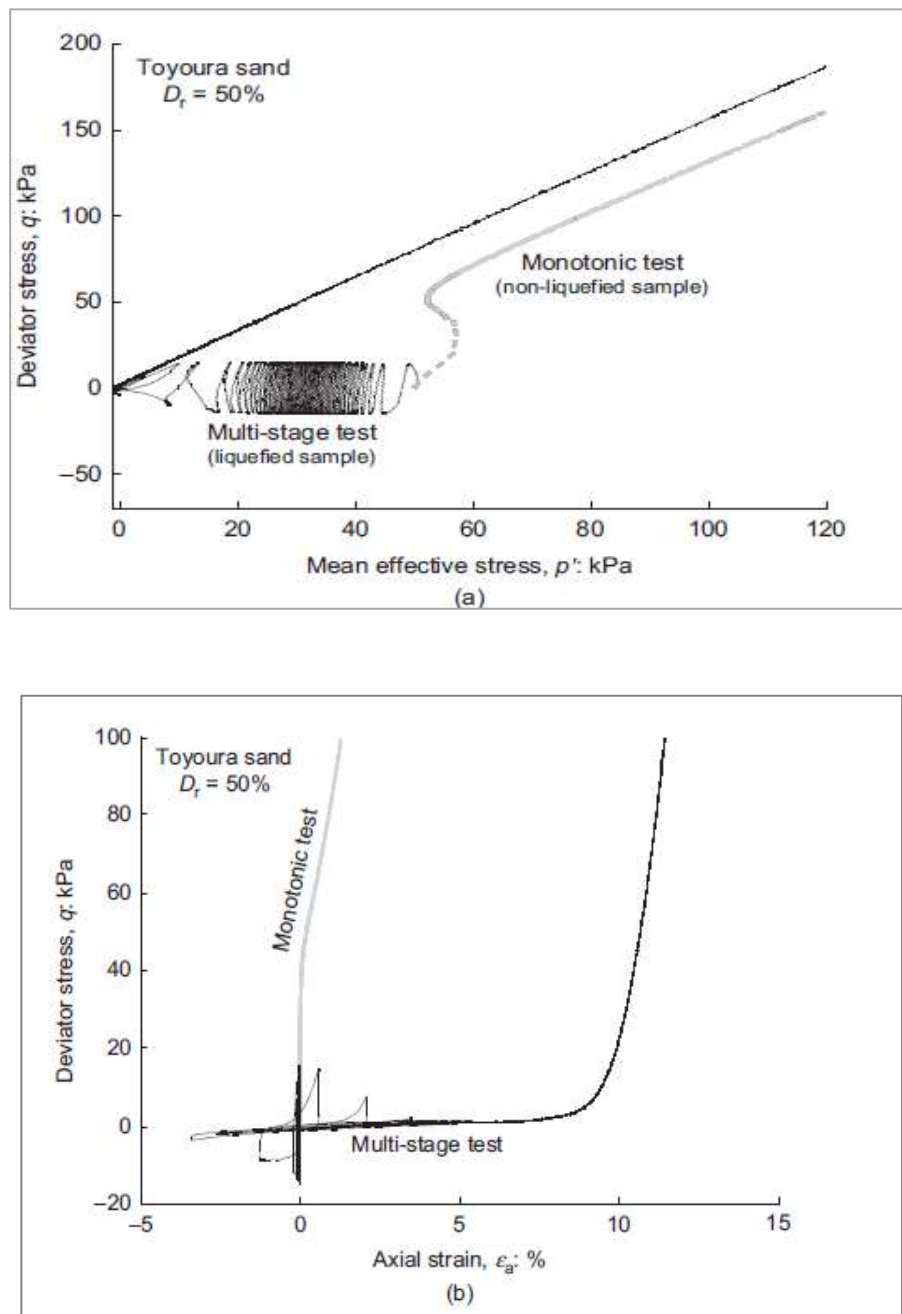
Figure 1.11: Undrained behavior of Toyoura sand loading by different stress path, monotonically (grey), cyclic followed by monotonic (black) a) effective stress path b) stress-strain curve (after Dash (2016))

Majority of the previous studies are conducted by conventional triaxial apparatus. Triaxial test is performed having a back pressure to improve sample saturation. Therefore, the sample that tends to dilate, as they are sheared undrained condition tend to generate negative excess pore water pressure, the mean effective stress becomes increasingly positive and drastic increase in the shear strength. The back pressure provides protection against the pore pressure to reduce to zero But continued dilation lead to excess pore pressure below -100kPa, at that point the water in the pore will cavitate and boil (Macmanus and Davis (1997) and Mokni and Desrues (1998)), resulting in the generation of gas in the pores and eventually become a drained test. Such kind of scenario is not exhibited in the field and raises a question on the reliability and simulation of the post liquefaction strength using conventional triaxial apparatus.

Simulation of post liquefaction large deformation of liquefied soils in laboratory element tests remains to be a significant challenge in geotechnical engineering, mainly due to the technical limitations. In addition to other limitations in triaxial tests, the axial strain levels are usually limited to 20% or less due to a larger extent of non-uniform deformation of the specimen at higher strain levels. Technical and mechanical limitations prevent the simulation of strains larger than 10-15% using conventional simple shear devices (Cappellaro et al. 2018). In contrast, by using a torsional shear apparatus on hollow cylindrical specimens, by increasing the amount of torsional shear displacement one can achieve higher strain levels that are applied to the specimen (Kiyota et al. 2008).

A considerable large strain level during cyclic shearing, liquefied soil gradually regains its strength and stiffness upon shearing upon dissipation of pore water pressure. However, after exceeding a threshold value of shear strain causing strain localization (concentration of shear deformation into a narrow zone of intense shearing commonly referred to as a shear band), a progressive deterioration of stiffness during cyclic mobility has been observed (Kiyota et al. 2008, 2013, Chiaro et al. 2013).

Generally, the shear banding process begins at the state when the mobilized strength of soil reaches its peak and gradually develops as shear deformation continues. Under the cyclic loading strain localization was investigated using modified torsional simple shear apparatus by Kiyota et al. (2008), Chiaro et al. (2011), Umar et al. (2016). Consistent with the USS for undrained monotonic loading(without any cyclic history), the post liquefaction undrained monotonic dilative behavior is expected to terminate at the large stress and strain level, following the path aa-cc in Figure 1.12 in contrast to stress strain path of aa-bb. This USS has significant importance with an increase in the cyclic stress history and corresponding influence on post cyclic undrained static strength deterioration. As per author knowledge and literature review, no research indicates the USS in the post liquefaction undrained monotonic loading.
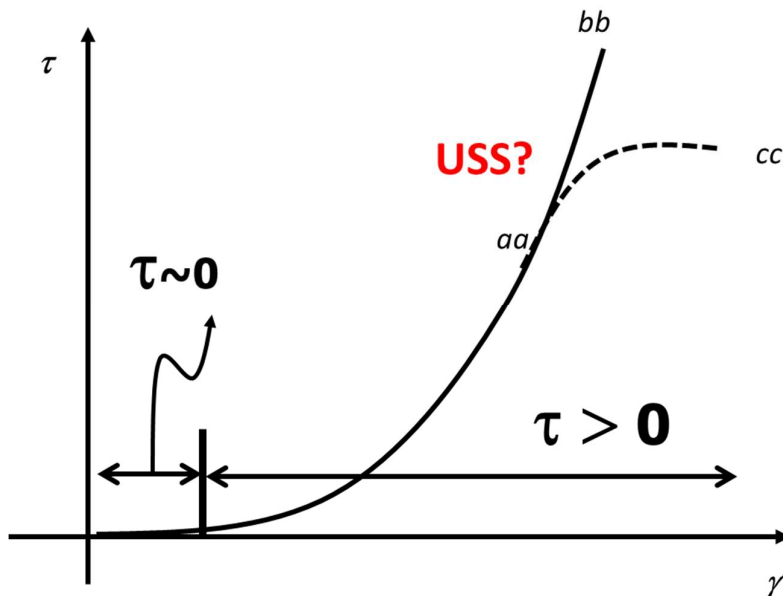
Figure 1.12:   Post liquefaction undrained monotonic stress-strain

schematic illustration during large strain

1.8   OBJECTIVE OF THIS STUDY

In the view of the above background, the primary objective of this studies is

1-1)   Investigate the large undrained strain monotonic behavior of saturated Toyoura sand having a relative density from 19% to 72% up to single amplitude shear strain of about 60%. Investigate the effect of density on the three states of the soil 1) undrained Instability state (UIS), 2) Phase transformation state (PTS), 3) Quasi steady-state (QSS), 4) Ultimate steady-state (USS). This study will emphasize on the USS, with the increase in the relative density, which in the previous studies was unable to address due to the mechanical or technical limiting of testing apparatus. For that, a torsional shear apparatus having specimen dimension of D_{out} =100, D_{in} = 60mm, H=200mm is used. The specimen will be sheared under simple shear condition (quasi simple shear by fixing the height of the specimen).

1-2)   Post liquefaction undrained static monotonic behavior with the increase in the amplitude of shear strain (herby referred to as damage strain) on the ultimate steady-state (USS). The specimen will be subjected to strain amplitude hereby define as damage strain with repeated cyclic loading to reach desired values. Following that without opening the drainage valve loaded monotonically. Majority of the existing studies assume that the strength and stiffness are unaffected by the amplitude and soil mobilized the same strength due to dilative behavior.

Effect of relative density, the effect of confining pressure, the effect of initial static shear (reversal and non-reversal) on the post liquefaction undrained static strength.

1-3)   Investigate the Fujinuma dam collapse with Newmark-D.

1.9   ORGANIZATION OF THESIS

CHAPTER 1

In this chapter in detail, existing experimental data and previous studies are reviewed and the research questions were raised.

CHAPTER 2

Described laboratory testing material, specimen preparation method, a saturation of specimen and shearing techniques are discussed in detail

CHAPTER 3:

Typical test results from the large strain undrained monotonic test results from a relative density of 19 to 72% is presented. The test results are presented and compared in terms of effective stress path, stress-strain relationship, stress ratio vs shear strain.

CHAPTER 4:

Post liquefaction undrained monotonic test are discussed in detail. Effect of damage strain from 1% to 92% is presented for level ground and for slope ground (reversal and non-reversal). Effect of confining pressure, cyclic stress ration and reconsolidation history on undrained peak strength.

CHAPTER 5:

Strain localization in the undrained monotonic test, as well as post liquefaction monotonic test, is discussed in detail. Effect of strain localization on the ultimate peak strength is provided.

The second part of this chapter discussed the development of 3D image analysis to understand strain localization. Comparison of image analysis with experimental data is provided.

CHAPTER 6:

This Chapter present the case study of Fujinuma dam analysis by incorporation the experimental data in the stability analysis software used by IGI cooperation.

CHAPTER 7:

This includes the major conclusions and research outcomes, and future suggestion and recommendation for addressing some other issues related to undrained strength degradation

1.10   References

1) Alarcon-Guzman, A., Leonards, G. A., and Chameau, J. L. [1988]: *Undrained monotonic and cyclic strength of sands*, Journal of Geotechnical Engineering., ASCE, 114(10), 1089-1110.

2) Been, K., Jefferies, M.G., and Hachey, J. [1991]: *The critical state of sands* Geotechnique,41:365ñ381.

3) Beaty, M.H. and Byrne, P.M. [2000]: *A Synthesized Approach for Predicting Liquefaction and Resulting Displacements*, Proc. 12th World Conf. on Earthquake Engineering., Paper No. 1589.

4) Bouckovalas, G.D, Andrianopoulos, K.I., and Papadimitriou, A.G. [2003]: *A critical state interpretation for the cyclic liquefaction resistance of silty sands*, Soil Dynamics Earthquake Engineering 2003; 23:115–25.

5) Castro, G. and Poulus, S.J. [1977]: *Factors affecting liquefaction and cyclic mobility*, Journal of the Geotechnical Engineering Division, ASCE, 103: 501-51.

6) Cappellaro, C., Cubrinovski, M., Bray, J. D., Chiaro, G., Riemer, M. F. and Stringer, M. E. [2018]: *Comparisons in the cyclic direct shear response of two sands from Christchurch, New Zealand,* ASCE Geotechnical Special Publication 293: 150-159.

7) Chiaro, G., Koseki, J., and Sato, T. [2012]: *Effects of initial static shear on liquefaction and large deformation properties of loose saturated Toyoura sand in undrained cyclic torsional shear tests*, Soil and Foundations 52(3): 498–510.

8) Chiaro, G., Kiyota, T. and Koseki, J. [2013]: *Strain localization of characteristics of loose saturated Toyoura sand in undrained cyclic torsional shear tests with initial static shear"* Soils and Foundation 53: 23-34.

9) Chiaro, G., Kiyota, T., Pokhrel, R.M., Goda, K., Katagiri, T. and Sharma, K. [2015]: *Reconnaissance report on geotechnical and structural damage caused by the 2015 Gorkha Earthquake, Nepal*, Soils and Foundations, 55: 1030-1043.

10) Chiaro, G., Alexander, G., Brabhaharan, P., Massey C., Koseki J., Yamada, S. and Aoyagi, Y. [2017a]: *Reconnaissance report on geotechnical and geological aspects of the 2016 Kumamoto Earthquake, Japan*, Bulletin of the New Zealand Society for Earthquake Engineering 50(3): 365-393.

11) Chiaro, G., Kiyota, T. and Miyamoto, H. [2017b]: *Liquefaction potential and large deformation properties of Christchurch liquefied sand subjected to undrained cyclic torsional simple shear loading,* Proceeding of the 19th International Conference on Soil Mechanics and Geotechnical Eng., Seoul, South Korea, 1497-1500.

12) Cubrinovski, M., Bray, J.D., Taylor, M., Giorgini, S., Bradley, B.A., Wotherspoon, L. and Zupan, J. [2011]: *Soil liquefaction effects in the Central Business Districts during the February 2011 Christchurch Earthquake*, Seismological Research Letters, 82: 893-904.

13) Dash, S. [2010]: *Lateral pile–soil interaction in liquefiable soils. PhD thesis, University of Oxford,* Oxford, UK.

14) Dash, S., Bhattacharya, S. and Blakeborough, A. [2010]: *Bending–buckling interaction as a failure mechanism of piles in liquefiable soils*. Soil Dynamics. Earthquake Engineering 30, No. 1–2, 32–39.

15) Duttine, A., Tatsuoka, F., Yazaki, S. and Mohri, Y. [2015a]: *Evaluation of seismic dam displacement by Newmark method taking into account soil strength reduction due to undrained cyclic loading*, Japan Geotechnical Society (JGS) Special Issue on earth dam seismic stability, 2015.03, 8-11, (in Japanese).

16) Duttine, A., Yazaki, S., Tatsuoka, F. and Mohri, Y. [2015b]: *Seismic stability analysis of small earth-fill dams by Newmark-D method, Japan Society of Irrigation, Drainage and Rural Engineering (JSIDRE)* Special Issue on irrigation dam seismic investigation and maintenance, 2015.12, 15-18, (in Japanese).

17) El Takch, A., Sadrekarimi, A., El Naggar, H. [2016]: *Cyclic resistance and liquefaction behavior of silt and sandy silt soils,* Soil Dynamics Earthquake Engineering 2016; 83:98–109.

18) Finn W.D.L. [2000]: "*Post liquefaction flow deformations*", Pak RYS and Yamamura J, Editors. Soil Dynamics and Liquefaction 2000, ASCE Geotechnical Special Publication No. 107, 2000: 108-122.

19) Georgiannou, V.N. [2006]: *The undrained response of sands with additions of particles of various shapes and sizes.* Géotechnique,56(9): 639–649. doi:10.1680/geot.2006.56.9.639.

20) Goto, S., Baba, K., Mori, S. and Nishio, S. [1992]: *Deformation behavior of saturated sand subjected to monotonic shear following cyclic undrained loading,* Proceeding, 28th Japan National Conf. on Soil Mechanic. and Foundation. Engineering.

21) Hamada, M., O'Rourke, T.D. and Yoshida, N. [1994]: *Liquefaction-induced large ground displacement, Performance of Ground and Soil Structures during Earthquakes*, 13th ICSMFE, 93-108.

22) Iwasaki, T. [1986]: *Soil liquefaction studies in Japan: state of the art*.: Journal of Soil Dynamics Earthquake Engineering1986;5(1).

23) Japanese geotechnical society: Committee report – Research Committee on a seismic measure for earth structures [2014]: Proceeding of JGS special symposium beyond the east Japan great earthquake disaster pp21-32, 2014(In Japanese).

24) Kamata T., Tsukamoto Y., and Ishihara K. [2009]: *Undrained shear strength of partially saturated sand in triaxial tests,* Bulletin of the New Zealand society for earthquake engineering.

25) Kiyota, T., Sato, T., Koseki, J. and Mohammad, A. [2008]: *Behavior of liquefied sands under extremely large strain levels in cyclic torsional shear tests*, Soils and Foundations 48(5): 727-739.

26) Kiyota, T., Kyokawa, H. and Konagai, K. [2011]: *Geo-disaster report on the 2011 Tohoku-Pacific Coast Earthquake*, Bulletin of Earthquake Resistant Structure Research Center, 44: 17-27.

27) Kiyota, T., Koseki, J. and Sato, T. [2013]: *Relationship between limiting shear strain and reduction of shear moduli due to liquefaction in large strain torsional shear tests*, Soils and Dynamics 49: 122-134.

28) Kiku, H. and Tsujino, S. [1996]: *Post liquefaction characteristics of sand*, Proceedings 11th world conference on earthquake engineering, Acapulco, Mexico, Paper No. 1088.

29) Kokusho, T., Hara, T. and Hiraoka, R. [2004]: *Undrained shear strength of granular soils with different particle gradations.* Journal of Geotechnical and Environmental. Engineering 130, No. 6, 621–629.

30) Macmanus, K. J. and Davis, R. O. [1997]: *Dilation induced pore fluid cavitation in sands*, Geotechnique, 47(1), 173}177 (1997).

31) Mohamad, R. and Dobry, R. [1986]: *Undrained monotonic and cyclic triaxial strength of sand,* Journal of Geotechnical Engineering 1986;112(10).

32) Mokni,M. and Desrues, J. [1999]: *Strain localization measurements in undrained plane-strain biaxial tests on Hostun RF sand,* mechanics of cohesive-frictional materials Mech. Cohes.-Frict. Mater. 4, 419}441 (1998)

33) Murthy, T. G., Loukidis, D., Carraro, J. A. H., Prezzi, M., and Salgado, R. [2007]: *Undrained monotonic response of clean and silty sands,* Géotechnique, 57(3), 273–288.

34) Nakata, H., Miyake, K., Muraoka, T., [1991]: *Shaking table tests of submerged tunnel in sandy ground*. Proceedings of Geo-Coast' 91, Yokohama-Japan.

35) Newmark, N. M. [1965]: *Effects of earthquakes on dams and embankments*, Geotechnique 1965, 15(2): 727-738.

36) Poulos, S.J., [1981]: *The steady state of deformation,* Journal of Geotechnical Engineering Division, ASCE, 107: 553-562.

37) Poorooshasb, H.B. [1989]: *Description of flow of sand using state parameters*, Computers and Geotechnics, 8: 195–218.

38) Poorooshasb, H.B., and Consoli, N.C. [1991]: *The ultimate state*, In Proceedings of the 9th Panamerican Conference on Soil Mechanics and Foundation Engineering, Vina del Mar, Chile,pp. 1083–1090.

39) Riemer, M.F., and Seed, R.B. [1997]: *Factors affecting apparent position of steady-state line*, Journal of Geotechnical Engineering, ASCE,123: 281-288.

40) *Re-evaluation of the Slide in the Lower San Fernando Dam in the Earthquake of Feb. 9, 197 1*, Report No. UCB/EERC-88/04, EERC and UC Berkeley.

41) Seed, H.B., Lee, K.L., Idriss, I.M. and Makadisi, F.I. [1975]: *The Slides in the San Fernando Dams during the Earthquake of February 9, 1971* – ASCE, J of the Geotechnical Engineering Division, GT7, pp. 651-688.

42) Seed, H.B., Idriss, I.M., Lee, K.L. and Makadisi, F.I. [1975]: *Dynamic Analysis of the Slide in the Lower San Fernando Dam during the Earthquake of February 9, 1971* – ASCE, J of the Geotechnical Engineering Division, GT9, pp. 889-911.

43) Seed, H. B. [1979]: *Considerations in the earthquake-resistant design of earth and rockfill dams*. Géotechnique 29, No. 3,215–263.

44) Stark, T.D., and Mesri, G. [1992]: Undrained shear strength of liquefied sands for stability analysis. Journal (ASCE)0733-9410(1992)118:11(1727)

45) Shamoto, Y., Zhang, J.M., and Goto, S., [1997]: *Mechanism of large post liquefaction deformation in saturated sand*. Soils Foundations, 37 (2), 71–80.

46) Sitharam, T. G., Vinod, J. S. and Ravishankar, B. R. [2009]: *Post-liquefaction undrained monotonic behavior of sands: experiments and DEM simulations*. Géotechnique 59, No. 9, 739–749.

47) Shamoto Y, Zhang JM, and Goto. S. [1997]: *Mechanism of large post-liquefaction deformation in saturated sand*. Soils Foundation 1997;37(2):71–80.

48) Sivathayalan, S. [1994]: *Static, cyclic and post liquefaction simple shear response of sands*, M.A.Sc. Thesis, University of British Columbia, Vancouver, BC, Canada.

49) Sivathayalan, S., and Yazdi A.M. [2004]: *Post liquefaction response of initially strain softening sand,* Triantafyllidis T. Editor. Cyclic Behavior of Soils and the Liquefaction Phenomena, Proceedings of the International Conference, Bochum, Germany, 31 March - 2 April 2004.

50) Sivathayalan, S. and Vaid, Y. P. [2004]: *Cyclic resistance and post liquefaction response of undisturbed in-situ sands*, Proceedings of the 13th world conference on earthquake engineering, Vancouver, BC, Canada, Paper No. 2940.

51) Sitharam, T. G., Vinod, J. S. and Ravishankar, B. R. [2009]: *Post-liquefaction undrained monotonic behavior of sands: experiments and DEM simulations*. Géotechnique 59, No. 9, 739–749.

52) Sivathayalan, S. and Vaid, Y. P. [2004*]: Cyclic resistance and post liquefaction response of undisturbed in-situ sands*, Proceedings of the 13th world conference on earthquake engineering, Vancouver, BC, Canada, Paper No. 2940.

53) Tatsuoka, F., Sasaki, T. and Yamada, S., [1987]: *Settlement of saturated sand induced by cyclic undrained simple shear*, Proceeding of 8th World Conference on Earthquake Engineering, 3, 398–405.

54) Tatsuoka, F., Duttine, A., Yazaki, S. and Mohri, Y. [2014]: *Evaluation of seismic slip displacement of slope by Newmark method taking into account soil strength reduction due to undrained cyclic loading and strain-softening,* Proc. Special JGS Symposium. Overcoming the Great East Japan Earthquake 394-403 (in Japanese).

55) Tatsuoka, F., Koseki,J., Takahashi, A., [2017]: *Earthquake induced damage to earth structures and proposal for revision of their design policy – based on a case history of the 2011 off the pacific coast of Tohoku earthquake*, Journal of JSCE Vol 5, 101-112, 2017.

56) Thomas, J. [1992]: *Static, cyclic and post liquefaction behavior of Fraser River sand*, M.A.Sc. Thesis, University of British Columbia, Vancouver, Canada.

57) Lee, K.L., Seed, H.B., Idriss, I.M., and Makadisi, F.I. [1975]: *Properties of Soil in the San Fernando Hydraulic Fill Dams* – ASCE Journal of the Geotechnical Engineering Division, GT8, pp. 801-821.

58) Tanaka, T., Tatsuoka, F. and Mohri, Y. [2012]: *Earthquake-induced failure of Fujinuma Dam*, Proceeding of International Symposium on Dams for a Changing World, 24th Congress ICOLD, Kyoto, 6.47-6.52.

59) Tanaka, T. [2016]: *Elasto-plastic dynamic response of fill-type dams: total and effective stress analyses,* International Symposium on the Qualification of Dynamic Analyses of Dams and their Equipments, 31 August-2 September 2016, Saint-Malo, France.

60) Umar, M., Chiaro, G. and Kiyota, T. [2016]: *On the influence of initial static shear on large deformation behavior of very loose Toyoura sand in undrained cyclic torsional shear tests,* JGS Special Publication, 4(2): 17-22 [Selected paper Proceedings of the 6th

Japan-Korea Geotechnical Workshop].

61) Verdugo, R. [1992]: *Characterization of sandy soil behavior under large deformation*, Ph.D. thesis, University of Tokyo, Tokyo.

62) Vaid, Y.P., Chung, E.K.F., and Kuerbis, R.H. [1990]: *Stress path and steady state*. Canadian Geotechnical Journal, 27: 1–7.

63) Vaid, Y.P., and Thomas, J. [1994]: *Post liquefaction behavior of sand",* Proceedings, of thirteenth International Conference on Soil Mechanics and Foundation Engineering, New Delhi, India, 1994: 1305 - 1310.

64) Vaid, Y.P., and Thomas, J. [1995]: *Liquefaction and post liquefaction behavior of sand*. Journal of Geotech Engineering, ASCE 1995;121(2):163–73.

65) Vaid, Y.P., and Sivathayalan, S. [1997]: *Post liquefaction behavior of saturated sand under simple shear loading*, Proceedings of Fourteenth International Conference on Soil Mechanics and Foundation Engineering, Hamburg, 6-12 Sept 1997, 1: 221-224.

66) Verdugo, R., and Ishihara, K. [1996]: *The steady state of sandy soils. Soils and Foundations,* 36(2): 81–92.

67) Wang, Y. and Wang, Y.L. [2017]: *Liquefaction characteristics of gravelly soil under cyclic loading with constant strain amplitude by experimental and numerical investigations,* Soil Dynamics Earthquake Engineering 2017;92:388–96.

68) Yasuda, S., Masuda, T., Yoshida, N., Nagase, H., Kiku, H., Itafuji, S., Mine, K. and Sato, K. [1994]: *Torsional shear and triaxial compression tests on deformation characters of sands before and after liquefaction*, Proceedings of the 5th US–Japan workshop on earthquake resistant design of lifelines and countermeasures.

69) Yasuda, S., Terauchi, T., Morimoto, M., Erken, A. and Yoshida, N. [1998]: *Post liquefaction behavior of several sands*, In Proceedings of the 11th European conference on earthquake engineering, Rotterdam, the Netherlands: Balkema (CD-ROM).

70) Yoshida, N., Yasuda, S., Kiku, M., Masuda, T. and Finn, W. D. L. [1994]: *Behavior of sand after liquefaction*, Proceedings of the US–Japan workshop on earthquake resistant design of lifeline facilities and countermeasures against soil liquefaction, Buffalo, NY, USA, vol. 5, pp. 181–198.

71) Yamamuro, J.A., and Lade, P.V. [1998]: *Steady-state concepts and static liquefaction of silty sands*, Journal of Geotechnical and Environmental Engineering, 124(9): 868–877.

72) Yoshimine, M. [1996]: *Undrained flow deformation of saturated sand under monotonic loading conditions*, Ph.D. thesis, University of Tokyo, Tokyo. (In Japanese).

73) Yoshimine, M., and Ishihara, K. [1998]: *Flow potential of sand during liquefaction*. Soils and Foundations, 38(3): 179–188.

74) Yoshimine, M., Ishihara, K., and Vargas, W. [1998]: *Effects of principal stress direction and intermediate principal stress on undrained shear behavior of sand,* Soils and Foundations, 38(3):189–198.

CHAPTER 2

Test Material, Apparatus and Procedure

CHAPTER 2: Material, apparatus and test procedure

LIST OF FIGURES

LIST OF TABLES

CHAPTER 2: Material, apparatus and test procedure

2.1 Introduction

To investigate undrained behavior of sand, torsional shear test on saturated Toyoura sand specimen was performed. To simulate the simple shear condition as closely as encountered in the field, vertical displacement of the top cap was prevented, during monotonic or cyclic shearing of the specimen in the undrained cyclic torsional shear test.

In this chapter, material properties are discussed in detail by analyzing their index properties. Modified torsional shear apparatus is explained in detailed, which was developed in the Institute of Industrial Science, University of Tokyo. In the last part of this chapter, the testing procedure was discussed in detail, which includes specimen preparation, testing procedure, and the loading procedure to apply the initial static shear and cyclic loading.

2.2 Index properties of sandy soil

Soil is heterogeneous in nature having three-phase, soil solids, having pore spaces filled by water and air. Therefore, mostly the soil exists in three-phase form i-e solid, water and air.

The proportion of solid, water and air is evaluated by five dimensionless quantities i-e *void ratio* (*e*), *Porosity* (*n*), *moisture content* (*w*), *saturation ratio* (*Sr*) and relative *density (Dr).*

The definition of all these dimensionless parameters is given below

Void ratio

$$\text{Void ratio, e} = \frac{V_v}{V_s},$$

Whereas, V_v = volume of voids,

` V_s = Volume of soil solids

Porosity

$$\text{Porosity, } n, = \frac{Vv}{V},$$

Whereas, Vv = volume of voids,

`   V = Total Volume

Water Content

$$\text{Moisture content, } w, = \frac{Ww}{Ws}$$

Whereas, Ww = weight of water,

`   Ws = weight of solid

Degree of Saturation

$$\text{Degree of Saturation, } Sr, = \frac{Vw}{Vv}x100$$

Degree of saturation ranges from 0 to 100%, depending on whether all the pore spaces is occupied by air or water respectively.

Relative Density

In case of soil consist of sand or gravels, the relative density is used to characterize the degree of compaction.

It is given by the following equation.

$$Dr, = \frac{e_{max} - e}{e_{max} - e_{min}} * \ 100\%$$

Wheres as,

e_{max} = maximum void ratio;

e_{min} = minimum void ratio;

e = current void ratio.

The relative density indicates the compactness of the soil deposit and greatly influences the

behavior of the soil. In Table 2.1 description of relative density from very loose to dense is

presented based on personal experience.

Table 2.1: Soil description based on relative density

Dr (%)	Description
0-20	Very loose
20-40	Loose
40-60	Medium dense
>60	Dense

2.3 Testing material

In this study Toyoura sand with negliglbe fine content (Fc<1%) has been used to conduct monotonic and cyclic undrained torsional shear test. Toyoura sand mainly consists of quartz and its particle are mostly subangular in shape. Properties of Toyoura sand are listed in detail in Table 2.2. Grain size distribution curve of Toyoura sand is shown in Figure 2.**1**. Due to a large amount of Toyoura sand used in one test (e.g 1.5kg), Toyoura sand was reused after air and oven drying.

Index properties of new batch of Toyoura sand and used one is compared and insignificant changes in index properties were observed.

Table 2.2: Material index properties

Material	Specific gravity G_s	Minimum void ratio e_{min}	Maximum void ratio e_{max}	Mean Diameter D_{50} (mm)	Fines content F_C (%)
Toyoura sand	2.659	0. 608	0.951	0.18	0.1
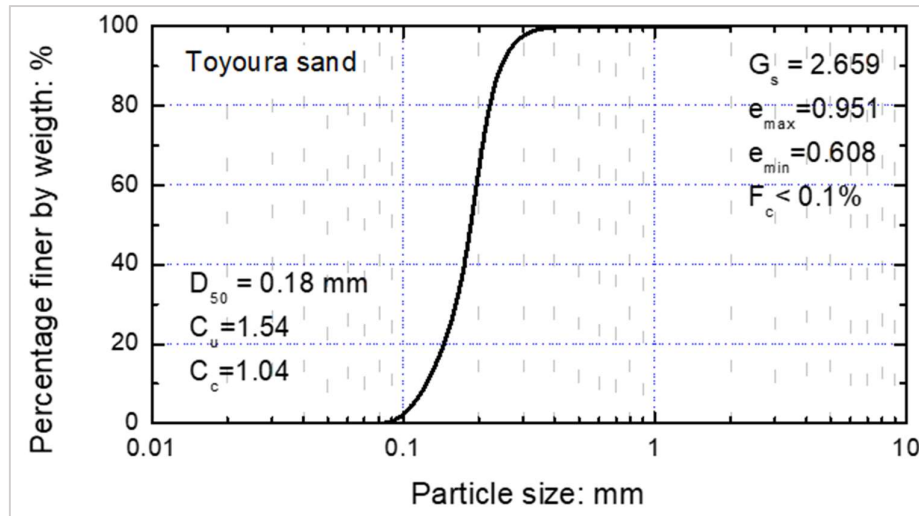
Figure 2.1: Grain size distribution curve of Toyoura sand.

2.4 Testing apparatus

Automated torsional shear apparatus was used to conduct the test as shown in Figure 2.2 which was developed by Kiyota et al. (2008) in the Institute of Industrial Science, University of Tokyo. In an effort to induce large shear strain on hollow cylindrical specimen, Kiyota et al. (2008) modified the conventional torsional shear apparatus to achieve double amplitude shear strain levels exceeding 100% on the specimen size of 30cm height, 15cm outer dia and 9cm inner dia by using a belt-driven torsional loading system that is connected to an AC servo motor through electro-magnetic clutches and a series of reduction gears. To reduce time and induce larger shear strain specimen size is reduced to of 20cm height, 10cm outer dia and 6cm inner dia to achieve double amplitude shear strain exceeding 150%. A series of experiment by Umar et al. (2018) showed that the specimen with different dimensions showed similar strength and deformation characteristics.

The main part of the apparatus includes loading devices, cell, and measurement devices. The loading system of this apparatus consists of servo-controlled axial and torque loading devices. The torque and axial load and are simultaneously, independently applied on the hollow

cylindrical specimen through two servo-motors at constant strain rates, in principle.

Each loading device has an electro-magnetic clutch which can reverse the loading direction instantly. The axial and torque loading and cell pressure are automatically controlled by a computer during the test including the consolidation stage before the shear loading. By drawing a grid on the external face of the outer membrane, specimen deformation behavior can be observed from the outside of the cell and its visual analysis can be performed by taking a series of pictures.

Torsional shear apparatus is capable of testing specimens with various dimensions ranging from 200mm in outer diameter, 120mm in inner diameter and 300mm in height to 90mm in outer diameter. For large size specimen, it is possible to investigate the properties of soil with different particle size from sand to gravel. Therefore, in this study, a hollow cylindrical specimen with inner diameter of 60mm and outer diameter of 100mm with 200mm in height is used in all the experiments.

2.5 Measurement devices

The whole system consists of 24 channels to measure stresses, strains and volume change. Seven channels were used in this study: two channels for the two-component load cell (axial and torque loads), one channel for the External Displacement Transducer (ETD) for vertical strain, one channels for external potentiometer for shear strain, and one channel each for High Capacity Differential Pressure Transducer (HCDPT) and Low Capacity Differential Pressure Transducer (LCDPT).
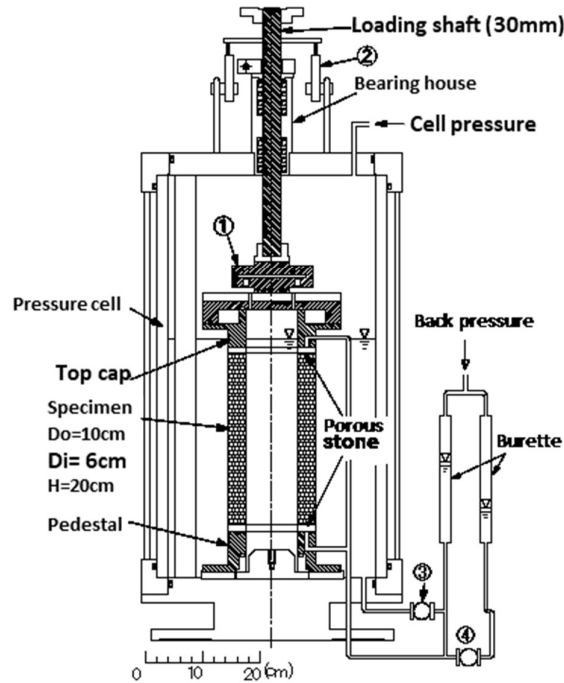
Figure 2.2: Torsional shear apparatus employed in this study

(after Kiyota et al. 2008)

2.5.1   Load cell

A two-component load cell and calibration data is shown in Figure 2.3, Figure 2.4 and Figure 2.5 with a negligible coupling effect (i.e., no effect of axial load on torque measurement and vice versa) located inside the cell is employed in this apparatus. The capacities of vertical load and torque are of 8 kN and 0.15 kNm, respectively.
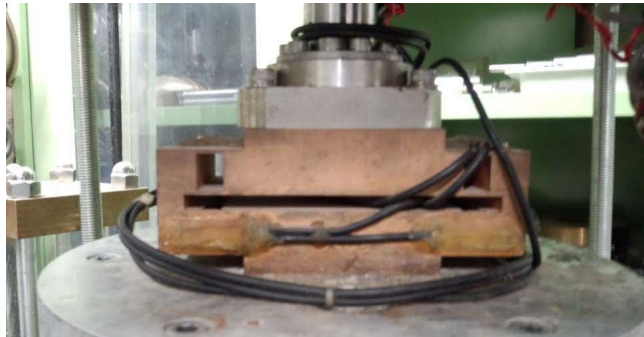
Figure 2.3: Two component load cell
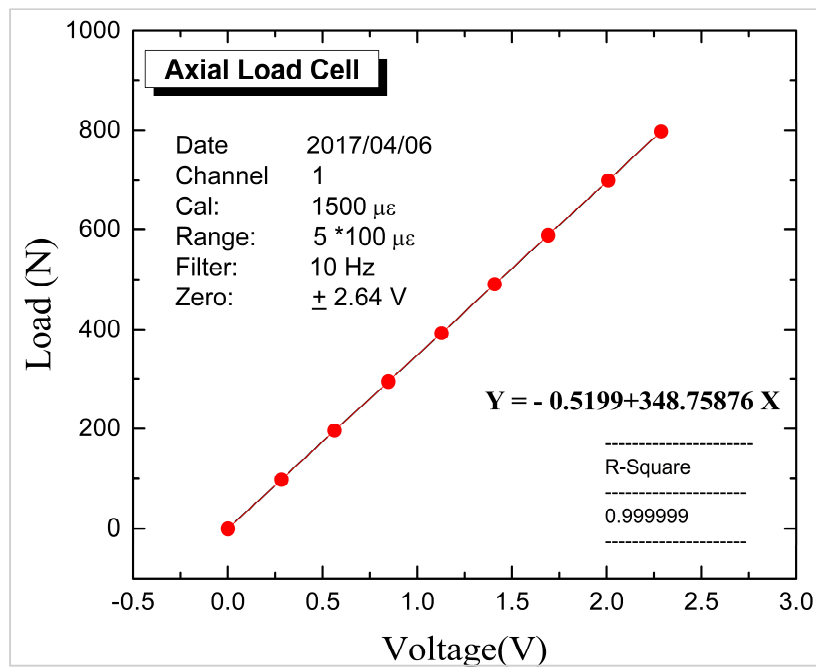
Figure 2.4: Axial load calibration
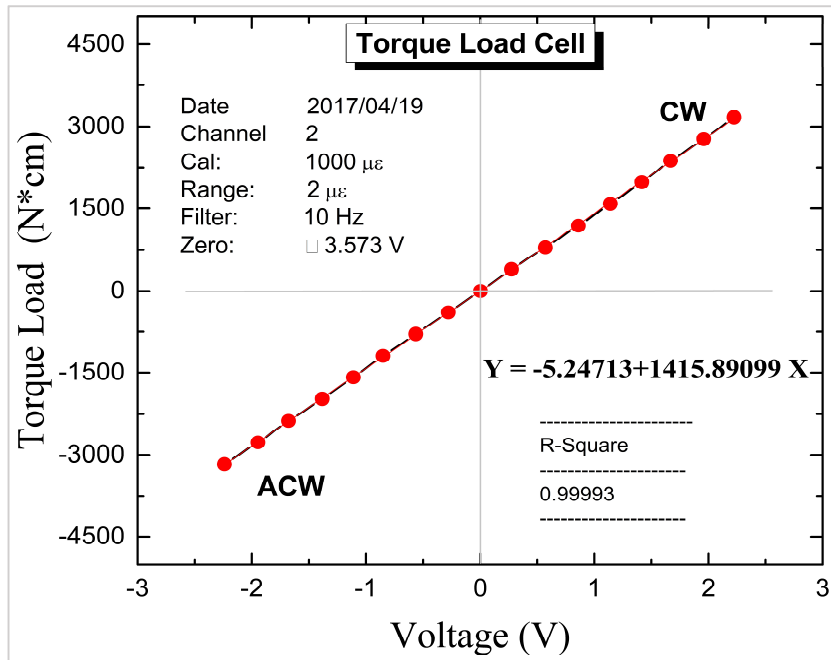
Figure 2.5: Torque calibration

2.5.2   External potentiometer

Large deformation exceeding 150% in term of double amplitude is measured by using

external potentiometer as shown in Figure 2.7 its calibration in

Figure 2.6.

Figure 2.6: External potentiometer
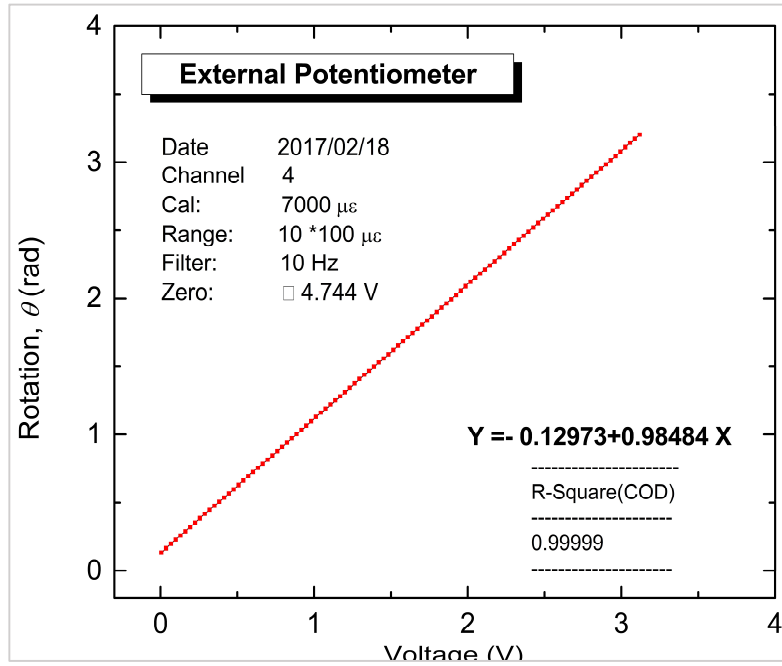
Figure 2.7: External potentiometer caliberation
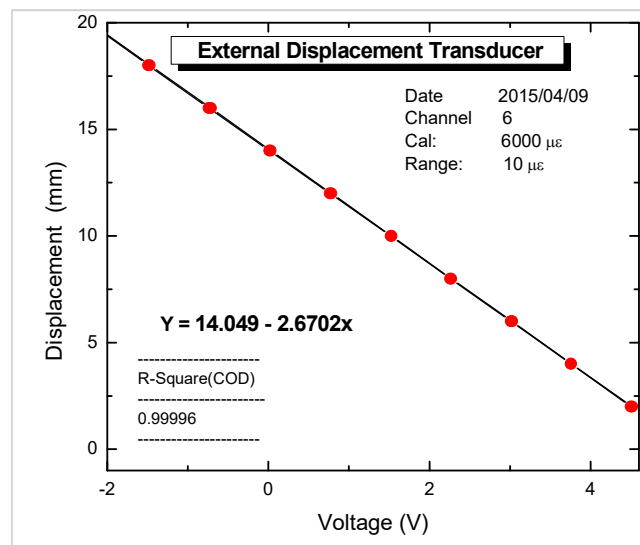
Figure 2.8: External Displacement Transducer (EDT) and its calibration

2.5.3 High Capacity Differential Pressure Transducer (HCDPT)

For measuring the confining pressure, HCDPT measures the difference in pressures between the cell pressure and the pore water pressure. HCDPT positive terminal is connected with the cell chamber to measure the cell pressure, while the negative is attached to both the top and bottom drainage valve of the specimen to measure the pore water pressure inside the specimen. The employed HCDPT has a maximum capacity over 600kPa. HCDPT and its calibration data is shown in Figure 2.9 and Figure 2.10 respectively.

Figure 2.9: High Capacity Differential Transducer (HCDPT)
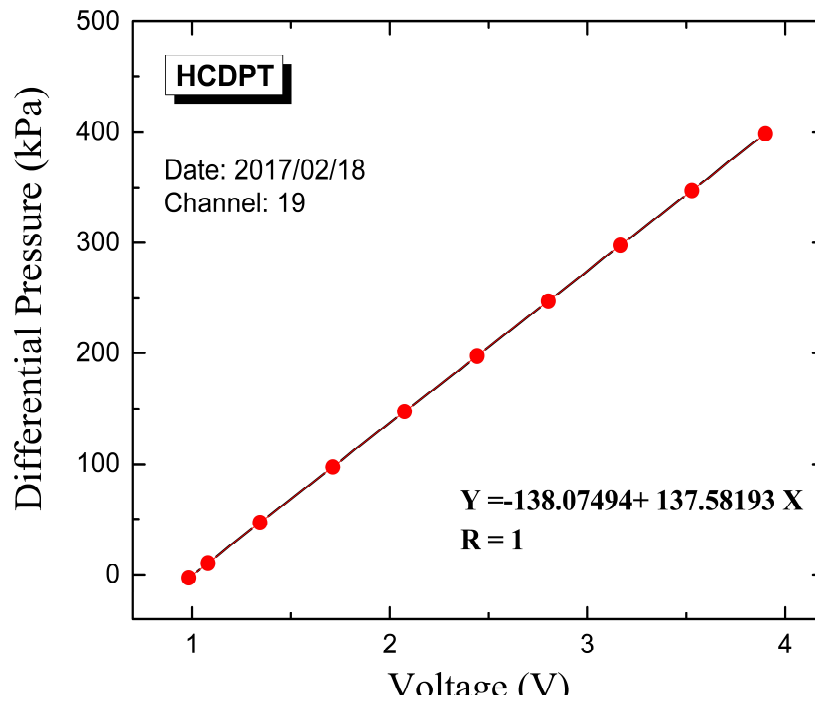
Figure 2.10: High Capacity Differential Transducer (HCDPT) calibration

2.5.4 Low Capacity Differential Pressure Transducer (LCDPT)

Volume changes during the consolidation are measured by the difference of water head in two burettes, one that collects drained water coming from the specimen and other used as a reference LCDPT and its calibration is shown in Figure 2.11 and Figure 2.12 respectively

Figure 2.11: Low Capacity Differential Pressure Transducer (LCDPT)
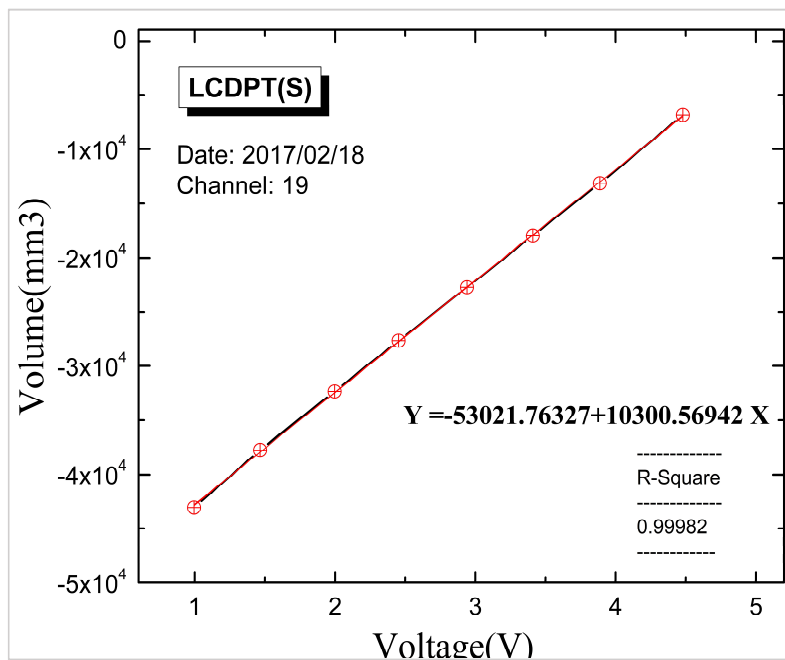
Figure 2.12: Low Capacity Differential Pressure Transducer (LCDPT) calibration

2.6   Experimental procedure

2.6.1   Specimen preparation methods

Fabric prepared by different preparation method significantly affect the soil behavior subjected to undrained cyclic loading (Oda(1972), Ladd(1974), Mulilis et al.(1977). Different sample preparation methods are employed in the laboratory (Figure 2.13), depending on the material and testing conditions.

For example, 1) Air pluviation 2) water pluviation 3) dry rodding has been mostly adopted methods for a sample preparation. In this study, the specimen was prepared by using the air pluviation technique suggested by Hong Nam (2004), which is a little different as described in the relevant standard procedure of JGS, 1998. This method minimizes the effect of inherent anisotropy in the radial direction of the hollow cylindrical sand specimens (Hong Nam, 2004, and De Silva et al. 2006). Air pluviation method produces horizontal bedding planes, and the shear stress is also applied in the horizontal bedding plane of the specimen in torsional shear apparatus. There this technique is most suitable to produce a sand fabric to investigate sandy soil behavior.
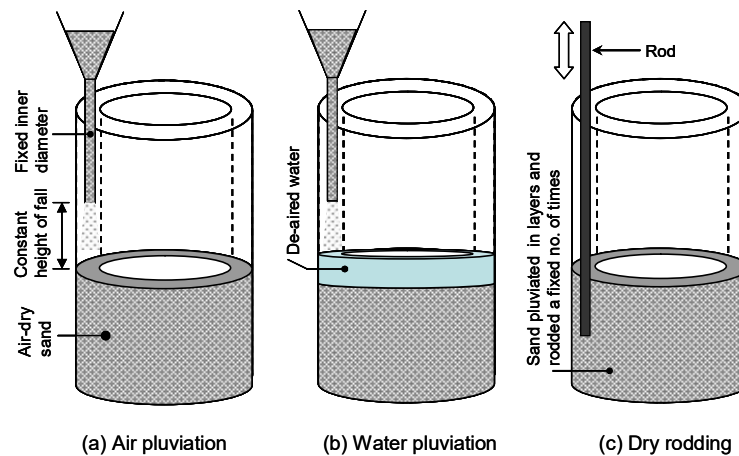
Figure 2.13: Different methods of sample preparation

2.6.2 Experimental procedure

The outer membrane (0.3 mm thick) was placed over the pedestal which contains a porous stone as shown in Figure 2.14A with blades in order to apply the necessary friction during the torsional shear loading. The gap between the outer membrane and the pedestal was sealed by using three rubber band.

The inner membrane of 0.3 mm thickness was placed over a metal ring as shown in Figure 2.14B. Following this the metal ring together with the membrane was placed into the pedestal hole (Figure 2.14C) while taking the inner membrane out from the hole of the pedestal as shown in Figure 2.14D.
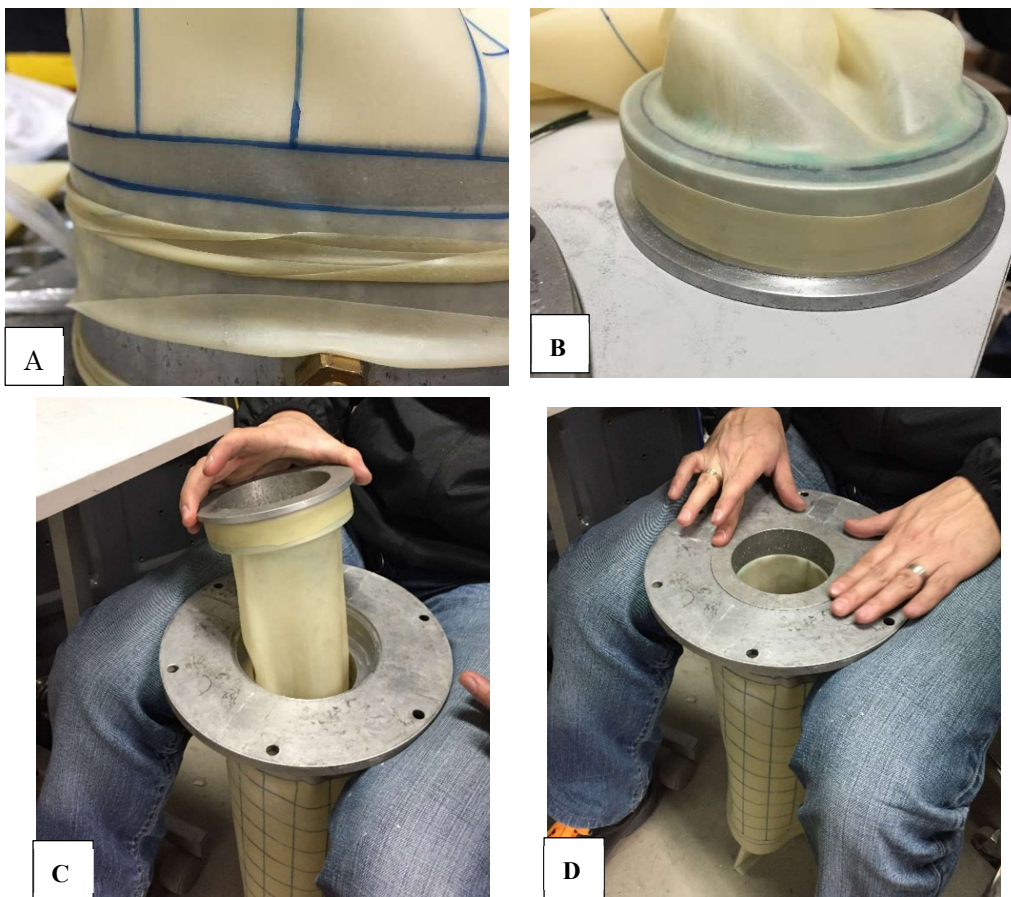
Figure 2.14: Procedure to place the two membranes on outer and inner mold

The pedestal was then firmly screwed into the apparatus base and the inner mold was then set

as shown in Figure 2.15A. The inner mold consists of four metal parts, which makes a perfect

cylinder. All four parts of the inner mold were placed inside the inner membrane, which comes

out from the pedestal, and the mold was firmly fixed using the ring and rod. Subsequently, the

outer mold was then fixed. This outer mold consists of two symmetrical metal parts with two

clamps to tighten them together as shown in Figure 2.15B. A small amount of lubricant (grease)

was applied along the edges of the outer mold before fixing it. After fixing the outer mold, the

extra part of the outer membrane was put over the outer mold, and it was ensured that the gap

between the outer membrane and the outer mold was perfectly sealed. A vacuum of 30 kPa was

then applied to the space between outer membrane and outer mold to adhere with the outer

mold.
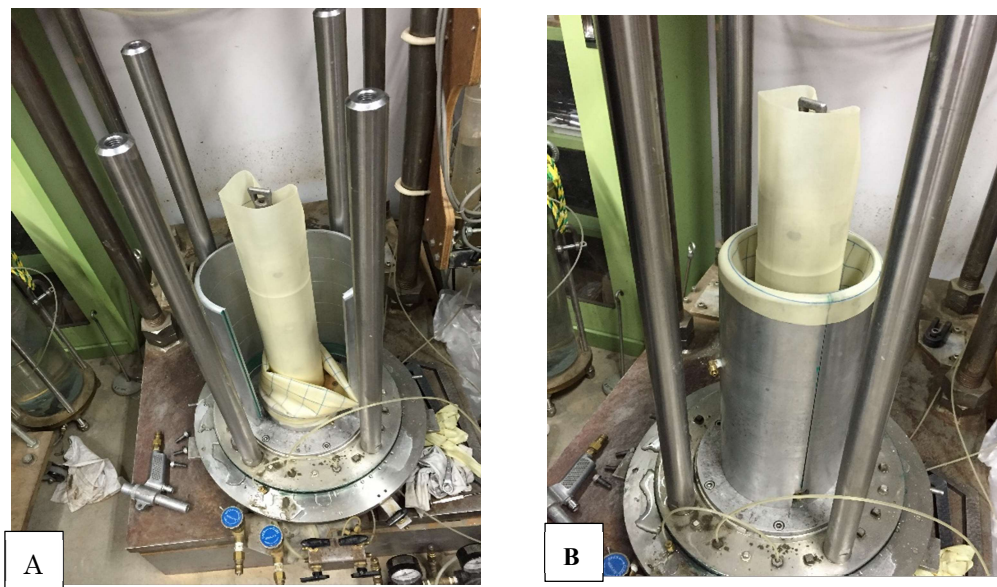
Figure 2.15:: Fixing of the inner and outer mold

By using the air pluviation method as shown in, the sand was poured from the nozzle in a radial

as well as circumferential direction. In this study to achieve a varying range of relative density

(D_r) (i.e., measured after achieving isotropic consolidation of 100 kPa) were achieved by

varying the height of nozzle. To obtain specimens with initial relative density (D_r) of about 27$\pm$3 %, the falling height was selected to be 4 cm and for relative density 20$\pm$2 %, nozzle of the pluviator was kept at 1.5cm. Whereas for achieving denser specimen, a pluviator height of 40cm was used. After pluviation the material to the full height of the specimen, the top surface of the specimen as leveled horizontally (Figure 2.17 by using a metal strip, and the waste material was collected and weighed. The relative density was also measured at this stage.
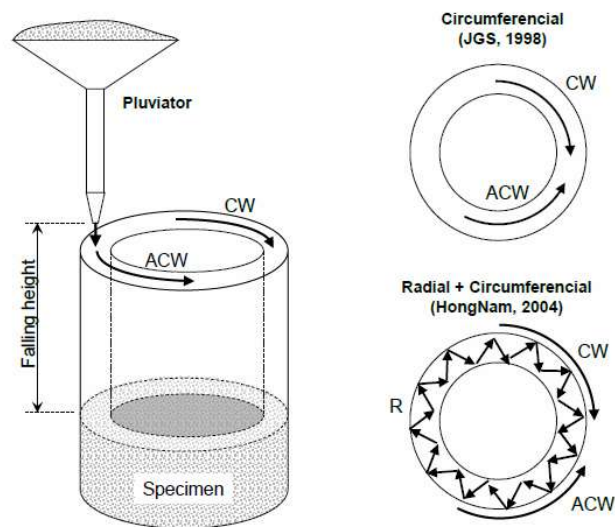
Figure 2.16: Pluviation technique used in this study (Chiaro (2010))

Figure 2.17: Pluviation into the mold

To place the top cap over the specimen, first, the top cap guider was fixed to one of the four steel poles that come from the base of the apparatus. Then a steel cable with three bolts connected to one end and with dead weight attached to the other end was attached to the top cap using the three bolts.

Then the cable was attached to the top cap was put over the pulleys of the guider and balanced using counterbalances. To keep the top cap horizontal, it was maintained by adjusting the three bolts before it was placed on the top of the specimen. Finally, the top cap was placed very carefully over the specimen until it touched the top surface. Two clamps were then fixed symmetrically to two steel poles and the top cap was held in position by attaching it to the clamps using the bolts. After clamping, the extra part of the inner membrane was pulled gently over the top cap inner ring, and the extra part of the outer membrane was placed over the top cap outer ring. The specimen was perfectly sealed by using rubber bands, covering the inner and outer rings of the top cap.

The counterbalance was then applied again, and the clamps were removed. After a partial vacuum of 30 kPa had been applied to the specimen, the outer mold was removed. The top cap was clamped again, and the inner mold was removed. After that, the diameter of the specimen at eight (8) different positions was measured by using measurement tape.

Before attaching the top cap, voltage reading was set to zero for all the voltage measuring transducers. Then the top cap was connected firmly to the load cell, followed the specimen is covered with the cell. The cell was pushed back, and the load cell is attached to the automatic loading system. The cell was filled with water and finally while keeping the vacuum to 30 kPa.

2.7   Saturation of the specimen

liquefaction resistance is significantly affected by the degree of saturation (Figure 2.18 (Okamura and Soga, 2006)). Higher degree of saturation is desirable to obtain precise undrained behavior and liquefaction characteristics. Two methods are extensively employed i-e Double

vacuum (Ampadu, 1991)) and injection of carbon dioxide (ref) to achieve high degree of saturation. In this study double vacuum method is employed with its ease of applicability to achieve high degree of saturation. Detailed procedure of double vacuum is described below.

In the double vacuum method, a complete vacuum (-98 kPa) was applied to the specimen as a back pressure, while keeping the effective stress constant at 28 kPa by applying a partial vacuum of 70 kPa to the cell. The specimen was kept for about 8 hours under this state before allowing the water to enter the specimen. Then the de-aired distilled water was allowed to enter the specimen. It takes about 6 hours, water start coming from top of the specimen into the drainage tank. Water was allowed to go through until the air bubbles stop coming into the drainage tank. When the air bubbles stop coming into the drainage tank, a back pressure (P_B) of 200 kPa was applied for one hour, while keeping the effective stress of 30kPa, in order to compress the air bubbles and further saturate the specimen. During the back pressure, the pipes of HCDPT are saturated in order to remove any entrapped air inside the pipe, and also to remove error in the measurement.

For measuring the degree of saturation, skepmton B values is used, for isotropic condition (($\Delta\sigma_1 = \Delta\sigma_3$) skepmton B value is given by following equation.

$$B = \frac{\Delta u}{\Delta\sigma_3}$$

Whereas:

Whereas:

Δu = increment of pore water pressure;

$\Delta\sigma_3$ = increment of minor total principal stress.

In isotropic loading, stress in the vertical and horizontal direction is applied in equal increments

to the specimen, therefore the degree of saturation, can be measured by, pore water pressure increment, with the theoretically value of fully saturated sand (i.e., for ideally and fully saturated specimen $B = 1.0$ and $\Delta u = \Delta \sigma_3$).

Towhata (2008) evaluated the varying of degree of saturation with Skempton 'B' value by varying the back pressure. It can be seen in Figure 2.19 saturation can be considered to be sufficient, when the B value is above 0.96. However, in scenario in which B value is not sufficiently high, back pressure is increases to compress the air bubbles.
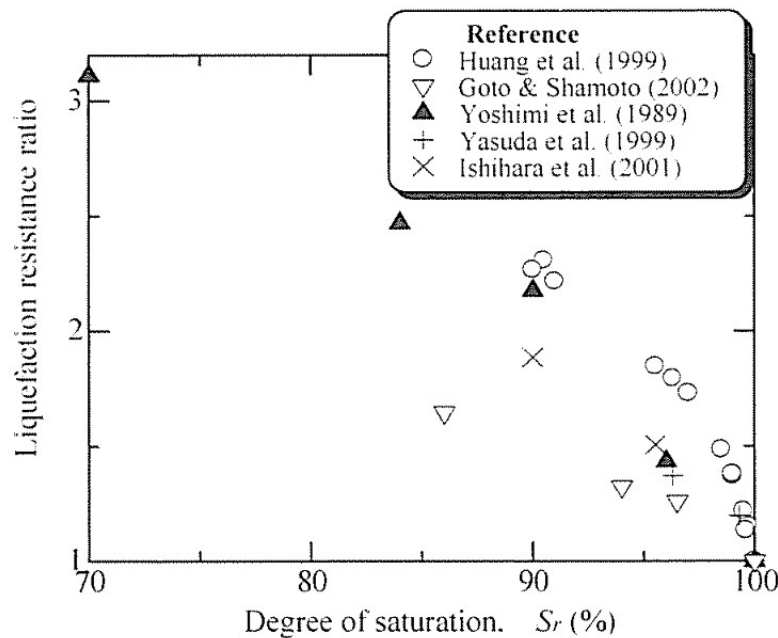
Figure 2.18: Effect of degree of saturation on the liquefaction resistance
(Okamura and Soga (2006))
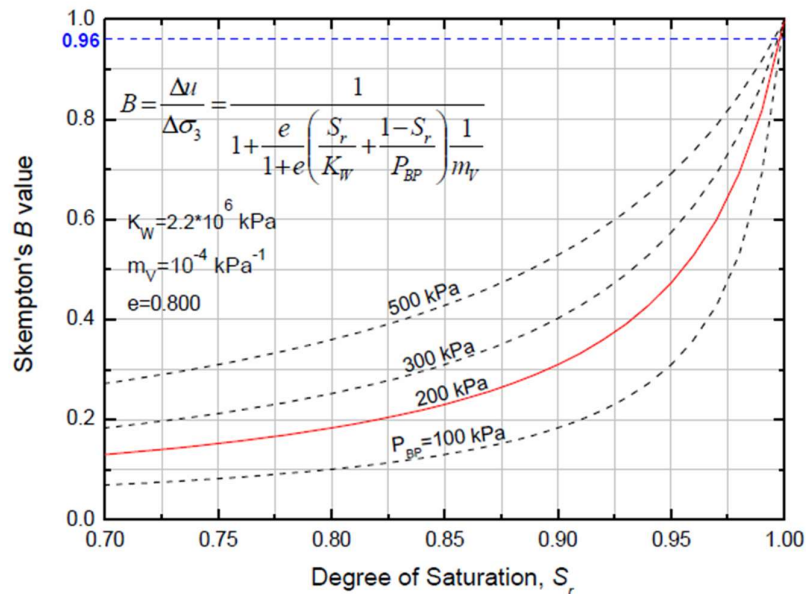
Figure 2.19: Relationship between Skempton's *B* value and the degree of saturation
(Towhata (2008))

2.8   Tests procedure

Series of tests as listed from Table 2.4 to 2.10, were performed on Toyoura sand specimens with relative density (*Dr*) from 27 to 71%, with a void ration of 0.69 to 0.88 after consolidation to mean effective stress. After completing the saturation process by employing the double vacuum method, and back pressure of 200 kPa was applied in order to achieve higher degree of saturation (*B* > 0.96). The specimens were subjected to the following steps, Schematic illustration of the steps are shown in

Figure 2.20.

i) Isotropic consolidation

The specimens were isotropically consolidated by increasing the effective stress state up to 100

kPa, with a constant back pressure of 200 kPa.

ii) Undrained cyclic torsional shear loading

Isotropically consolidated specimens were cyclic sheared at strain rate of 0.5 %/min under

undrained conditions, in order to apply a specified value of damage strain.

iii) Undrained monotonic torsional shear loading

Without allowing the draininage, undrained monotonic torsional loading with constant amplitude of shear stress was applied at a constant shear strain rate of about 0.5 %/min in investigate the static undrained strength.
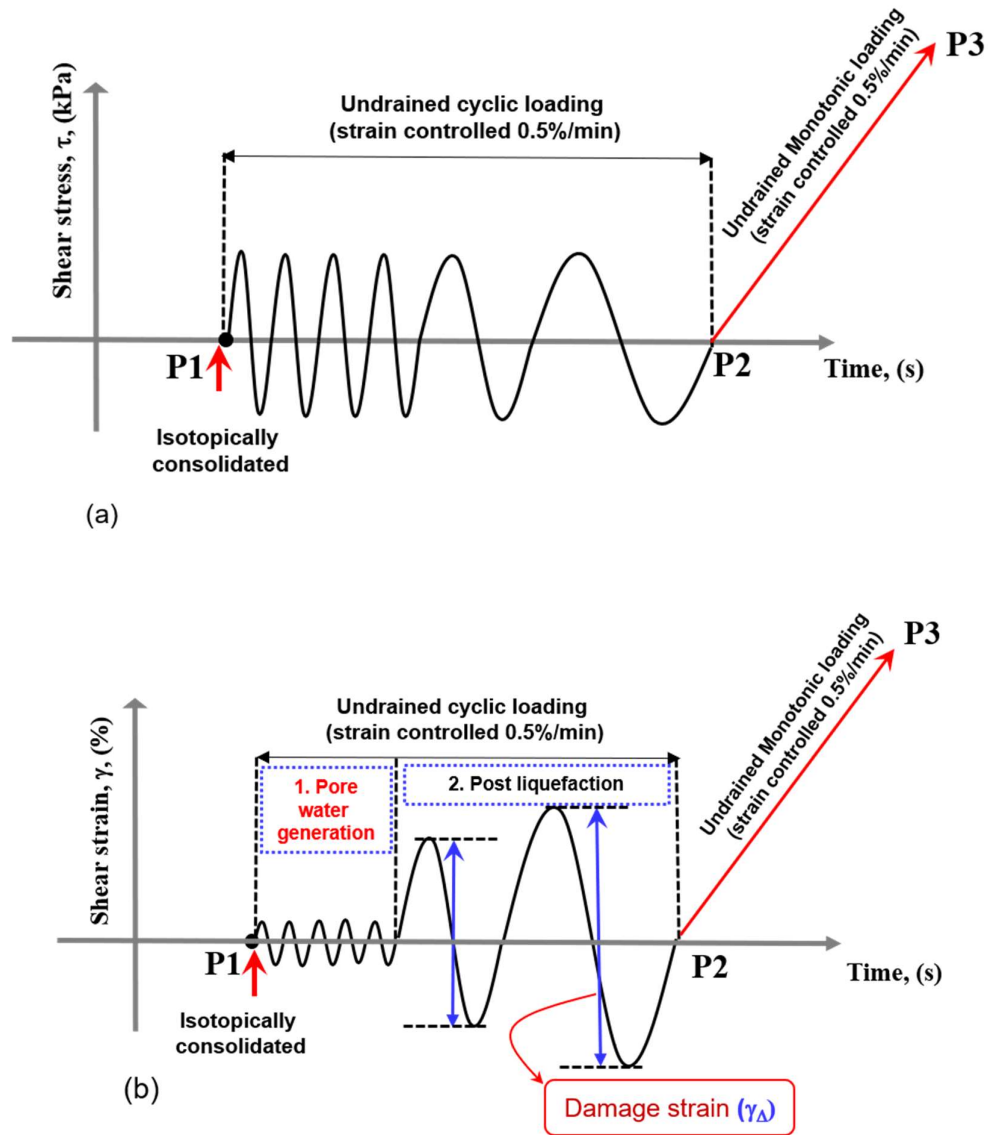
Figure 2.20: Schematic illustration of test procedure from P1 to P3

Table 2.4: Large strain undrained Monotonic test

Test No.	Relative Density, Dr (%)	Void ratio, e	Mean effective stress ($p^{'}$) (kPa)	Shear stress (kPa)
1-1	19.0	0.884	100	
1-2	28.5	0.857	100	
1-3	36.8	0.823	100	
1-4	47.9	0.766	100	undrained monotonic loading
1-5	51.6	0.766	200	
1-6	49.0	0.768	400	
1-7	60.3	0.739	100	
1-8	72.0	0.693	100	

Table 2.5: Undrained cyclic test

Test No.	Relative Density, Dr (%)	Void ratio, e	Mean effective stress ($p^{'}$) (kPa)	Shear stress (kPa)
2-1	48.2	0.767	100	12
2-2	52.0	0.768	100	17
2-3	48.4	0.784	100	20
2-4	71.0	0.701	20	30

Table 2.6: Undrained cyclic test with damage strain

Test No.	Relative Density, Dr (%)	Void ratio, e	Cyclic damage strain, γ_{Δ}, (%)	Mean effective stress ($p^{'}$), (kPa)	Shear stress (kPa)
3-1	47.9	0.768	1	100	20
3-2	48.3	0.772	6	100	20
3-3	52.2	0.771	13	100	20
3-4	50.8	0.772	22	100	20
3-5	49.0	0.785	25	100	20
3-6	48.4	0.784	92	100	20
5-1	68.7	0.711	3	100	20
5-2	72.1	0.700	7	100	20
5-3	67.9	0.714	12	100	20

Table 2.7: Undrained cyclic test with damage strain – stress level effect

Test No.	Relative Density, Dr (%)	Void ratio, e	Cyclic damage strain, $\gamma_{\Delta,}$ (%)	Mean effective stress (p'), (kPa)	Shear stress (kPa)	Static shear
6-1	49.5	0.762	6%	100	12	0
6-2	46.3	0.774	6%	100	12	0
6-3	45.7	0.776	6%	100	12	15

Table 2.8: Undrained cyclic test with damage strain – with static shear

Test No.	Relative Density, Dr (%)	Void ratio, e	Cyclic damage strain, $\gamma_{\Delta,}$ (%)	Mean effective stress (p') (kPa)	Shear stress (kPa)	Static stress (kPa)
7-1	48.3	0.771	0	100	Mono	0
7-2	46.0	0.775	3	100	12	15
7-3	45.7	0.776	6	100	12	15
7-4	48.0	0.776	8	100	12	15
7-5	46.0	0.772	11	100	12	15
7-6	47.0	0.785	13	100	12	15
7-7	45.5	0.776	17	100	12	15
7-8	47.0	0.765	13	100	0.2	15
7-9	47.0	0.772	13	100	0.2	10

Table 2.9: Undrained cyclic test with damage strain with Pressure level

Test No.	Relative Density, Dr (%)	Void ratio, e	Cyclic damage strain, $\gamma_{\Delta,}$ (%)	Mean effective stress (p') (kPa)	Shear stress (kPa)	Static shear
8-1	49.5	0.762	7	200	0.20	0
8-2	45.7	0.776	11	100	0.20	0

Table 2.10: Undrained monotonic test with damage strain with reconsolidation history

Test No.	Relative Density, Dr^1 (%)	Cyclic damage strain, $\gamma_{\Delta,}$ (%)	Relative Density, Dr^2 (%)	Mean effective stress ($p\,'$) (kPa)	Shear stress (kPa)
9-1	48.0	7	72.0	100	0.20
9-2	48	11	66.0	100	0.20

2.8.1   Correction for membrane force

Koseki et al. (2005), among others, pointed out that in performing torsional shear tests on hollow cylindrical soil specimens, due to the presence of inner and outer membranes, the effect of membrane force on measured torsional shear stress cannot be neglected (i.e. to calculate the actual shear stress applied on soils, the total stress measured by the load cell needs to be corrected for the apparent shear stress induced by the presence of the membrane, namely membrane force). Furthermore, membrane force becomes significantly important when shear strain reaches an extremely large level (Kiyota et al. 2008; Chiaro et al., 2012).

Usually, the membrane force is corrected based on the linear elasticity theory, which assumes cylindrical deformation of a specimen. Accordingly, the theoretical apparent shear stress (τm) induced by the inner and the outer membranes can be evaluated as follows:

$$\tau_m = \frac{t_m E_m \left(r_o^3 + r_i^3\right)\theta}{\left(r_o^3 - r_i^3\right)H} \tag{1}$$

$$\theta = \frac{3\left(r_o^2 - r_i^2\right)H}{2\left(r_o^3 - r_i^3\right)}\gamma \tag{2}$$

here θ is the rotational angle of the top cap detected by external potentiometer; H is the height of the specimen; ro and ri are the outer and inner radii of the specimen; τm and Em are, respectively, the thickness and the Young's modulus (= 1470 kPa; Tatsuoka et al., 1986) of the membrane.

Nevertheless, experimental evidence clearly demonstrates that at large shear strains, deformation of a hollow cylindrical sand specimen is not uniform along specimen height. In addition, specimen shape is far from being perfectly cylindrical (Kiyota et al., 2010; Chiaro et al., 2013). Accordingly, to confirm the validity of Eq. (1) in correcting for the effect of the membrane force, an apposite testing procedure was developed over the years (Kiyota et al. 2008, Chiaro et al. 2012, Chiaro et al. 2015a). Umar et. al (2016) showed the hyperbolic correlation between γ and τ_m for specimen size having height 300mm, outer diameter 150mm and inner diameter of 90mm. In order to validate the correlating, specimen dimensions was changed to height 200mm, outer diameter 100mm and inner diameter of 60mm.

A hollow cylindrical water specimen, monotonic torsional shear test was performed and results is plotted in Figure 2.21, to compare the specimen size effect on membrane force. From the Figure 2.21, it can be observed, changing the size of the membrane, membrane force is not greatly influenced. Therefore, it implies that existing correlation for the correction of membrane force is applicable irrespective of specimen dimensions.
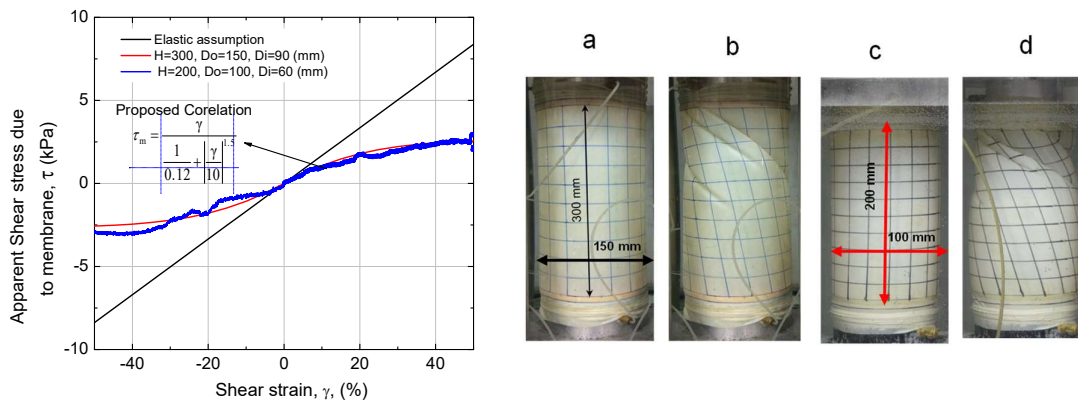
Figure 2.21: Membrane force a) Comparison of membrane force between two different specimens b) water specimen prepared for measurement of membrance force

2.9   References

1) Ampadu, S. I. K. [1991]: *Undrained behavior of kaolin in torsional simple shear*, Ph.D. thesis, Dep. of Civil Engineering, University of Tokyo, Japan

2) Chiaro, G., Koseki, and Sato, T. [2012]: *Effects of initial static shear on liquefaction and large deformation properties of loose saturated Toyoura sand in undrained cyclic torsional shear tests*, Soil and Foundations, 52(3), 498–510

3) Chiaro, G., Kiyota, T. and Koseki, J. [2013]: *Strain localization of characteristics of loose saturated Toyoura sand in undrained cyclic torsional shear tests with initial static shear,* Soils and Foundations, 53(1), 23-34.

4) Chiaro, G., Kiyota, T. and Miyamoto, H. [2015a]*: Large deformation properties of reconstituted Christchurch sand subjected to undrained cyclic torsional simple shear loading*, Proceeding of the 2015 NZSEE Conference, Rotorua, New Zealand, April 2015, 529-536.

5) De Silva, L.I.N., Koseki, J., and Sato, T. [2006]: *Effect of different pluviation techniques on deformation property of hollow cylinder sand specimens*, Proceeding of International Symposium on Geomechanics and Geotechnics of Particle Media, Ube, Yamaguchi, Japan, 29-33

6) Hong Nam, N. [2004]: *Locally measured quasi-elastic properties of Toyoura sand in cyclic triaxial and torsional loadings,* Ph.D. thesis, Dep. of Civil Engineering, University of Tokyo, Japan

7) JGS [1998]: *Standards of Japanese geotechnical society for laboratory shear tests*, Japanese Geotechnical Society, 5550-1998 (English version)

8) Ladd, R. S. [1974]: *Specimen Preparation and Liquefaction of Sands*, Journal of Soil Mechanics Foundation Division, ASCE, Vol. 100, No. GT10, pp. 1180–1184.

9) Mulilis, J. P., Arulanandan, K., Mitchell, J. K., Chan, C. K., and Seed, H. B. [1977]:

Effects of Sample Preparation on Sand Liquefaction, Journal of Geotechnical Engineering Division, ASCE, Vol. 103, No. GT2, pp. 91‑108.

10) Oda, M. [1972]: *Initial Fabric and Their Relations to Mechanical Properties of Granular Material,* Soils Foundation, Vol. 12, No. 1, pp. 17‑36.

11) Kiyota, T., Koseki, J. and Sato, T. [2010]: *Comparison of liquefaction-induced ground deformation between results from undrained cyclic torsional shear tests and observations from previous model tests and case studies*, Soils and Foundations, 50(3), 421-429.

12) Koseki, J., Yoshida, T. and Sato, T. [2005]: *Liquefaction properties of Toyoura sand in cyclic torsional shear tests under low confining stress*, Soils and Foundations, 45(5), 103-113

13) Okamura, M. and Soga, Y. [2006]: *Effects of pore fluid compressibility on liquefaction resistance of partially saturated sand,* Soils and Foundations, 46 (5), 695-700

14) Tatsuoka, F., Sonoda, S., Hara, K., Fukushima S. and Pradhan, T. B. S. [1986]: *Failure and deformation of sand in torsional shear*, Soils and Foundations, 26(4), 79-97.

15) Towhata, I. [2008]: *Geotechnical Earthquake Engineering*, Springer

16) Umar, M., Chiaro,G., and Kiyota, T. [2016]: *On the influence of initial static shear on large deformation behavior of very loose Toyoura sand in undrained cyclic torsional shear tests*, Proceedings of the 6th Japan-Korea Workshop.

17) Umar M., Kiyota T. and Chiaro G. [2018] *Effect of specimen size on behavior of dense sand in large strain torsional shear apparatus.* Bulletin of Earthquake Resistant Structure Research Center, Institute of Industrial Science, University of Tokyo, 51: in press.

CHAPTER 3

Characterization of undrained monotonic behavior under extremely large strain

CHAPTER 3: Characterization of undrained monotonic behavior under extremely large strain

LIST OF FIGURES

LIST OF TABLES

Table 3.1: List of undrained large strain monotonic test

CHAPTER 3: Characterization of undrained monotonic behavior under extremely large strain

3.1. Introduction

Ultimate Steady-state (USS) is defined as the state at which granular material continues to deform at constant stress and constant void ratio. Critical state soil mechanics is an effective way of modeling soil behavior. Granular material sheared reaches an ultimate state under a unique combination of effective stress and void ratio.

The term "steady-state" in connection with experimental studies on the undrained response of sand has often been used to refer to the same concept as the term 'critical state'. Recent studies showing two states are the same (Verdugo and Ishihara, 1996, Reimer and Seed, 1997).

Soil fabric formed under gravity has anisotropic in nature, such that the material response is stiffer in the vertical compression. A sand sample compressed in the direction perpendicular to the bedding plane, the behavior is more dilative. Samples that dilate, as they are sheared under undrained triaxial condition – tend to generate negative pore pressure. While the pore pressure is becoming increasingly negative the mean effective stress becomes increasingly positive and the strength increases. Consequently, the observed resistance at the steady-state becomes increasingly higher than what is expected from field experience.

Vaid et al. (1990) recognized the importance of shear mode in laboratory testing. However, most of the studies conducted using simple shear devices have mechanical limitation to measure strain level up to 20%, as well as the measurement of high negative excess pore water pressure during undrained monotonic shearing.

In a torsional shear test on hollow cylindrical specimens, one can achieve higher strain levels by increasing torsional shear displacements that is applied to the specimen through rotating the top cap. (Kiyota et al. 2008).

Contrary to triaxial, shear stress in a torsional shear is more representative of specimen response to the field during cyclic or monotonic shearing in the undrained condition under simple shear condition.

The goal of this chapter is to examine the key features of the undrained response of clean sand, focusing on the Residual state(Ultimate steady-state), undrained peak strength, phase transformation state, Quasi steady-state and the flow liquefaction state exceeding shear strain of 50% in single amplitude as well as measurement of large negative excess pore water pressure. For this purpose, this chapter reports a series of the undrained monotonic test result from a strain-controlled hollow cylindrical torsional shear apparatus, isotropically consolidated Toyoura sand as shown in Table 1.

Table 3.1: List of undrained large strain monotonic test

Test No.	Relative Density, Dr (%)	Void ratio, e	Mean effective stress (p_0'), (kPa)
1-1*	19.0	0.884	100
1-2*	28.5	0.857	100
1-3*	36.8	0.823	100
1-4**	47.9	0.766	100
1-5**	51.6	0.766	200
1-6**	60.3	0.739	100
1-7**	72.0	0.693	100

*Specimen dimension: 300x150x90mm, **Specimen dimension:200x100x60mm [Height, Outer dia, Inner dia]

3.2.   Definition of undrained strength

Under low confining pressure and low relative density, the steady-state may appear at two stages during undrained monotonic loading. The first is the shear strength at quasi-steady-state (QSS), after the peak shear stress (the onset of flow liquefaction, (Ishihara et. al. 1993)). It is associated with the temporary local minimum shear stress. QSS has significant importance for

engineers because it corresponds to the peak and minimum undrained shear strength of the sand at small strain level (< 1%). The second is an ultimate steady-state (USS) at the final stage of deformation after exceeding the peak strength. In the following section, undrained shear strength at QSS, undrained peak strength and residual strength at USS is investigated with the deceases in the void ratio.

3.3. Effective stress path during undrained monotonic loading

Figure 3.1 to Figure 3.4 corresponds to the effective stress path during undrained monotonic loading of loose to dense Toyoura sand isotropically consolidated at effective stress of 100kPa. As expected we can observe, Toyoura sand becomes less contractive (more dilative) with the decreasing void ratio from 0.884 to 0.693. When the void ratio of the sand is less than 0.788, (Figure 3.2 to Figure 3.4) the point of minimum mean effective stress appears where the dilatancy behavior changes from contractive to dilative. This point is named as phase transformation (PTL) by Ishihara et al. (1975). Whereas for the sample with void ratio 0.884 (Figure 3.1), PTL did not reach and sample behaved contractive, reaching a state of $p'=0$. It is noteworthy that the inclination of PTL, irrespective of the initial void state is uniquely defined at an angle of 30°.

Figure 3.2 to Figure 3.4 shows with a decrease in the void ratio, shear stress increased at quasi-steady-state (QSS). Whereas, the inclination of flow liquefaction line (FLL) is uniquely defined at 28° irrespective of initial void ratio, consistent with the PTL. This implies that the PTL and FLL are material dependent, unaffected by a state of initial density.

Stress-strain response Figure 3.5 to Figure 3. 8 from very loose to dense Toyoura sand during undrained monotonic torsional shear loading. It is evident from Figure 3.6 to Figure 3. 8, after exceeding PTL, it continued to dilate. This dilation behavior reached at the peak at state B marked in Figure 3.6 to Figure 3. 8. As the material becomes denser, the change from strain

hardening behavior reaching an ultimate peak lead to a strain-softening behavior reaching a residual state. This residual state is defined as the ultimate steady-state in the current study (deformation of the specimen under a constant state of stress). The shear stress along this state is referred to as residual undrained shear stress.

The peak undrained shear stress increased from 200kPa to 298kPa with a decrease in the void ratio from 0.766 to 0.693. Extremely loose specimen (Figure 3.5) did not reach the peak undrained strength (state B) after exceeding the peak shear stress at undrained instability state(UIS), consequently the development of large shear strain. The shear strain continues to develop and gradually recovered after a shear strain of 60% (Figure 3a, top right mini window). The inclination of the critical state line on the effective stress path (Figure 3.1 to Figure 3.4) increased with a decreased in the void ratio, representing an increased in the friction angle from 32° to 34°.

It is noteworthy the specimen that did not exhibit a phase transformation, tend to develop large deformation after exceeding the small amplitude of shear stress. Whereas for medium dense to dense sand, a large shear strain was developed after exceeding the peak undrained shear stress. Therefore, it can be concluded that the loose, as well as dense sand, are prone to large deformation depending on the density state as well as the amplitude of shear stress.
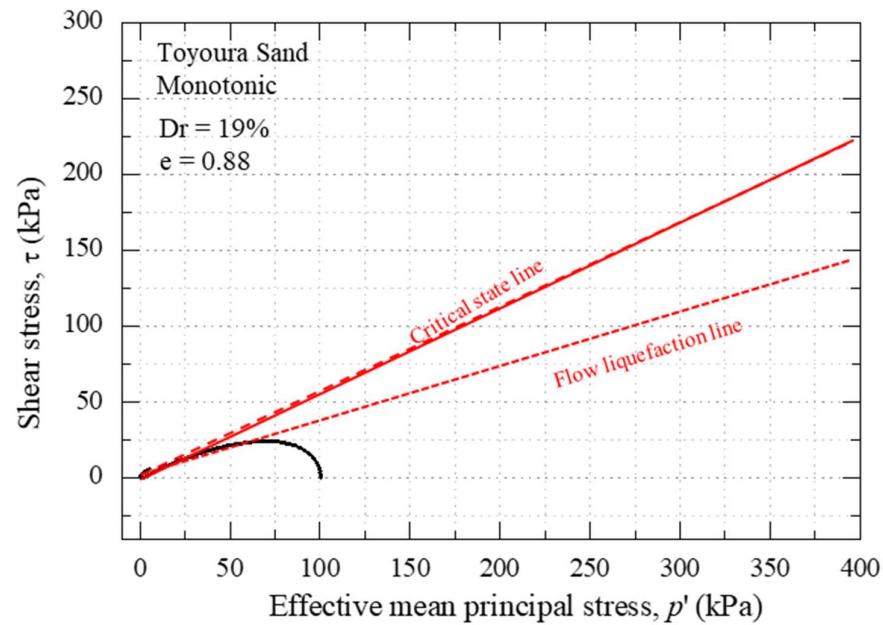
Figure 3.1: Effective stress path during undrained monotonic loading(Dr = 19.0%)
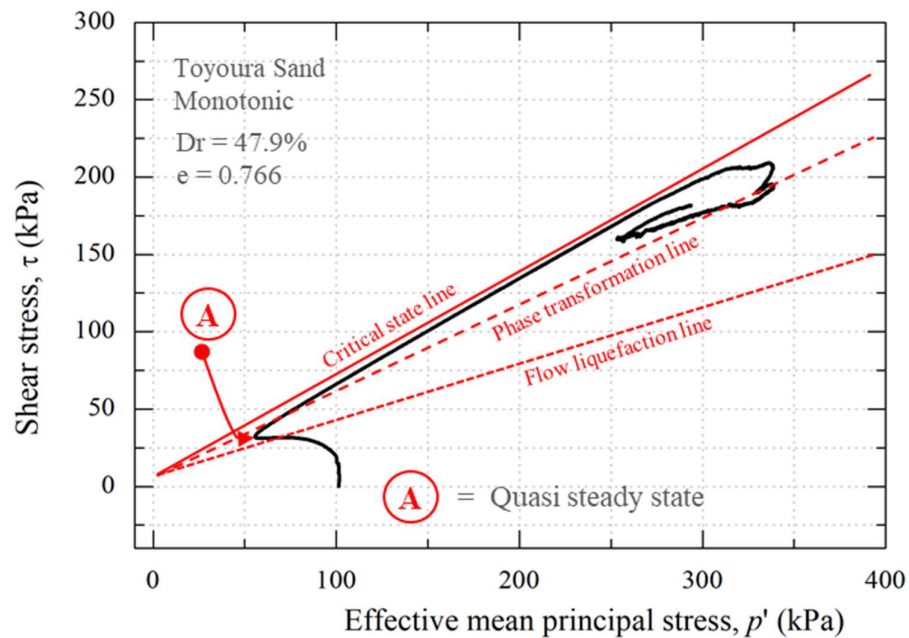
Figure 3.2: Effective stress path during undrained monotonic loading (Dr 47.9%)
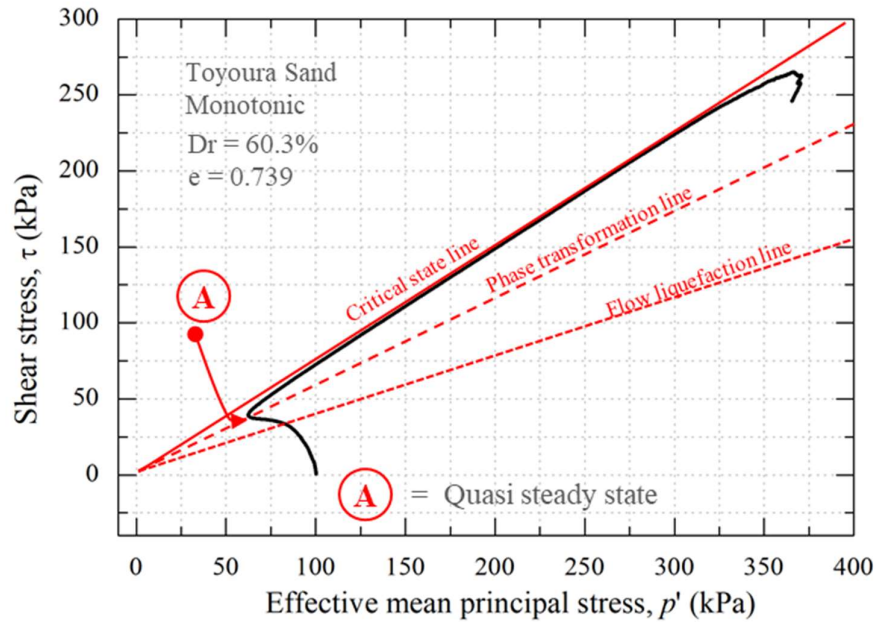
Figure 3.3: Effective stress path during undrained monotonic loading (Dr = 60.3%)
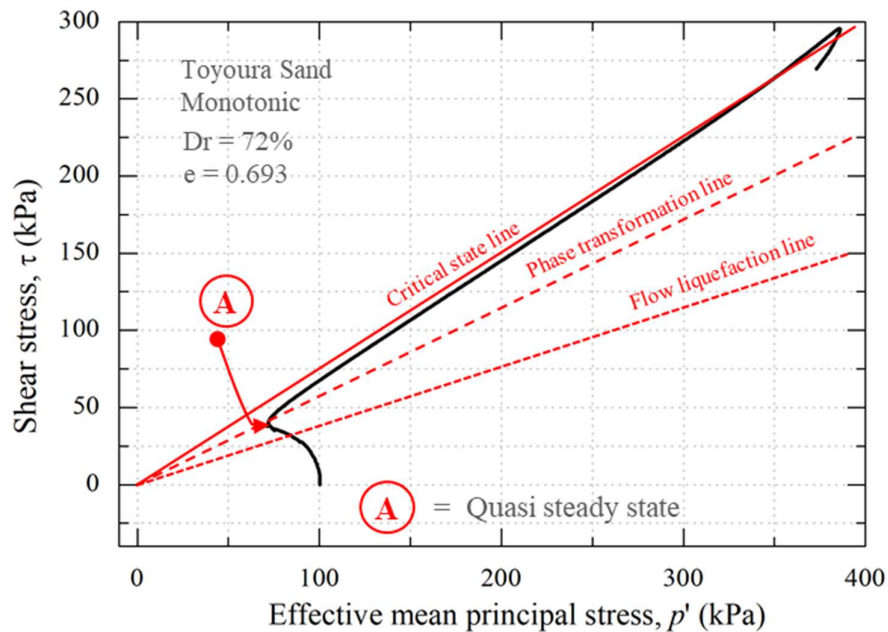
Figure 3.4: Effective stress path during undrained monotonic loading (Dr = 72%)
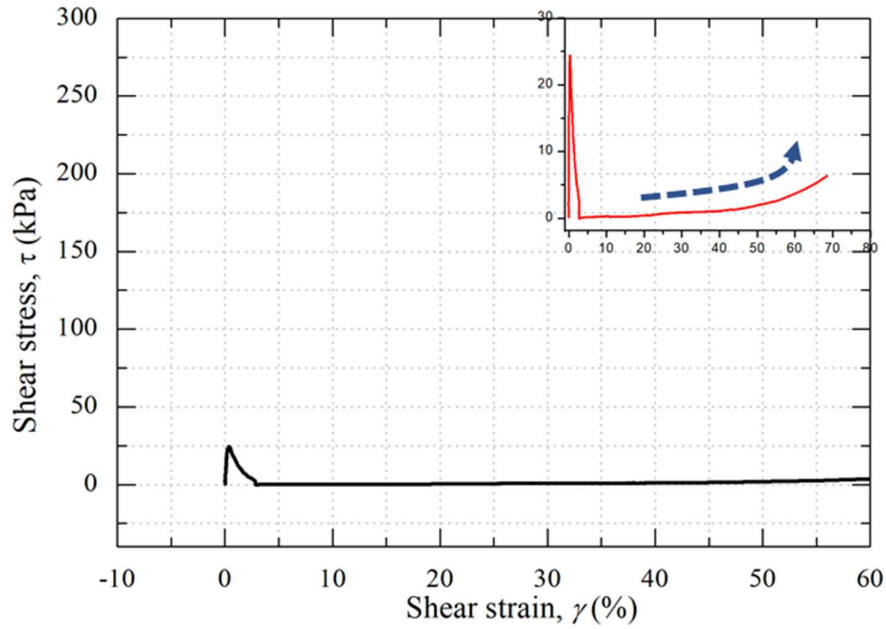
Figure 3.5: Stress-strain relationship during undrained monotonic loading (Dr = 19.0%)
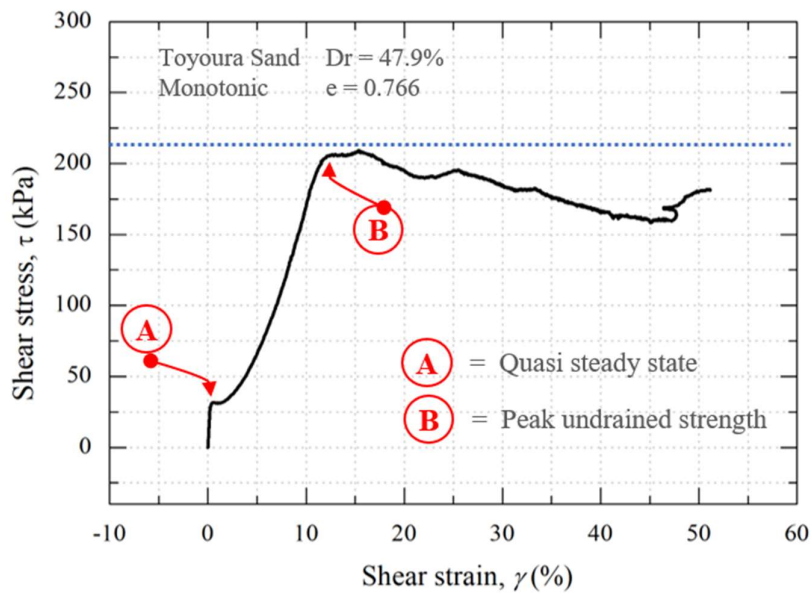
Figure 3.6: Stress-strain relationship during undrained monotonic loading (Dr 47.9%)
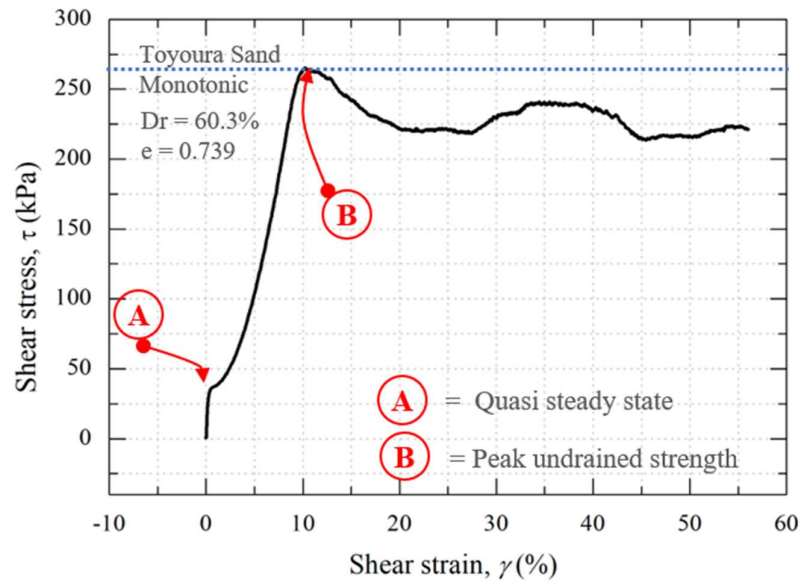
Figure 3. 7: Stress-strain relationship during undrained monotonic loading (Dr = 60.3%)
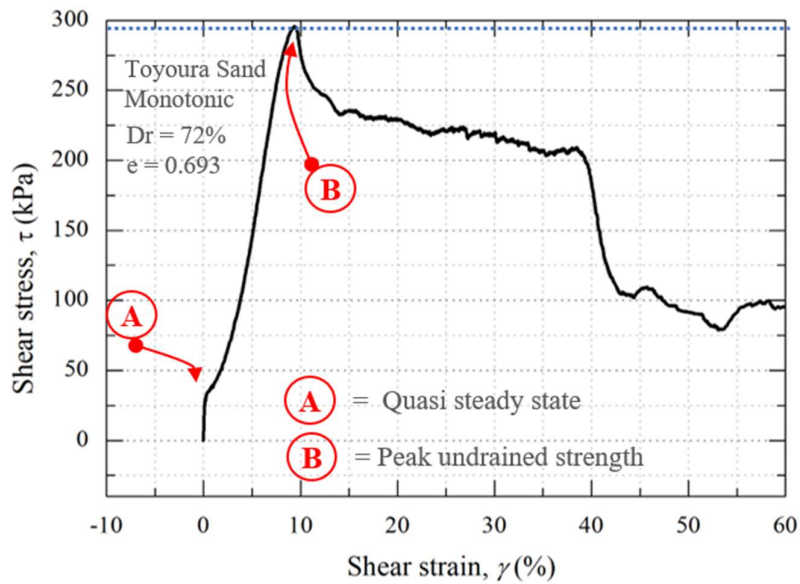
Figure 3. 8: Stress-strain relationship during undrained monotonic loading (Dr = 72%)

3.4. Influence of relative density on excess pore water generation

With the increase in the cyclic loading result in the generation of excess pore water pressure. During monotonic undrained loading, after exceeding the phase transformation phase, sandy soil tends to generate changes from negative to positive. As loading is increased further, this positive excess pore water, tend to increase more. During the triaxial loading as investigated by the past researcher, they is no termination of excess pore water pressure, due to the pressure of back pressure as well as the mode of the loading in the compression loading. As the compression loading is increased, the greater the negative pore water is developed. This behavior ends up result in the "boiling" in the triaxial specimen in compression.

However, in torsional shear loading, the shear stress is applied directly on the bedding plane by torque on top of the specimen. This torsional loading also results in the generation of excess pore water pressure after the specimen behavior change from contractive to dilative. From Figure 3.9 to Figure 3.12 shows a typical test result in term of a generation of excess pore water pressure during undrained torsional shear loading with the increase in relative density from 19% to 72%.

For extremely loose specimen (Figure 3.9), the soil tends to develop positive excess pore water pressure during the process of undrained loading. Whereas the specimen partially contractive and partially dilative (Figure 3.10 to Figure 3.12) during the generation of negative excess pore water reached an ultimate state followed by linear increase with the increase in the shear strain. This reaffirms that the positive excess pore water pressure contributes to high undrained shear stress during monotonic loading. However, it will ultimately reach a peak point, whereas the generation of negative excess pore water pressure becomes linear.
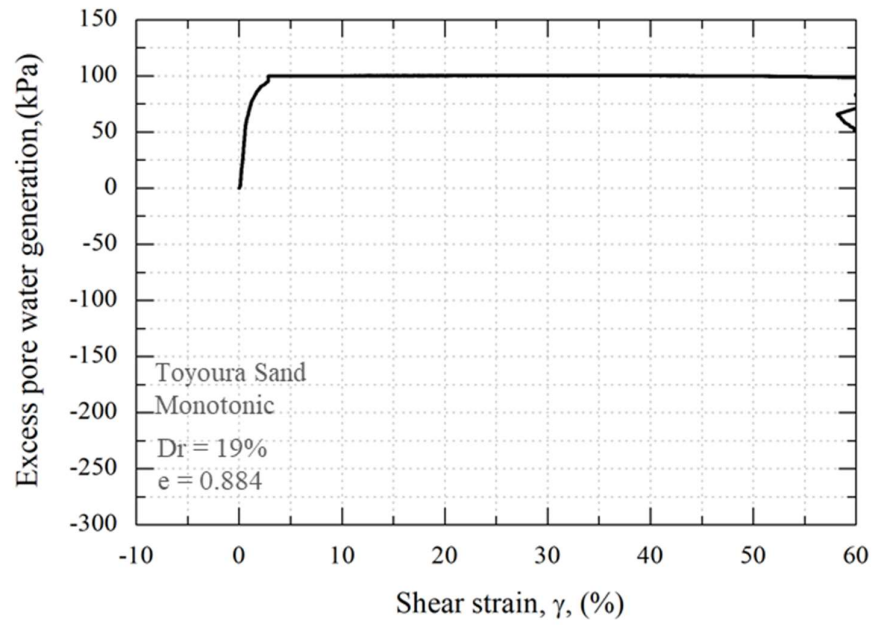
Figure 3.9: Excess pore water generation during undrained monotonic loading
(Dr = 19.0%)
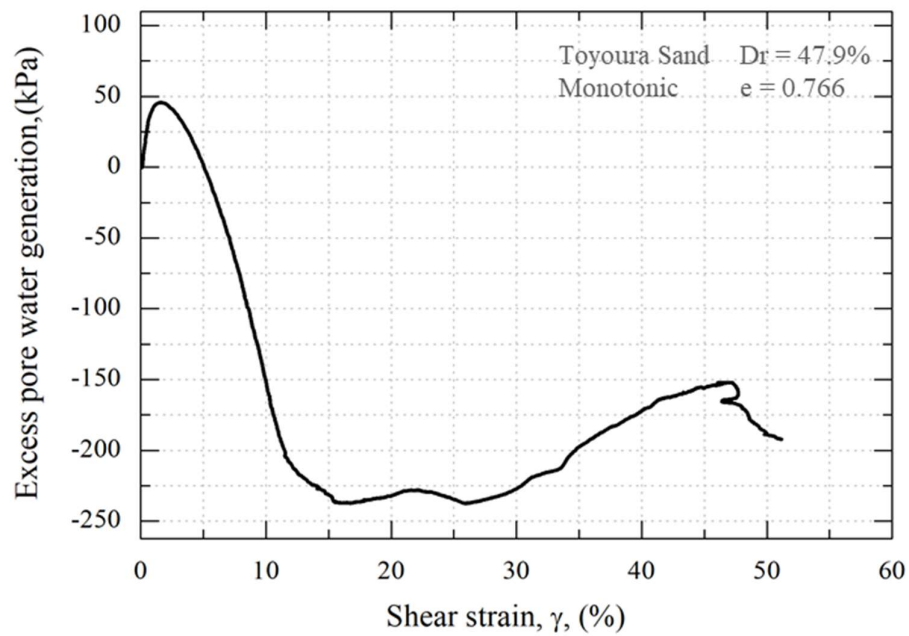
Figure 3.10: Excess pore water generation during undrained monotonic loading **(Dr 47.9%)**
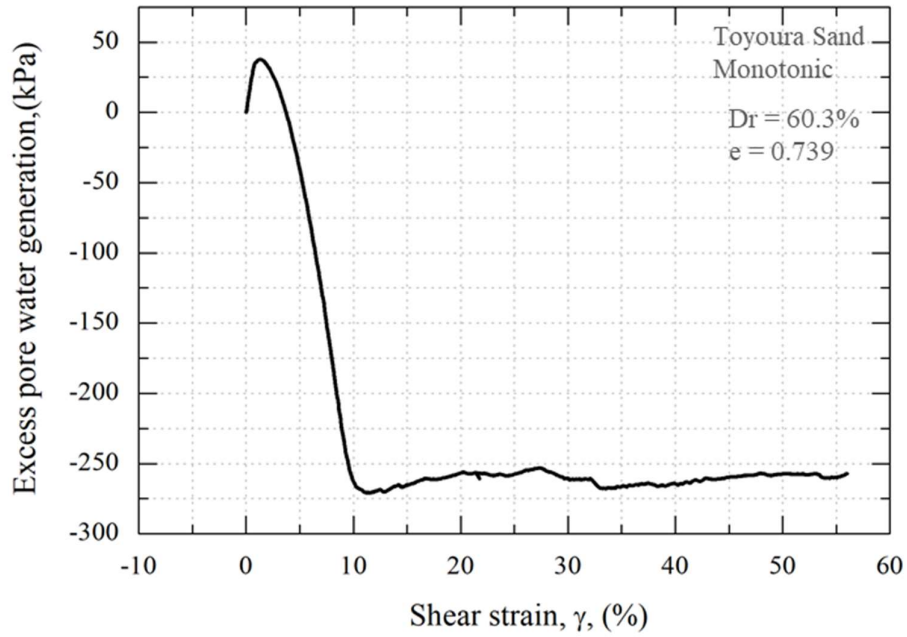
Figure 3.11: Excess pore water generation during undrained monotonic loading (Dr = 60.3%)
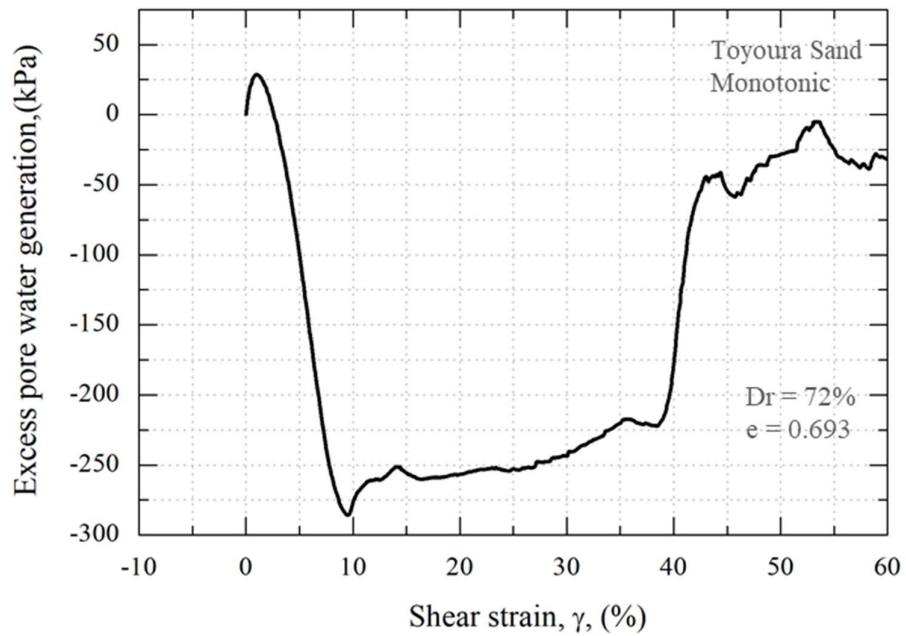
Figure 3.12: Excess pore water generation during undrained monotonic loading (Dr = 72%)

3.5. Cavitation in dense sands and influence of back pressure

In dense sand possibility of caviation of pore fluid induced by dilation has a significant important to the undrained strength of the soils. As a result of cavitation, the loading will change from undrained to drained. Lee (1965) observed cavitation by conduction a series of undrained triaxial tests on denser samples. He noted that as the confining pressure becomes higher cavitatin did not occur, there being less potential to dilate as the confining pressure is increased. Figure 3.13 shows a comparison of series of undrained triaxial test performed by Macmanus et al. (1997) on dense sand by varying the back pressure from 150kPa to 500kPa, while keeping a mean effective stress of 50kPa. It can be observed from Figure 3.13b, the pore pressure begins at the imposed back pressure that the with the increase in the back pressure, and then continue to decrease until the cavitation occur at the pressure of -95kPa and at a strain level of 0.0185, 0.0222 and 0.0273 respectively.

Mokni and Desrues (1998) conducted biaxial test on Houston sand to investigate the relation between strain localizaito and caviation during undrained shearing. They concluded that in all the tests the pore pressure move toward the same final value of -85kPa, consistant with the fining of Macmanus et al. (1997). In additions they concluded that the strain localization coincides with the occurrence of cavitation in the specimen.

However in this study by using the torsional shear apparatus, from Figure 3.11 and 3.12, during undrained monotonic loading, the results showed contracdictory behavior as by previous researchers. In these test higher the relative the generation of negative excess pore water pressure. Cavitation pressure was unoabserved in the above test. In order to further investigate caviation, another test were performed under the similar testing condition as Figure 3.12, however under a higher back pressure of i-e 300kPa.
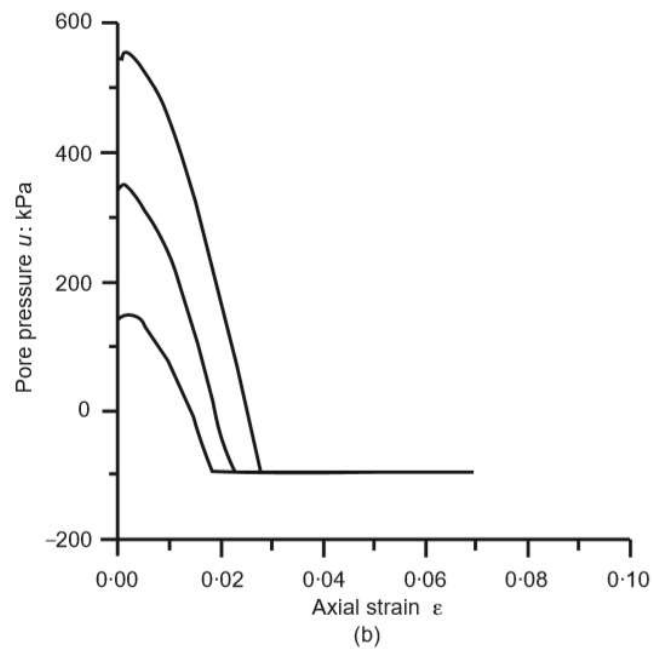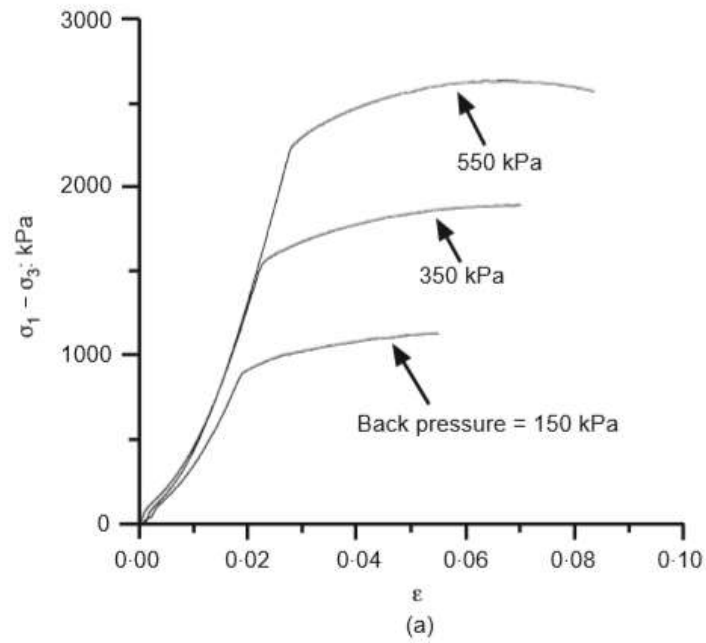
Figure 3.13: (a) Undrained stress±strain response, (b) undrained pore pressure response
(after Macmanus et al. (1997)

Figure 3.15 shows the stress-strain relationship of two test under the initial mean effective stress of 100 kPa with a back pressure of 200kPa and 300kPa respectively. Both the specimen shows similar behavior during small strain, reaching a quasi steady state (QSS). The specimen showed higher ultimate peak resistance subjected to 300kPa backpressure.

The pore water generation shown in Figure 3.16, shows consistant behavior irrespective of high initial back pressure. The specimen subjecte of 300kPa back pressure shows slightly high negative pore water generation i-e -95kPa, which can be attributed to the higher shear strength during stress strain response.
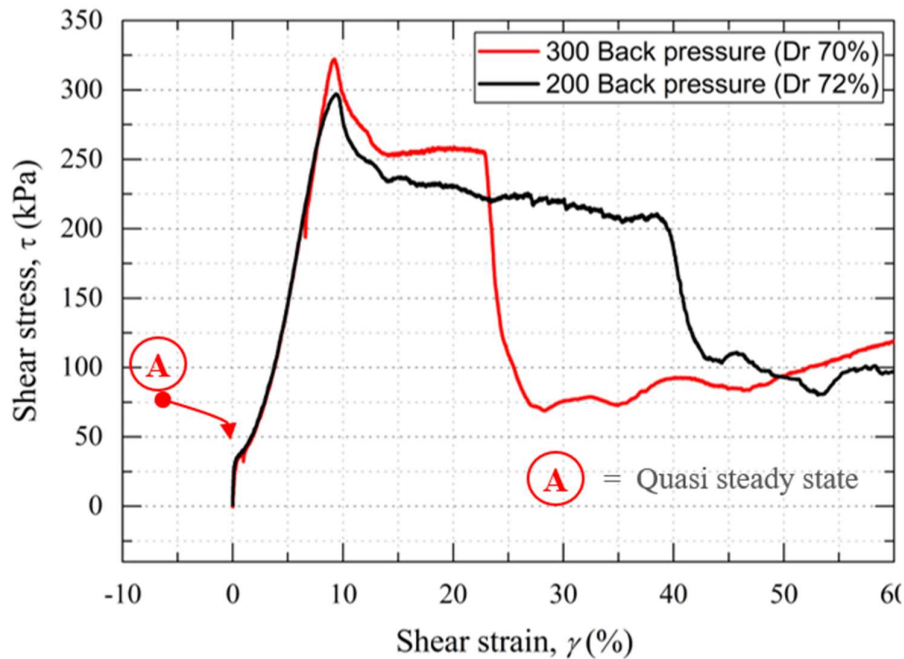
Figure 3.14: Undrained stress±strain response of Toyoura sand with different back pressure

Macmanus et al.(1997) shown that after initiation of cavitation, the specimen mean effective stress path chaned to drained from undraind as shown in Figure 3.16. However, the effective stress path shown in Figure 3.17 shows a contracdictory as observed by Macmanus et al.(1997).
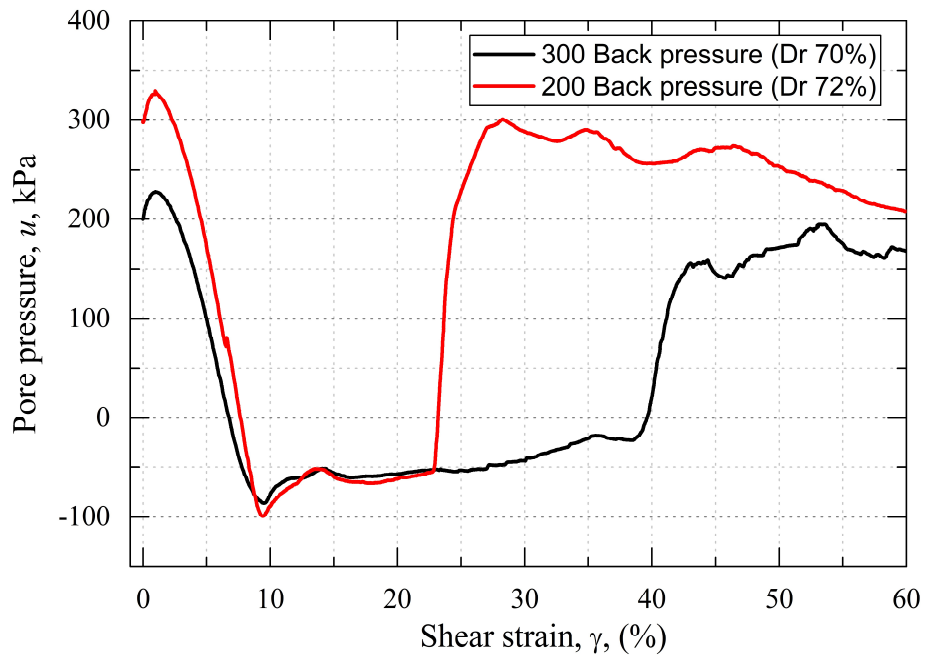
Figure 3.15: Variation of pore pressure with different back pressure for dense specimen
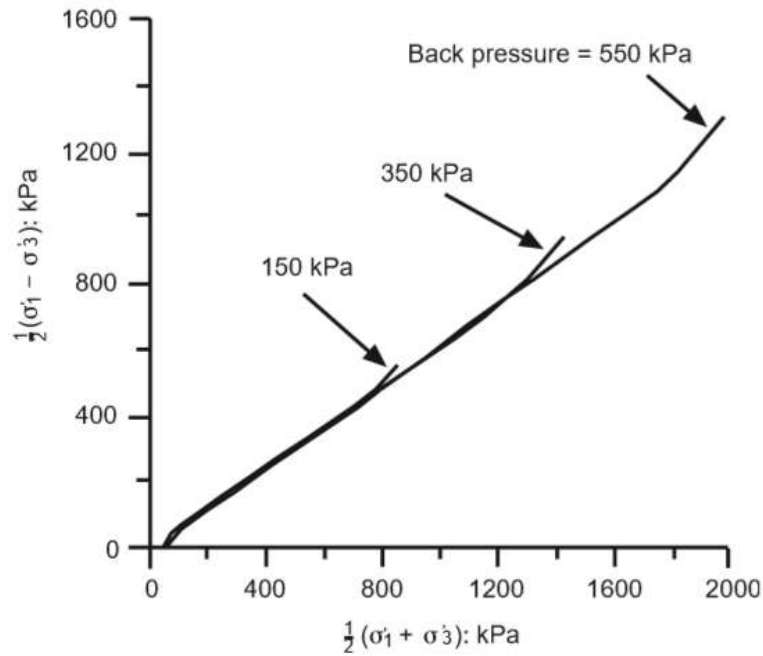
Figure 3.16: Variation of pore pressure with different back pressure

In Figure 3.17, it is evident that the stress path after reaching a peak state moved toward the residual state, as clearly evident from the stress strain path (Figure 3.14).. This contractrion can be associated with the mode of shear experience by the specimen. The boundary effect is more pre-dominant in triaxial undraeind testing during compression loading as compared to torsional simple shear. Furthermore, the back pressure did not influence the phase transformation state of the specimen
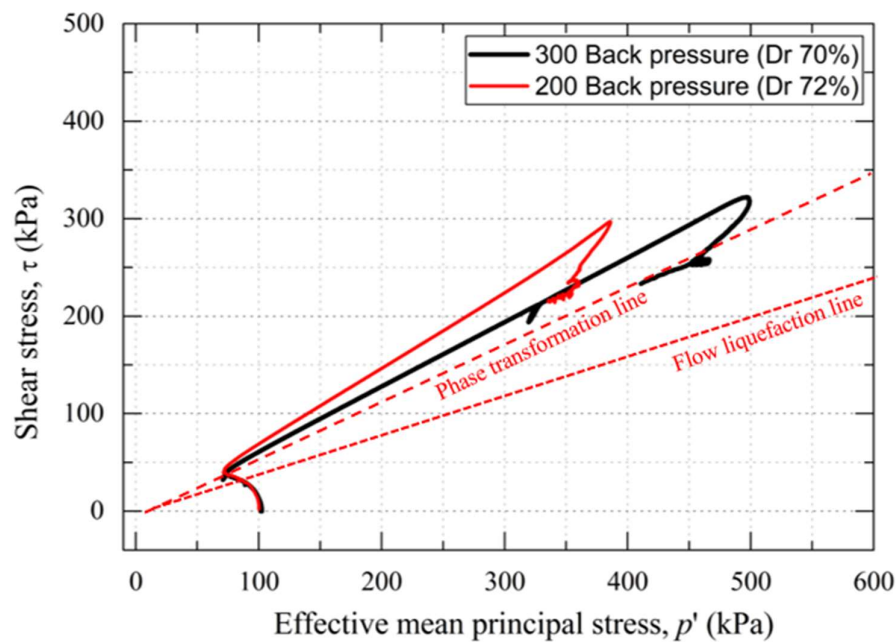
Figure 3.17: Effective stress path with different back pressure

3.6.   Influence of relative density on stress ratio

To have a more precise interpretation of a Quasi-steady state (QSS) and ultimate steady-state (USS), Figure 3.18 to Figure 3.21 report test results in terms of stress ratio and shear strain from loose to dense Toyoura sand. Consistent with the increased in the shear stress with the decrease in a void ratio (Figure 3.6 to Figure 3. 8), the stress ratio initially increased to a peak value and with a further increase in shear strain, it reached a residual stress ratio (Figure 3.19 to Figure 3.21). For the dense specimen with the void ratio of 0.693, peak stress ratio of 0.74

was observed. Whereas for every loose specimen exceeding peak stress ratio, the collapse was observed, which is associated with flow failure during liquefaction. Therefore, a stress ratio of 0.54 provides a threshold. Exceeding this threshold value stress ratio, the specimen will show initially a stain hardening followed by strain-softening leading to residual state. Whereas, below this threshold value the specimen will show a strain hardening accompanied by a loss in shear strength.

Specimen deformation at several states (numbered as to 1 through 4) is shown in Photo 1 to 3 for a void ratio of 0.884, 0.766 and 0.693 respectively. State 1 corresponds to the initial state ($\gamma_{SA} = 0\%$) – a vertical reference line marked in red color.

Dense specimen (Photo 2 and 3) from state 2 ($\gamma_{SA} = 5\%$) to 3 ($\gamma_{SA} = 10\%$), the deformation was uniform throughout the height of the specimen. The shear band(s) appeared between state 3 ($\gamma_{SA} = 10\%$) and 4 ($\gamma_{SA} = 20\%$). At state 5 ($\gamma_{SA} = 30\%$), the region near the top cap experienced larger deformation than that near pedestal indicating a non-uniform deformation distribution along with the height of the specimen. Whereas loose specimen (Photo 1), after exceeding a shear strain of 2% (state 2), the region near the pedestal collapsed (Figure 3.5). This collapse is associated with the loss of shear stress in the specimen, and consequently the development of extremely large strain.
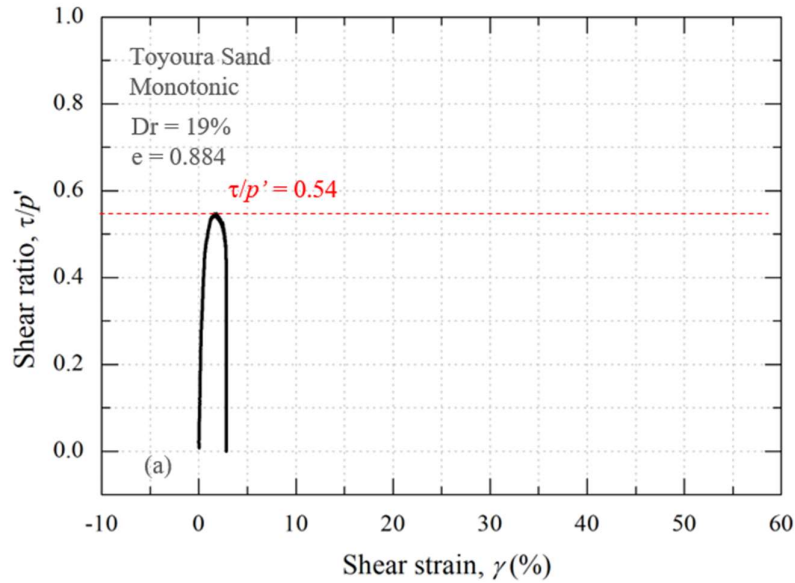
Figure 3.18: Relationship between stress ratio vs shear strain during undrained monotonic loading (Dr = 19.0%)
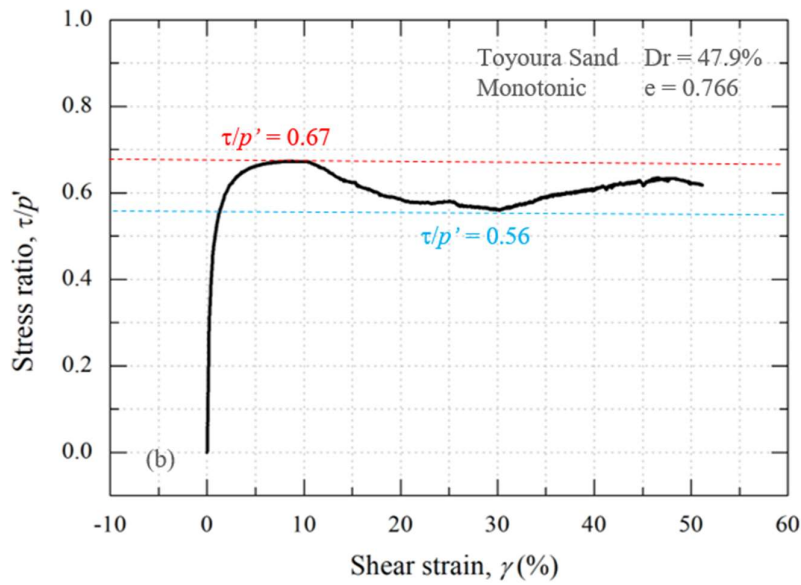
Figure 3.19: Relationship between stress ratio vs shear strain during undrained monotonic loading (Dr = 47.9%)
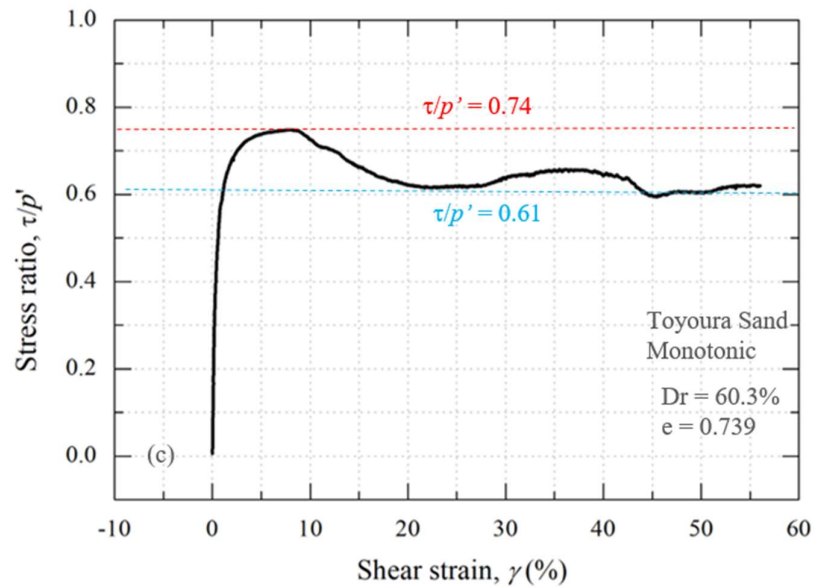
Figure 3.20: Relationship between stress ratio vs shear strain during undrained monotonic loading (Dr = 60.3%)
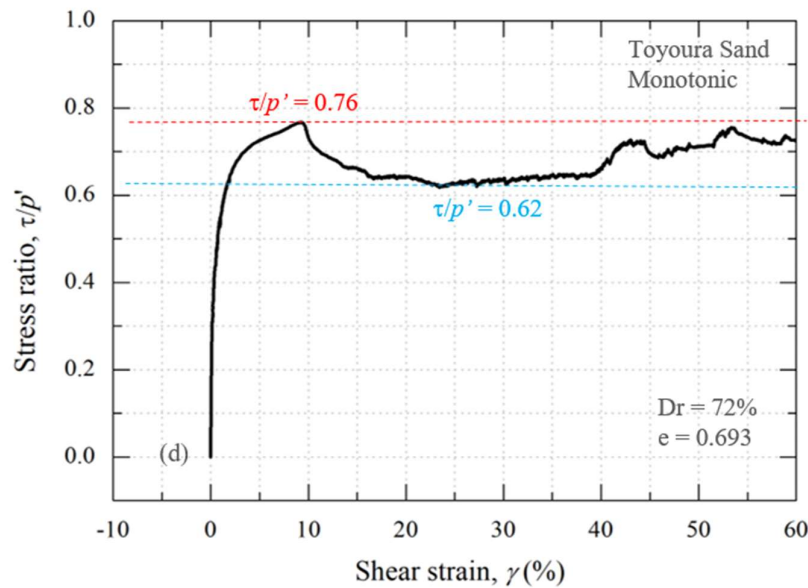
Figure 3.21: Relationship between stress ratio vs shear strain during undrained monotonic loading (Dr = 72%)
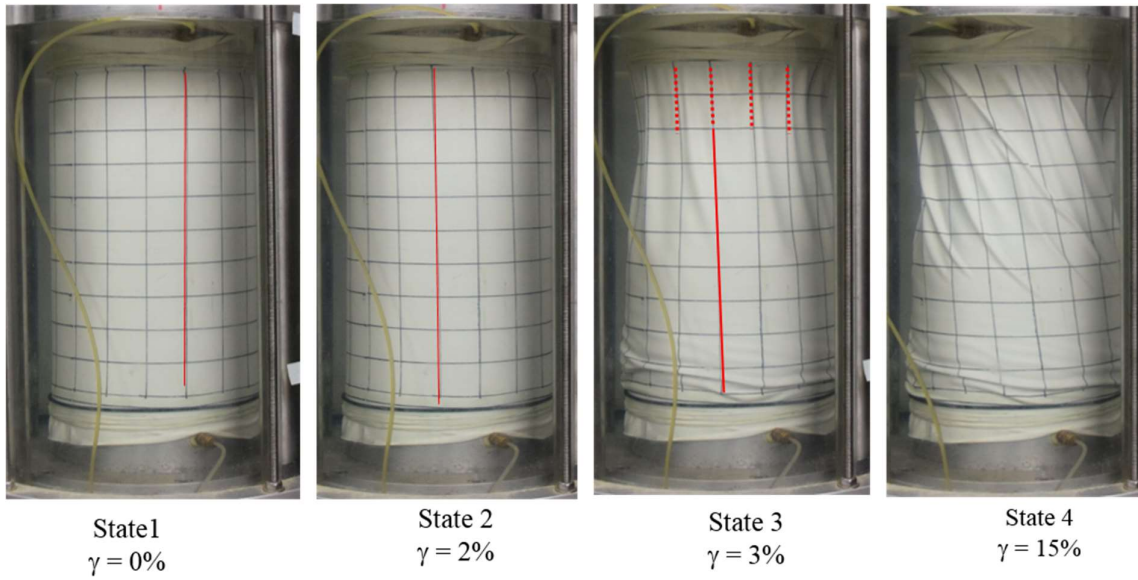
Photo 1: Specimen deformation at various stages for Test 1-1, (Dr=19.0%)
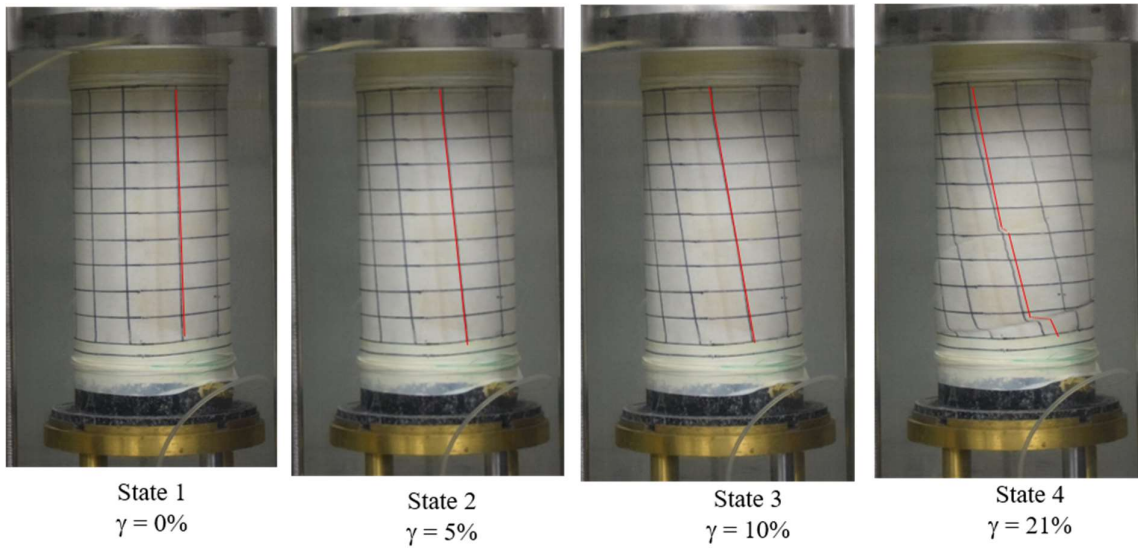
Photo 2: Specimen deformation at various stages for Test 1-4 (Dr=47.9%)

| State A | State B | State C | State D |
| $\gamma = 0\%$ | $\gamma = 5\%$ | $\gamma = 10\%$ | $\gamma = 21\%$ |
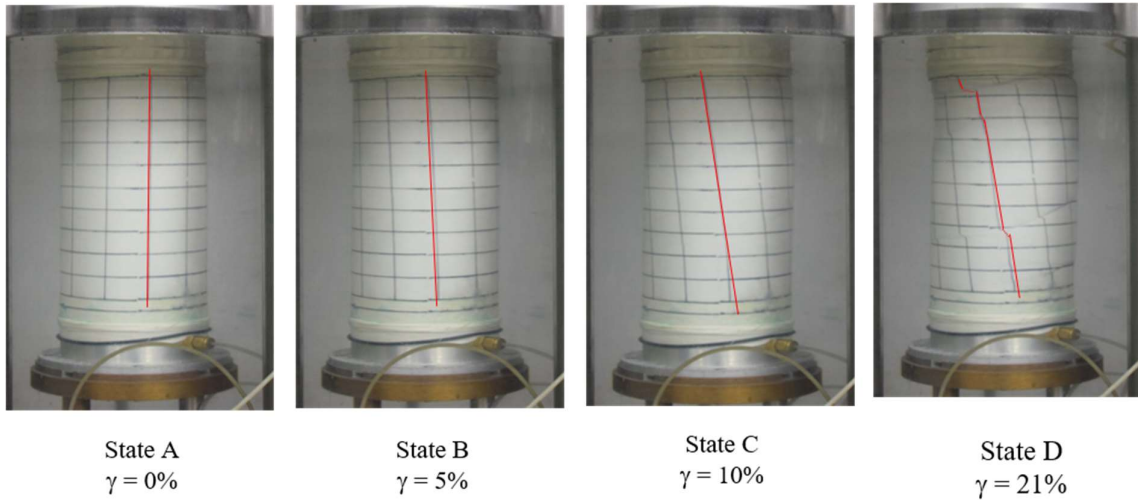
Photo 3: Specimen deformation at various stages for Test 1-7 (Dr=72%)

3.7. Variation of undrained shear strength during monotonic loading along Quasi steady-state, peak state and residual state (Ultimate steady state)

The undrained shear strength at QSS is taken by plotting at a vertical tangent at PTL. Whereas the shear strength at the ultimate peak is taken at the beginning of non-uniformity in the specimen (Kiyota et al. 2008). Whereas residual strength is taken at along the residual state (ultimate steady-state, USS). Figure 3.22 shows the correlation of undrained shear strength at QSS and with the increase in the void ratio. It can be observed that, at the void ratio of 0.857, the shear strength at QSS and USS are 5kpa and 32kPa respectively. Whereas, as the void ratio decreases, the difference between shear stress at QSS and USS becomes significant i-e at the void ratio of 0.693, shear strength is 40kPa and 297kPa at QSS and TSS respectively. This implies that denser specimen exhibits higher shear strength at QSS and USS with the decrease in the void ratio.
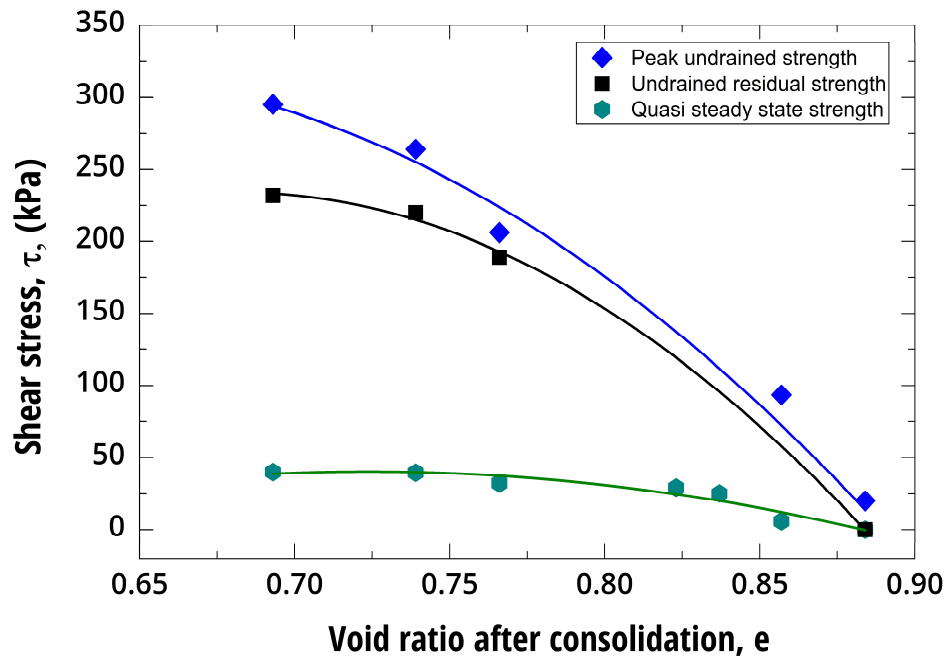
Figure 3.22: Void ratio and undrained shear stress at peak undrained strength, residual strength, and quasi-steady state strength

3.8.   References

1) Ampadu, S.I.K. [1991]: *Undrained behavior of kaolin in torsional simple shear*, Ph.D. Thesis, Department of Civil Engineering, University of Tokyo, Japan.

2) Chiaro, G., Kiyota, T. and Miyamoto, H. [2017]: *Liquefaction potential and large deformation properties of Christchurch liquefied sand subjected to undrained cyclic torsional simple shear loading*, Proceeding of the 19th International Conference on Soil Mechanics and Geotechnical Eng., Seoul, South Korea, 1497-1500.

3) De Silva, L.I.N., Koseki, J. and Sato, T. [2006]: *Effects of different pluviation techniques on deformation property of hollow cylinder sand specimens*, Proceedings of the International Symposium on Geomechanics and Geotechnics of Particulate Media, Ube, Yamaguchi, Japan, 29-33.

4) Ishihara. K., Tatsuoka, E. and Yasuda, S. [1975]: *Undrained deformation and liquefaction of sand under cyclic stresses*, Soils and Found.,15(1), 29-44.

5) Ishihara, K. [1993]: *Liquefaction and flow failure during earthquakes*, Geotechnique, 43(3), 351-415.

6) Kiyota, T., Sato, T., Koseki, J. and Mohammad, A. [2008]: *Behavior of liquefied sands under extremely large strain levels in cyclic torsional shear tests*, Soils and Foundations 48(5): 727-739.

7) Lee, K. L. [1965]: *Triaxial compressive strength of saturated sand under seismic loading conditions,* University of California, Berkeley, PhD thesis.

8) Reimer, M. F. and Seed, R. B. [1997]: *Factors affecting apparent position of steady-state line*, J. Geotech. Geoenviron. Engrg., ASCE, 123(3), 281-288.

9) Umar, M., Kiyota, T., Chiaro,   G., Duttine, A.,[2019]: *Undrained Monotonic Behavior Of Sand In Large Strain Torsional Shear Apparatus*, ERS bulletin, Institute of industrial science, University of Tokyo, 2019.

10) Vaid, Y.P., Chung, E.K.F., and Kuerbis, R. [1990]: *Stress path and steady state*. Canadian GeotechnicalJournal, 27: 1–7.

11) Verdugo, R. and Ishihara, K. [1996]: *The steady state of sandy soils*, Soils and Foundations, 36(2), 8192.

CHAPTER 4
Influence of damage strain on undrained static shear strength

CHAPTER 4: Influence of damage strain on undrained static shear strength

LIST OF FIGURES

LIST OF TABLES

CHAPTER 4: Influence of damage strain on undrained static strength

4.1   Introduction

The contact forces between the grains of soil contribute to stiffness and strength of granular materials. However, repeated cyclic shearing results in the degradation of these contact forces resulting in the deterioration. Numerous efforts have been made to investigate and quantify the post cyclic degradation of granular materials -i-e clays, silt, and sand (Castro et al. (1989) Kuebis (1988), Marcuson et al. (1990), Seed et al. (1989), Vaid (1994), Yoshida et al. (1995), Shamoto et al. (1997), Kokusho (2004) and Dash (2016).

Particularly for clean sands to investigate the post cyclic undrained static strength, the specimens were subjected to repeated constant amplitude cyclic loading, upon reaching a specific value of the double amplitude of strains (hereby refer as damage strain), the loading mode was changed to monotonic until the end of the test. Vaid (1994), Dash (2016) and Mehdi (2017) concluded the strength and stiffness are comparable among the monotonic test(non-liquefied) with the specimen with the cyclic strain history.

It is a challenging task to simulate large deformation of liquefied soils in laboratory element tests. In triaxial tests, for example, the axial strain levels employed are usually limited to 20% or less due to a larger extent of non-uniform deformation of the specimen at higher strain levels. Back pressure is employed in a triaxial test to improve saturation. Samples that tend to dilate, as they are sheared under undrained condition – tend to generate negative pore pressure. While the pore pressure is becoming increasingly negative, the mean effective stress becomes increasingly positive, and the strength increases. Consequently, the stress-strain curve becomes linear and no termination of post liquefaction ultimate strength was unobserved (Vaid et al. 1995, Shamoto et al. 1997, Dash (2016), Lombardi et al. 2016).

In contrast, in torsional shear test on hollow cylindrical specimen, one can achieve higher strain levels by increasing the number of torsional shear displacements that is applied to the specimen through rotating the top cap (i-shear strain exceeding 100%, Kiyota et al. 2008). Contrary to triaxial, shear stress is directly applied to the specimen on the horizontal bedding plane and evaluated by applied torque and specimen dimensions.

Therefore, to simulate the simple shear in addition to large post liquefaction strain, this chapter provides new insight into the post liquefaction undrained static strength degradation and deformation characteristic using the modified torsional simple shear for different densities, initial static shear, cyclic stress ratios, and reconsolidation histories.

4.1.1   Test procedure for level ground

Higher degree of saturation (i.e., Skempton's B-value > 0.95) was achieved by the double vacuum method (Ampadu, 1991) while circulating de-aired water into the specimen. The specimens were isotropically consolidated by increasing the effective stress state up to a $p' = 100$ kPa, with a back pressure of 200 kPa till state A as shown in Figure 4. **1**.

Following that, undrained constant-amplitude cyclic torsional shear stress ($\tau_{cyclic} = 20$ kPa) was applied at a shear strain rate of 0.5%/min from state P1 to state P2 (Figure 4. **1**). The loading direction was reversed when the amplitude of τ_{cyclic} (membrane force corrected following Chiaro et al. 2017b).

Cyclic loading was terminated at the target value (Table 4.1) of cyclic damage strain (γ_Δ) at state P2 (Figure 4. **1**)). Afterward, while keeping undrained conditions, monotonic shear loading was applied until a single amplitude shear strain (γ_{SA}) exceeding 50% was achieved, from state P2 to P3 (Figure 4. **1**). During the process of undrained torsional loading, the vertical

displacement of the top cap was prevented to replicate as much as possible the simple shear

condition. A summary of the tests performed is provided in Table 4.1.
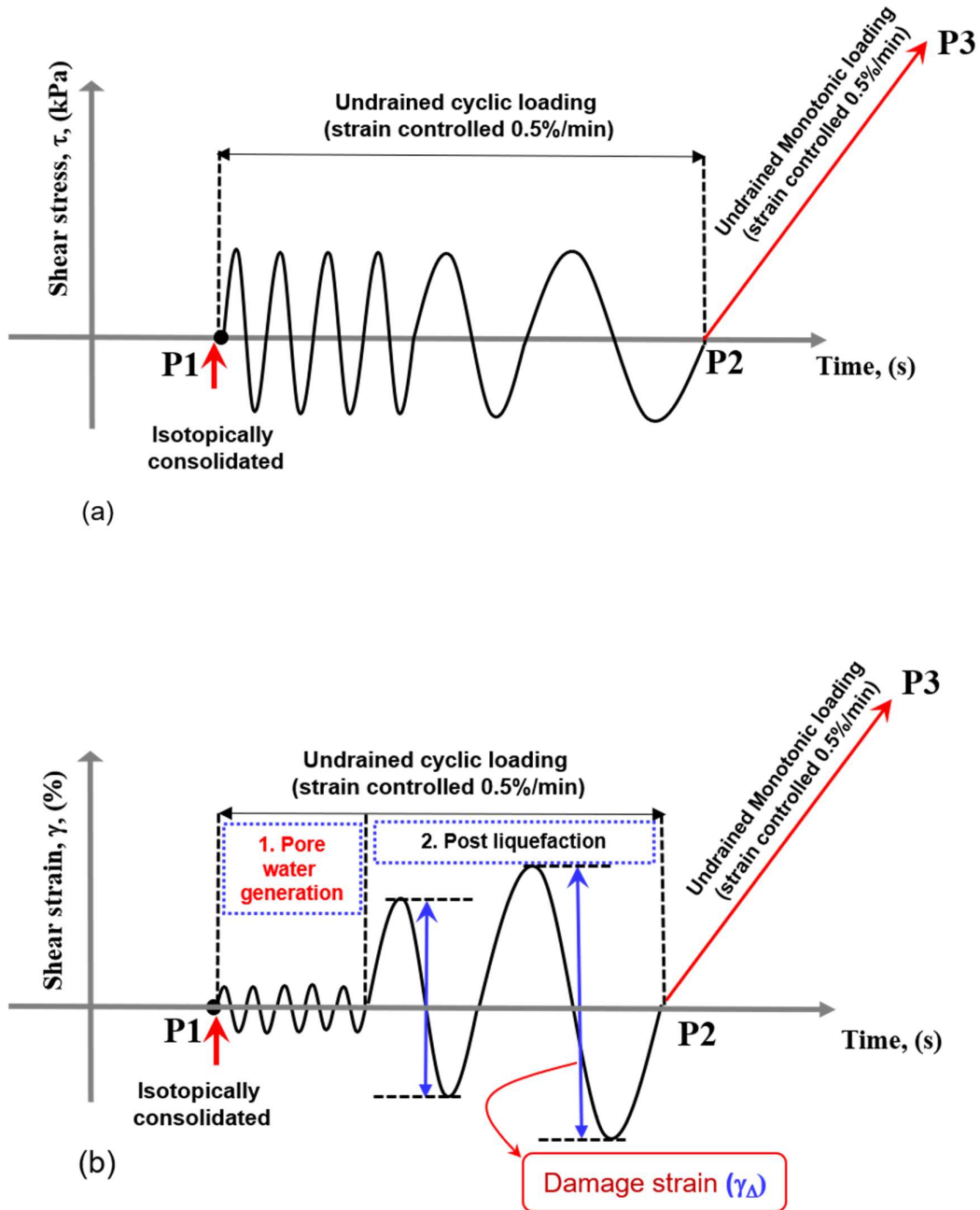
Figure 4. 1: Test procedure and illustration from state P1 to state P3 without static shear

Table 4.1: Summary of test performed for level ground

Test No.	Relative Density, Dr (%)	Void ratio, e	Cyclic damage strain, γ_Δ, (%)	Mean effective stress (p') (kPa)	Cyclic shear stress (kPa)
3-1	47.9	0.768	1	100	20
3-2	48.3	0.772	6	100	20
3-3	52.2	0.771	13	100	20
3-4	50.8	0.772	24	100	20
3-5	49.0	0.785	26	100	20
3-6	48.4	0.784	92	100	20
4-1	68.7	0.711	3	100	20
4-2	72.1	0.700	7	100	20
4-3	67.9	0.714	12	100	20
4-4	70.1	0.704	19	100	30

4.2   Effect of damage strain on strength characteristics

4.2.1 Effect of damage strain on post liquefaction undrained static shear strength without static shear on medium dense (Dr 48$\pm$3)

Only a limited amount of studies has focused on the post-liquefaction behavior of liquefied soil, due mainly to the mechanical limitation of the element test to simulate extremely large deformation. Studies conducted by Yoshida et al. (1994), Vaid et al. (1995) and Kokusho et al. (2004) concluded that the post-liquefaction behavior of sand subjected to undrained monotonic loading is dilative, even if the sand showed contractive and strain-softening behavior before liquefaction. Dash (2010) compared the undrained monotonic behavior of liquefied and non-liquefied samples at the same initial density. Dash (2010) showed that liquefied sample with axial strain exceeding 5%, subsequently sheared monotonically without dissipating the excess pore water pressure exhibited comparable stiffness with the non-liquefied sample.

In this section, post-liquefaction undrained monotonic behavior of Toyoura sand is presented in terms of stress-strain for cyclic damage strain levels listed in Table 4.1. Typical test results in term of stress-strain relationship of the medium dense sand (Dr 48$\pm$3) with a damage strain i-e γ_Δ = 1%, 6%,13%, 24%,26%, and 92%, is shown in Figure 4.2 to Figure 4.4 respectively.

Excess pore water generated as a resulte of of constant amplitude cyclic stress. Soil strength recovered as a result of cyclic mobility and develops shear strain during constant amplitude cyclic loading. In Figure 4.2, with a damage strain 1%, during undrained monotonic loading the specimen recover its stiffness during loading and ultimately reaching a peak shear stress of 156kpa. Following that peak state, the specimen develops large shear strain exceeding 40% under the constant shear stress. Consistant with the undrained monotonic loading (Chapter 3), the peak state is defined at the ultimate peak state in post liquefaction undrained monotonic loading.

From Figure 4.2 to Figure 4.4, with the increase in the damage strain, the specimen achieved an ultimate peak shear stress of 150kpa, 122kPa, 80kPa, 70kPa, respectively. This shows a significant deterioration in the ultimate peak shear stress with the increase in the damage strain from 6% to 26%.

Figure 4.4c shows a test with a damage strain of 92%, and the ultimate peak strength observed was 15kPa. From this result, it is evident that under substantial deformation, soil possesses shear resistance by mobilization of dilatancy. However, during this test, significant non-uniform deformation was observed in the specimen.

In summary, from these test result, it is evident that the post liquefaction undrained static strength degraded with the increase in the damage strain. From a practical point of view, during the earthquake loading, each cyclic induces a damage strain which consequently results in the degradation of from initial peak undrained measured strength.
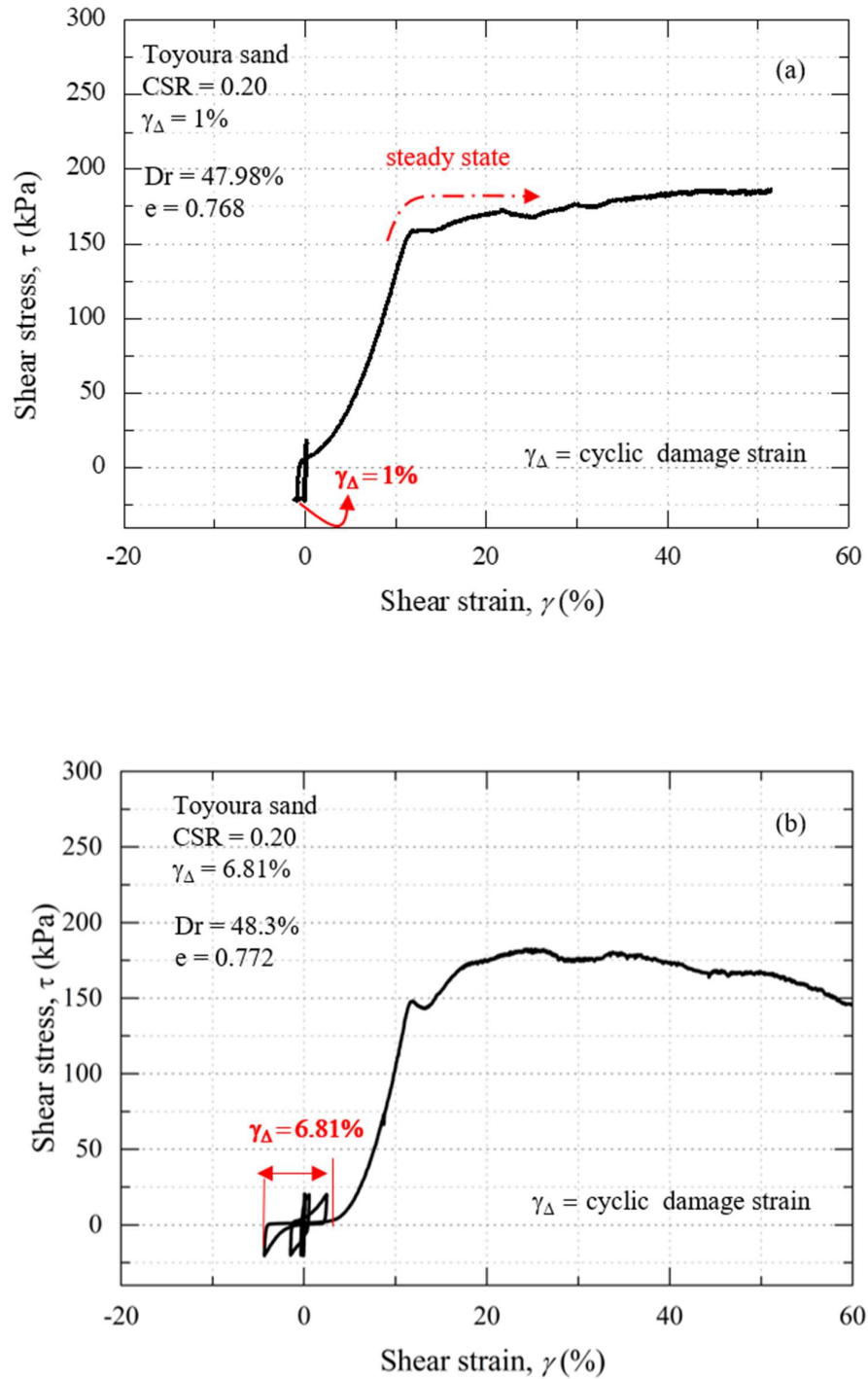
Figure 4.2:   Typical stress-strain relationship with damage strain (Medium dense Dr 48±3)

a) $\gamma_\Delta = 1\%$,   b) $\gamma_\Delta = 13\%$
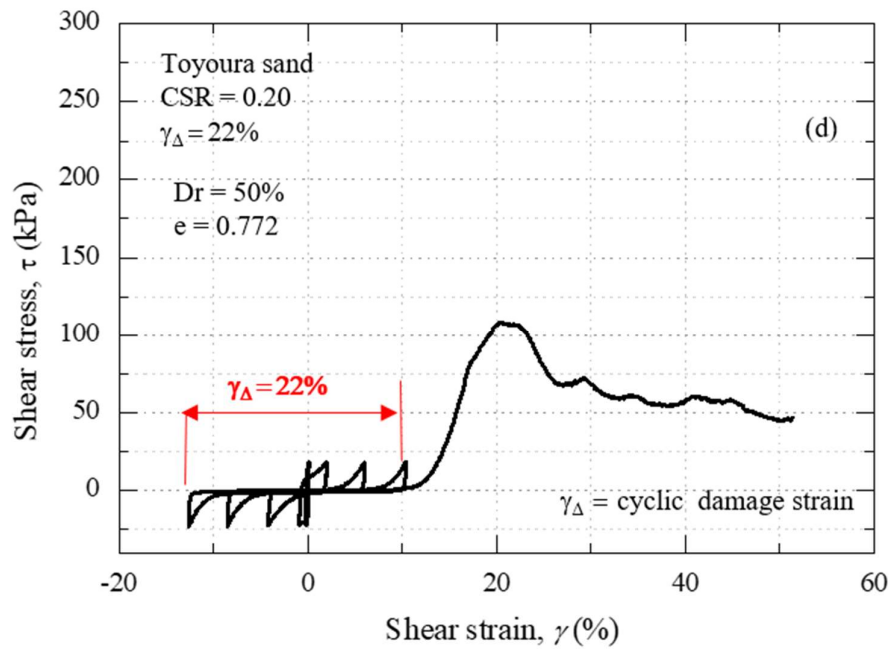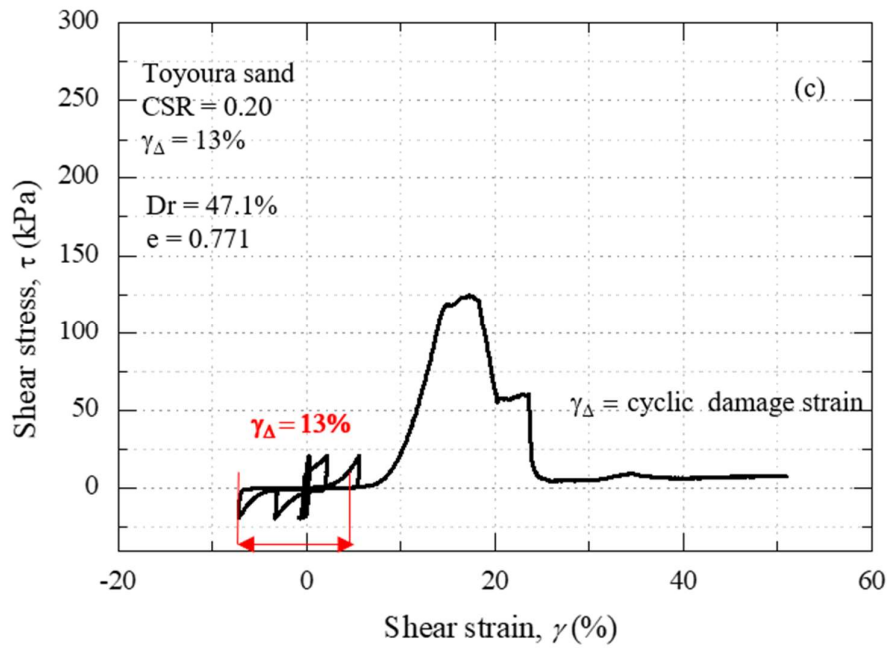
Figure 4.3: Typical stress-strain relationship with damage strain (Medium dense Dr 48$\pm$3)

c) γ_Δ = 13%,   d) γ_Δ = 22%
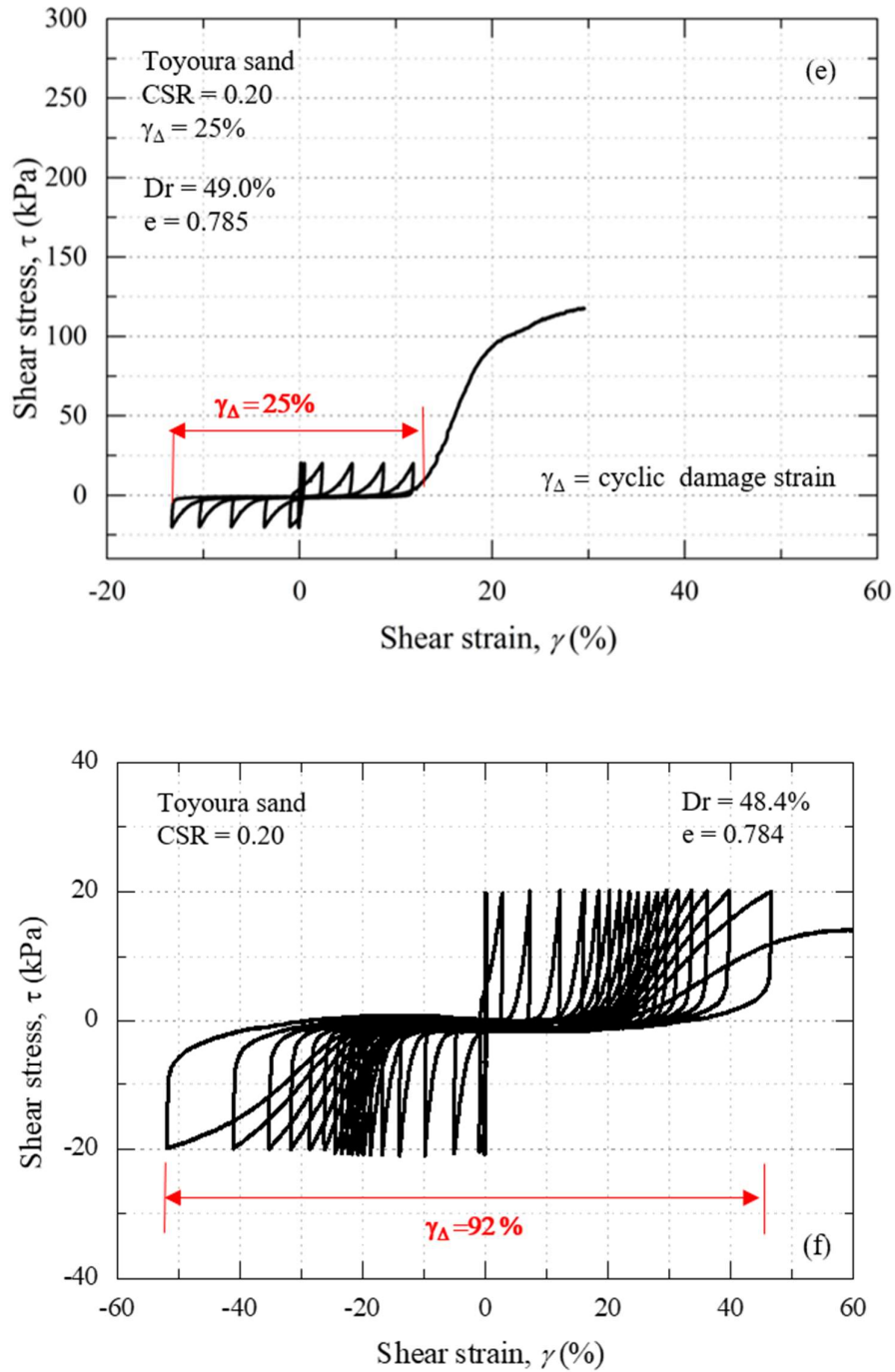
Figure 4.4: Typical stress-strain relationship with damage strain (Medium dense Dr 48$\pm$3)

e) γ_Δ = 26%,   f) γ_Δ = 92%

4.2.2 Effect of damage strain on post liquefaction undrained static strength without static shear on dense sand (68±3)

It is well known and understood that dense sand is unlikely to liquefy and is highly resistant against large deformation mainly due to high cyclic resistance against liquefaction ($p'=0$) and it has the ability to dilate excessively during undrained shearing. Therefore, densification is being used as a countermeasure against liquefaction. However, clean sand showed susceptibility of liquefaction under long-duration strong shaking such as observed during the Tohoku Earthquake 2011.

Figure 4.5 to Figure 4.6 shows a typical stress-strain relationship of a dense Toyoura sand (68±3). The specimen was liquefied ($p'=0$) by a constant amplitude cyclic stress (20kPa). Following liquefaction, specimen develops the shear strain with the increase in the number of loading cycles. The mode of loading was changed to monotonic after reaching the desired value of damage strain 3%. 7%, 12% and 19% respectively. Consistent with the medium dense sand, during undrained monotonic loading, specimen recovered its stiffness and consequently the shear strength increased, ultimately reaching a peak state followed by large deformation.

With the increase in the damage strain from 3% to 19%, undrained peak static strength degraded from 297kPa to 100kPa. From this, it can conclude two things. Firstly, the dense sand shows degradation in the undrained ultimate peak strength consistant with the medium dense sand. Secondly, dense sand is also susceptible to large deformation after exceeding undrained peak strength. From a practical point of view, a large amplitude earthquake having long duration lead to large deformation of clean sand earth structures.
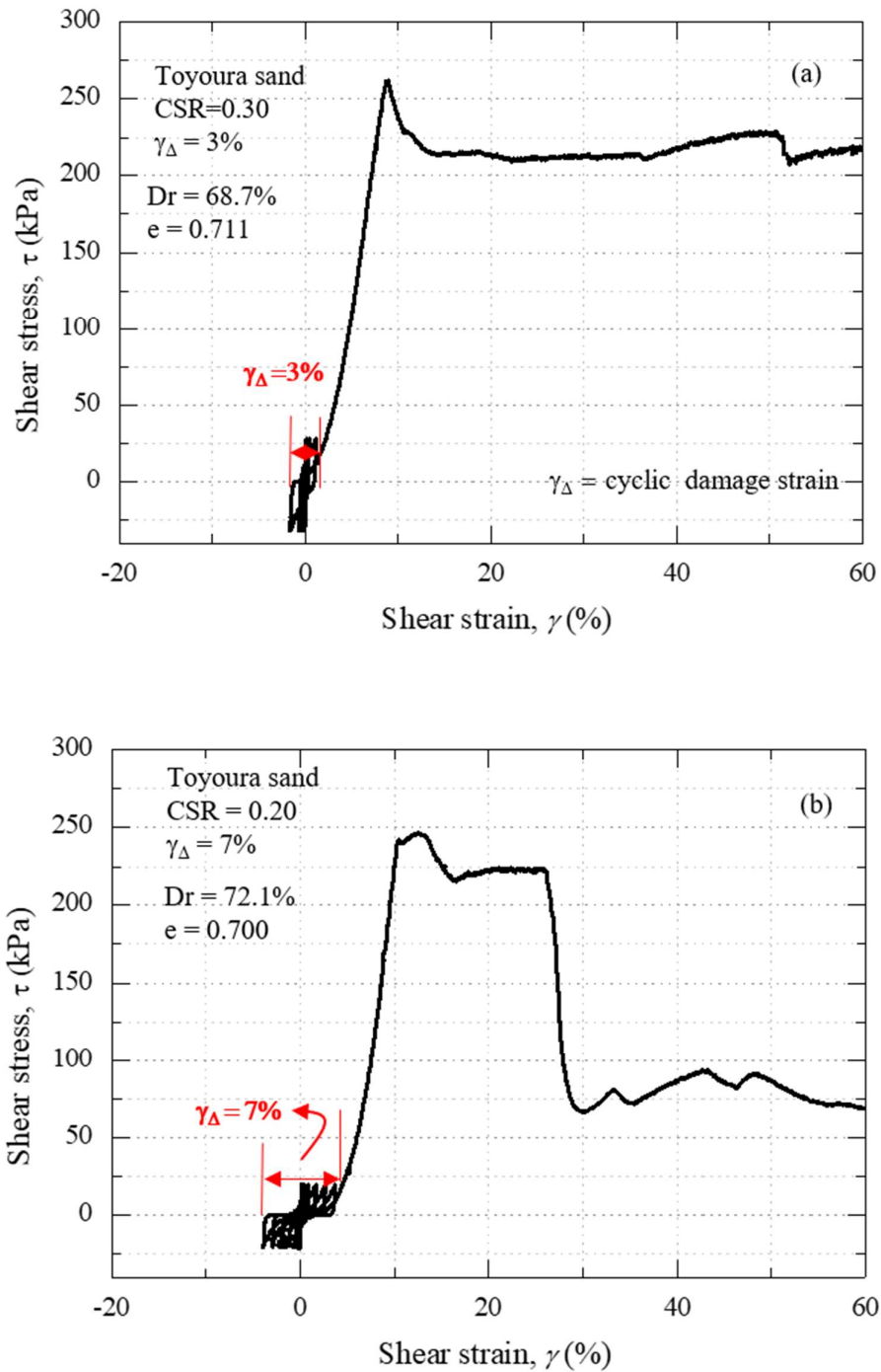
Figure 4.5:   Typical stress strain relationship with damage strain (Dr 68±3)

a) $\gamma_\Delta = 1\%$, b) $\gamma_\Delta = 8\%$
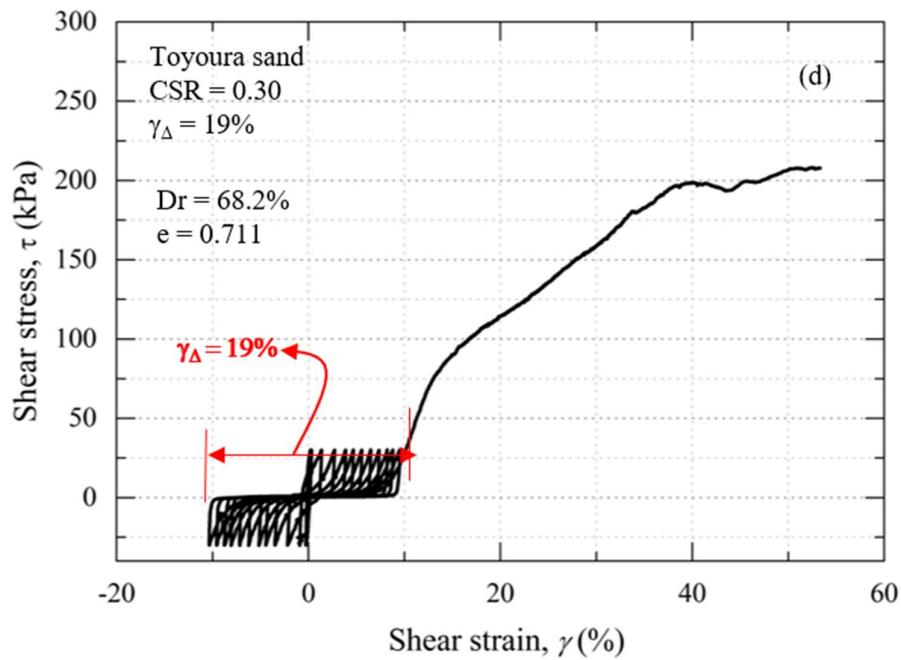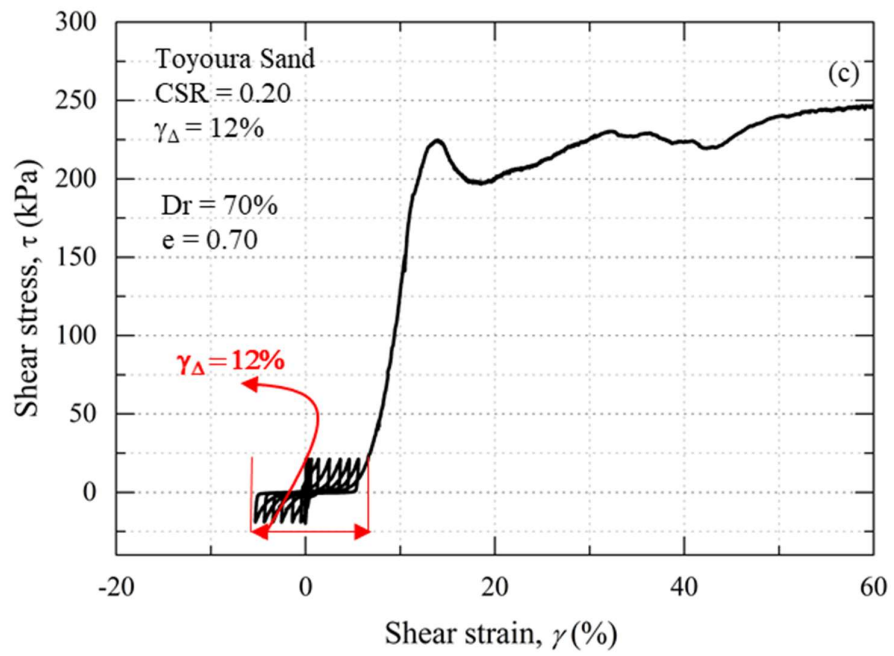
Figure 4.6:   Typical stress-strain relationship with damage strain (Dr 68$\pm$3)

a) γ_Δ = 12%, b) γ_Δ = 19%

4.2.3 Effect of damage strain on phase transformation and critical state line for medium dense Toyoura sand

Figure 4.7 to Figure 4.8 corresponds to the effective stress path during undrained monotonic loading of medium dense Toyoura sand isotopically consolidated at effective stress of 100kPa with a damage strain of 1%, 13%, 24% and 92% under constant amplitude cyclic stress of 20kPa. Increase in the number of cycles resulted in the excess pore water pressure increase. Consequently, a decrease in the mean effective principal stress.

The point of minimum mean effective stress appears where the dilatancy behavior changes from contractive to dilative. This point is named as phase transformation line (PTL) by Ishihara et al. (1975). After exceeding the PTL specimen reached a state of liquefaction ($p'=0$). It is noteworthy that the inclination of PTL, at the same initial void ratio with different level of damage strain, is insignificantly affected and uniquely defined at an angle of 30°. After $p_o'= 0$, effective stress repeatedly recovered during cyclic constant amplitude loading with the increase in the development of shear strain in the proceeding cycle.

During undrained monotonic loading, specimen followed the critical state line (CSL) irrespective of the initial void ratio (shown in chapter 3). In the test from Figure 4.7 to Figure 4.8 for medium dense sand, with different level of damage strain, specimen reached same CSL, consistent with the existing studies (Ishihara 1993, Verdugo & Ishihara, 1996,   , 1997, Papadimitriou et al. 2005 and Zlatovic and Ishihara (1997) that any history of initial fabric is erased at the large shear stain level. It is also interesting to note that compare to degradation in the ultimate peak strength in the stress-strain curve (section 4.2.1 and 4.2.2), CSL lines did not show degradation and attained the same inclination of about ~ 30-31˚
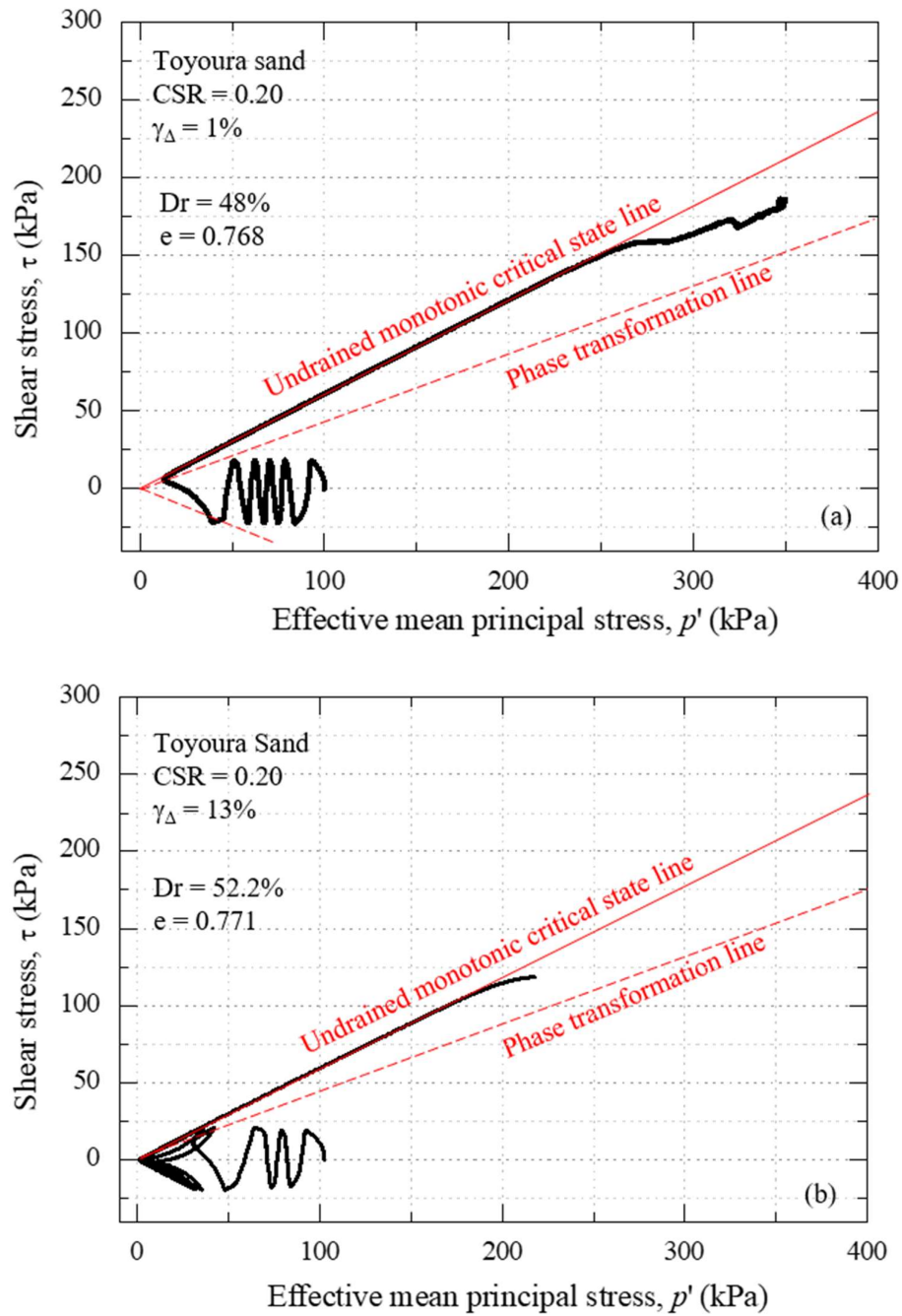
Figure 4.7:   Effective stress path with damage strain (Medium dense Dr 48±3)

a) $\gamma_\Delta = 1\%$,   b) γ_Δ = 13%
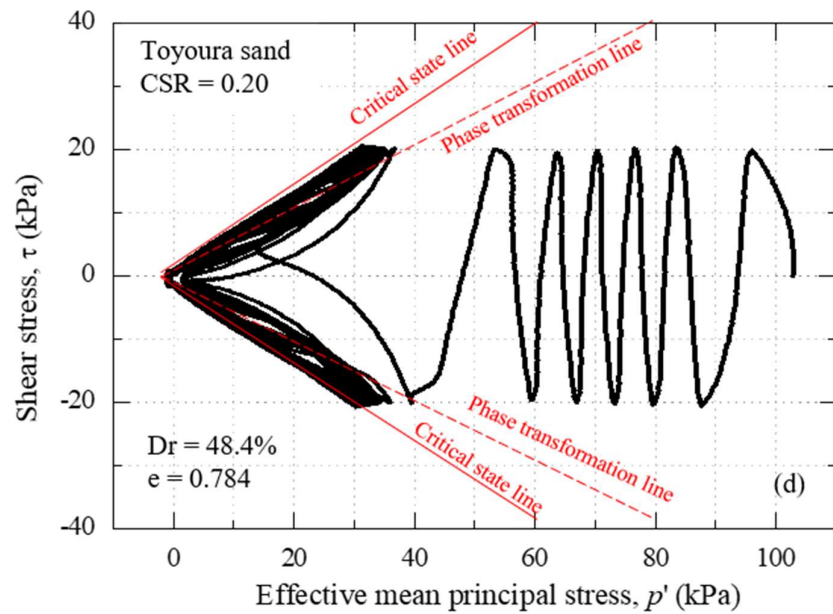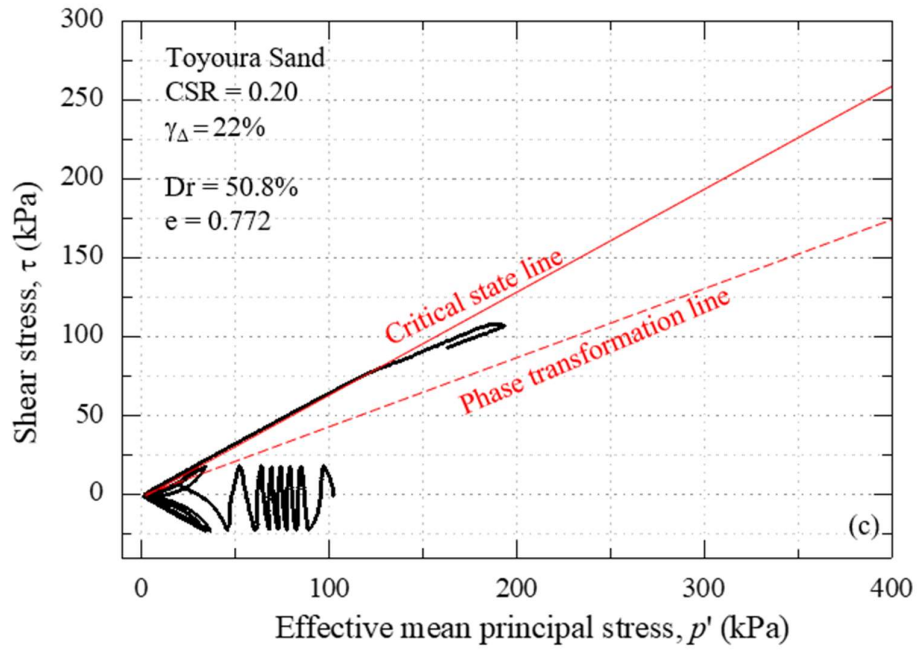
Figure 4.8:   Effective stress path with damage strain (Medium dense Dr 48±3)

c) $\gamma_\Delta = 24\%$,   d) $\gamma_\Delta = 92\%$

Figure 4.9 to Figure 4.10 shows a Typical effective stress path of dense sand with different level of damage strain i-e 3%, 7%, 12%, and 19% respectively. With the increase in the cyclic constant amplitude, loading increased positive excess pore water pressure leading to a decrease in the effective stress and consequently reached a state of liquefaction (p'=0)

Consistent with the medium dense Toyoura sand, PTL inclination plot on the effective stress plot shows an inclination of 20˚ with different level of damage strain, that reaffirms that the PTL is unaffected by the initial density (Ishihara 1993). Whereas, as expected contrary to medium dense, dense sand exhibit a steeper inclination of about 39 ˚ of CSL. Increase in the damage strain unaffected the inclination of CSL line.

4.2.4   Discussion

Investigation of effective stress path comparison of the cyclic test followed by undrained monotonic loading revealed (Figure 4.7to Figure 4.10) that the PTL line is unaffected by the initial relative density. Whereas irrespective of the damage strain level, the critical state line reached the same inclination at the same initial density level. This can be possibly explained, the failure line depends on the intrinsic friction between the particle. Intrinsic parameter did not show deterioration with the increase in the damage strain.
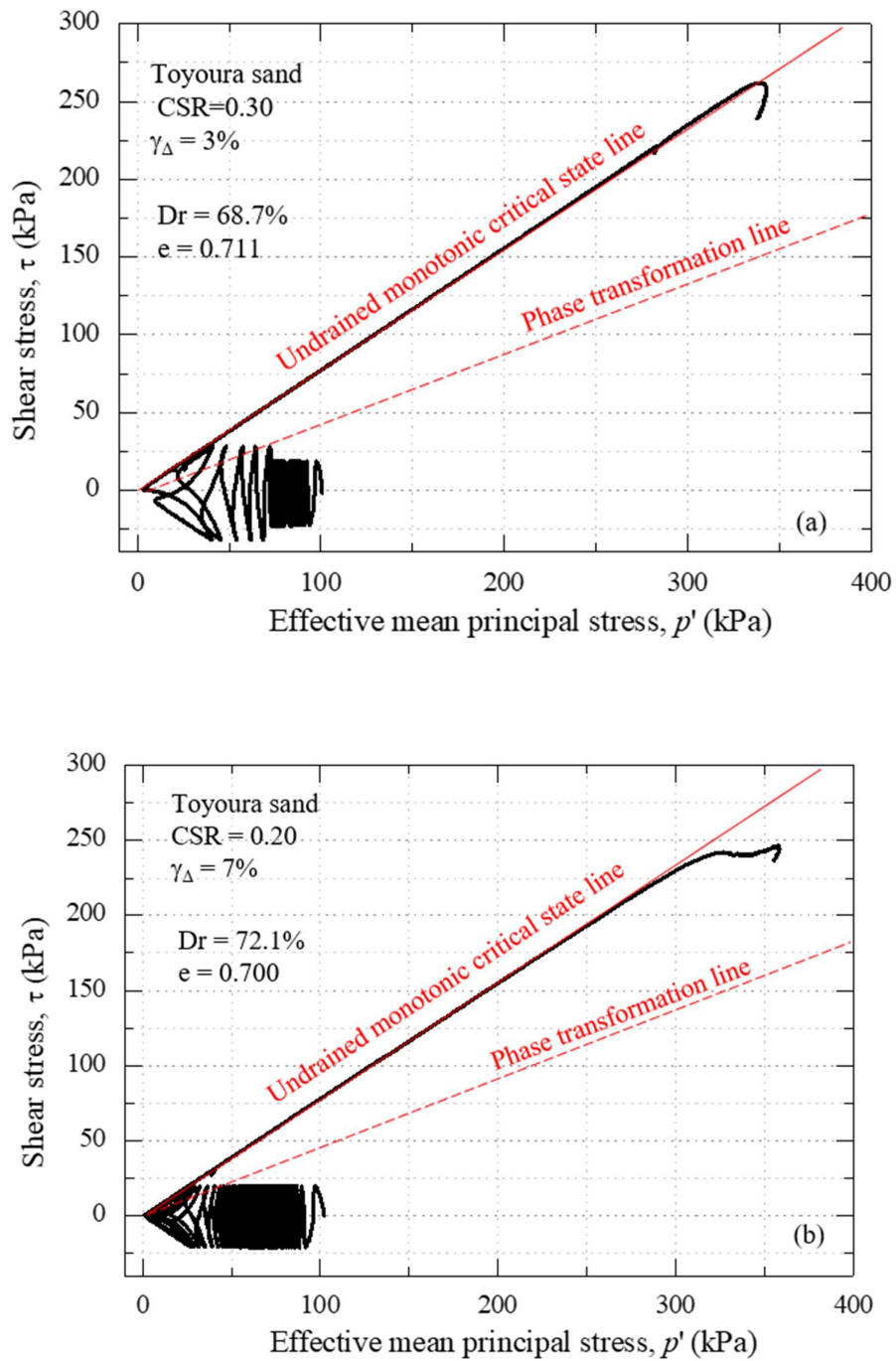
Figure 4.9:   Effective stress path with damage strain (Dense sand Dr 68±3)

a) $\gamma_\Delta = 3\%$,   b) $\gamma_\Delta = 7\%$
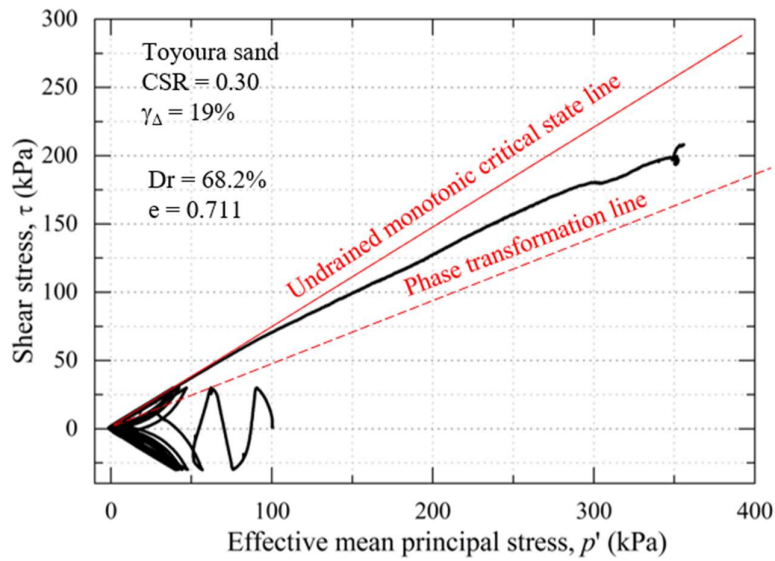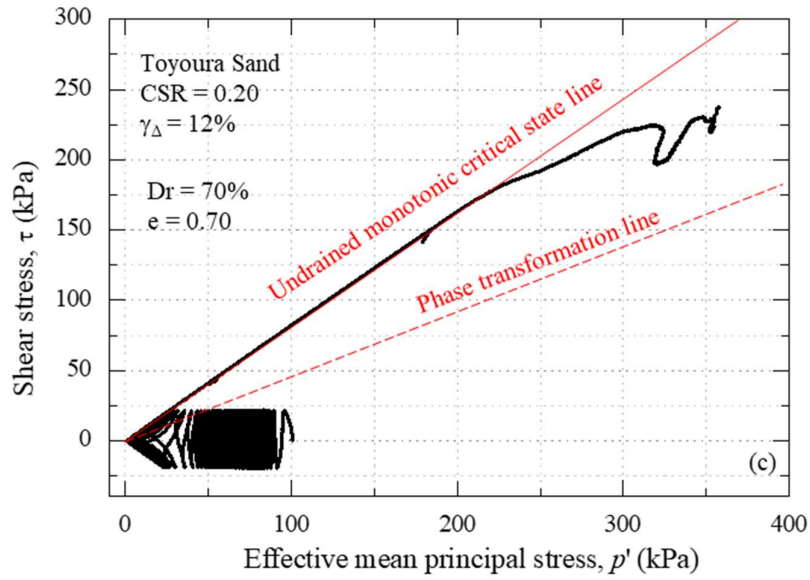
Figure 4.10:   Effective stress path with damage strain (Dense sand Dr 68$\pm$3)

c) $\gamma_\Delta = 12\%$,   d) $\gamma_\Delta = 19\%$

4.2.5   Effect of damage strain on stress ratio of medium dense sand

Figure 4.11 to Figure 4.14 shows the typical test result between corrected stress ratio (Chiaro et al. (2012) and shear strain of cyclic test followed by an undrained monotonic test with 1%, 13%, 24%, and 92% respectively for medium dense sand. During cyclic loading, the stress ratio changes from positive to negative during cyclic loading as a result of cyclic mobility. Whereas during post liquefaction undrained monotonic loading, the specimen achieved a peak stress ratio followed by a residual state. It is interesting to observe that with different level of damage strain; peak stress ratio is different. However, all the test irrespective of damage strain achieved similar residual stress of 0.6 during undrained monotonic loading. From this comparison, it is evident that the residual stress ratio is independent of the damage strain and no degradation of stress ratio was observed.
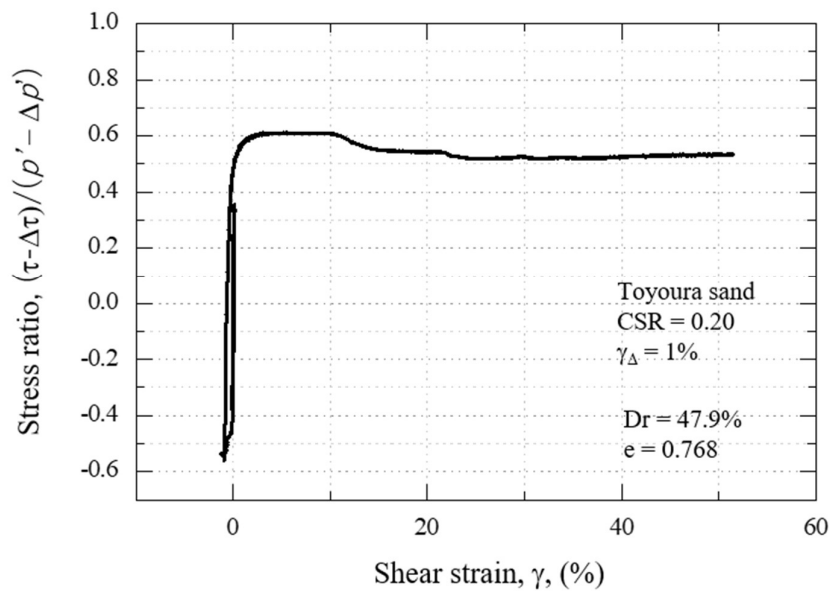
Figure 4.11: Corrected stress ratio vs shear strain
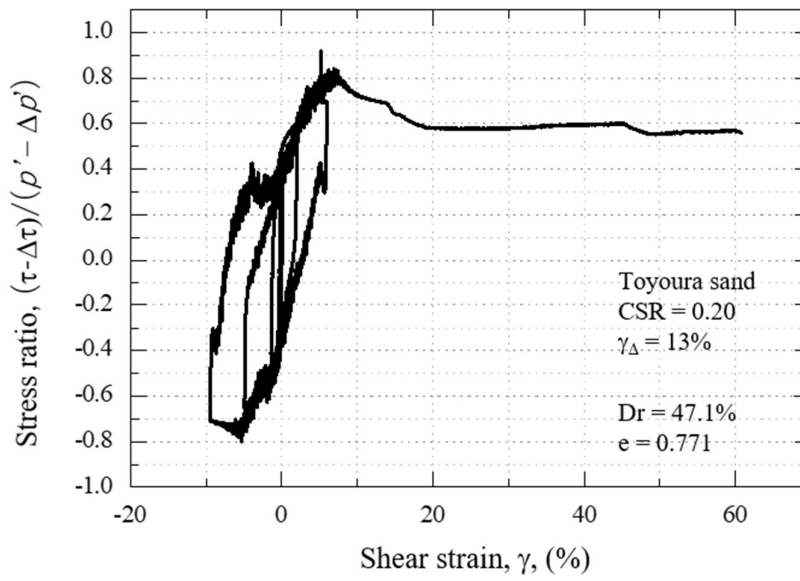
Figure 4.12:   Corrected stress ratio vs shear strain
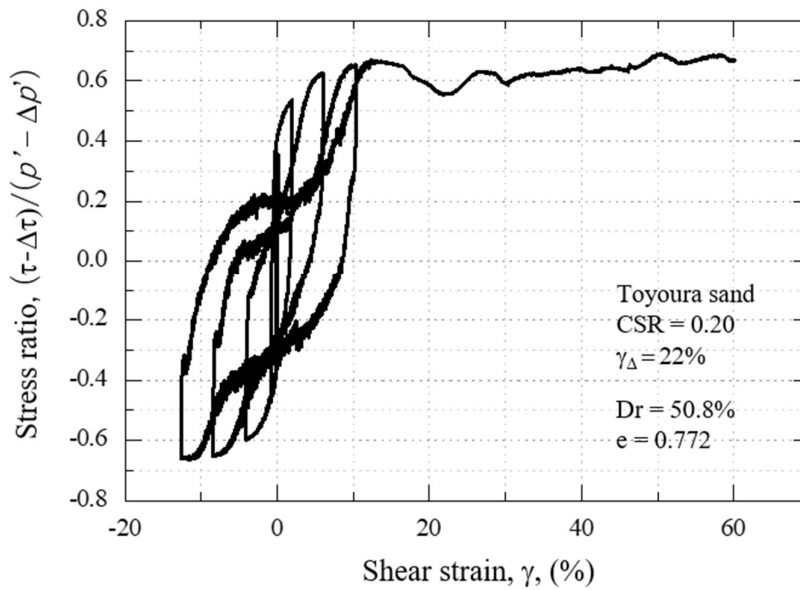
Figure 4.13: Corrected stress ratio vs shear strain
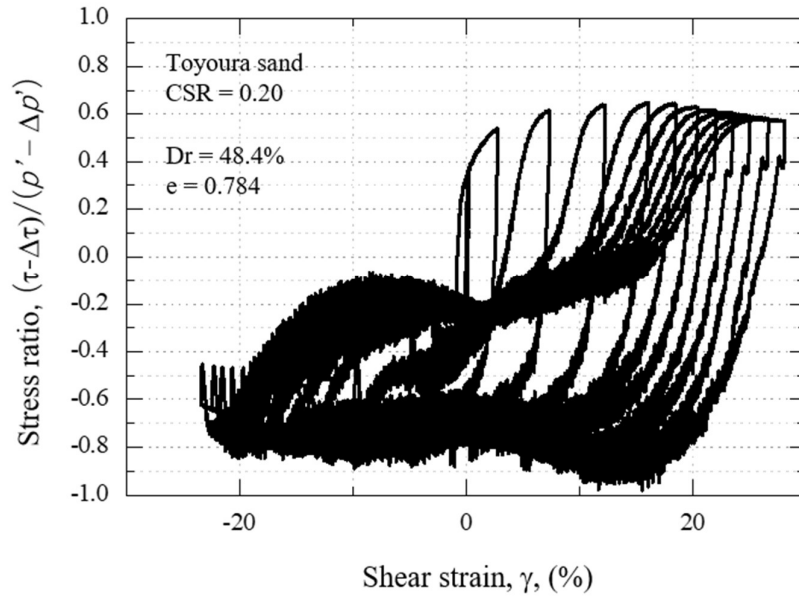
Figure 4.14: Corrected stress ratio vs shear strain

4.2.6 Post liquefaction static shear strength degradation curves

Figure 4. 15 shows strength degradation curve with damage strain for medium dense and dense sand. The post liquefaction undrained static strength deteriorated irrespective of the relative density with the increase in the damage strain. For a damage strain of 24%, strength degradation in medium dense was 111kPa, as compared to dense sand 167kpa. The dotted lines show the extrapolation of degradation correlation for both the relative density. The experimental data become unreliable due to non-uniformity in the specimen as a result of extremely large strain and strain accumulation near the top cap of the specimen.
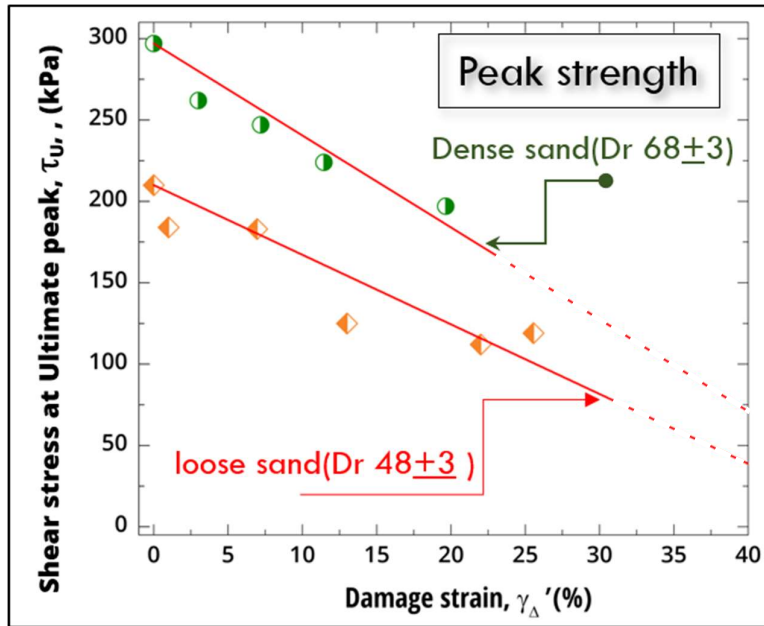
Figure 4. 15: Peak undrained strength deterioration with damage strain

4.3 Effect of damage strain on undrained static strength with static shear

In case of slope ground, a soil element beneath is subjected to an initial static shear(τ_{static}) in before an earthquake, as shown in Figure 1. During the seismic loading, the coupling of cyclic stress(τ_{cyclic}) and initial static shear (τ_{static}), the soil element can either experience reversal or non-reversal loading, as shown in Figure 4. 16.
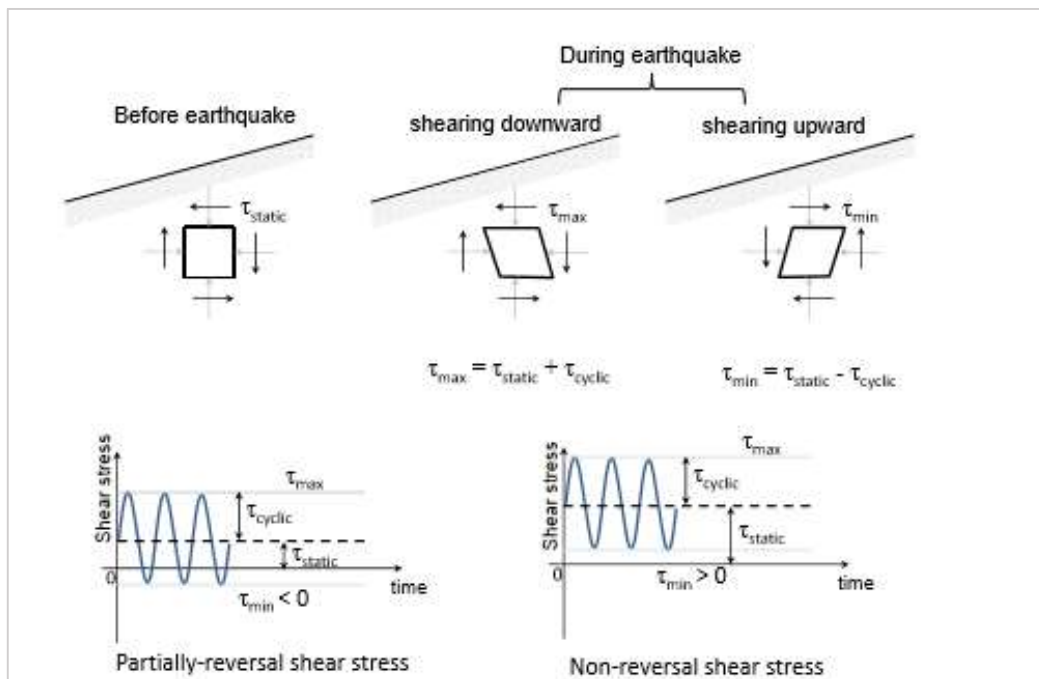
Figure 4. 16: Slope ground stress conditions during earthquakes

When initial static shear (τ_{static}) is larger than cyclic shear stress (τ_{cyclic},) i-e $\tau_{static} < \tau_{cyclic}$, the cyclic shear stress changes within the amplitude of maximum positive i-e $\tau_{max} = \tau_{static} + \tau_{cyclic} > 0$ and minimum negative value i-e $\tau_{min} = \tau_{static} - \tau_{cyclic} < 0$. This loading scenario is called reversal loading as shown in Figure 4.17.

Whereas, as shown in Figure 4.18, when $\tau_{static} > \tau_{cyclic}$, shear stress remains positive (i.e. $\tau_{max} > 0$ and $\tau_{min} > 0$). This type of loading is termed non-reversal stress (Yoshimi and Oh-oka 1975, Hyodo et al. 1991).

4.4   Test procedure for simulating sloping ground

4.4.1   Definition of Damage strain in case of initial static shear

As the level of initial static shear increases, shear strain started to accumulate in the direction of applied initial static shear (Chiaro et al. (2012), Umar et al. 2016). In this study, it is assumed that damage strain amplitude is defined as double amplitude (γ_{DA}) as it's given by the following equation

$$\gamma_\Delta = \gamma_{max} - \gamma_{min}$$

Whereas γ_Δ is the damage strain, $\gamma_{max\ is}$ the maximum shear stain applied before undrained monotonic loading and γ_{min} is the initial shear strain before cyclic loading.
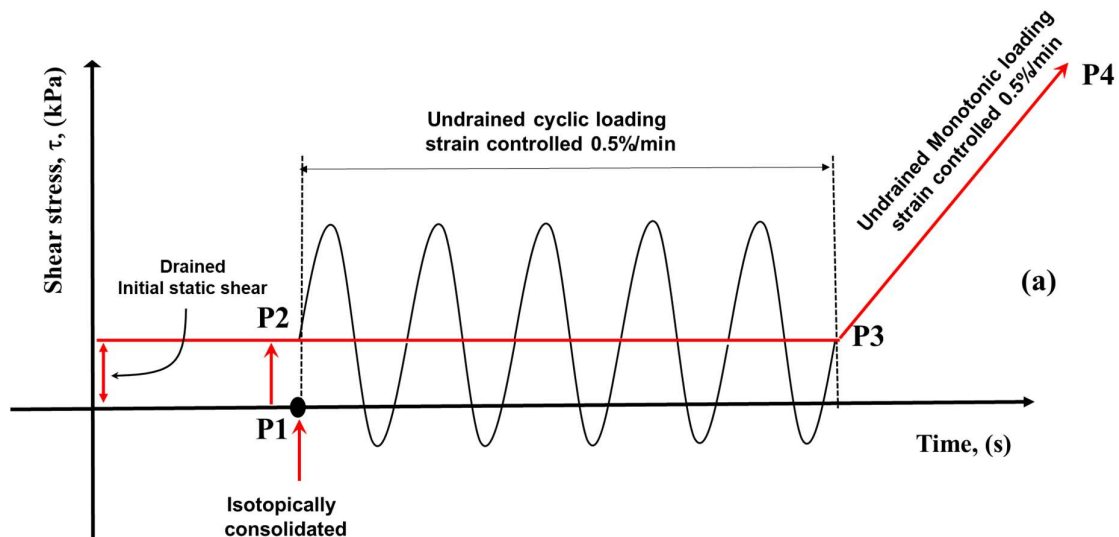
Figure 4.17: Test procedure with a static shear Reversal loading
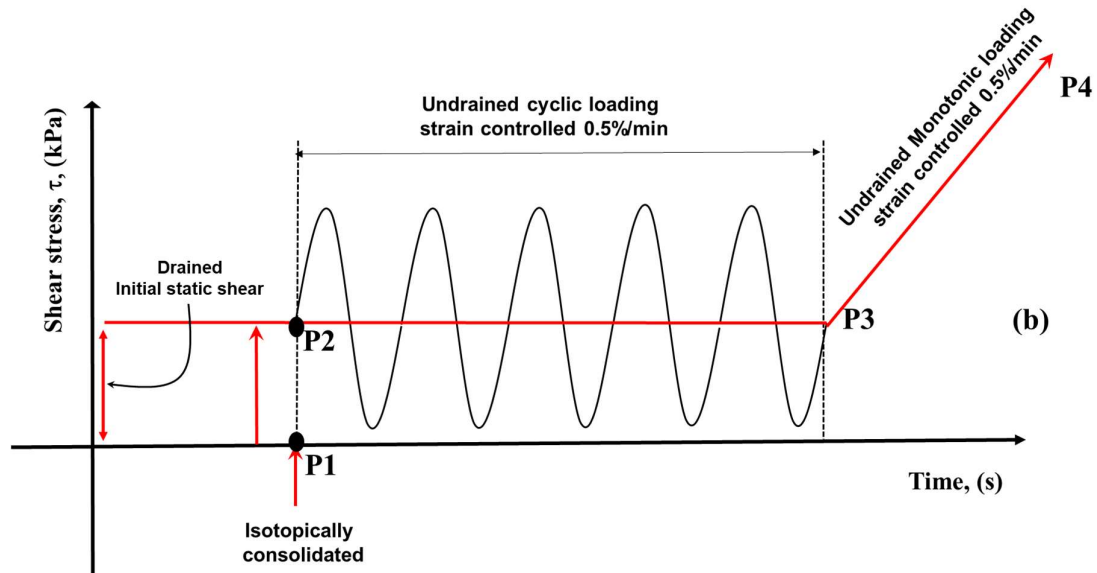
Figure 4.18: Test procedure with a static shear during non-reversal loading

Table 4.1. Summary of test performed with initial static shear

Test No.	Relative Density, Dr (%)	Void ratio, e	Cyclic damage strain, γ_Δ, (%)	Mean effective stress (p_o'), (kPa)	Shear stress (kPa)	Static shear stress(kPa)
5-1	47.9	0.77	0	100	Mono	15
5-2	52.2	0.78	11	100	20	10
5-3	49.0	0.79	16	100	20	10
Non-reversal loading						
6-1	46.0	0.775	3	100	12	20
6-2	45.7	0.776	6	100	12	20
6-3	48.0	0.776	8	100	16	20
6-4	46.2	0.777	9	100	16	20
6-5	46.0	0.771	12	100	16	20
6-6	47.1	0.776	14	100	16	20
6-7	45.5	0.776	17	100	16	20

4.5   Effect of Damage strain on undrained static strength with initial static shear for reversal loading

Initial static shear plays a significant role in determining the deformation characteristic of sand. Superimposition of static shear leads to a decrease in the liquefaction resistance during reversal loading during large deformation (Chiaro et al. 2011). Investigation on plastic silty sand with initial static shear by Yasuhara et al. (1997) showed the degradation of ultimate strength with increase in the cyclic loading as compared with the monotonic loading (without cyclic). However, as per author knowledge, no investigation has been done on the influence of static shear on the post liquefaction undrained monotonic strength on clean sand.

In this section effect of initial static shear on the ultimate peak, strength is investigated under reversal condition ($\tau_{cyclic} > \tau_{static.}$ **Error! Reference source not found.** to Figure 4. 22 shows the typical effective stress path and the stress-strain relationship of test performed with initial static shear for reversal loading with an initial static shear stress of 10kPa and cyclic stress of 20kPa. It is evident that the by constant amplitude cyclic shear stress, shear strain develops predominantly in the direction of applied static shear. After reaching a damage strain of 11% (**Error! Reference source not found.**b), the mode of loading was changed to monotonic. During undrained monotonic loading, specimen recovered its stiffness and ultimately reaching a peak strength of 200kPa. Whereas in Figure 4. 22b, with a damage strain of 16% with initial static shear of 10kPa, ultimate shear strength during undrained monotonic loading was 175kPa. The results of the above reversal loading indicate that the ultimate strength deteriorated with the increased in the damage strain irrespective of the initial static shear under reversal. On the other hand, the comparison of effective stress path **Error! Reference source not found.**a and Figure 4. 22a shows that the phase transformation line is unaffected by the initial static shear. Analogous to the level ground, effective stress path followed the CSL line during undrained monotonic loading. However, CSL inclination increases from 30 to 32 degree with

superimposition of static shear.
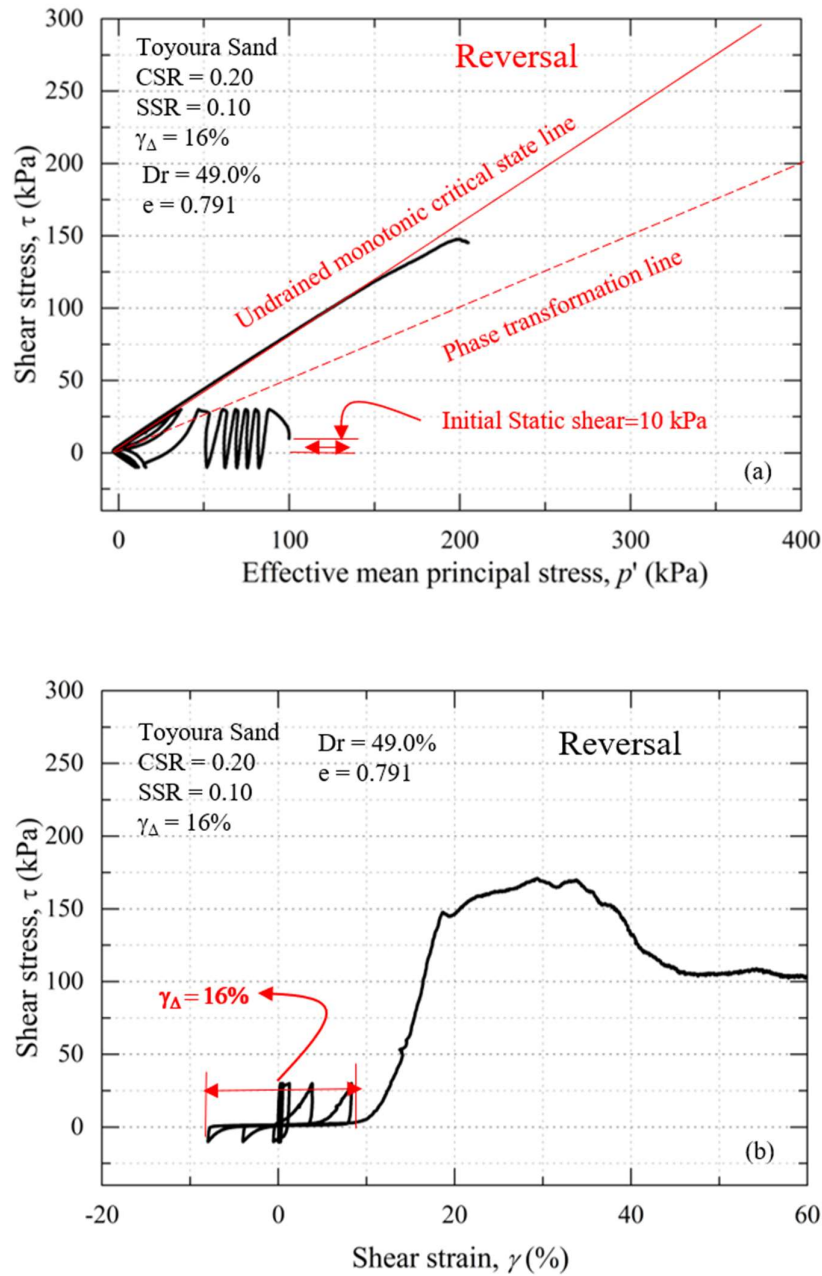
Figure 4.19: Typical test results with initial static shear reversal loading
SSR=0.10, γ_Δ =11%, CSR = 0.20
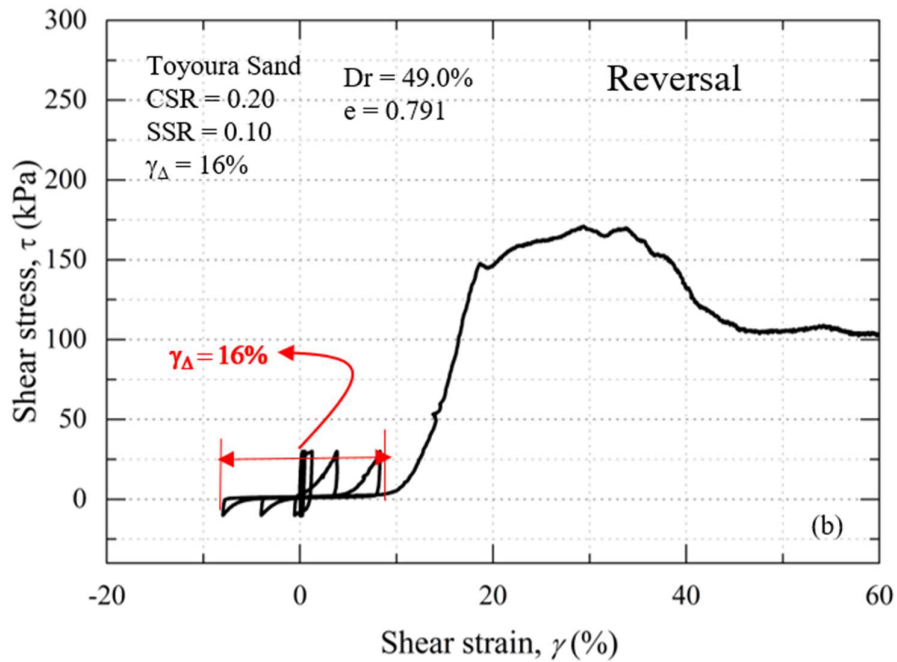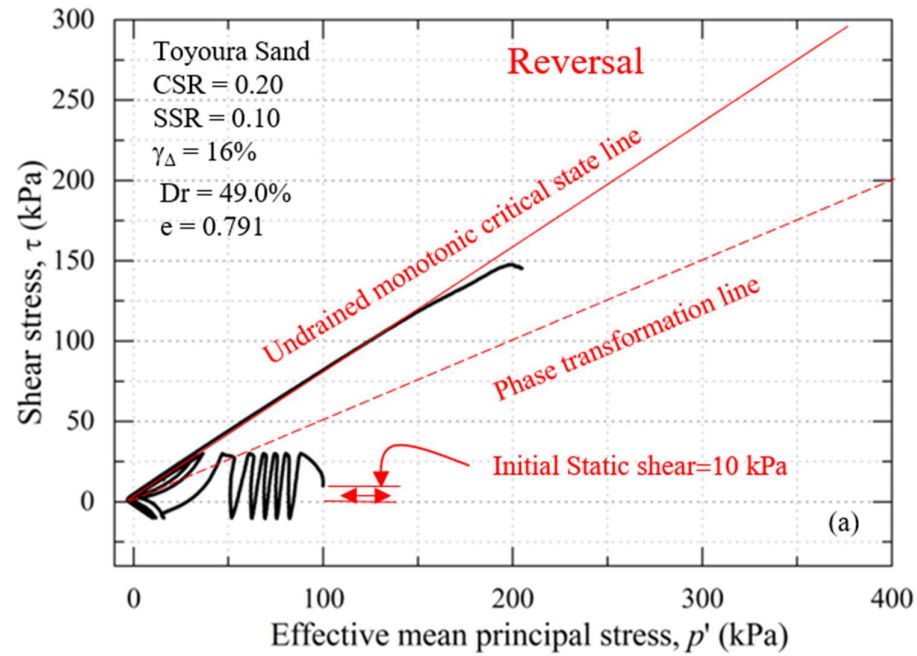
Figure 4.20: Typical test results with initial static shear Reversal loading
SSR=0.10, γ_Δ =16%, CSR = 0.20

4.6 Effect of damage strain on undrained static strength with initial static shear for reversal loading

Typical test results in term of effective stress path and stress-strain for non-reversal loading ($\tau_{static} > \tau_{cyclic}$) for a damage strain of 3%, 8%, and 12% respectively is shown in Figure 4.21 to Figure 4.23. It can be observed that that during undrained cyclic loading, excess pore water pressure was generated resulted in the decrease in the effective stress. However, in the case of non-reversal loading specimen did not reach the state of liquefaction (p'=0). cyclic mobility was observed, soil strength recovered by repeated cyclic loading.

Following the undrained cyclic loading to induce the damage strain, during undrained monotonic loading, specimen followed the CSL. With the increase in the damage strain 3 t0 12%, the inclination of CSL increased from 30 to 34. Such an increase in the inclination is the indication of specimen stiffness by repeated cyclic loading.
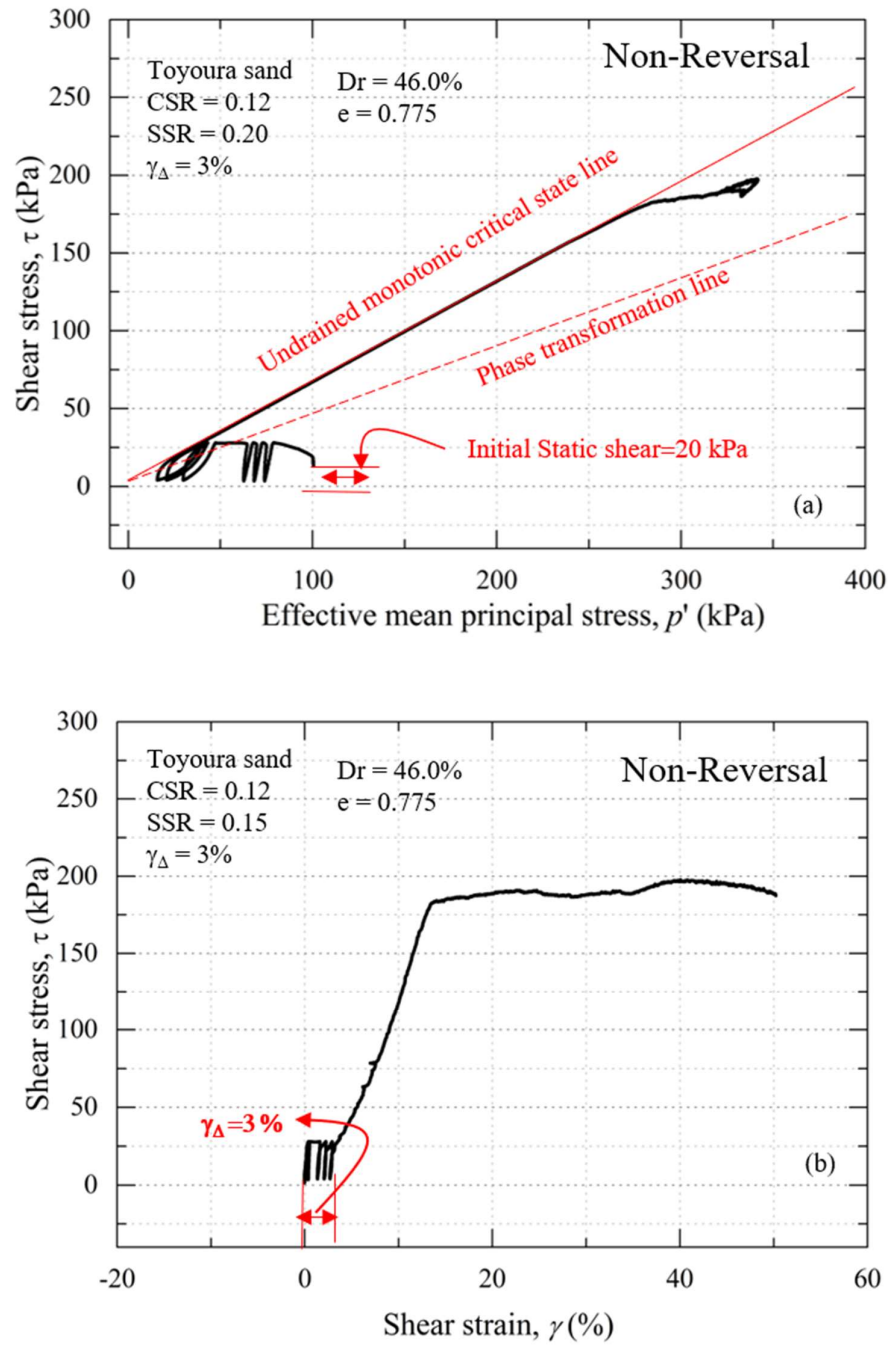
Figure 4.21: Typical test results with initial static shear Non- Reversal loading
SSR=0.12, CSR = 0.20, γ_Δ =3%,
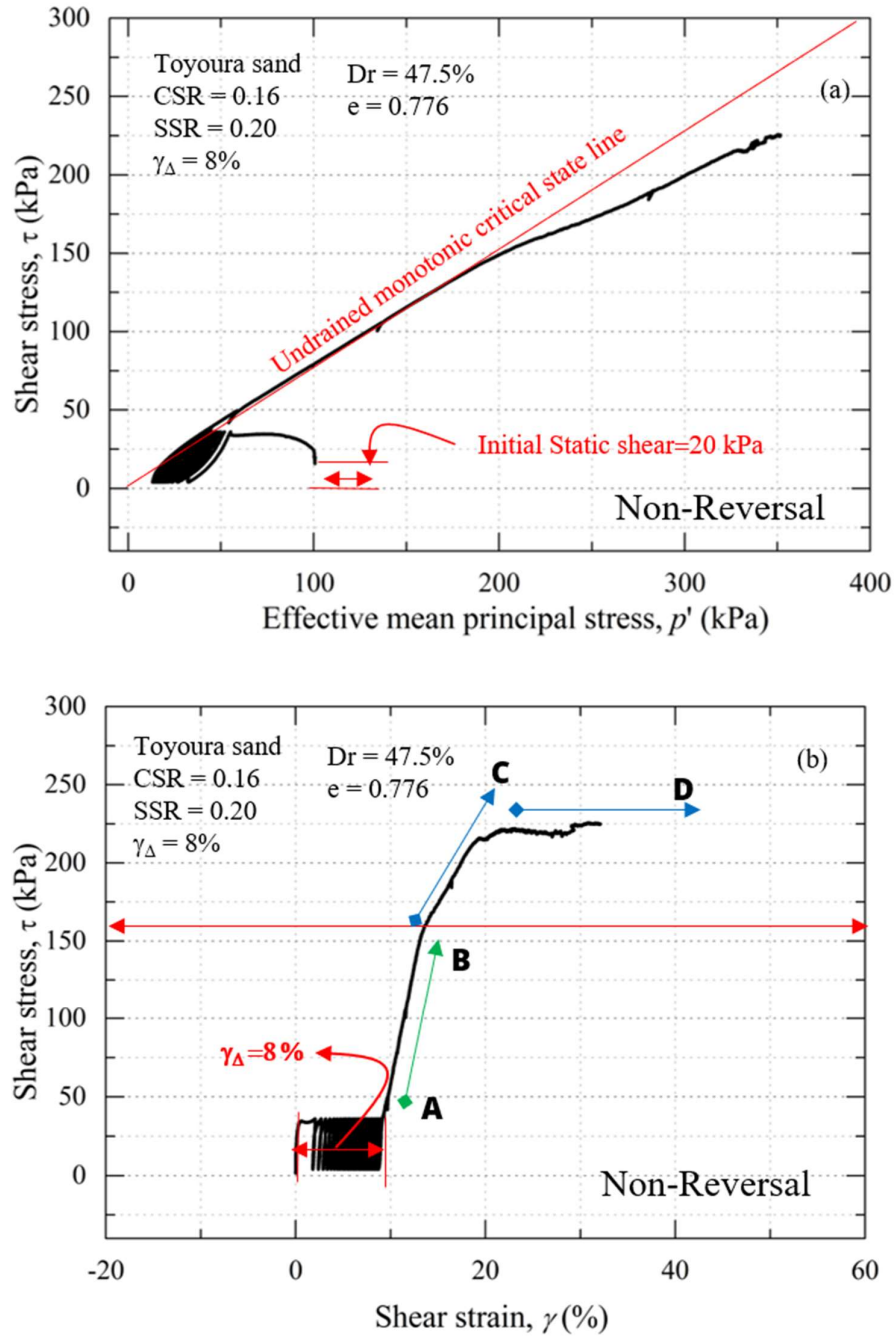
Figure 4. 22: Typical test results with initial static shear Non- Reversal loading
SSR=0.20, CSR = 0.16, γ_Δ =8%
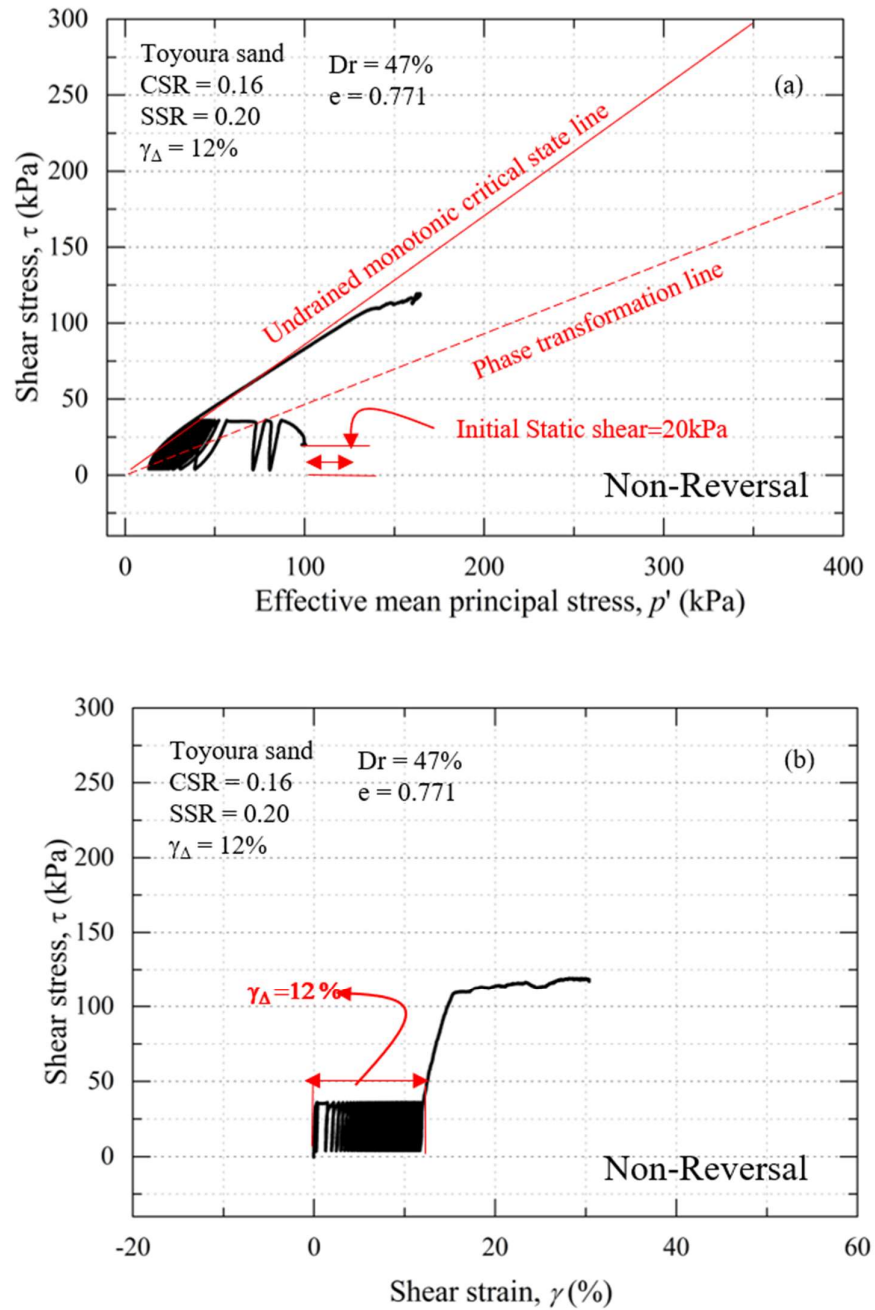
Figure 4.23: Typical test results with initial static shear Non-Reversal loading
SSR=0.20, CSR = 0.16, γ_Δ =12%

4.7 Effect of cyclic stress ratio on the post liquefaction undrained strength

From a practical point of view, the ground can accumulate shear strain by the different amplitude of cyclic stress. Therefore a series of test were conducted by reaching the same amplitude of double amplitude of damage strain of 6% by different amplitude of cyclic stress ratio.

Figure 4.24 to Figure 4.26 typical stress-strain relationship with a damage strain of 6%, with a cyclic stress ratio from 0.12 to 0.20. As the amplitude of cyclic stress increased, the number of cycles to reach a damge strain 6% decreased. During the monotonic undrained loading, the soil recovered its stiffness and strength and ultimately reached the undrained peak strength followed by the residual state. A red dotted line is marked the limiting undrained strength (discussed in chapter 5). Limiting undrained strength is defined as the beginning of non-uniformities in the specimen. The strain at limiting strength is referred to as limiting strain(Kiyota et al. (2008)). It is evident that the irrespective of the cyclic stress ratio, all the specimen reached the same limiting undrained strength. Whereas the undrained residual strength also reached the same peak shear stress state. From this comparison, it is evident that the undrained peak strength is independent of the cyclic stress amplitude and mainly dependent on the experience damage strain.

Whereas in Figure 4.26, a damage strain of 6% under non-reversal stress condition is applied. Under such a non-reversal stress condition, the shear strain developed progressively in the applied direction of initial static shear. During the undrained monotonic specimen recovered its stiffness and reached ultimate peak stress followed by the residual state of deformation. It is interesting to note that, under such combination of loading specimen did not reach the state of $p_o{'} = 0$, and reached the same ultimate undrained peak strength as compared with the cyclic stress of 0.12 and 0.20, where the specimen reached the state of $p_o{'} = 0$. This concludes that a

sandy soil recovered its stiffness and strength and its history of liquefaction is erased.
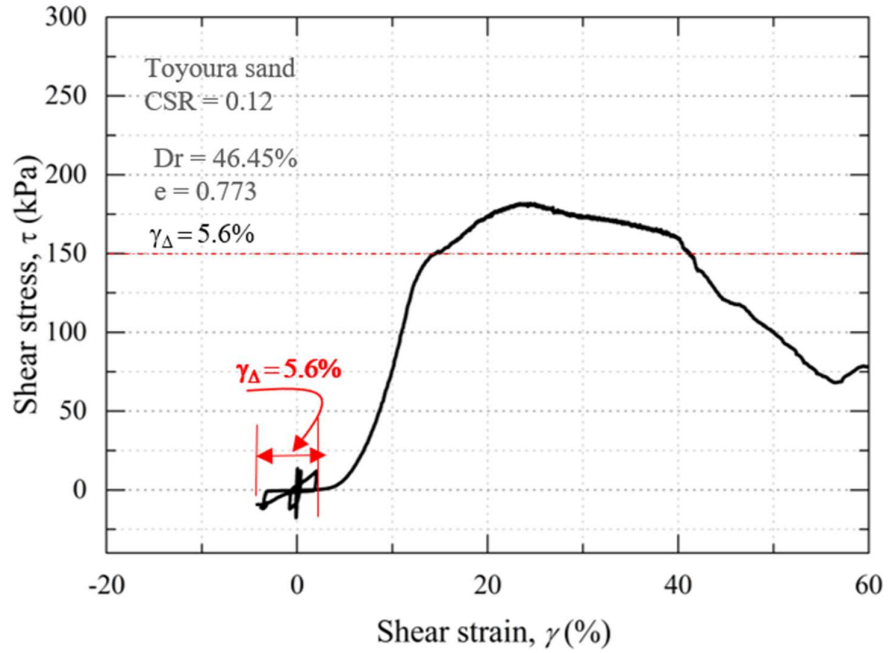
Figure 4.24: Typical stress-strain with CSR 0.12, and γ_Δ =6%
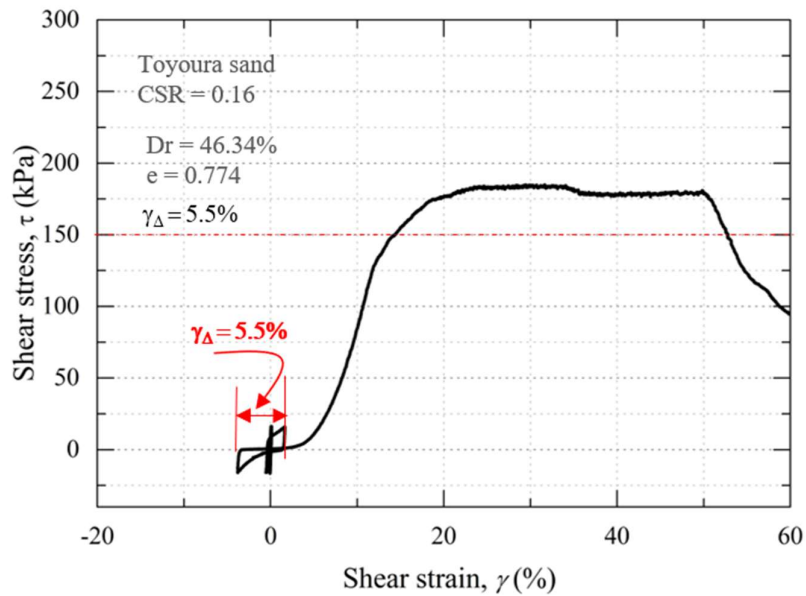
Figure 4.25: Typical stress-strain with CSR 0.16, and γ_Δ =6%
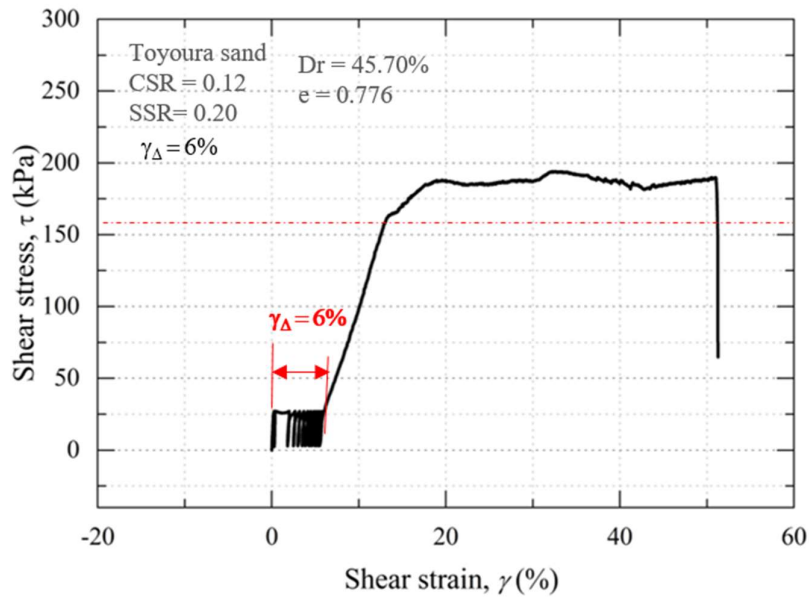
Figure 4.26: Typical stress strain with CSR 0.12 and SSR =0.10, and γ_Δ =6%

4.8 Effect of cyclic stress ratio on the effective stress path with damage strain

In

Figure 4.27 to Figure 4.29 results are presented in effective stress of Toyoura sand specimen with the different amplitude of stress ratio and achieving the same damage strain. As expected, higher cyclic stress ratio resulted in the faster development of excess pore pressure. The number of cycles to reach a damage strain of 6% decreased from 145 to 20 by the increase in the amplitude in the cyclic stress ratio from 0.12 to 0.20 respectively (

Figure 4.27 and Figure 4.28). During undrained monotonic loading, specimen followed undrained critical state line. The inclination of CSL remains unaffected by the amplitude of the cyclic stress ratio and can be defined as 32°. In addition, the phase transformation line (PTL) is also unaffected by the change in the amplitude of the cyclic stress ratio.

Effective stress path in non-reversal loading is presented in Figure 4.29. Excess pore water was

generated during non-reversal loading and effective stress moved toward failure envelope.

During undrained monotonic loading, it followed a critical state. The inclination of critical under non-reversal loading is also unaffected by mode of loading and inclination is consistent with the reversal loading discussed above.

The result in section 4.4.5 and 4.4.6 can be concluded that the damage strain is the influential factor in determining the ultimate peak strength of sandy soil whereas the amplitude of cyclic stress or static stress did not affect the ultimate peak strength. From a practical point of view, earthquake having different amplitude but accumulating the same amplitude will result in the same degradation of undrained peak strength.
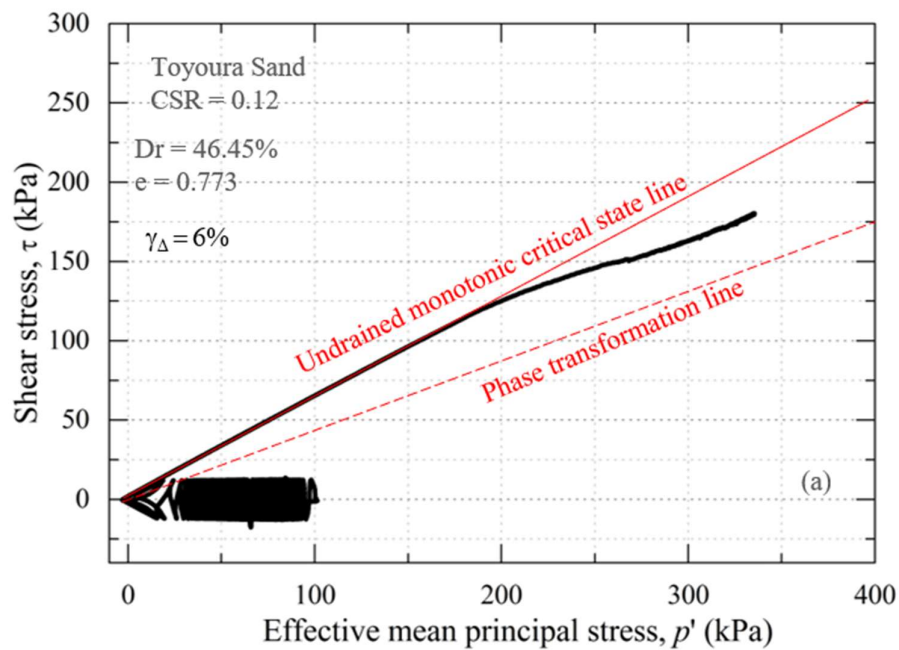
Figure 4.27: Typical effective stress path with CSR 0.12, and γ_Δ =6%
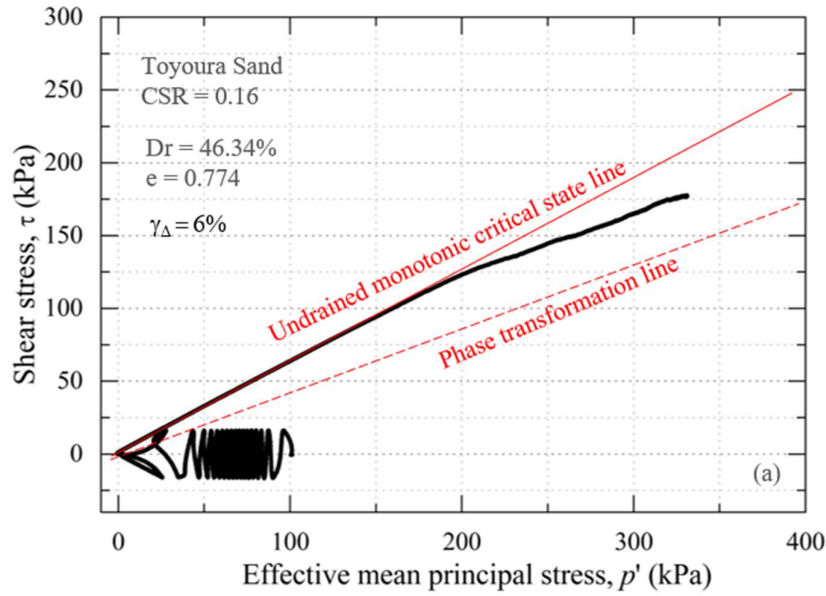
Figure 4.28: Typical effective stress path with CSR 0.16, and γ_Δ =6%
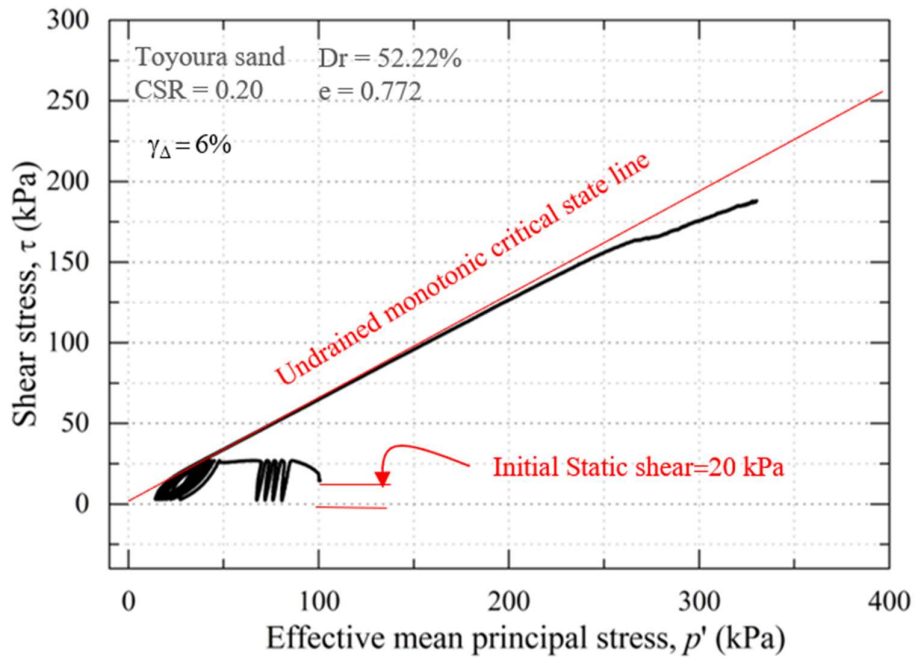
Figure 4.29: Typical effective stress path with CSR 0.12, SSR=0.20 and γ_Δ =6%

4.9 Effect of confining pressure the post liquefaction undrained strength

Typical test results in term of effective stress path and stress-strain are presented in Figure 4.30, and Figure 4.31 for the specimen consolidated at the confining pressure of 200kPa and 400kPa, respectively. A constant amplitude cyclic stress ratio of 0.20 is applied to achieve a damage strain of 13% and 17.6% respectively. Following that undrained monotonic loading is applied exceeding a shear strain of 60% single amplitude.

From the effective stress, the critical state line is unaffected by the consolidation pressure and achieve an inclination of 33˚ for 200kPa and 400kPa. Whereas, the phase transformation line is also unaffected by the consolidation pressure.

Whereas during the undrained monotonic loading reached an ultimate undrained strength followed by residual state exceeding a shear strain of 60%. The undrained peak resistance deteriorated with the damage strain as compared with the undrained monotonic test (without cyclic loading). Therefore, it can be concluded that the damage strain deteriorated the undrained peak resistance irrespective of the confining pressure.
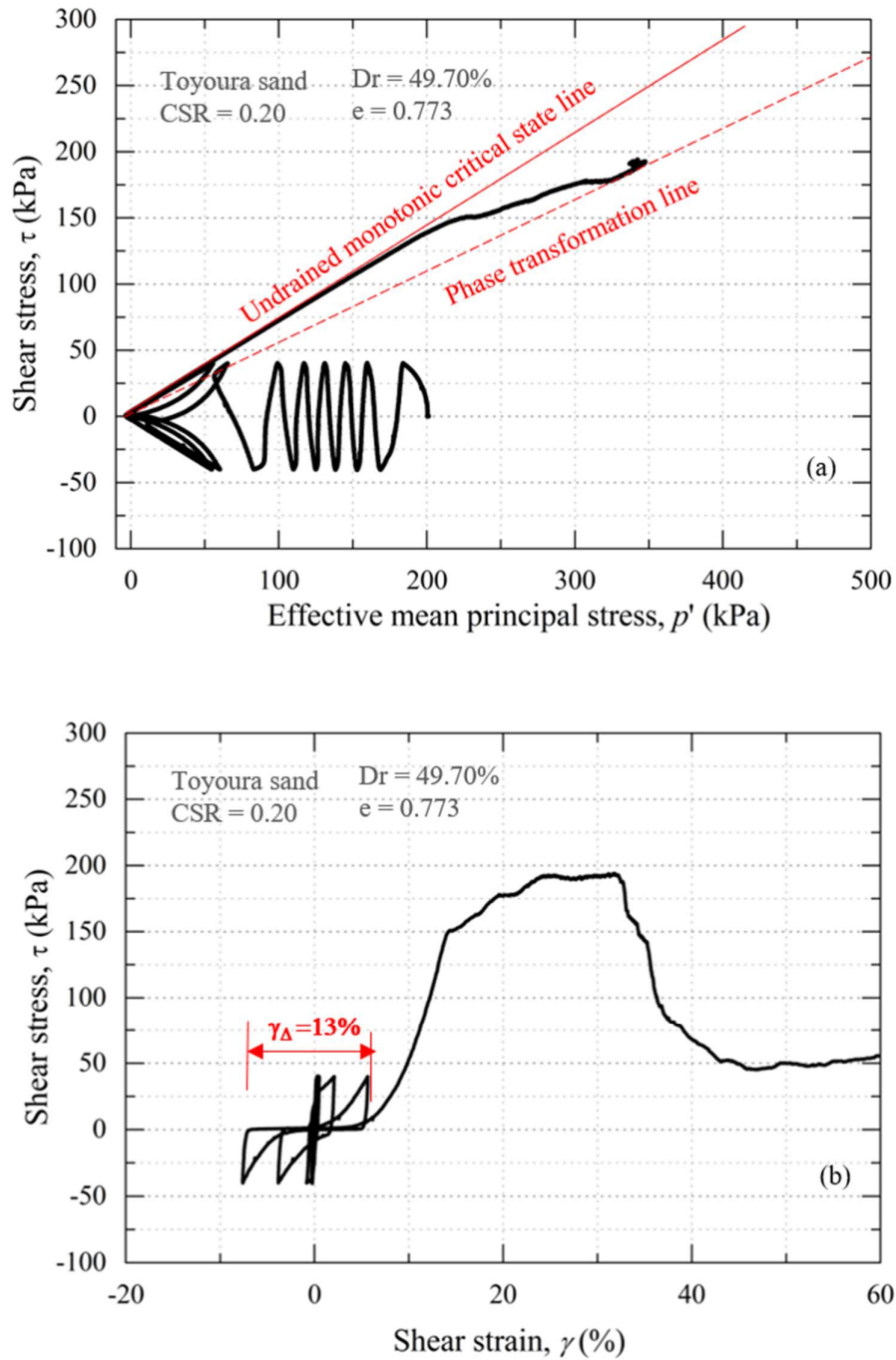
Figure 4.30: Typical test result with damage strain for $p'=200$kPa
a) Effective stress path b) stress strain relationship
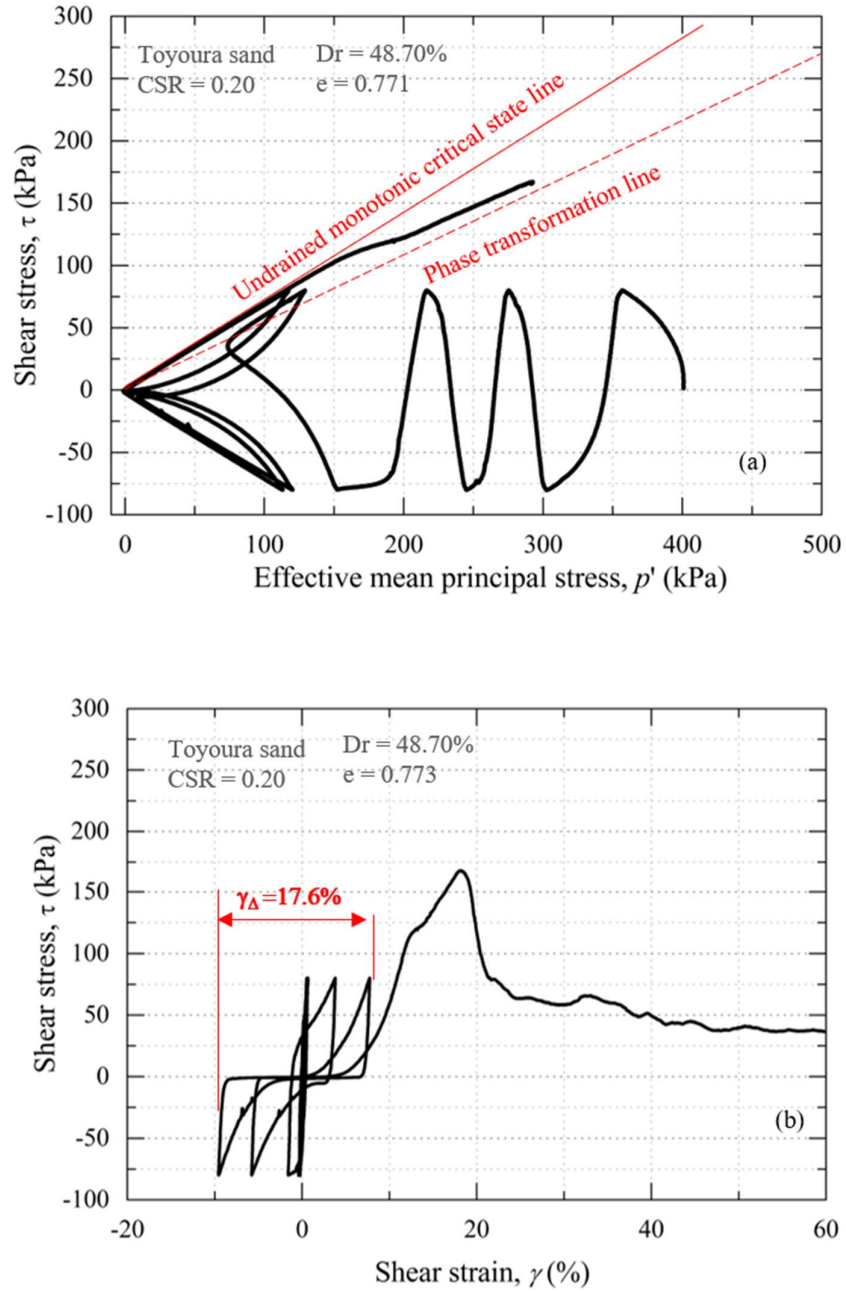
Figure 4.31: Typical test result with damage strain for $p'=400$kPa
a) Effective stress path b) stress-strain relationship

4.10   References

1) Ampadu, S. I. K. [1991]: *Undrained behavior of kaolin in simple torsional shear*, Ph.D. thesis, Dep. of Civil Engineering, University of Tokyo, Japan.

2) Castro, G., Keller, T. O., and Boynton, S. S.[1989]: *Re-evaluation of the Lower San Fernando Dam: Report 1, an investigation of the Feb-ruary 9, 1971 slide,* U.S. Army Corps of Engineers Contract Rep. No.GL-89-2, Vols. 1 and 2, U.S. Army Corps of Engineers Water ways Experiment Station, Vicksburg, Miss.

3) Castro, G. [1969]: *Liquefaction of Sands*, Ph.D. Thesis, Harvard University, Cambridge, Mass.

4) Chiaro, G., Koseki, J. and Sato, T. [2012]: *Effects of initial static shear on liquefaction and large deformation properties of loose saturated Toyoura sand in undrained cyclic torsional shear tests* Soil and Foundations 52(3): 498–510.

5) Chiaro, G., Kiyota, T. and Koseki, J. [2013]: *Strain localization of characteristics of loose saturated Toyoura sand in undrained cyclic torsional shear tests with initial static shear*, Soils and Found. 53: 23-34.

6) Chiaro, G., Kiyota, T. and Miyamoto, H. [2017b]: *Liquefaction potential and large deformation properties of Christchurch liquefied sand subjected to undrained cyclic torsional simple shear loading*, Proceeding of the 19th International Conference. on Soil Mechanics and Geotechnical Eng., Seoul, South Korea, 1497-1500.

7) Dash, S. [2010]: *Lateral pile–soil interaction in liquefiable soils*, PhD thesis, University of Oxford, Oxford, UK.

8) Dash, S., Bhattacharya, S. and Blakeborough, A. [2010]: *Bending–buckling interaction as a failure mechanism of piles in liquefiable soils*, Soil Dynamics Earthquake Engng 30, No. 1–2, 32–39.

9) Hyodo, M., Murata, H., Yasufuku, N., and Fujii, T. [1991]: *Undrained cyclic shear strength and residual shear strain of saturated sand bycyclic triaxial tests*, Soils Found.,313, 60–76.

10) Ishihara, K., Tatsuoka, F. and Yasuda, S. [1975]: *Undrained Deformation and Liquefaction of Sand Under Cyclic Stresses,* Soils and Foundations, Vol. 18, No. 4, pp.31-45.

11) Ishihara, K. and Yoshimine, M. [1992]: *Evaluation of Settlements in Sand Deposits Following Liquefaction during Earthquakes*, Soils and Foundations, Vol. 32, No.l, pp. 173-188.

12) Koester, J. P. [1993*]: Effects of fines type and content on liquefaction potential of low-to-medium plasticity fine-grained soils*."Proceeding of 1993 National Earthquake Conference, Central United States Earthquake Consortium,Memphis, Tenn., 1, 67–75.

13) Kokusho, T., Hara, T. and Hiraoka, R. [2004]: *Undrained shear strength of granular soils with different particle gradations*. Jouranl of Geotech. Geoenvironmental. Engineering 130, No. 6, 621–629.

14) Kiyota, T., Sato, T., Koseki, J. and Mohammad, A. [2008]: *Behavior of liquefied sands under extremely large strain levels in cyclic torsional shear tests*, Soils and Foundations 48(5): 727-739.

15) Kuerbis, R., Negussey, D., and Vaid, Y. P. [1988]: *Effect of gradation and fines content on the undrained response of sand*, Hydraulic fill structures, ASCE Geotechnical Engineering Division Specialty Publication No. 21, D. J. A. Van Zyl and S. G. Vick, eds., Fort Collins,Colo., 330–345.

16) Lombardi D, Dash SR, Bhattacharya S, Ibraim E, Wood DM, Taylor CA. [2017]: Construction of simplified design p-y curves for liquefied soils. Geotechnique 2017. http://dx.doi.org/10.1680/igeot.15.P.116.

17) Marcuson, W.M., Hynes, M.E., and Franklin, A.G. [1990]: Evaluation of use of residual strength in the seismic stability of embankments. Earthquake Spectra, 6(3): 529-572.

18) Okura, Y., Ochiai, H., and Sammori, T. [2002]: "The effect of void ratio on flow failure generation caused by monotonic liquefaction" International congress, congress publication, Volume 2. Pp 537-545

19) Papadimitriou, A. G., Dafalias, Y. F., and Yoshimine, M. [2005]:"Plasticity modeling of the effect of sample preparation method on sand response. "Soils Found., 45(2), 109–123.

20) Riemer, M.F., and Seed, R.B. [1997]: *Factors affecting apparent position of steady-state line.* Journal of Geotechnical Engineering, ASCE,123: 281ñ288.

21) Ross W. Boulanger, Ph.D., P.E [2010]: *Final technical report: Predicting void redistribution induced strength loss in liquefied soil*

22) Seed HB, Lee KL. [1996]: *Liquefaction of saturated sands during cyclic loading.* Journal of Soil Mechanics and Foundation Engineering ASCE 1966;92:105–34.

23) Seed, H. B., Seed, R. B., Harder, L. F., and Jong, H.-L.[1989]: *Re-evaluation of the Lower San Fernando Dam: Report 2, examination of the post-earthquake slide of February 9, 1971*, U.S. Army Corps of Engineers Contract Rep. No. GL-89-2, U.S. Army Corps of Engineers Waterways Experiment Station, Vicksburg, Miss.

24) Shamoto Y., Zhang JM, Goto, S., [1997]: *Mechanism of large post-liquefaction deformation in saturated sand*, Soils Foundation 1997;37(2):71–80.

25) Umar, M., Chiaro,G., and Kiyota, T., [2016]: *On the influence of initial static shear on large deformation behavior of very loose Toyoura sand in undrained cyclic torsional shear tests,* Proceeding of the 6th Japan-Korea Workshop.

26) Vaid Y.P. and Thomas, J. [1994]: *Post liquefaction behavior of sand*, Proceeding of Thirteenth International Conference on Soil Mechanics and Foundation Engineering, New Delhi, India, 1994: 1305 - 1310.

27) Vaid Y.P., Thomas, J. [1995]: *Liquefaction and post liquefaction behavior of sand,* Journal of Geotechnical Engineering ASCE 1995;121(2):163–73.

28) Vaid, Y.P., & Sivathayalan, S, [1997]: *Post liquefaction behavior of saturated sand under simple shear loading*, Proceeding of Fourteenth International Conference on Soil Mechanics and Foundation Engineering, Hamburg, 6-12 Sept 1997, 1: 221-224.

29) Verdugo, R., and Ishihara, K. [1996]: *The steady state of sandy soils*, Soils and Foundations, 36(2): 81–92.

30) Yoshimi, Y., and Oh-Oka, H. [1975]. I*nfluence of degree of shear stress reversal on the liquefaction potential of satu rated sand*, Soils and Foundations, 15(3), pp. 27-40.

31) Yoshida, N. [1995]: *Earthquake Response Analysis at Port Island during the 1995 Hyogoken-nanbu Earthquake*, Tsuchi-to-Kiso, 43, 10, pp49-54 (in Japanese)

32) Zlatovic, S., and Ishihara, K. [1997]: *Normalized behavior of very loose non-plastic soils Effects of fabric*. "Soils Foundation., 37(4), 47–56

CHAPTER 5

Strain localization influence on undrained strength

CHAPTER 5: Strain localization influence on undrained shear strength

LIST OF FIGURES

CHAPTER 5: Strain localization influence on undrained shear strength

5.1. Introduction

Strain localization (or the formation of the shear band) is frequently observed in sandy soils undergoing shear loadings and is considered an essential precursor of the failure of soils and relevant   geo-structures. During shearing, as the deformation becomes larger, the concentration of strain at a local zone within the element can occur, or to be precise the concentration of shear deformation into a narrow zone of intense shearing commonly referred to as a shear band.

Field observations from past and recent earthquakes have shown that very often liquefied soils have the potential to undergo substantial deformation. During the 1964 Niigata and 1983 Nihonkai-Chubu earthquakes, Japan, liquefaction-induced ground displacement reached several meters (Hamada et al. 1994). In 1971, the San Fernando earth-dam liquefied and collapsed during a powerful earthquake that hit Southern California, USA (Seed et al., 1975). More recently, during the 2011 Canterbury Earthquake Sequence (New Zealand) and 2011 Off the Pacific Coast of Tohoku Earthquake (Japan), extensive liquefaction-induced lateral spreading occurred and caused severe damage to residential buildings, lifeline facilities and major road infrastructures (Cubrinovski et al., 2011, Kiyota et al., 2011). Lateral spreading and liquefaction were also observed in a gentle slope nearby a damaged earth dam-embankment following the 2015 Gorkha Nepal Earthquake (Chiaro et al., 2015). The flow-type slope failure that produced the deadly Takanodai landslide has been associated with liquefaction-induced large deformation during the 2016 Kumamoto earthquake (Chiaro et al. 2017a). Attempt to methodically characterize such liquefaction-induced large displacement, physical model tests (e.g. Yasuda et al. (1994) and element tests (Kiyota et al. 2008 and Chiaro et al. 2012) have been carried out.

Due to its importance, since the 1950s, efforts have been made in measuring the shear band properties (thickness and orientation) and the stress-strain behavior within shear bands (e.g. Chu et al. 1996, Vardoulakis (1996), Mokni and Desrues (1998), Desrues and Viggiani (2004); Rechenmacher (2006), Daouadji et al. 2011, Kiyota et al. 2008, Chiaro et al. 2013, and Chiaro et al.2015). These studies identified some of the critical factors which influence the strain localization in the sand, i.e. density, confining pressure, initial static shear, boundary conditions, and the drainage conditions. Although these studies have provided much information, still many uncertainties exist about the initiation of shear bands and especially the influence on substantial deformation (Kiyota et al. 2008 and Chiaro et al. 2013, 2015).

Laboratory element tests enable evaluation of soil behavior under well-defined density-stress conditions. However, the simulation of large deformation of liquefied soils in laboratory element tests remains to be a significant challenge in geotechnical engineering, due mainly to technical limitation. In triaxial tests, for example, the axial strain levels employed are usually limited to 20% or less due to a more significant extent of non-uniform deformation of the specimen at higher strain levels. Moreover, commonly used triaxial devices fail to reproduce realistic stress conditions and soil deformation modes (Chiaro et al. 2013) that soils elements experience during earthquake, shakings, i.e. simple shear conditions. Conversely, technical limitations prevent the simulation of strains larger than 10-15% using conventional simple shear devices (Cappellaro et al., 2018). In contrast, by using a torsional shear apparatus on hollow cylindrical specimens, one can achieve higher strain levels by increasing the amount of torsional shear displacement that is applied to the specimen (Kiyota et al., 2008).

At substantial large strain level during cyclic shearing, liquefied soil gradually regains its strength and stiffness upon shearing upon dissipation of pore water pressure. However, after exceeding a threshold value of shear strain causing strain localization (concentration of shear deformation into a narrow zone of intense shearing commonly referred to as a shear band), a

progressive deterioration of stiffness and strength during cyclic mobility has been observed (Kiyota et al. 2008, 2013; Chiaro et al. 2013). Generally, the shear banding process begins at the state when the mobilized strength of soil reaches its peak and gradually develops as shear deformation continues. Full understanding of strain localization mechanisms (formation and evolution) is essential to most geotechnical problems, including liquefaction-induced large deformation (Kiyota et al. 2008, 2013, Chiaro et al. 2013). However, this is not an easy task due to the vast number of factors that need to be considered, such as density state, mean effective stress level, cyclic and static shear stresses, pre-shearing, soil type, etc. In this chapter, it providing new insights into the effect of liquefaction-induced cyclic shear strain (hereby referred to as "cyclic damage strain", γ_Δ) on the post-liquefaction undrained monotonic stress-strain response and peak strength of Toyoura sand by means of a series of tests performed in a modified torsional shear apparatus capable of achieving double amplitude shear strain (γ_{DA}) exceeding 120% under simple shear condition.

5.2. Large strain undrained monotonic test result and strain localization

5.2.1. Stress-strain relationship

In Figure 5.2 typical stress-strain relationship of Toyoura sand undergoing monotonic loading during undrained shearing is shown. The specimen initially showed a contractive behavior and achieved a transient speak shear stress marked by at a state A. Subsequently, as the shear strain level increased, the shear strength increased until reaching its peak of 207 kPa at state B. Whereas in Figure 5.1, in the effective stress path, during undrained loading specimen reached a state A (phase transformation), the behavior become dilative exceeding phase transformation. The dilation behavior continues with the increase in the monotonic loading. The behavior terminates reaching at state B and effective stress path continue to move toward zero.

Figure 5.3 shows excess pore water generation during undrained monotonic loading. During contractive behavior, positive excess pore water is generated. Exceeding phase transformation behavior, negative pore water was generated. Negative excess pore water pressure continues to generate during undrained monotonic loading and even exceed the state B, the ultimate shear stress on stress-strain relation, it continues to generate and reach the ultimate point. In contrary to effective stress path, negative excess pore water stabilizes and continuously generated in a linear manner which helps in maintaining the specimen shear resistant.

Specimen deformation at several states (numbered as to 1 through 5) is shown in Photo 1. State 1 corresponds to the initial state ($\gamma_{SA} = 0\%$) – a vertical reference line marked in red col-or is reported. From state 2 ($\gamma_{SA} = 5\%$) to 3 ($\gamma_{SA} = 10\%$), the deformation was uniform throughout the height of the specimen. The shear band(s) appeared between state 3 ($\gamma_{SA} = 10\%$) and 4 ($\gamma_{SA} = 20\%$). At state 5 ($\gamma_{SA} = 30\%$), the region near the top cap experienced larger deformation than that near pedestal indicating a non-uniform deformation distribution along with the height of the specimen.

The shear banding process is initiated at a state when the mobilized strength of geomaterial reaches its peak and develops as shear deformation with a strain softening. However, during undrained monotonic shearing, evaluation of shear band initiation and evolution is more complicated as compared to drained monotonic shearing. Shear strength in undrained shearing is mobilized by the combination of positive dilatancy as well as negative excess pore water pressure (Figure 5.3). Therefore, the stress-strain, effective stress path and generation of excess pore water pressure curves are insufficient to describe precisely initiation of strain localization (shear band formation) and its evolution. In addition, size-dependent stress-strain parameters in torsional shear strain lead to unreliable test results. Therefore, it is crucial to identify the region of non-uniformity in the specimen to avoid misleading experimental data.
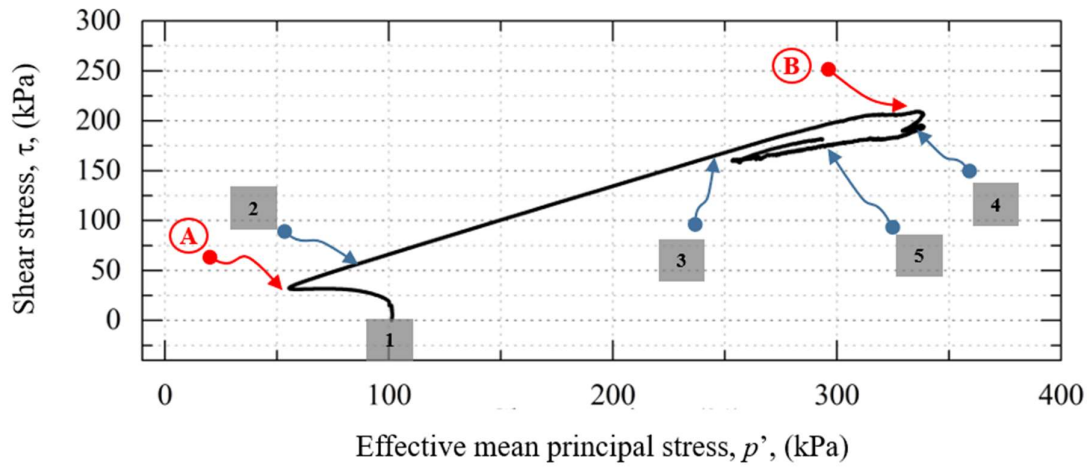
Figure 5.1: Effective stress path during undrained monotonic loading (Dr 47%)
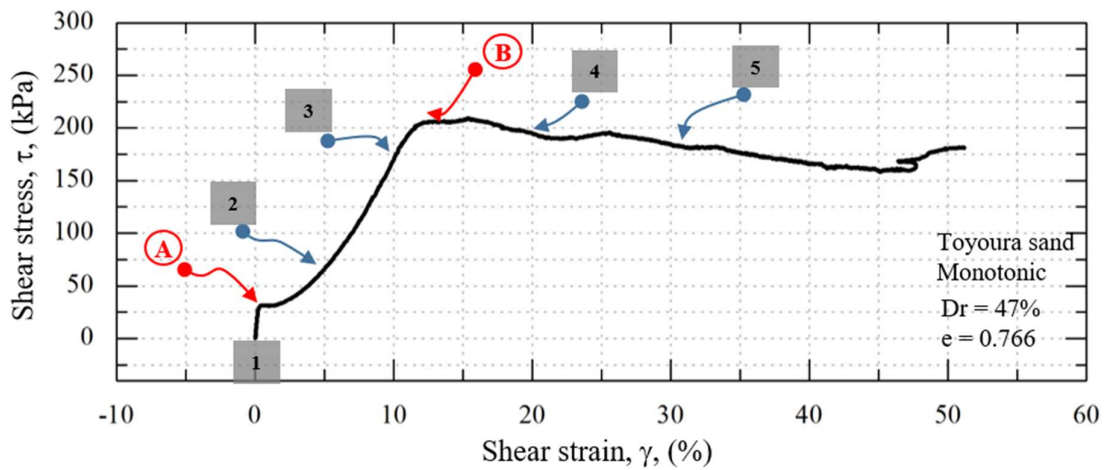
Figure 5.2: Stress strain relationship during undrained monotonic loading (Dr 47%)
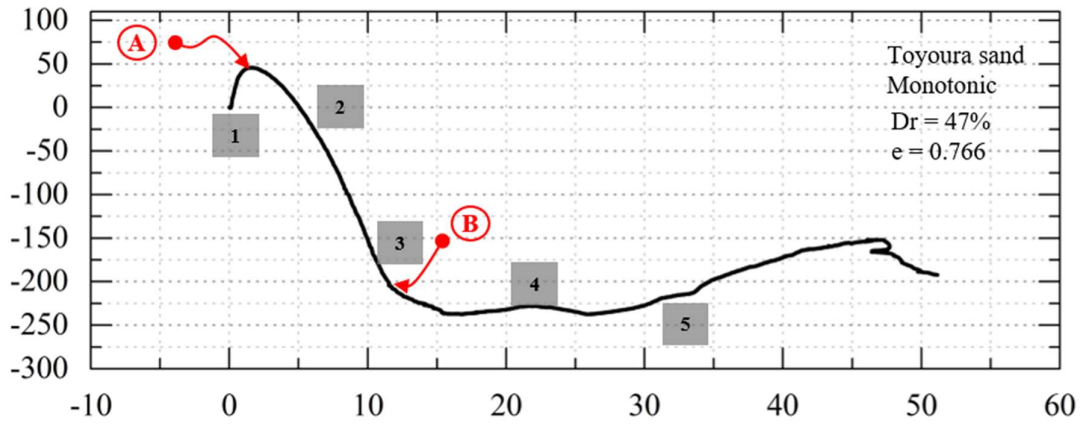
Figure 5.3: Excess pore water generation during undrained monotonic loading (Dr 47%)
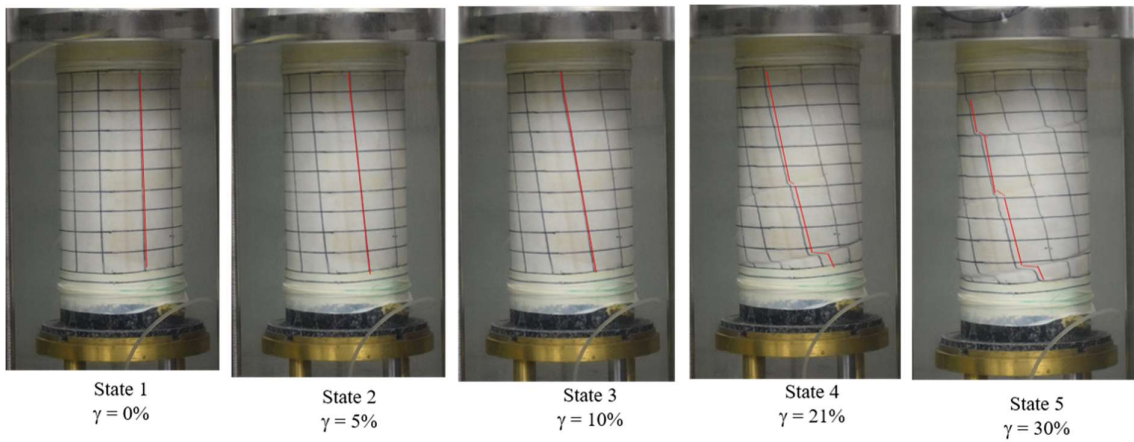
Photo 1: Specimen deformation during undrained monotonic loading (Dr 47%)

5.2.2. Variation of differential stress with shear strain

For the same test results shown in Figure 5.2 the variation of differential stress ($\sigma_d = \sigma_v - \sigma_h$) with shear strain is shown in Figure 5.4. Toyoura sand exhibited a peak value of 46 kPa at a shear strain of $\gamma_{SA} = 10.8\%$ (state AA in Figure 5.4), beyond which q value abruptly dropped to a negative value of -95 kPa at a shear strain of $\gamma_{SA} = 21\%$.

Recent studies by Kiyota et al. (2008) and Chiaro et al. (2013) on undrained torsional cyclic liquefaction test associated the sudden drop in σ_d value with the initiation of the shear band. Such a sudden drop in σ_d value is associated with the change in specimen response from volume expansion to contraction during undrained torsional shearing. More precisely, change in dilatancy characteristic from positive to negative, that is exhibited by volume expansion or contraction under fixed height.

In agreement with the above, the σ_d value drop in Figure 5.4 at state B ($\gamma_{SA} = 10.80\%$) can be considered s as the initiation of strain localization (i.e., limiting shear strain) under undrained monotonic loading. Differently from q, after at State AA, the shear stress continued to increase to a peak state B (Figure 5.2). Such a dissimilar response between shear stress and deviator stress is attributed to the mobilization of dilatancy as well as negative buildup pore water pressure locally (Figure 5.3) around and inside the shear band increased the shear stress. After exceeding the limiting shear strain to initiate strain localization, test results become defective due to specimen non-uniformity. Therefore, undrained peak shear stress was evaluated in correspondence of the limiting shear strain. This reduction in σ_d reached at the minimum value which is referred to as the end strain refers to as the formation of the shear band.

The shear stress at the limiting strain is defined as the limiting undrained shear strength and shear strength at the end strain is defined as the residual shear stress. Limiting shear stress has significant importance as it refers to as the shear strength achieved by the specimen before exhibiting a local non-uniform behavior.

Comparison of differential stress(σ_d) from a relative of 47%, 60% and 72% in Figure 5.4, Figure 5.6, and Figure 5.8 respectively shows that the with the increase in the relative density, differential stress increased, whereas limiting strain to cause strain localization reduced from 10.80% to 8.8%. The corresponding limiting undrained shear stress increased from 180kPa to 296kPa at state AA (Figure 5.5 and Figure 5.9). From this, it can be deduced that the limiting undrained shear to cause strain localization increased with the decrease in the limiting strain, with the increase in the relative density. This behavior resulted due to the denser specimen ability to reach faster dilative earlier under the undrained monotonic loading as compared to medium dense. Whereas the end strain at which the specimen reached the minimum value of differential stress (σ_d) referred as a residual state fluctuated between the shear of 16% to 21% with the increase in the relative density. Residual undrained strength increased with the increase in the relative density from 47% to 72%.

Figure 5.10 and Figure 5.11 shows the relationship between stress and strain, differential stress and shear strain for a relative density of 51% consolidated at effective stress of 200kPa. The specimen achieved a limiting strain at 10.80% (Figure 5.10), the same level as compared to the specimen consolidated at the 100kPa (Figure 5.5). This concludes that the limiting strain and end strain are independent of the confining pressure and dependent on the relative density.
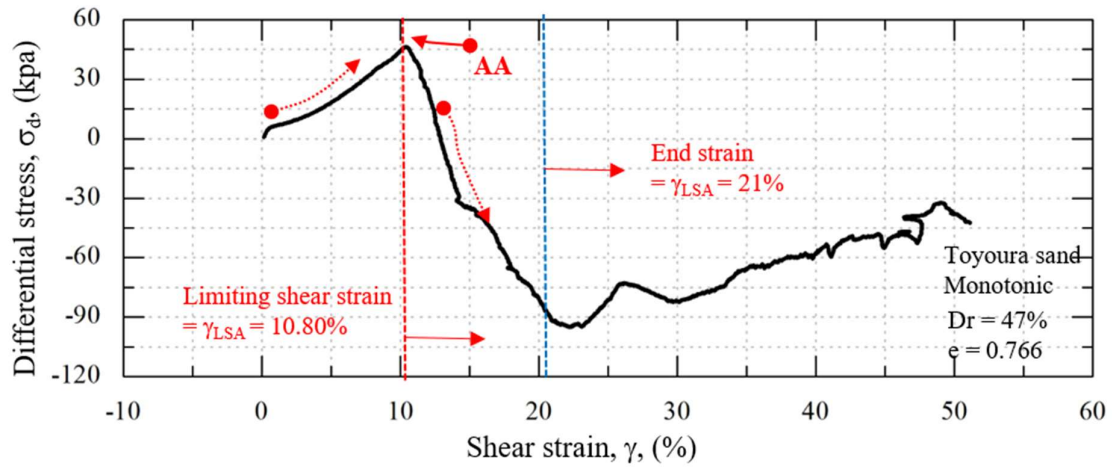
Figure 5.4: Differential stress(σ_d) variation during undrainedmonotonic loading (Dr 47%, , p'=100kPa)
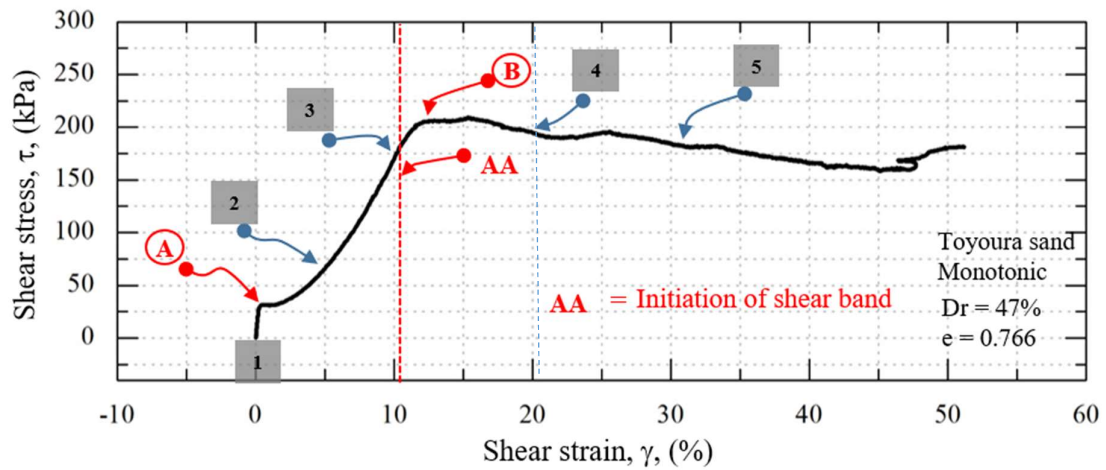
Figure 5.5: stress strain relationship during undrained monotonic loading

(Dr 47%, , p'=100kPa)
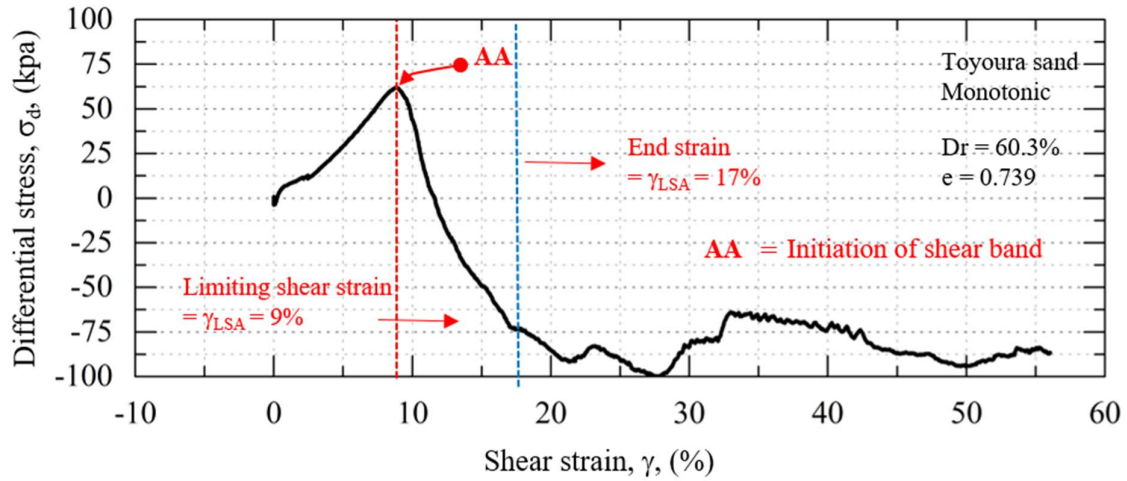
Figure 5.6: Differential stress(σ_d) variation during undrained monotonic loading
(Dr 60%, $p'=100$kPa)
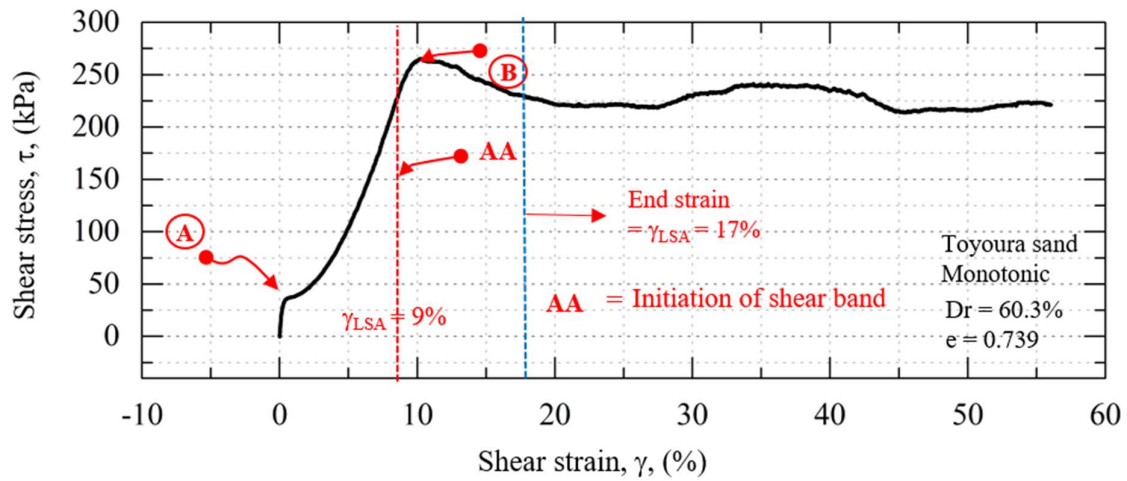
Figure 5.7: stress strain relationship during undrained monotonic loading
(Dr 60%, $p'=100$kPa)
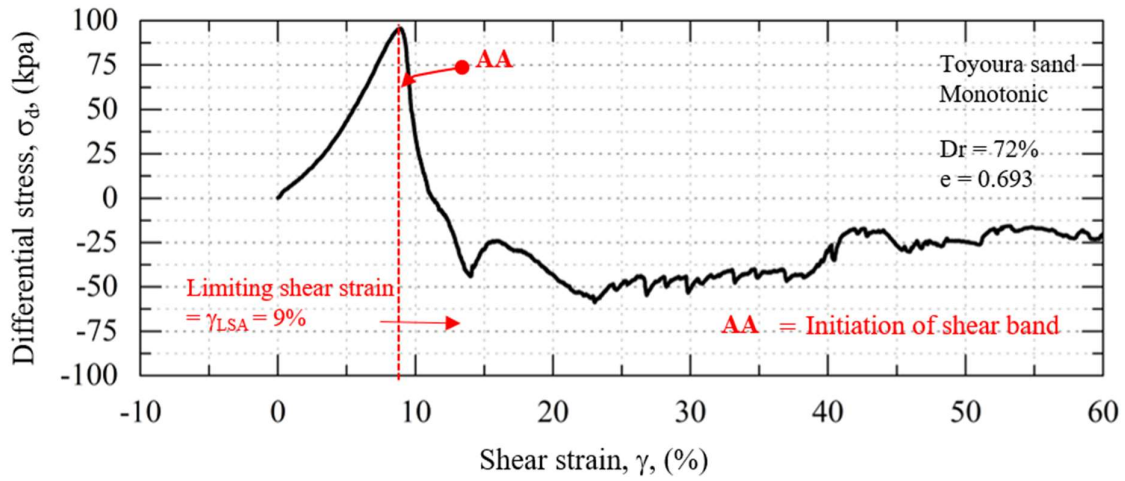
Figure 5.8: Differential stress(σ_d) variation during undrained monotonic loading
(Dr 72% , p'=100kPa)
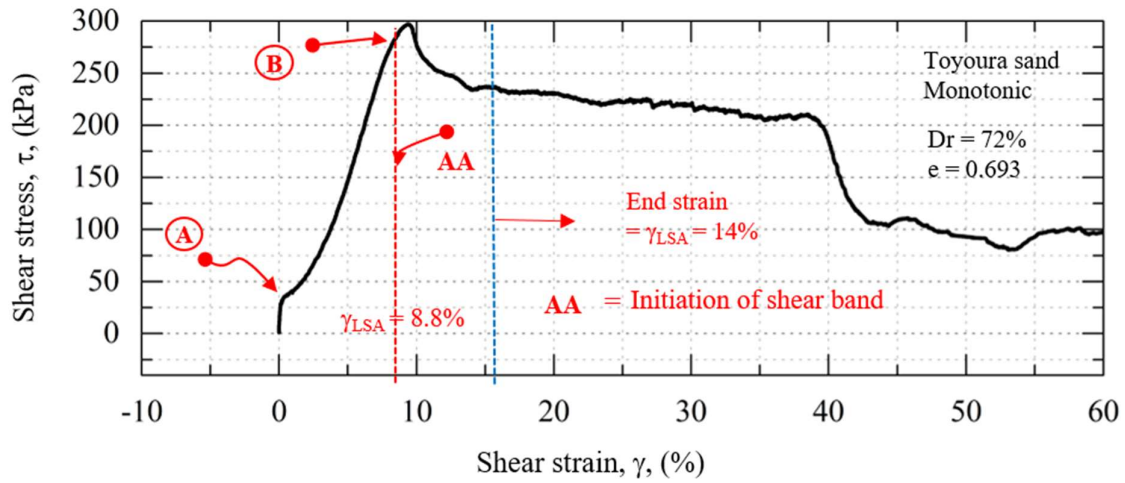
Figure 5.9: stress strain relationship during undrained monotonic loading

(Dr 72%, p'=100kPa)
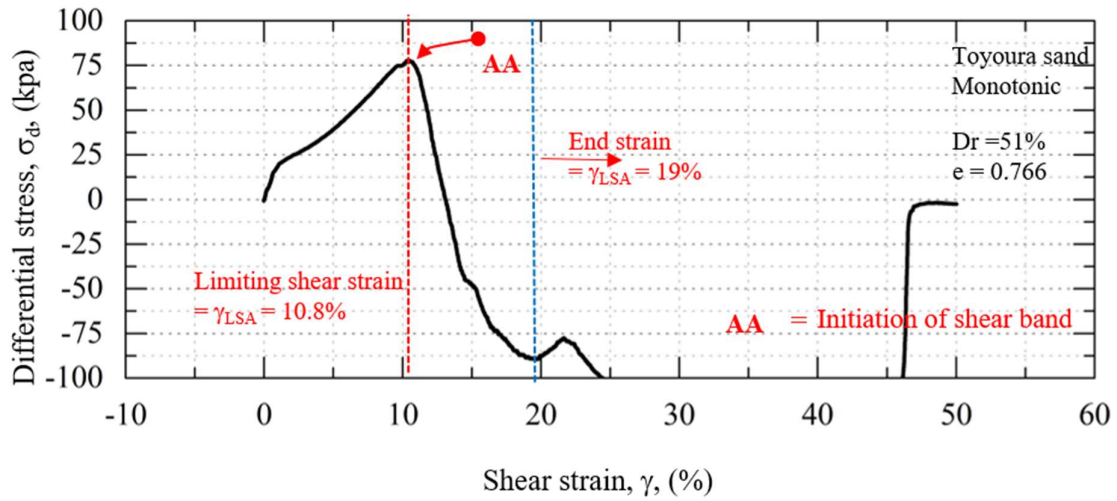
Figure 5.10: Differential stress(σ_d) variation during undrained monotonic loading
(Dr 51% , p_o'=200kPa)
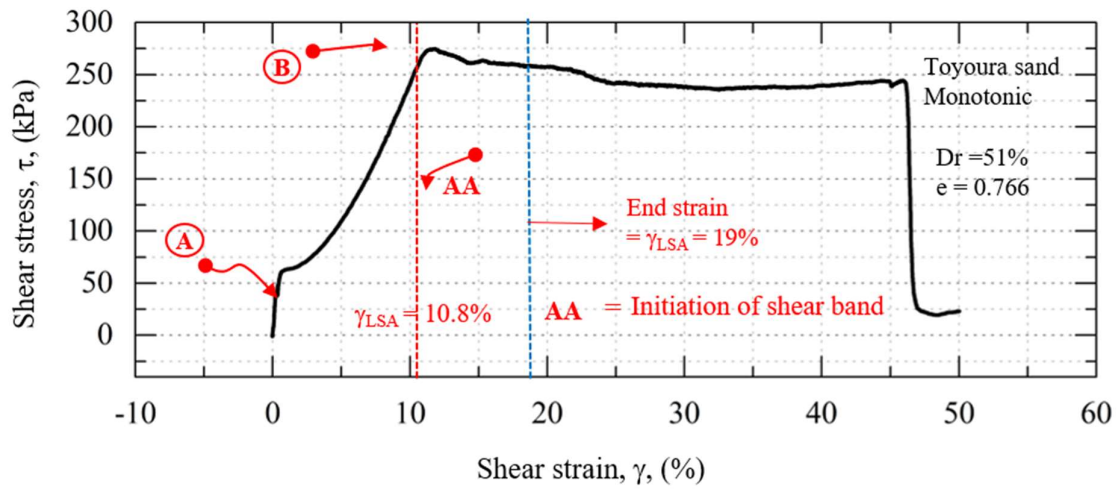
Figure 5.11: stress strain relationship during undrained monotonic loading
(Dr 51%, p'=200kPa)

5.2.3. Post-liquefaction monotonic stress-strain response and strain localization

Only a limited amount of studies have focused on the post-liquefaction behavior of liquefied soil, due mainly to the mechanical limitation of the element test to simulate extremely large deformation. Studies conducted by Yoshida et al. (1994), Vaid et al. (1995,1997) and Kokusho et al. (2004) concluded that the post-liquefaction behavior of sand subjected to undrained monotonic loading is dilative. Strictly speaking, the dilative behavior of granular material termites at the beginning of the formation of the shear band. As shown in section 5.2.3, non-liquefied specimen, shear band initiate before reaching the ultimate peak undrained strength. Using the same concept of development of shear and in undrained monotonic behavior in section 5.2.3, In this section undrained monotonic behavior of Toyoura sand is presented in terms of stress-strain for cyclic damage strain levels of of γ_Δ = 6, 13, and 22%, as shown in in Figure 5.13, Figure 5.15 and Figure 5.17 respectively. Following the initial liquefaction state (p_o'=0), soil strength recovered by cyclic mobility. During post-liquefaction undrained monotonic shearing, there is an initial deformation with zero stiffness with the increase in the shear strain and with further shearing, a gradual increase in the shear stress with an increase in the shear strain is observed. Similarly, to monotonic test, ultimate peak shear stress at which the non-uniform deformation imitated is marked by state AA in Figure 5.13, Figure 5.15 and Figure 5.17. Limiting undrained shear stress deteriorated from 135 kPa to 57 kPa with the increase of cyclic damage strain from 6 to 24%. This decay of shear strength is associated with a decrease in the stiffness during large strain with the increase in the cyclic damage strain.

Differential stress (σ_d) exhibit the same characteristics as observed in the non-liquefied specimen. During the undrained monotonic loading, the stiffness is recovered due to dilatancy and increased in the σ_d can be observed with different level of damage strain in Figure 5.12, Figure 5.14 and Figure 5.16 respectively. However, exceeding the point AA, it drops to the minimum point with the development of shear strain in the specimen.

It is interesting to note that the amplitude of σ_d decreased with the increase in the damage strain from 6% to 24%. As the amplitude of the damage strain is increased, it resulted in the deterioration in the capacity of the specimen to dilate. Which consequently resulted in the lower σ_d under quasi simple shear condition. Figure 5.18 and Figure 5.19 compares the variation of σ_d with the increase in the damage strain for medium dense and dense Toyoura sand. Consistent deterioration was observed in σ_d with the increase in damage strain regardless of the initial density state.

In the case of the liquefied specimen, the residual strength is higher due to strain hardening behavior of specimen during the evolution of the shear band. Presence of negative excess pore water pressure presence contributes to this increase in the residual strength. Whereas in case of drained loading, after strain hardening, a strain-softening behavior is observed mainly due to the absence of excess pore water pressure.
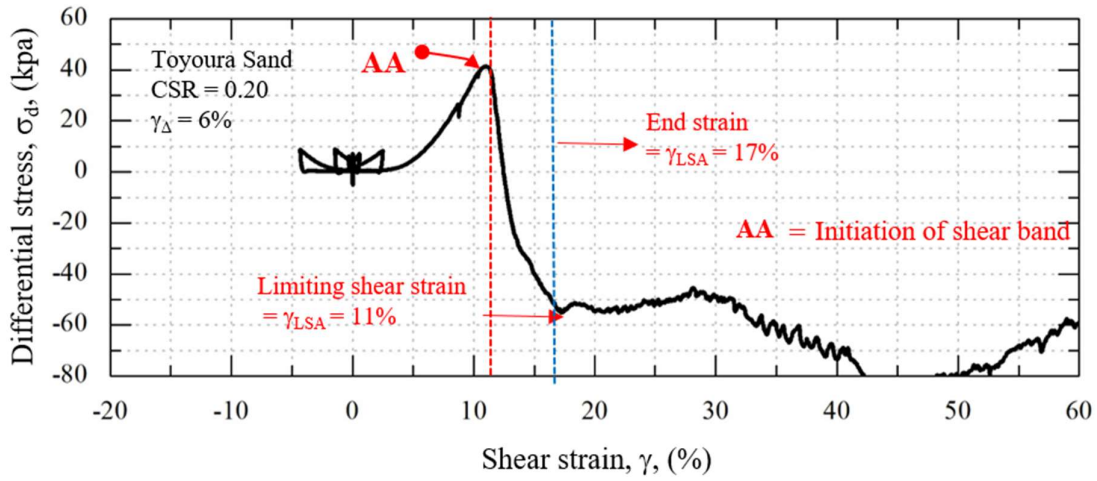
Figure 5.12: Differential stress(σ_d) variation during undrained monotonic loading
(Dr 52% , γ_Δ = 6%)
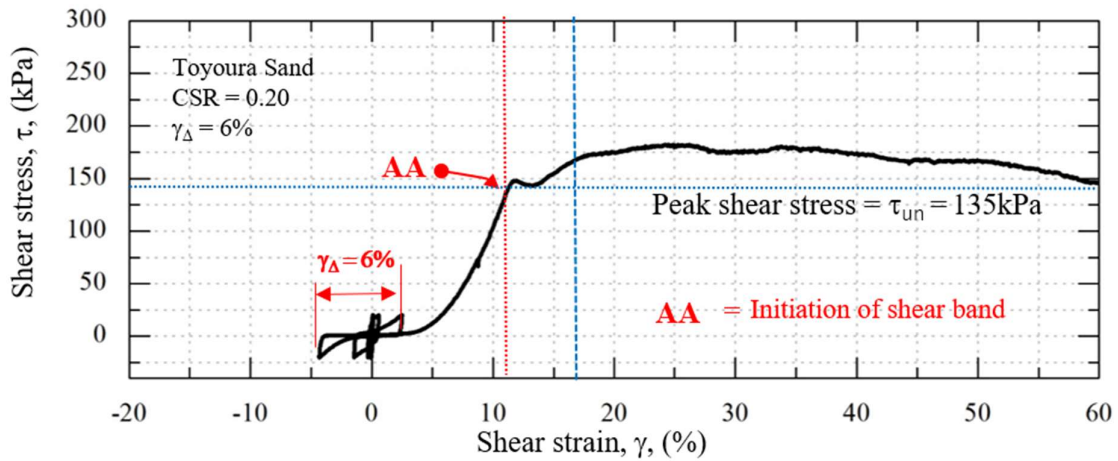
Figure 5.13: stress strain relationship during undrained monotonic loading
(Dr 52%, γ_Δ = 6%)
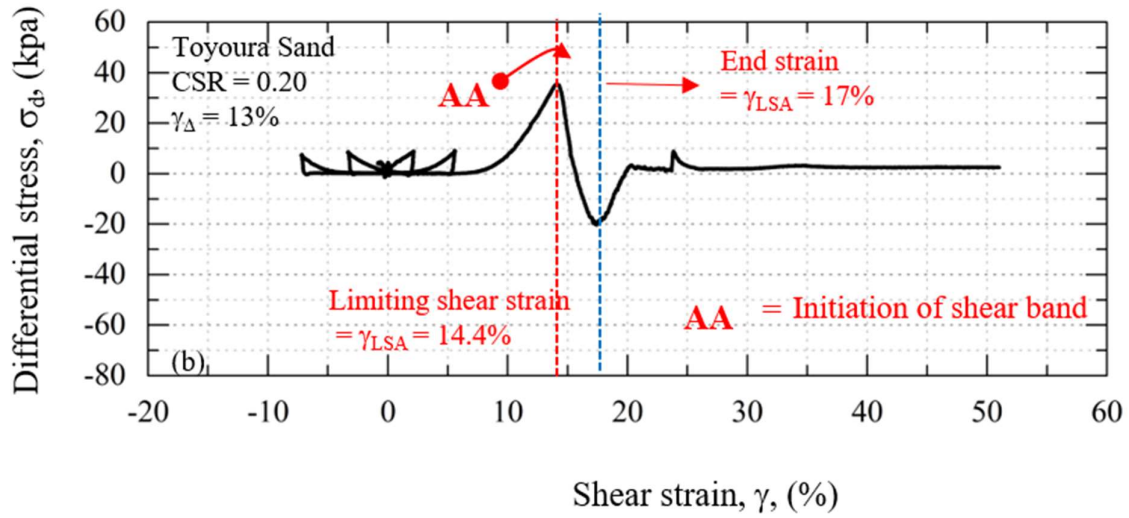
Figure 5.14: Differential stress(σ_d) variation during undrained monotonic loading
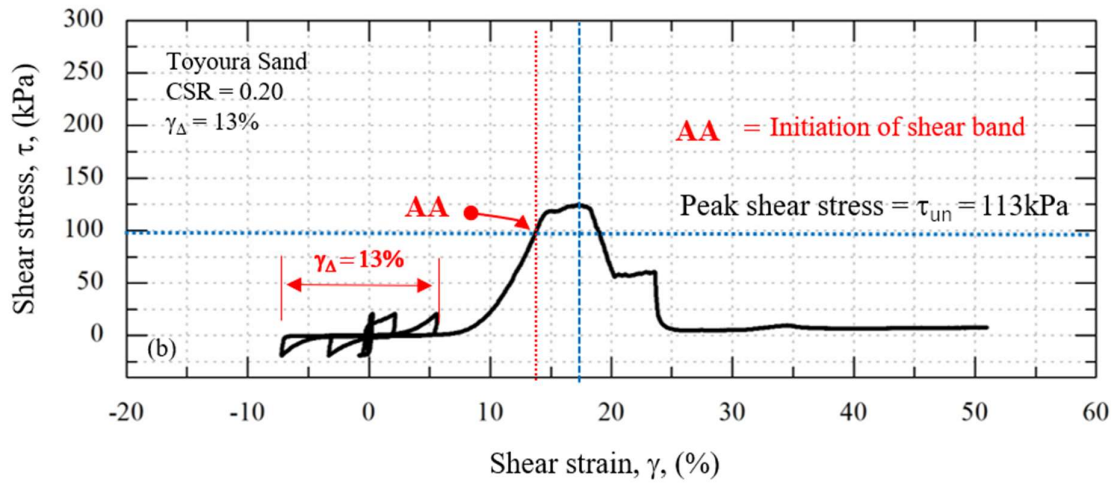
(Dr 47% , $\gamma_\Delta = 13\%$)

Figure 5.15: stress strain relationship during undrained monotonic loading

(Dr 47%, $\gamma_\Delta = 13\%$)
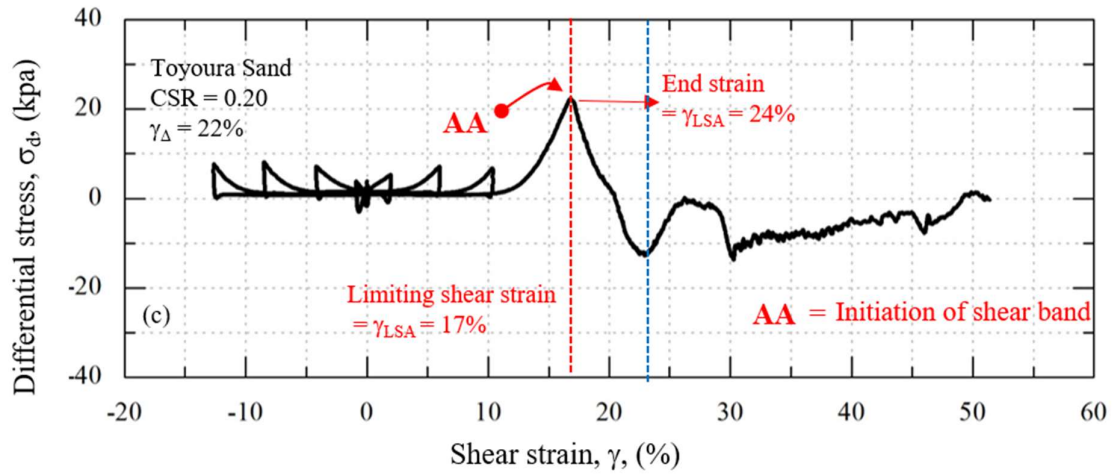
Figure 5.16: Differential stress(σ_d) variation during undrained monotonic loading
(Dr 50% , γ_Δ = 24%)
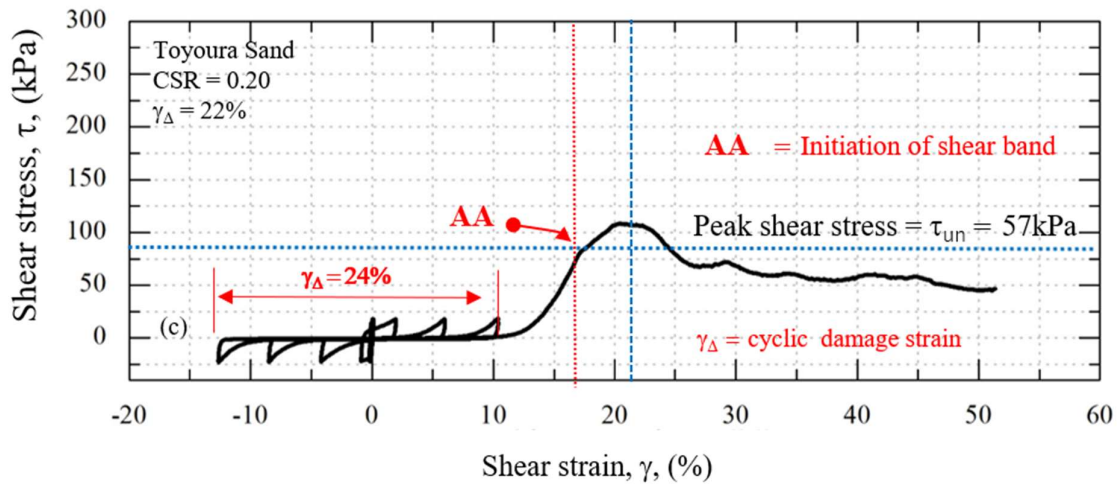
Figure 5.17: stress strain relationship during undrained monotonic loading
(Dr 50%, γ_Δ = 24%)
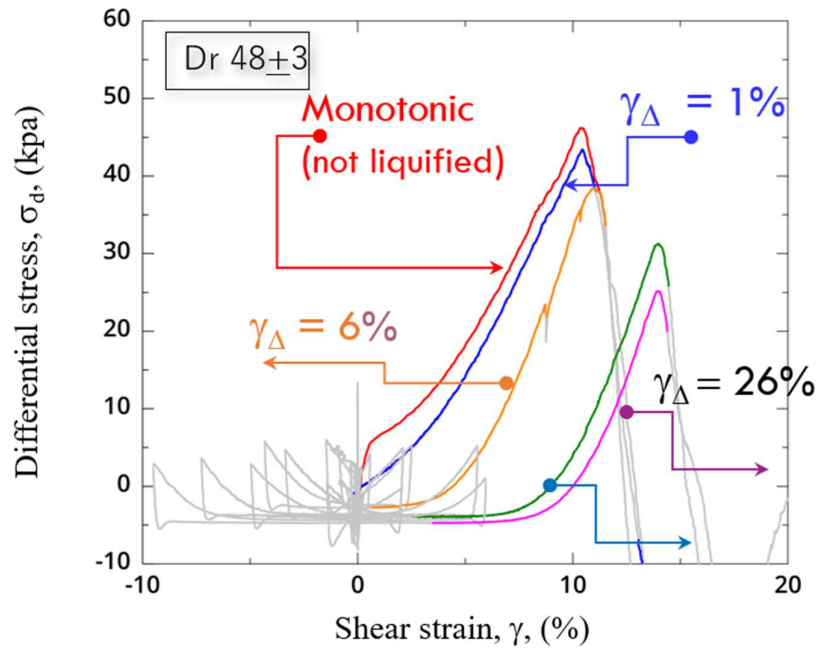
Figure 5.18: Variation of differential stress, σ_d with different amplitude of damage strain
(Dr 48$\pm$3%)
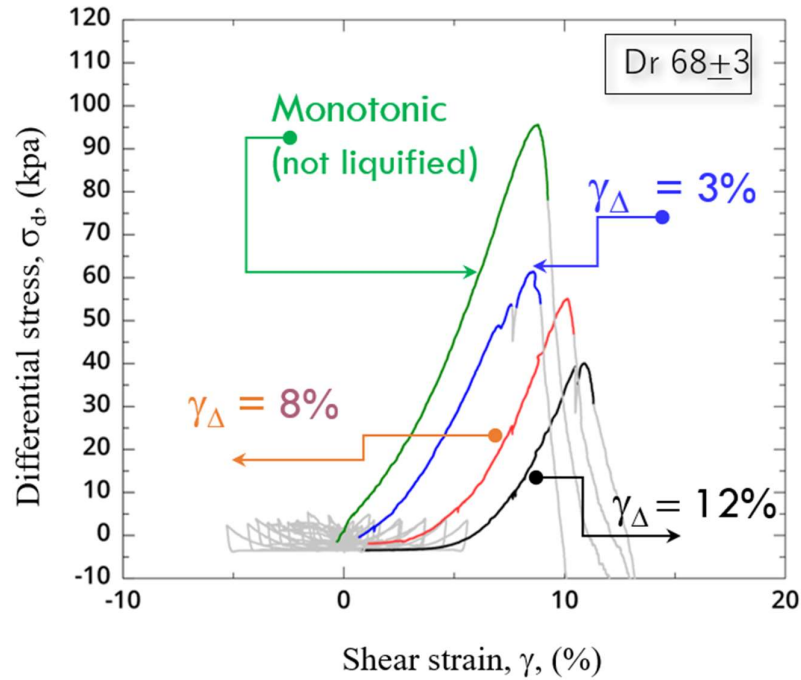
Figure 5.19: Variation of differential stress, σ_d with different amplitude of damage strain
(Dr 68$\pm$3%)

5.2.4. Relationship between damage strain and limiting strain

Exceeding a threshold shear strain called "limiting strain" under a monotonic or cyclic loading result in the formation of the shear band. This threshold acts as a barrier in the development of large strain. Previous studies by Kiyota et al. (2012) and Chiaro et al. (2011) showed that the limiting strain in undrained cyclic loading is the density-dependent and does not depend on the cyclic stress ratio. Figure 5.20 shows the relationship between damage strain and limiting shear strain in a single amplitude of shear strain for medium dense (48±3) and dense (68±3) Toyoura sand. It can be evident from the figure with the increase in the relative density, limiting strain is decreased. Whereas, for each density, there is a lower bound of limiting stain which is achieved without damage. The upper bound is achieved by applying constant amplitude cyclic loading. The combination of cyclic and monotonic loading resulted in the limiting strain higher that the monotonic test and small amplitude cyclic loading. This can be concluded that the cyclic loading delays the formation of shear strain and also lower the limiting undrained shear strength to cause strain localization.
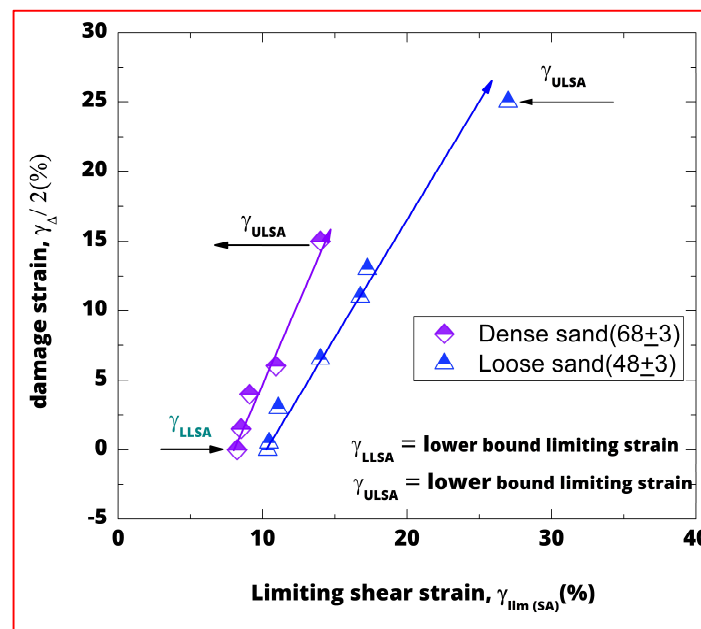
Figure 5.20: Relationship between limiting strain and damage strain

5.2.5. Degradation correlation considering strain localization

In this chapter, stain localization was discussed in detail. It can be concluded that the specimen failed due to strain localization during undrained loading. Exceeding limiting strain, significant non-uniformities was observed in the specimen. Therefore, the definition of limiting undrained strength is introduced to take strength until the specimen behaved uniformly. Figure 5.21 and Figure 5.22 shows the degradation of residual and limiting undrained strength evaluation based on the differential stress. Both the strength provides a good correlation along the data set obtained. As expected with higher density for the same level of damage strain, denser specimen exhibited lower strength deterioration as compared to medium dense.

An effective way of achieving a one degradation correlation is normalization each degraded strength with its undrained monotonic (without cyclic history). Figure 5.23 shows the normalized degraded strength which is defined by the following definition

$$\tau^* = \frac{\text{limiting shear stress at } (\tau_l)}{\text{limiting monotonic shear stress } (\tau_{l.mono})}$$

Where τ_l is the limiting undrained static strength after applying the damage strain, $\tau_{l.mono}$ is the limiting undrained monotonic strength(without any cyclic damage strain) and τ^* is the rate of degradation.
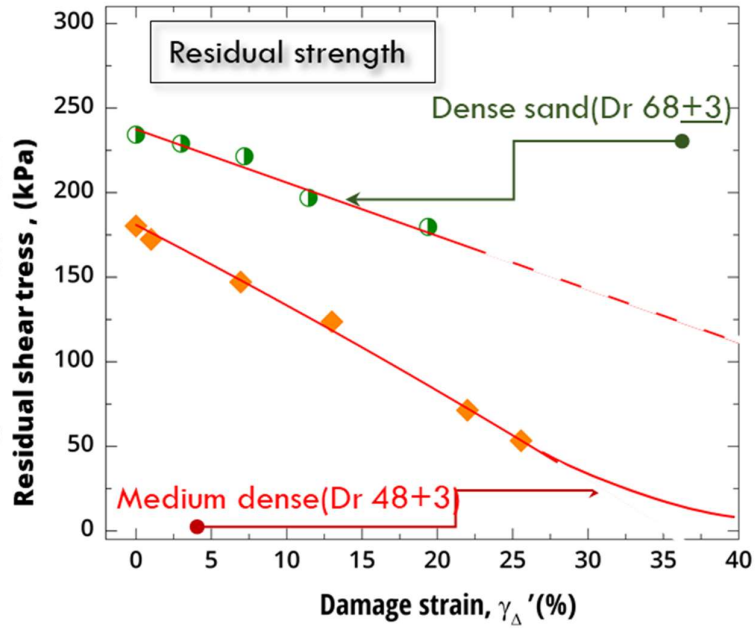
Figure 5.21: Degradation of undrained residual strength with damage strain
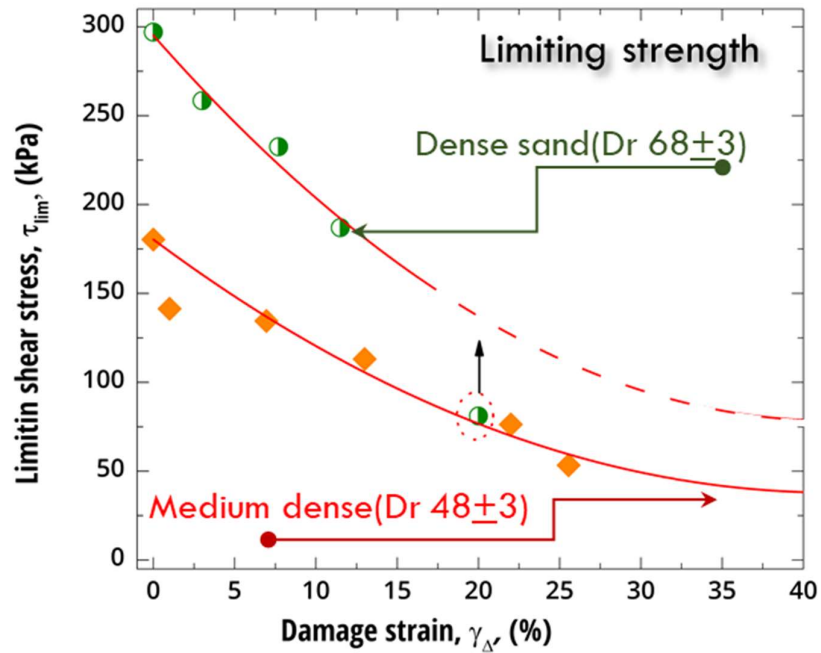
Figure 5.22: Degradation of limiting undrained strength with damage strain
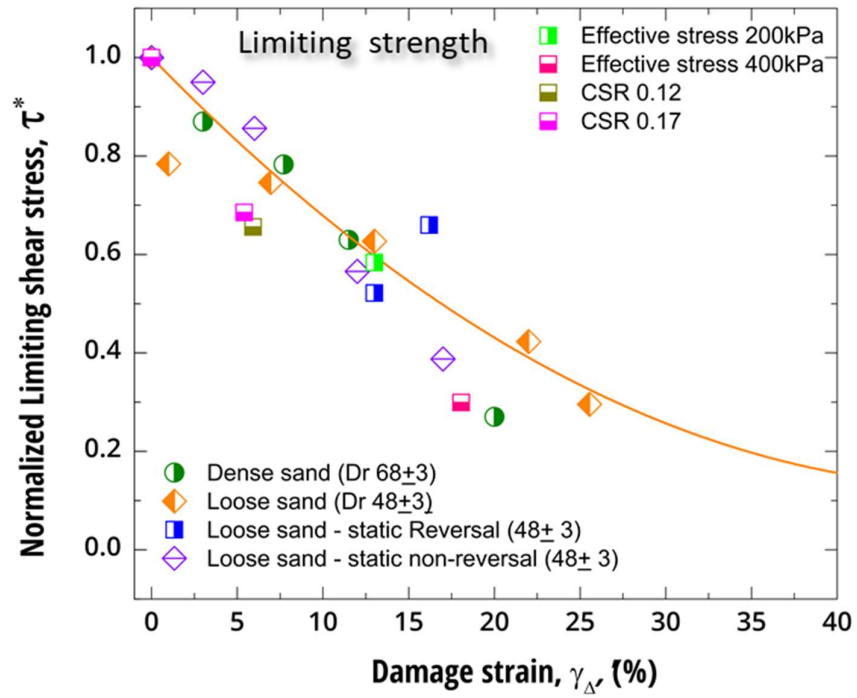
Figure 5.23: Normalized degradation of limiting undrained strength with damage strain

5.3. References

1) Cappellaro, C., Cubrinovski, M., Bray, J. D., Chiaro, G., Riemer, M. F. & Stringer, M. E. [2018]: *Comparisons in the cyclic direct shear response of two sands from Christchurch*, New Zealand, ASCE Geotechnical Special Publication 293: 150-159.

2) Cubrinovski, M., Bray, J.D., Taylor, M., Giorgini, S., Bradley, B.A., Wotherspoon, L. and Zupan, J. [2011]: *Soil liquefaction effects in the Central Business Districts during the February 2011 Christchurch Earthquake*, Seismological Research Letters, 82: 893-904.

3) Chiaro, G., Koseki, and Sato, T. [2012]: *Effects of initial static shear on liquefaction and large deformation properties of loose saturated Toyoura sand in undrained cyclic torsional shear tests*, *Soil and Foundations*, 52: 498–510

4) Chiaro, G., Kiyota, T. and Koseki, J. [2013a]: *Strain localization characteristics of loose saturated Toyoura sand in undrained cyclic torsional shear tests with initial static shear*, Soils and Foundations, 53: 23-34.

5) Chiaro, G., Koseki, J. and De Silva L.I.N. [2013b]: *A density- and stress-dependent elasto-plastic model for sands subjected to monotonic torsional shear loading*, SEAGS Geotechnical Engineering Journal, 44(2): 18-26.

6) Chiaro, G., Kiyota, T., Pokhrel, R.M., Goda, K., Katagiri, T. and Sharma, K. [2015]: *Reconnaissance report on geotechnical and structural damage caused by the 2015 Gorkha Earthquake, Nepal*, Soils and Foundations, 55: 1030-1043.

7) Chiaro, G., Alexander, G., Brabhaharan, P., Massey, C., Koseki, J., Yamada, S. and Aoyagi, Y. [2017]: *Reconnaissance report on geotechnical and geological aspects of the 2016 Kumamoto Earthquake, Japan*, Bulletin of the New Zealand Society for Earthquake Engineering, in press.

8) Chu, J., Lo, S.-C.R., Lee, I.K., [1996]: *Strain softening and shear band formation of sandin multi-axial testing,* Geotechnique 46 (1), 63–82.

9) Daouadji, A., Darve, F., Al Gali, H., Hicher, P.Y., Laouafa, F., Lignon, S., Nicot, F., Nova, R., Pinheir, M., Prunier, F., Sibille, L., Wan, R., [2011]: *Diffuse failure in geomaterials: experiments, theory and modeling.* Int. J. Numer. Anal. Methods Geomech. 35, 1731–1773.

10) Desrues, J., Viggiani, G. [2004]: *Strain localization in sand: an overview of the experimental results obtained in Grenoble using stereophotogrammetry.* Int. J. Numer. Anal. Meth. Geomech., 279–321.

11) Hamada, M., O'Rourke, T.D. and Yoshida, N. [1994]: *Liquefaction-induced large ground displacement,* Performance of Ground and Soil Structures during Earthquakes, 13th ICSMFE, 93-108.

12) Kiyota, T., Sato, T., Koseki, J., and Mohammad, A. [2008]: *Behavior of liquefied sands under extremely large strain levels in cyclic torsional shear tests*, Soils and Foundations, 48: 727-739.

13) Kiyota, T., Kyokawa, H. and Konagai, K. [2011]: *Geo-disaster report on the 2011 Tohoku-Pacific Coast Earthquake*, Bulletin of Earthquake Resistant Structure Research Center, 44: 17-27.

14) Kokusho, T., Hara, T. & Hiraoka, R. [2004]: *Undrained shear strength of granular soils with different particle gradations*, J. Geotech. Geoenviron. Engng 130, No. 6, 621–629.

15) Koseki, J., Yoshida, T. and Sato, T. [2005]: *Liquefaction properties of Toyoura sand in cyclic torsional shear tests under low confining stress*, Soils and Foundations, 45: 103-113.

16) Mokni, M., Desrues, J. [1998]: *Strain localization measurements in undrained planestrain biaxial tests on Hostun RF sand*, Mech. Cohes.-Frict. Mater. 4, 419–441.

17) Rechenmacher, A.L. [2006]: *Grain-scale processes governing shear band initiation and evolution in sands*. Int. J. Solids Struct. 54 (1), 22–45.

18) Seed, H.B., Idriss, I M., Lee, K.L. and Makadisi, F.I. [1975]: *Dynamic analysis of the slide in the Lower San Fernando Dam during the Earthquake of February 9*, Journal of Geotechnical.

19) Vaid Y, Thomas J. [1995]: *Liquefaction and post liquefaction behavior of sand,* J Geotech Eng ASCE 1995;121(2):163–73.

20) Vaid Y.P. and Sivathayalan S. [1997]: *Post liquefaction behavior of saturated sand under simple shear loading*, Proceeding Fourteenth International Conference on Soil Mechanics and Foundation Engineering, Hamburg, 6-12 Sept 1997, 1: 221-224.

21) Vardoulakis, I., [1996]: *Deformation of water-saturated sand*, I. Uniform undrained deformation and shear band. Geotechnique 46 (3), 441–456.

22) Yoshida, N. [1995]: *Earthquake Response Analysis at Port Island during the 1995 Hyogoken-nanbu Earthquake*," Tsuchi-to-Kiso, 43, 10, pp49-54 (in Japanese)

CHAPTER 6

3D image analysis to capture strain localization

CHAPTER 6: 3D image analysis to capture strain localization

LIST OF FIGURES

LIST OF TABLES

CHAPTER 6: 3D image analysis to capture strain localization

6.1.   Introduction

The onset of strain localisation is considered an important precursor of strength degradation leading to the failure of soils. During shearing, as shear deformations of a soil element becomes relatively larger, concentration of strain into a narrow zone of intense shearing occurs. Fully understanding of strain localisation onset and its mechanism are essential to study the failure and collapse characteristics of soils in most of earthquake-related geotechnical problems, including liquefaction-induced deformations.

In this instance, previous investigations conducted by Tatsuoka et al. (1986) via drained monotonic torsional shear tests on Toyoura sand under constant vertical and horizontal effective stress, reported that the formation of a shear band in sand specimen was attributed to a sudden reduction of the vertical strain (extension side) accumulated due to the mobilisation of positive dilatancy. Later, Kiyota et al. (2008), after performing undrained torsional shear tests on Toyoura sand, found out that the state response of the deviator stress q (i.e. the difference of vertical to horizontal stress $\sigma_d = \sigma_v - \sigma_h$,) to be consistent with the generation of the shear band observed by Tatsuoka et al. (1986), i.e. the state at which q suddenly drops. Kiyota et al. (2008) indicate that the shear strain defined at the moment of a sudden drop of σ_d is defined as that the limiting value of shear strain that causes strain localisation.

Kiyota et al (2008)'s limiting shear strain considers global measurement of shear strains in hollow-cylindrical sand specimens (i.e. shear strain in the whole specimen) which is calculated based on the torsional rotation of the specimen induced by the torsional torque applied to its top end. However, global strain measurement may underestimate the extent of strains in the specimen within the localised zone. This is, due to the effect of sustained shearing, shear strain development within the whole specimen varies significantly due to strain localisation, i.e.

strains develops largely, later shown in Figure 4 and 7, within the localised zone in contrast to zones outside the localised zone.

Therefore, in this chapter digital image correlation (DIC) is used to shed insights into local shear strain development and the formation of shear band(s) under simple shear conditions applied to Toyoura sand under undrained condition by a torsional shear apparatus. Figure 6.1 shows the comparison between a single camera and two camera used in 2D and 3D digital image correlation.
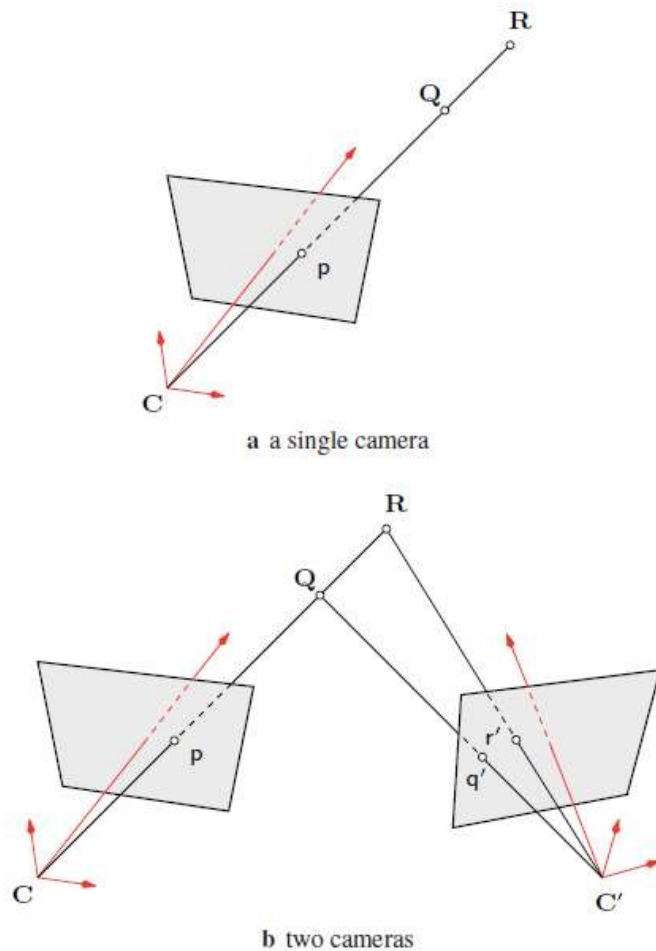
Figure 6.1: Recovering the third dimension by using two cameras

6.2.   Torsional shearing tests

6.2.1.   Torsional loading set-up

A fully automated torsional apparatus, developed by Kiyota et al. (2008) at the University of Tokyo, shown in Figure 1, was used in this study. The apparatus consists of a belt-driven torsional loading system that is connected to an AC servomotor through electro-magnetic clutches and a series of gears for velocity control. Torque and axial load are measured by a two-component load cell (axial load and torque capacities of 8kN and 0.15kNm, respectively) which is installed inside a pressure cell. Difference in pressure levels between the cell pressure and the pore water pressure are measured by a high-capacity differential pressure transducer (HCDPT) with a capacity of over 600kPa. Volume changes during the consolidation and initial shearing of a specimen are measured by a low-capacity differential pressure transducer (LCDPT). Shear stress amplitude is controlled by a computer, which monitors the outputs from the load cells and calculates the shear stress. The measured shear stress is then corrected to account the effects of membrane force.

6.2.2.   Specimen preparation and shear loading method

Toyoura sand (Gs = 2.659, e_{max} = 0.951, e_{min} = 0.608), a uniform sand with fines content <0.1%, was used in this investigation. Medium-size hollow cylindrical specimens, with dimensions of 100 mm in outer diameter, 60mm in inner diameter and 200mm in height, were prepared by air pluviation method, thus producing a sand fabric with horizontal bedding planes, at a relative density of 49 ± 3%. High degree of saturation (i.e. Skempton's B-value > 0.95) was achieved by the double vacuum method, while circulating de-aired water into the specimens. The specimens were isotropically consolidated by increasing the effective stress state up to a p_0' = 100 kPa, with a backpressure of 200 kPa.

Subsequently, to replicate seismic conditions in the field, a constant-amplitude cyclic torsional

shear stress (τ_{cyclic}) to a prescribed cyclic stress ratio (CSR) was applied to the sample at a shear strain rate of 0.5%/min. (Table 1). To mimic gentle slope condition, a static shear ratio was applied in drained monotonic shearing (SSR). During the process of undrained cyclic torsional loading, the vertical displacement of the top cap was prevented as much as possible to comply with simple shear conditions similar to that the ground undergoing horizontal seismic excitation.

Table 6.1 Torsional shear tests performed for 3D DIC

Test No.	Relative density Dr (%)	SSR	CSR	Mean effective stress (kPa) p_0'	Cyclic damage strain, γ_Δ (%)
1	47.0	0	Monotonic	100	0
2	47.9	0.15	0.12	100	3%
3	48.0	0.15	0.12	100	8%
4	45.8	0	0.20	100	24%
5	48.2	0	Monotonic (Dry sand)	100	0
6	47.0	0	Monotonic (inside cell dry sand)	100	0

6.2.3. Single-Camera 3D Digital Image Correlation

Digital image correlation (DIC) refers to the class of non-contact measurements methods that acquire images of an object, store images in digital form and perform image analysis to extract the full-field shape, deformation and motion measurements (Sutton M A, 2009).

3D DIC technique encompasses the use of two digital cameras (i.e. Two-Stereo Camera rig systems) positioned in the manner that the surface of the specimen is viewed from two different

angles that allow three-dimensional displacement measurements of a deformed object (Munoz et al, 2016a, b, Munoz et al, 2017a, b). Implementing this system generally, result costly. Therefore, this study firstly, presents the implementation of a low-cost 3DIC system by using a Single-Stereo Camera, see Yu et al. (2016) (Figure 6.2). Secondly, calibrate the system. The reflective effects of the cell and infilled water on the specimen were taken into account to extract correctly strains in the surface of the specimen. The complete stress-strain behavior of Toyoura sand in torsional shearing was coupled with the field of shear strains obtained via 3D DIC.
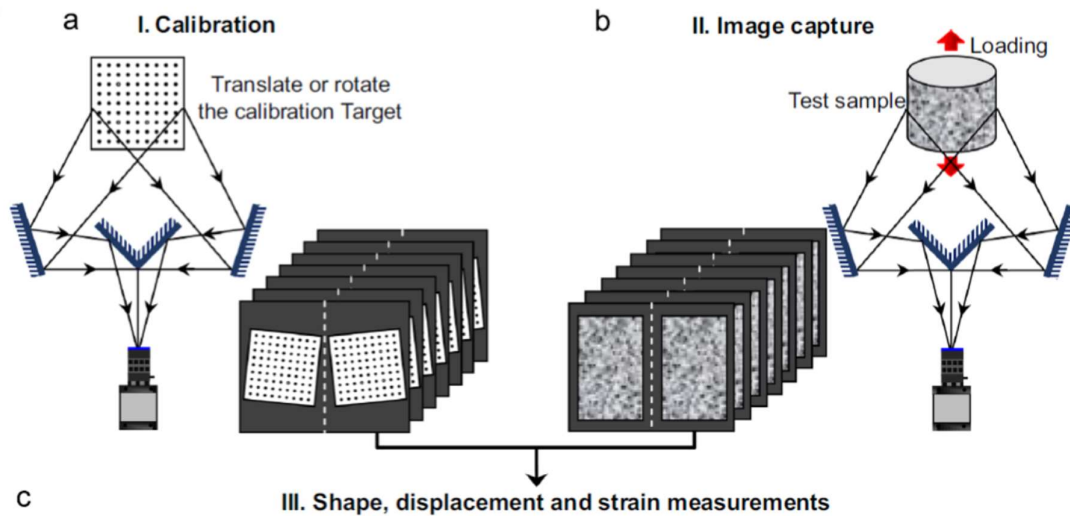
Figure 6.2: Illustration of the optical path of a single camera 3D DIC (Yu et. al 2016)

6.2.4. Speckle pattern preparation

DIC method relies on a contrasting random texture as speckle pattern in the surface of the specimen (Sutton et al. 2009). To this end, spray painting to speckle pattern the surface of an object is commonly used practice (Munoz et al, 2016a, b, Munoz et al, 2017a, b). In study, a speckle pattern was adhered to the surface of the membrane, which deformed with the surface of the soil sample, so no loss of correlation occurred (Figure 6. 4).

To achieve effective correlation, the speckle pattern was non-repetitive, isotropic and high in contrast, i.e. random pattern exhibiting no bias to an orientation and showing dark blacks and bright whites, adequate in size for high-strain resolution. By doing so, very sensitive defocus was avoided (Sutton et al. 2009).
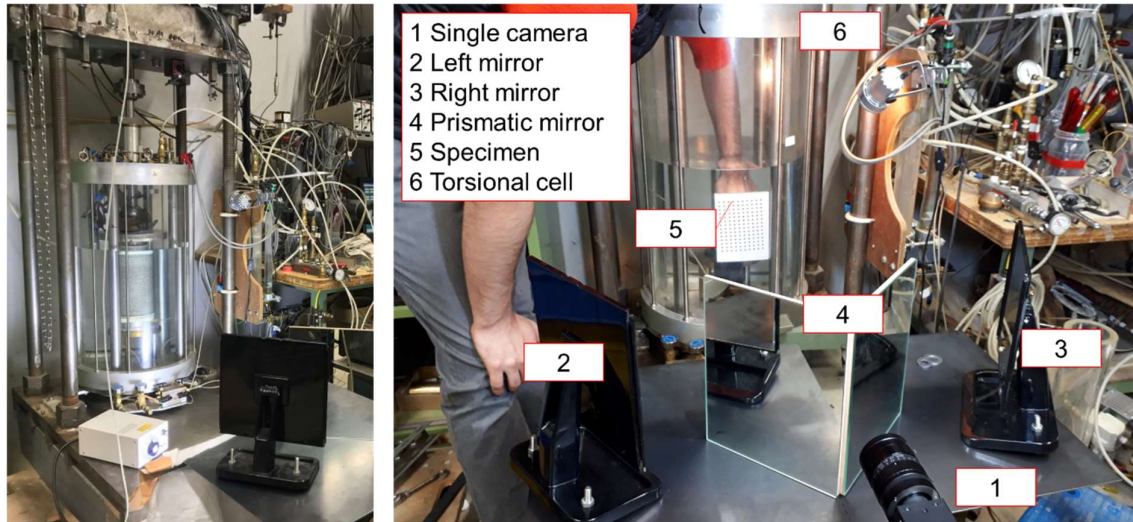
Figure 6. 3: Torsional apparatus and in-house DIC system.
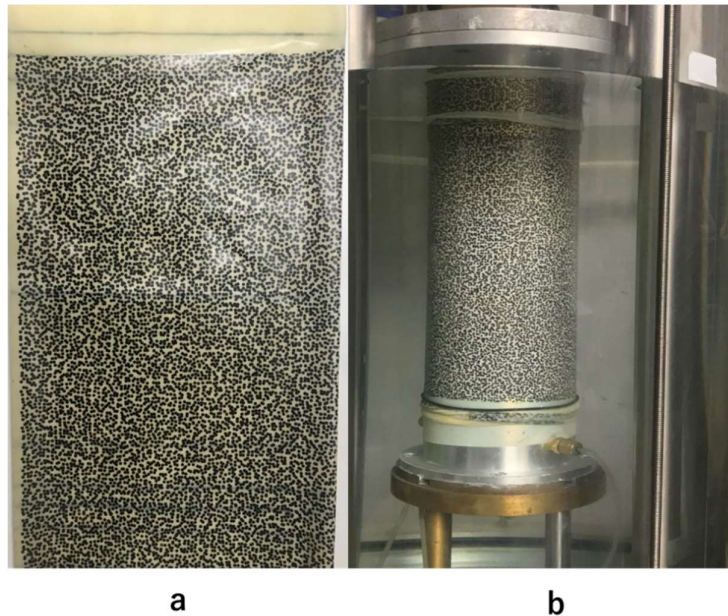
Figure 6. 4: Single camera 3D DIC setup and torsional apparatus used in the present study
a) Speckle pattern on b) Cylindrical specimen

6.2.5. Single-camera 3D DIC setup

Figure 6. 3: Torsional apparatus and in-house DIC system.shows the Single-Stereo camera system. The camera captured simultaneously the left and right digital grey-scale images. Typical left and right image pairs obtained by the camera during calibration are shown in Figure 2. The camera consisted of two high-resolution monochrome stereo cameras (i.e. Fujinon HF75SA-1, 1:1.8/75mm, 3 Megapixels resolution). Continuous and uniform illumination across the entire specimen was provided by a conveniently adjusted halogen light to ensure adequate contrast. The images were captured by a Snap software using an exposure time of 37 ms.

Prior to the shear torsional tests, each camera was stereo calibrated using a standard target having uniformly spaced markers. To do so, a calibration target was tilted and rotated, in and out of plane, nearby the site occupied by speckled specimen, as shown in Figure 6. 5.

The total images acquired during calibration were computed and analysed by VIC-3D software, see Figure 6. 5 VIC-3D software has been used effectively in a number of DIC material testing, e.g. Munoz et al. 2016a,b, 2017a,b. Stereo calibration results produced a standard deviation of residuals of 0.050-0.060 (in pixels), in general for all the tests. During the loading tests, the digital cameras were programmed to capture the images automatically at a frequency 1 Hz. A one-to-one correspondence between load, deformations, and respective digital images during the shear tests allowed studying strain development with stresses. Deformation measurements were concentrated within a portion of the specimen (i.e. the area of interest) as shown in Figure 2. VIC-3D software (produced by Correlated Solutions Inc.) was used for the analysis. This software implements image-processing algorithms for tracking surface coordinates and deformation from image to image. A subset size of 55 pixels was selected for accurate displacements measurements. Upon completion of image processing, the field of strains of the specimen's surface was obtained.
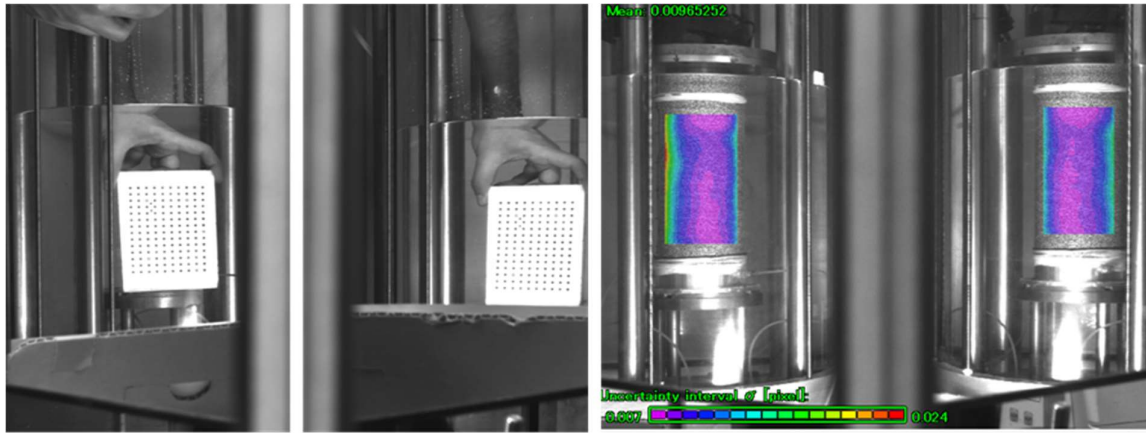
Figure 6. 5: a) Calibration target in water and b) example of results of a good quality pattern and lightening.

6.3.   Test results and discussion

6.3.1.   Field of shear strain during monotonic shearing

6.3.1.1.Typical global measurements

Typical shear stress, differential stress ($\sigma_d= \sigma_v-\sigma_h$) and excess pore water pressure versus shear strain (global) of the specimen is shown in Figure 3. Stress-strain curve exhibits the following: a strain hardening behavior from the beginning of loading at state A towards loading state B and E. Correspondingly, σ_d increased due to the mobilization of positive dilatancy until state D, consistent with the stress-strain relationship.

However, the amplitude of σ_d suddenly dropped from state D, whereas, shear stress continues to increase further towards state E. The sudden drop of σ_d is regarded as the change of specimen response from volume expansion to contraction by a formation of a shear band. Whereas, shear stress sustainably increased due to mobilization of dilatancy as well as negative buildup pore water pressure locally around and inside the shear band, i.e. from state D to E.

It was deemed that steady state for Toyoura sand under monotonic undrained loading, which is

defined as regime at which the specimen continues to deform under constant stress, begins at E at a global shear strain of 12%. The peak strength with this case reached 200 kPa at E.

6.3.1.2. Local measurements

Digital image correlation highly depends on the tracking of the speckle patter and their speckle distance between the points. However, when such a speckle pattern is submerged in the water, the distance between the speckle pattern is magnified. Therefore, it is important to validate DIC reliability to be used in the submerged specimen. Therefore, two serios of test was conducted, the one in which the vacuum is applied 100kPa, while keeping the sand unsaturated, followed by a torque on the top. In the second series of test the specimen were submerged in the water, followed by rotation on the top. The deformation is compared in the Figure 6.6 between rotation on the top and extraction local deformation by VIC 3D. It is evident from the comparison that the VIC 3D results are unaffected by the medium used to measure the local deformation. However when the rotation becomes significant large (at point 2 in Figure 6.6) small disagreement is observed between the measurement in the air and water.
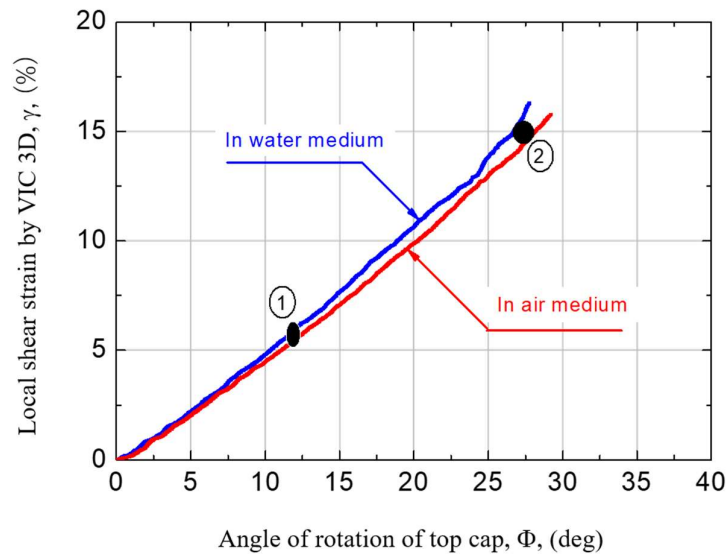
Figure 6.6: Comparison of local deformation of specimen in water and air

The corresponding local field of engineering shear strain evaluated by the VIC 3D is shown in Figure 6.9 The following features were observed:

Strain develops uniformly in the whole specimen in A to B. This can be seen by a single colour pattern, associated to strains in the order of 1%.

Stage C shows strain localising at a thin zone in the sample. In stage C, shear stress is about half of the peak stress at E. At stage C, outside the localised zone (green colour pattern) strains developed in the order of 8%, while inside the localised zones (cyan colour pattern) strains developed in the order of 15% in two localised zones. This feature shows that strains in localised zones can double the strains outside the localised zone.

At stage D, strain develops faster in the localised zones, i.e. in the first localised zone (purple colour pattern) in the order of 23% and the second (blue colour pattern) in the order 17%. Outside the localised zones, strains in the order 12% took place. Again, the ratio of strain in and out the localised zone seems in the two-fold order.

At peak stress at stage E, the shear band zone continues to expand (purple colour pattern) at a strain in order to 27%.

By the above discussion, at stage E, the global shear strain (global strain 12%) seems to underestimate the extent of local shear strains taking place in the localised zone (in the order of 27%) by at least two-fold.
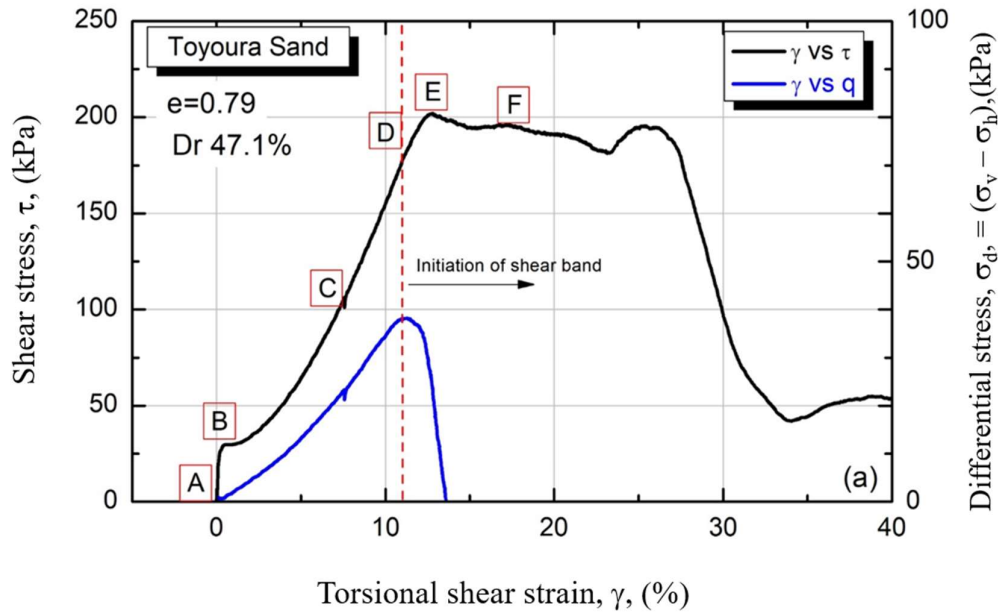
Figure 6.7: Stress vs strain and σ_d vs shear strain global plots during undrained monotonic torsional shearing. Letters A to F are loading stages
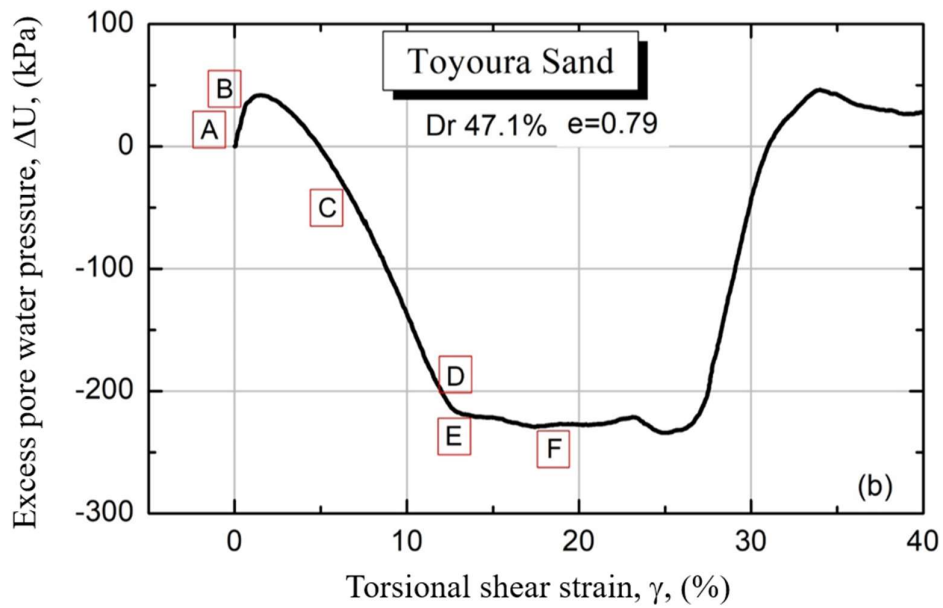
Figure 6.8: Excess pore water pressure vs strain global plots during undrained monotonic torsional shearing. Letters A to F are loading stages
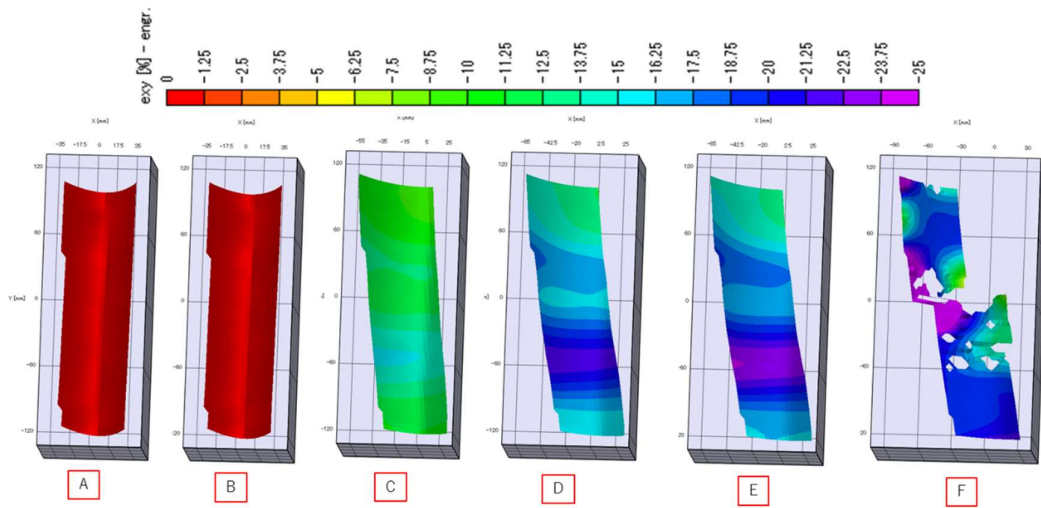
Figure 6.9: Field of strain in the specimen for loading stages A to F by DIC during monotonic load by VIC 3D
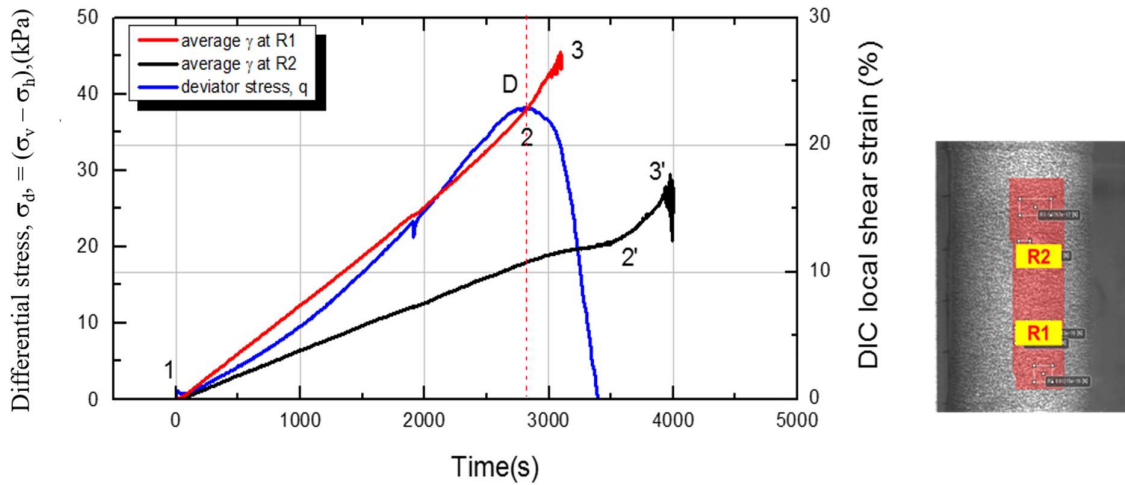
Figure 6.10: Field of strain in the specimen for loading stages A to F by DIC during monotonic load by VIC 3D

Further examination of the local strain characteristics supports the observations above. In Figure 6.10, local shear strain within (Region, R1) and outside (Region, R2) the localised zone have been extracted from the DIC measurements and compared with the time history of the change of q during the test. The following observations can be drawn:

Local strain for R1 show a constant rate of strain increment until state D, from point 1 to 2, of about 8×10^{-3} %/s. On the other hand, immediately after D takes place and the sample keeps experiencing stress and strains from D towards E, the local rate of strain increment increased faster to about 16×10^{-3} %/s, from point 2 to 3. This result indicates that the state of q sudden dropping at D can be associated to a faster increase in the development of strains inside the localised zone, i.e. a two-fold faster.

Similarly, local strain for R2 region show a constant rate of strain increment from 1 to 2', even after passing over state D and E, about 6×10^{-3} %/s, and then an increasing in strain rate from 2' to 3' of 14×10^{-3} %/s.

In additon the bifurcation between the magnitude of development of strain in R1, from 1 to 2 and 3, together with the magnitude of strain development in R2, from 1 to 2' and 3', suggest that the onset of non-homogeneous strains in the whole speciem, associated to the onset of localisation, takes place much before stage D. It seem that the onset of non-homogeneous strains takes place immediately after stage B.

Therefore, the stage where the deviator stress q drops seems to be the state at where shear strains inside the localised zone start to increase at a faster rate. This is important, as a faster increase in shear strains in the shear band can be associated to a faster degradation in strength of the specimen. By this behaviour, it seems that the strength capacity of the specimen after D could only attained and additional extra ~10% to reach the peak strength, from 180 kPa at D to 200 kPa at stage E.

6.3.2. Field of shear strain during cyclic excitation followed by monotonic loading

6.3.2.1. Typical global measurements:

Typical shear stress, deviator stress ($\sigma_d = \sigma_v\text{-}\sigma_h$) and excess pore water pressure versus shear strain (global) of the specimen is shown in Figure 6. This case corresponds to a non-reversal cyclic loading ($\tau_{static} > \tau_{cyclic}$) test. A specific cyclic damage strain ($\gamma_\Delta = 3\%$) from state A to B was induced to the specimen (i.e. cyclic excitation), after that a sustained monotonic loading was applied, i.e. from B following C to E until the end of the test, similarly to the monotonic test described above.

At state D in Figure 6.11, σ_d is suddenly drops, whereas shear stress sustainably increased to the end of the test. The peak strength at E only reached 182 kPa.

2.6.1. Local measurements

Figure 6.13 shows the field strain developed in the sample evaluated by VIC 3D at different loading states from A to F. This figure suggests the following.

The applied damage strain of 3% ($\gamma_\Delta = 3\%$) to the specimen induced a nearly homogeneous distribution of strain damage in the whole sample. This feature can be seen by comparing stages A and B in Figure 6.13, see the homogeneous light orange colour pattern in the sample in stage B.

After the end of the application of the cyclic damaging strain, further application of monotonic shear stress, induced further local shear strain growing in the sample in the order of 10 to 15% distributed nearly homogeneously in the sample as presented stage C. This feature can be seen by a nearly homogeneous green and cyan colour pattern in the sample. Although, a thin zone having a strain about 16% can be observed in stage C.

In Figure 6. 14, local time history of shear strain within (Region, R1) and outside (Region, R2) the localised zone is compared with the drop of q over time. Stage D is located in this figure. Consistent with a monotonic test, the rate in the increase of local strain in region R1 developed showing that before reaching state D, from point 1 to 2, about $7x10^{-3}$ %/s. On the other hand, immediately after D takes place towards E, the local rate of strain increment increased faster to about $21x10^{-3}$ %/s, from point 2 to 3, a three-fold faster. This result indicates that the state of σ_d sudden dropping at D can be associated to a faster increase in the development of strains inside the localised zone.

This feature can be seen through the colour patter at E, with strain in the order of 20-25% were observed, while at stage F, a broad localised zone was observed in the middle height of the specimen, > 25% (purple colour pattern).
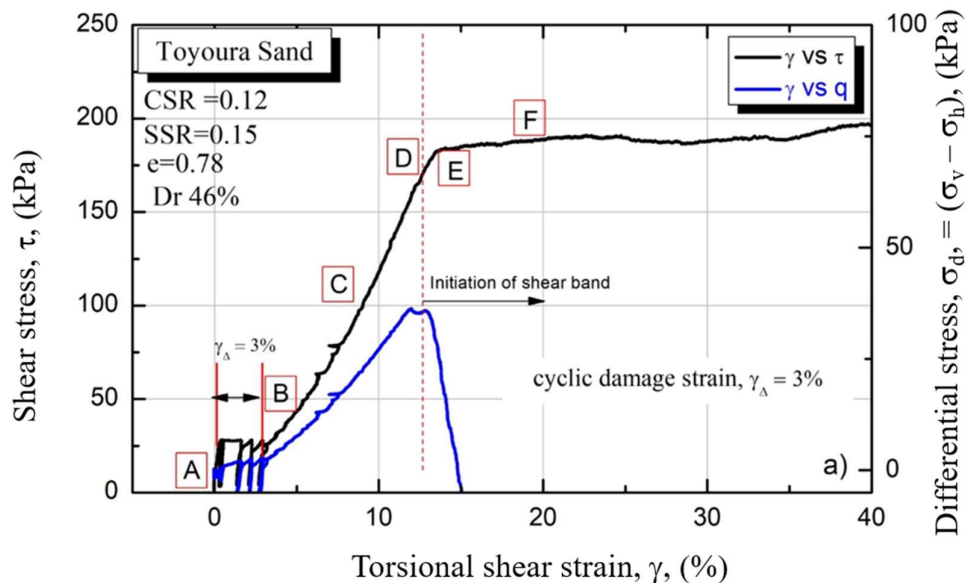
Figure 6.11: Stress vs strain and σ_d vs shear strain global plots during undrained monotonic torsional shearing. Letters A to F are loading stages for damage strain 3%
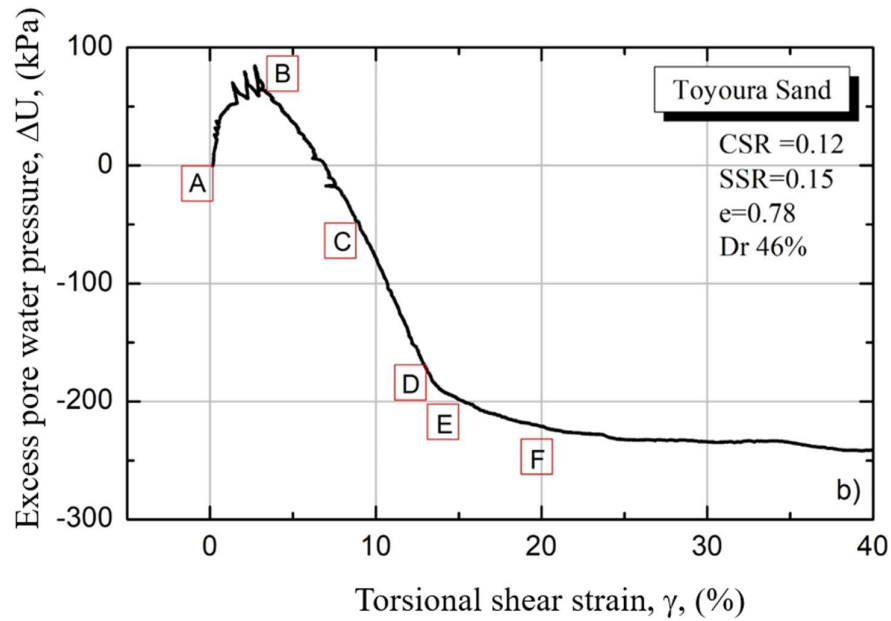
Figure 6.12: Excess pore water pressure vs strain global plots during undrained monotonic torsional shearing. Letters A to F are loading stages for damage strain 3%
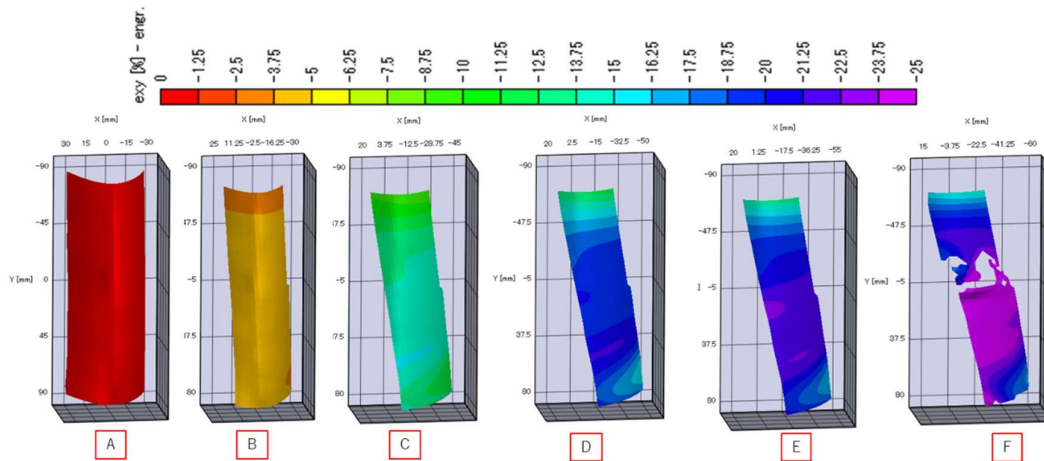
Figure 6.13: Field of strain in the specimen for loading stages A to F by DIC during cyclic load
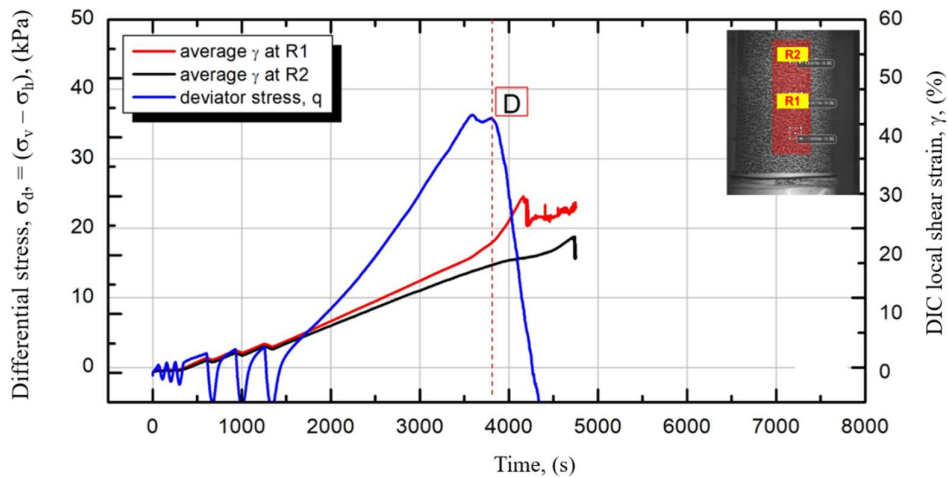
Figure 6. 14: Field of strain in the specimen for loading stages A to F by DIC during monotonic load by VIC 3D for damage strain 3%

Further comparisons between the rate of strain development to reach D indicates that with the specimen that was loaded monotonically from beginning to end was slightly faster, i.e. 8×10^{-3} %/s, in contrast with the specimen which was initially cyclically damaged to then loaded monotonically, i.e. 7×10^{-3} %/s. However, after D takes place, the rate of strain development in the former was 16×10^{-3} %/s and much faster about 21×10^{-3} %/s in the latter. This is important, as a faster increase in shear strains in the shear band can be associated with a faster degradation in strength of the specimen.

By this behaviour, it seems that the initial damaging strain of 3% induced a faster degradation of the strength capacity of the specimen after D, so that the peak strength with this case only reached 182 kPa, which is much lower than that 200 kPa with the case of the specimen without initial damage, a 10% lower.

Therefore, it can be speculated that an initial damage strain in the specimen take its toll in the specimen by accelerating further the strain development within the localised zone after D which can be the main contributor for a high degradation of strength after D. More research is needed in this regard.

By the above discussion, at stage E the global shear strain seems to underestimate (global strain

14%) the extent of local shear strains taking place in the localised zone (in the order of 27%) by a two-fold.

Studies by Kiyota et al. (2008) and Chiaro et al. (2015a) reported that the strain localisation with initial static shear is independent of the stress or strain loading. However, in this study, it was found localisation and the formation of a shear band may depend on the different rates of strain accumulation, after D, under monotonic and damaging strain cases. This can be a major factor for the degradation of the strength of the specimen. Other thing can be concluded that the D state on σ_d represent the initiation of shear band (strain localisation)

6.4.   Discussion

An in-house Single-Stereo Camera was employed to evaluate in field shear stain by 3D DIC for non-contact local shear strain measurement. The results shows that local strains taking place in the localise zone (a shear band) was larger, in the order of two-fold, to that the global average shear strain in the whole specimen) calculated based on the torsional force applied to the top of the specimen, in the order of two-fold. It is found that the rate of shear strain development inside a localised zone can be the major contributor to the strength degradation of the specimen.

6.5.   References

1) Chiaro, G., Kiyota, T. & Koseki, J. [2015]: *Strain localization characteristics of liquefied sands inundrained cyclic torsional shear tests*, Advances in Soil Mechanics and Geotechnical Engineering, IOS Press, 6 (1): 832-839.

2) Kiyota, T., Sato, T., Koseki, J. & Mohammad, A. [2008]: *Behavior of liquefied sands under extremely large strain levels in cyclic torsional shear tests*, Soils and Foundations, 48(5): 727-739.

3) Munoz, H., Taheri. A., and Chanda, E. [2016a]: *Fracture energy-based brittleness index development and brittleness quantification by pre-peak strength parameters in rock uniaxial compression*. Rock Mechanics and Rock Engineering, 49 (12): 4587–4606.

4) Munoz, H., Taheri, A., and Chanda, E. [2016b]: *Pre-peak and post-peak rock strain characteristics during uniaxial compression by 3D digital image correlation*, Rock Mechanics and Rock Engineering, 49 (7): 2541–2554.

5) Munoz, H., Taheri A. & Chanda, E. [2017a]: *Local damage and progressive localisation in porous sandstone*, Rock Mechanics and Rock Engineering, 50 (1): 3253–3259.

6) Munoz, H., Taheri, A., & Chanda, E. [2017b]: *Specimen aspect ratio and progressive field strain development of sandstone under uniaxial compression by three-dimensional digital image correlation*. Journal of Rock Mechanics and Geotechnical Engineering, 9 (1): 599-610.

7) Tatsuoka, F., Sonoda, S., Hara, K., Fukushima S. & Pradhan, T. B. S. [1986]: *Failure and deformation of sand in torsional shear,* Soils and Foundations, 26(4): 79-97.

8) Yu, L. and Pan B., [2016]: *Single-camera stereo-digital image correlation with a four-mirror adapter: optimised design and validation*. Optics and Lasers in Engineering, 87

(1): 120-128.

CHAPTER 7
Fujinuma Dam Stability Analysis by Newmark-D

CHAPTER 7: Fujinuma dam stability analysis by Newmark-D

TABLE OF FIGURES

CHAPTER 7: Fujinuma dam stability analysis by Newmark-D

7.1. Introduction

After World War 2, several irrigation dams were constructed. Fujinuma dam, whose purpose to serve as an irrigation reservation was located in Sukagawa city, Fukushima, Japan. It had a main and auxiliary dam. Both dam construction started in April 1937, then suspended in the world war II duration and latter completed in 1949. The main dam was earthen fill dam with a crest length of 133.3m and height of 18.5m. This dam was constructed in a layered manner and had no central impervious core (Figure 7.1) The auxiliary was an earthen fill with a crest length of 72.5m and height of 10.5m. Figure 7.1 shows the cross-section of the dam.

Fuji main dam and auxiliary dam collapsed during the 2011 Tohoku earthquake, resulted in the impounding of water (Figure 7. 2) downstream causing loss to infrastructure and loss of human life whereas 750 irrigation dams were partially damaged.

Successive studies were done to investigate the reason of the collapse of Fujinuma dam. Most of the studies is in agreement that the dam had a loosely compacted sandy fill (Figure 7. 3), which resulted in the low undrained strength. Tanaka et al. (2013) also added the deteriorated of undrained strength during long exposure of stress history of the Tohoku earthquake, a possible cause of failure.

Gradation curves and compaction of different layer calculated by retrieved material from collapsed Fujinuma dam is presented in Figure 7. 4.The details of other measures were presented in Tatsuoka et al. (2017).
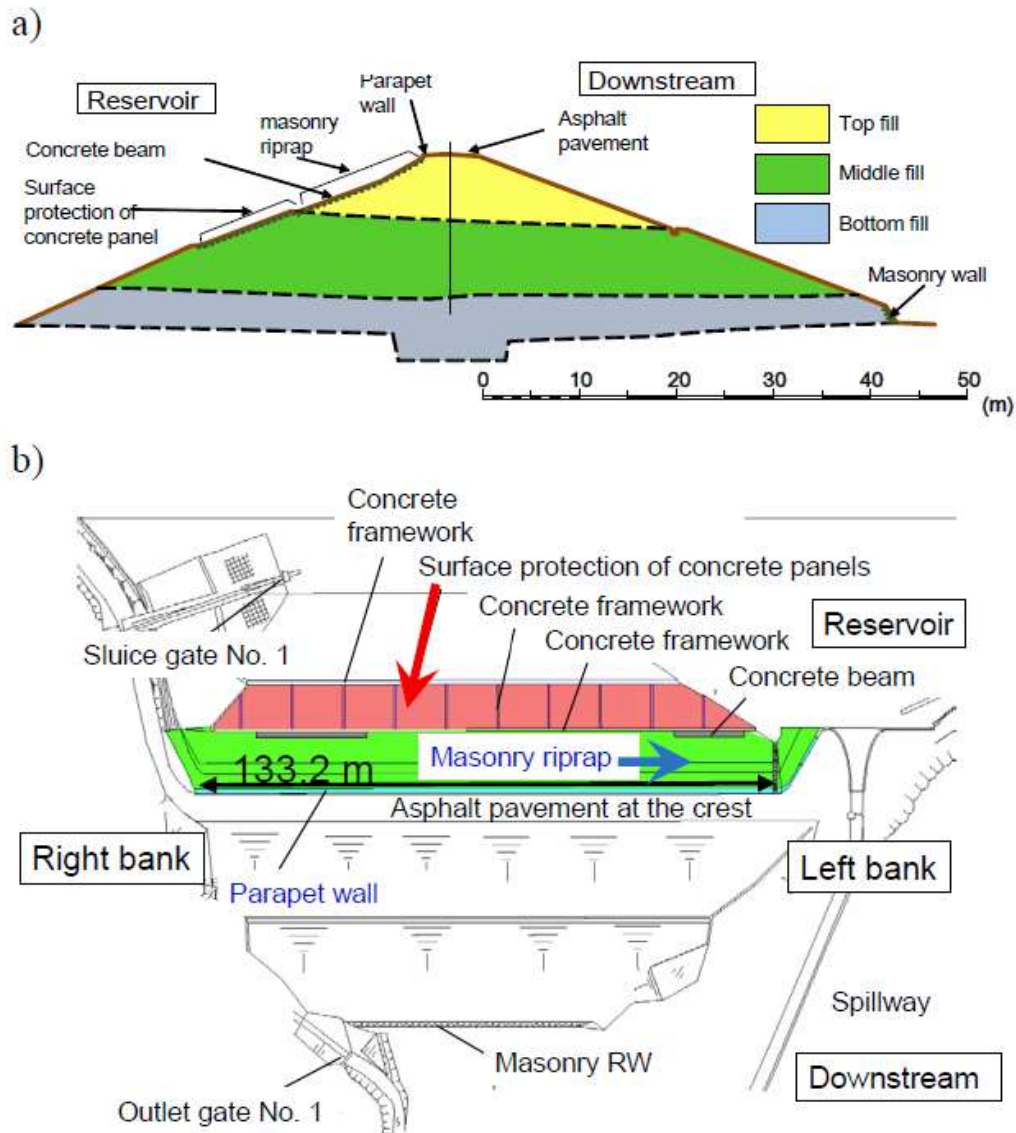
Figure 7.1 a) Typical cross section b) plan view of main dam (after Tanaka et al. 2012)

Figure 7. 2: Breaching and flooding of water after Tohoku earthquake (after Tanaka et al. 2012)
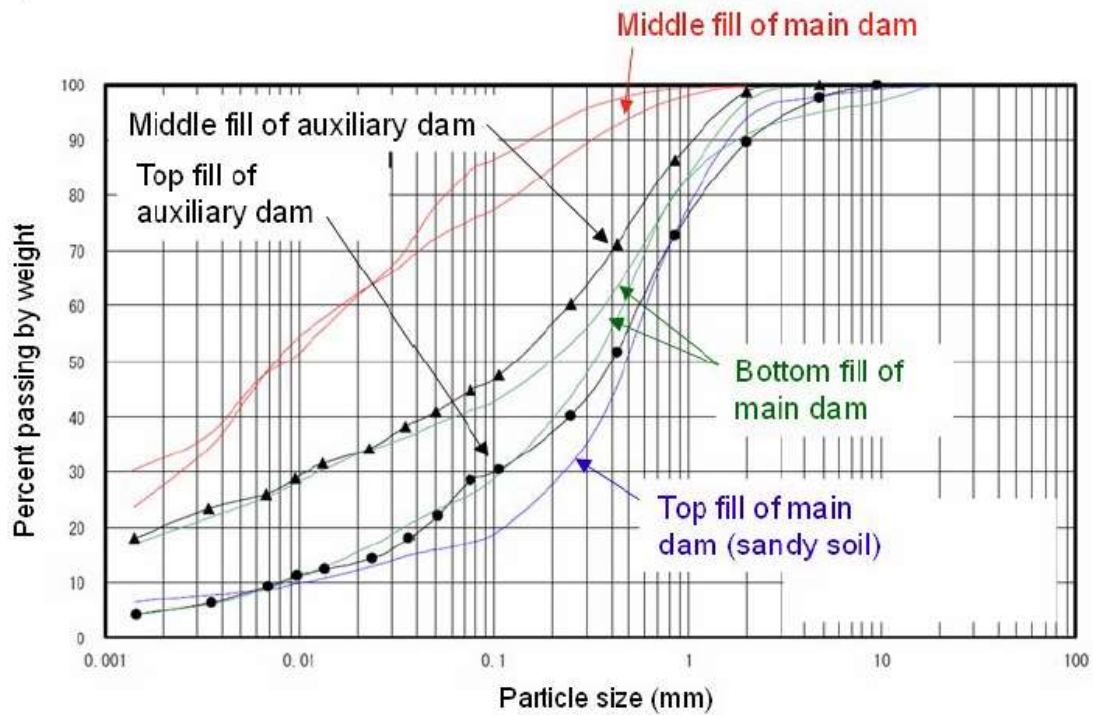
Figure 7. 3: Particle size distribution of Fujinuma Dam material from bottom to top fill of Auxiliary dam (after Tanaka et al. 2012)
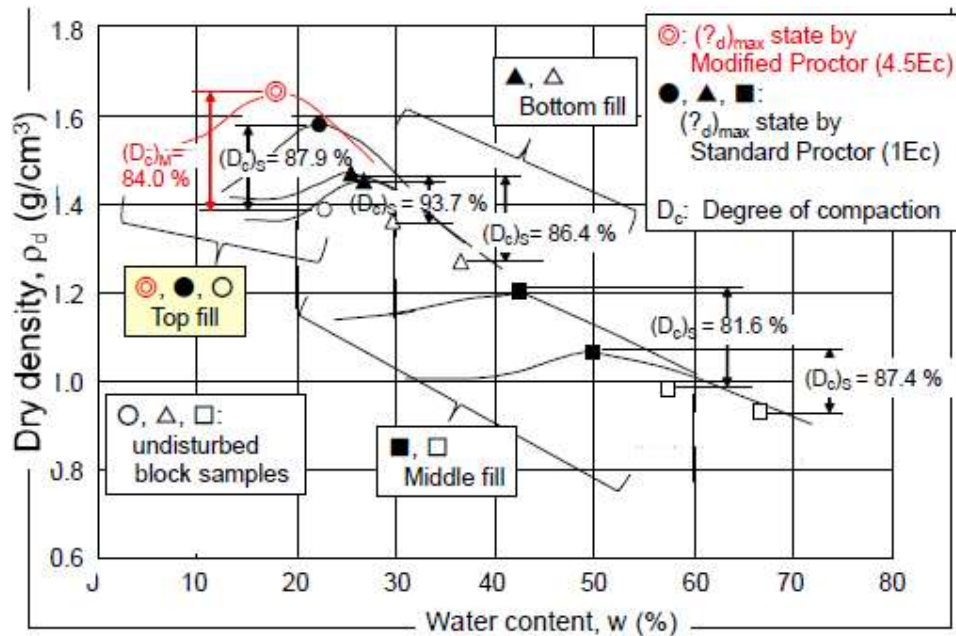
Figure 7. 4: Compacted states of the top, bottom and middle fill near the right bank
(after Tanaka et al. 2012)

Comprehensive field investigation of retrieved material and the triaxial undrained test revealed the following conclusions draw by Tatusuoka et al. (2017.)

i)   The dam was compacted poorly (top, middle and bottom fill). This was likely due to the absence of compaction machinery to achieved high compaction.

ii)   Mostly sandy soil was used in the construction, which is not the suitable type of soil due to high susceptibility to liquefy during an earthquake. Knowledge and understanding of sandy soil behavior were unavailable at that time.

iii)   At the time of the Tohoku earthquake, the water level in the Fujinuma reservoir was high for the start of the sowing season of rice. This led to the saturated condition for the bottom, medium and top fill.

iv)   Under saturated condition sandy soil exposed to undrained loading by Tohoku earthquake of long-time history resulted in the deterioration of undrained strength from initial value, which was already low due to low compaction.

7.2.   Design of Fujinuma dam

Design of earthfall dams or evaluating safely of existing earthfall dams and its safety against the earthquakes remains a challenge. Mainly due to the inconsistency between from the actual behavior of stress-strain during the earthquake and apparent behavior by assumptions used in the conventional design methods. The old irrigation code specified the stability of earthen fill dams to be evaluated by the pseudo-static limit equilibrium method (Figure 7.5) by considering the horizontal seismic coefficient of k_h =0.15 and design shear strength (drained shear strength) and the required factor of safety should be more than 1.2. The irrigation design code is revised in 2015, considering the relevant level 2 design earthquake and saturated soil, undrained shear strength (consider the degradation by undrained cyclic loading).

Conventional Newmark method has been used to design of seismic resistant earth-fill structures. Newmark stability analysis assumes the soil to behavior to rigid plastic. The Newmark sliding block method assumes a rigid body on a failure plane. When the seismic motion is subjected along the failure surface exceeds a threshold acceleration, displacements accumulate over time resulting in the permanent slope displacements. The mechanism of original Newmark is shown in Figure 7. 6. The threshold acceleration is also referred s yielding acceleration and is defined as the horizontal acceleration having a factor of safety of 1.0 under pseudo-static limit equilibriums stability analysis.
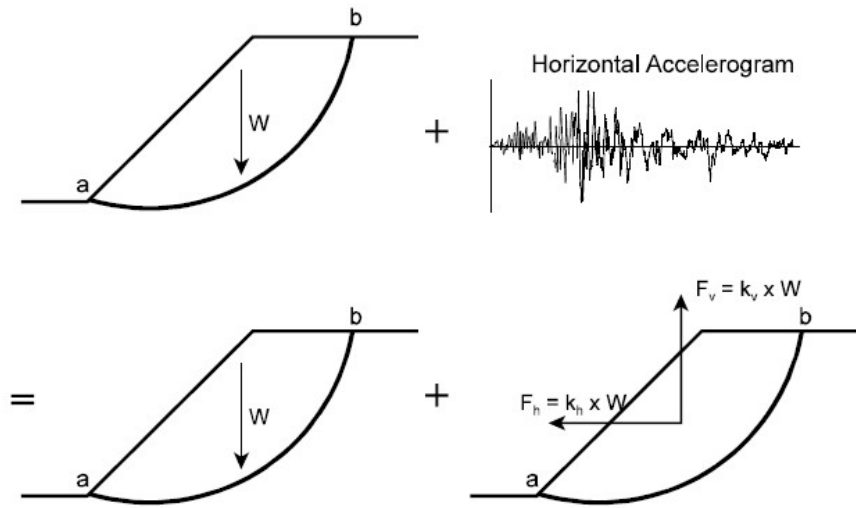
Figure 7.5: Psuedo static approach
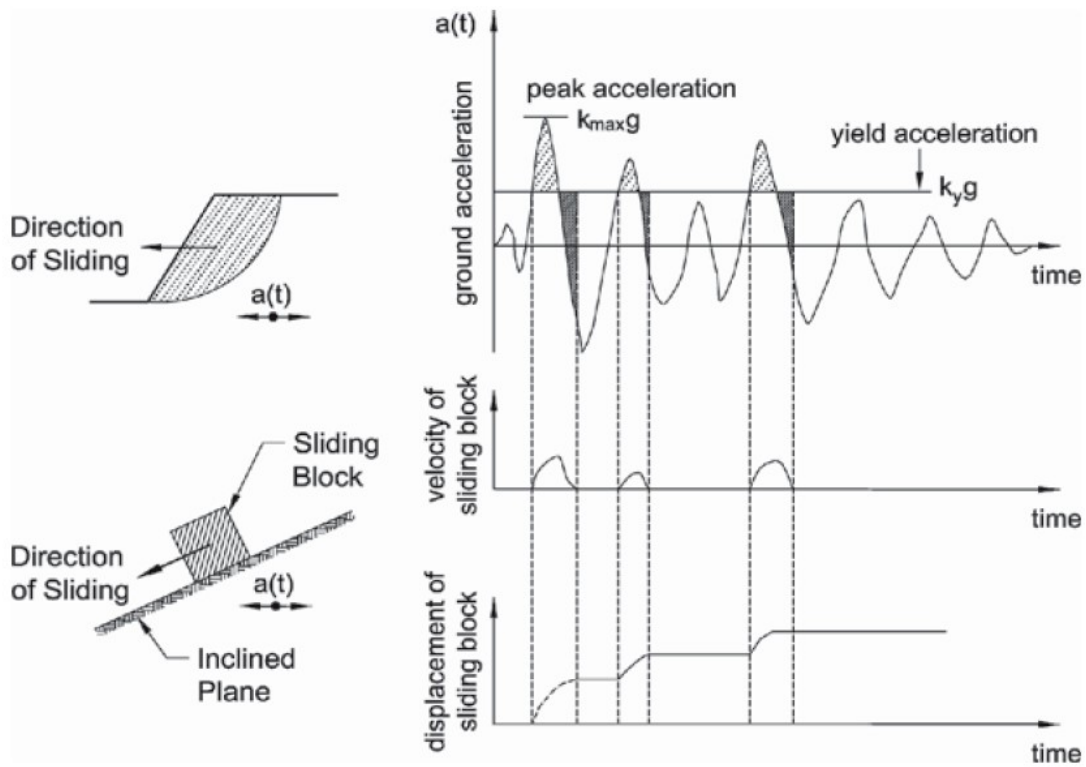
Figure 7. 6: Conventional Newmark stability mechanism (HCHRP report 611)

The reliable and accurate simulation of earth fill structures by sophisticated non-linear FEM effective stress analysis is costly and still difficult in engineering practice. Several numbers of issues should be taken into consideration such as the process of excess pore water pressure buildup and dissipation globally as well as locally inside and around the shear band. That is also being affected by particle size, strain level and many others. Therefore, a more simplified stability analysis with a small number of parameter easy to calculate is desired in practice. Duttine et al. (2015) modified the original Newmark seismic stability analysis to a simplified seismic stability analysis considering into account degradation of undrained soil strength (Newmark-D). The modified Newmark analysis is discussed in detail in Duttine et al. (2015) and schematically shown in Figure 7. 7.
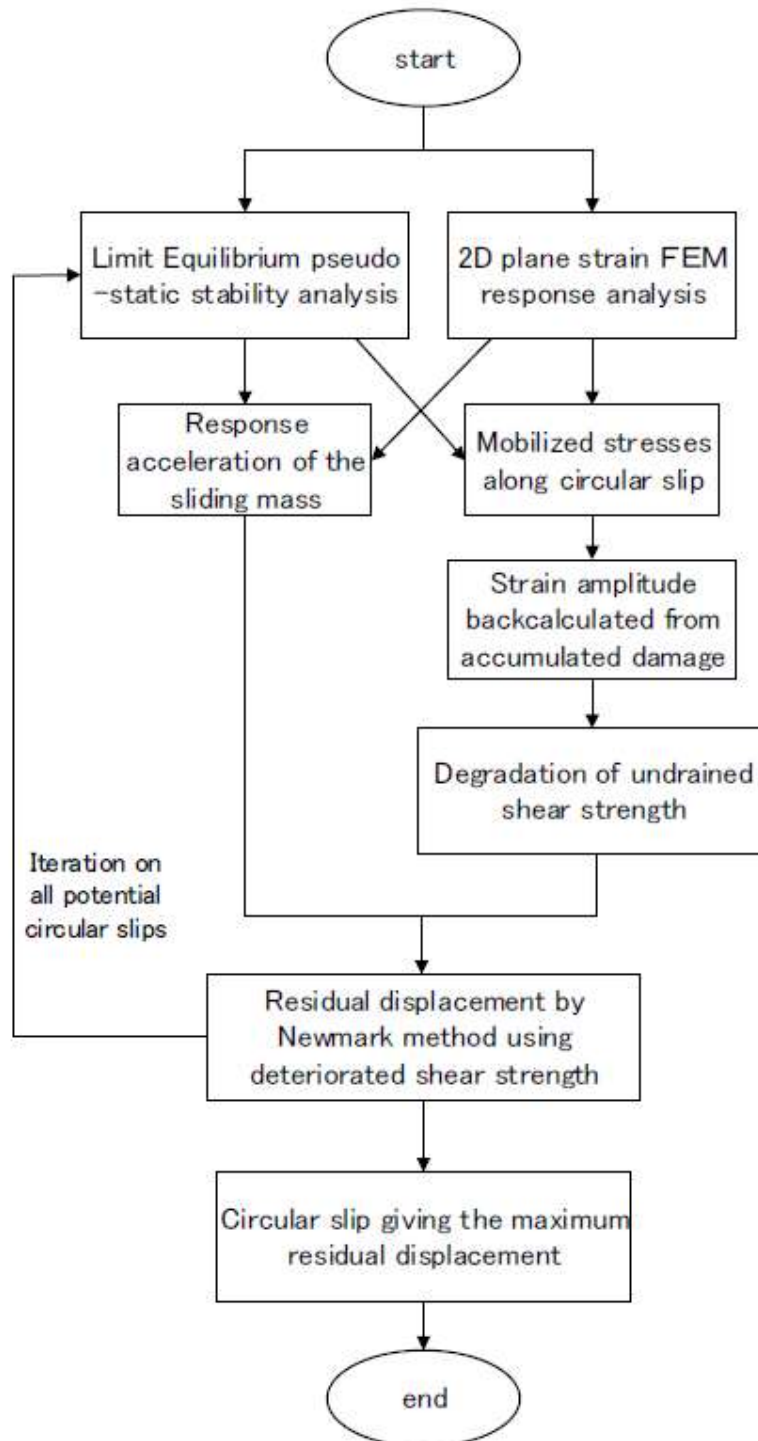
Figure 7. 7:   Schematic illustration on the stability analysis procedure by Newmark-D
(Duttine et al. 2015)

7.3.   Seismic stability analysis of Fujinuma dam with Newmark-D

Stability analysis software developed at IGI corporation was modified with the developed degradation correlation to take into account the degradation of stress-strain relationship during input motion. Material properties calculated from the retrieved material of Fujinuma dam (top, middle, and bottom) was used in the stability analysis. The inferred mechanism of the collapse of Fujinuma dam is shown in Figure 7. 8, failure alone slide 1(C1) first initiated resulted in the overtopping followed by slide 2,3 and 4.
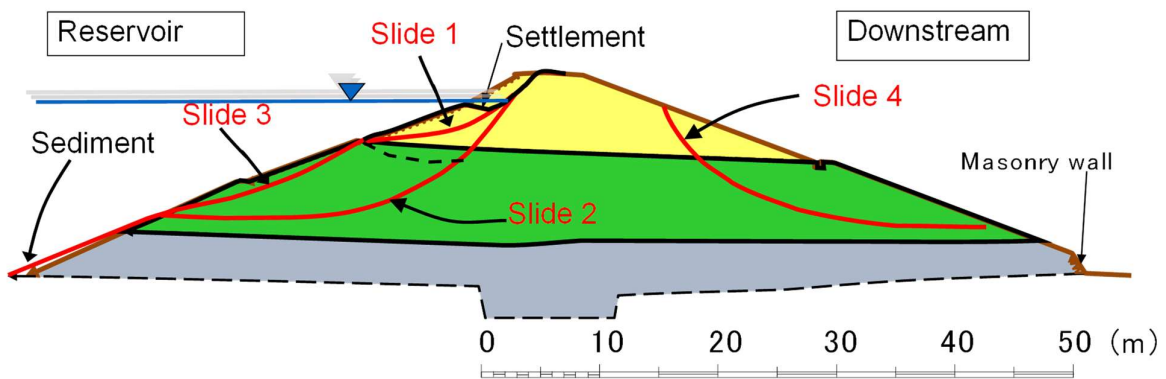
Figure 7. 8:   Inferred collapse mechanism of Fujinuma dam (after Tanaka et al. 2012)

The model of Fujinuma dam after stability analysis with top, middle and bottom fill with yellow, pink and magenta color respectively is shown in Figure 7.9. A critical failure line along the inferred failure plane after Tatsuoka et al. (2017) is also shown in Figure 7.9. The degradation correlation used in the simplified analysis is shown in Figure 7.10
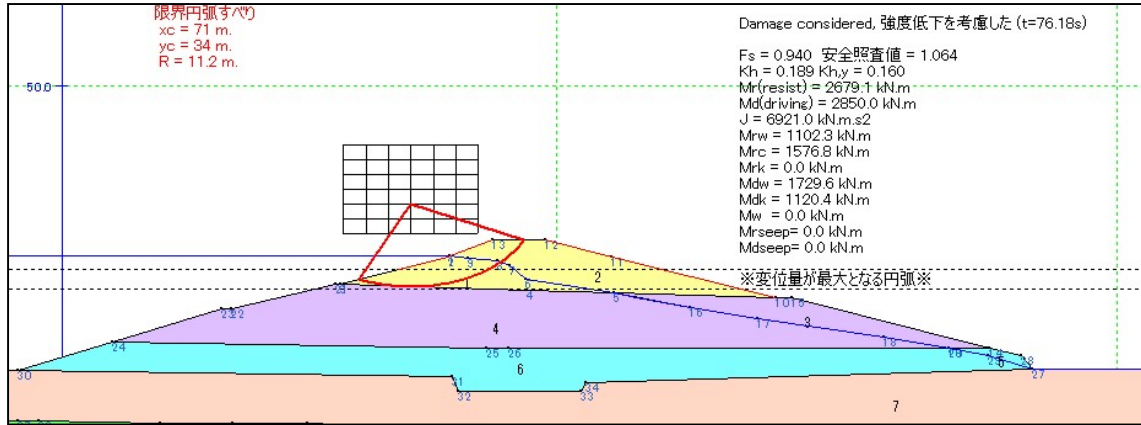
Figure 7.9:   Fujinuma dam model in stability analysis software by IGI
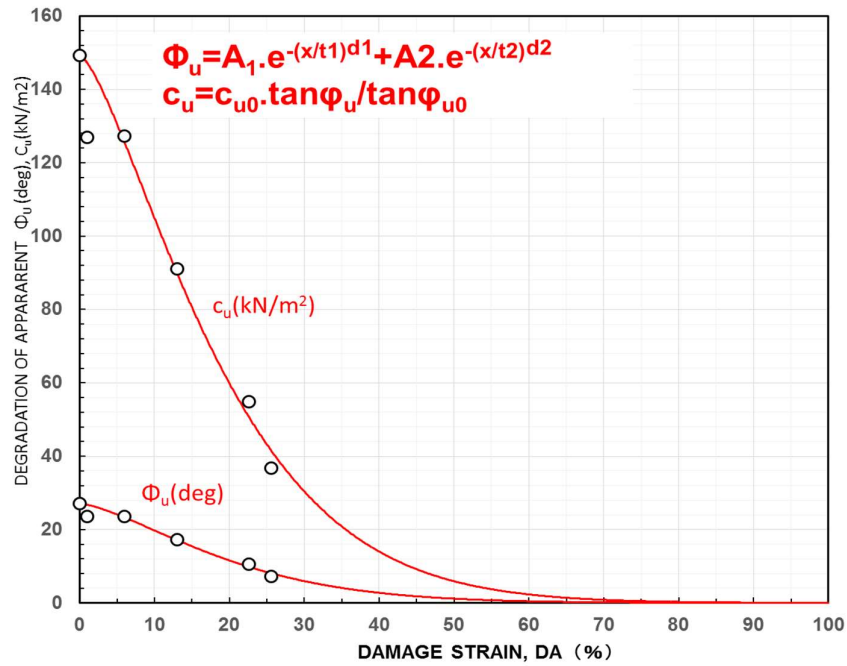
Figure 7.10:   Degradation correlation incorporated in IGI stability analysis on Fujimua sand assuming the tendency of deterioration similar as Toyoura sand

7.4. Summary of Seismic stability analysis results of Fujinuma dam with Newmark-D

Figure 7. 11 shows a summary of test result with the simplified stability analysis software by IGI corporation by Newmark-D with 2011 Tohoku earthquake as input earthquake motion. In Figure 7. 11b with the increase in the input motion, the deterioration of the yield seismic acceleration. The yield acceleration deteriorated from an initial value of 0.331 to 0.009 at the end of the seismic input motion.   Whereas Figure 7. 11the accumulated displacement reached 2.1m at the end of the seismic motion.

Figure 7. 11c shows the summary of calculated settlement by using conventional Newmark and Newmark-D stability analysis of Fujinuma dam. The calculated settlement from conventional Newmark method is 0.15m. The settlement by Newmark-D by previous triaxial data and updated by using the current study. From the comparison, the updated torsional shear degradation correlation calculated settlement is close to the observed settlement, which is more than 2m.

It can be concluded that the proposed degradation correlation in the current study successful calculated the settlement close to the observed settlement. In order to validate further the reliability of the proposed degradation correlation, further analysis with existing dams should be investigated.
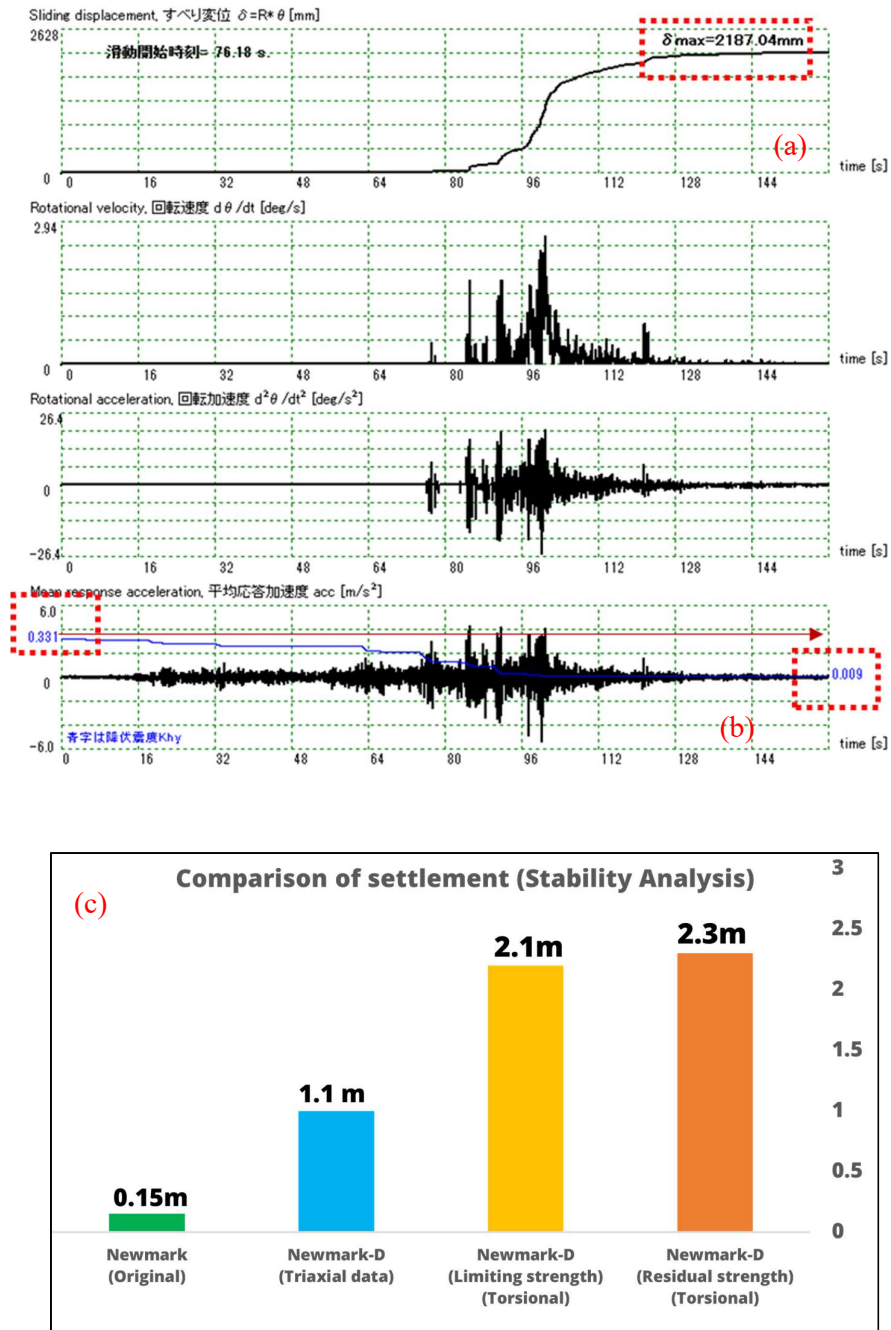
Figure 7. 11:   Summary of test results in terms of
a) sliding displacement b) deterioration of yielding acceleration c) comparison of settlement
among different cases of stability analysis

7.5. References

1) Duttine, A., Tatsuoka, F., Yazaki, S. and Mohri, Y. [2015a]: *Evaluation of seismic dam displacement by Newmark method taking into account soil strength reduction due to undrained cyclic loading*, Japan Geotechnical Society (JGS) Special Issue on earth dam seismic stability, 2015.03, 8-11, (in Japanese).

2) Duttine, A., Yazaki, S., Tatsuoka, F. and Mohri, Y. [2015b]: *Seismic stability analysis of small earth-fill dams by Newmark-D method*, Japan Society of Irrigation, Drainage and Rural Engineering (JSIDRE) Special Issue on irrigation dam seismic investigation and maintenance, 2015.12, 15-18, (in Japanese).

3) Newmark N.M. [1965]: *Effects of earthquakes on dams and embankments,* Géotechnique, 1965, Vol. 15, No. 2, pp. 139-160.

4) Tatsuoka, F., Koseki,J., Takahashi, A., [2017]: *Earthquake-induced damage to earth structures and proposal for revision of their design policy – based on a case history of the 2011 off the pacific coast of Tohoku earthquake*, Journal of JSCE Vol 5, 101-112, 2017.

CHAPTER 8

Conclusions and recommendations

CHAPTER 8: Conclusions and recommendations

8.1   Conclusions and recommendations

This study investigated the undrained behavior of Toyoura sand during the extremely large shear strain of about 120% in double amplitude. Five series of test were performed on saturated Toyoura sand sheared under quasi simple shear using hollow cylindrical Torsional shear apparatus. All the specimens were prepared by air pluviation to achieve desired density from loose to dense.

i)   Undrained monotonic behavior (without cyclic history)

The influence of relative density on undrained monotonic is investigated using large strain hollow cylindrical torsional shear apparatus. Except for very loose specimen, the ultimate critical state was observed for medium dense and dense Toyoura sand. Influence of two types of undrained shear strength encountered during undrained monotonic loading showed that the shear strength at flow, quasi-state increased with the increased in the density, as well as shear strength at ultimate steady-state. The increment of undrained shear strength at true critical state is significant as compared to undrained shear strength increase at quasi-state. Large deformation developed after exceeding the undrained shear strength at a true critical state. Whereas for loose sand, large deformation developed after exceeding shear stress at flow liquefaction state. The specimen exhibited contractive behavior having stress ratio of 0.54, whereas above this threshold stress ratio it will behave initially contractive followed by the dilative response. Undrained shear strength at Quasi steady state (QSS), undrained peak strength and residual strength (Ultimate steady state) is plotted against a decrease in the void ratio.

ii)   *Quantification of Undrained Strength degradation (Undrained monotonic behavior*

    with undrained cyclic history)

In this multistage test, the specimen was subjected to constant stress amplitude cyclic stress to achieved desired damage strain. Following that undrained monotonic loading is applied exceeding shear strain of 60% in single amplitude. Investigation of all the test revealed that specimen was brought to failure by the formation of the shear band during undrained monotonic loading.

Comparison of effective stress path, stress-strain relationship, and differential stress, two types of undrained strength were defined such as 1) Limiting undrained strength 2) residual strength. Limiting undrained refers to the stage, the initiation of the shear band. Residual strength refers to the stage of formation of the shear band. Due to the presence of negative excess pore water pressure, residual strength observed was higher than the limiting undrained strength.

The first series of test on medium dense sand revealed that the limiting undrained strength, as well as residual strength, deteriorated with the increase in the damage strain and ultimately reaching a minimum value of 6kPa subjected to 92% damage strain. Consistently dense limiting and residua undrained strength deteriorated with the increase in the damage strain. At the same amplitude of damage strain, deteriorated limiting and residual undrained strength of dense sand is higher as compared to medium dense sand.

The second series of test with initial static shear in reversal and non-reversal stress loading for medium dense sand revealed that the limiting and residual strength deteriorated with the increase in the damage strain.

Effect of confining pressure revealed the consistent result of deteriorating of limiting and residual strength.

A normalized limiting undrained shear strength degradation correlation is proposed considering, density state, confining pressure, stress amplitude level, reconsolidation history, and effect of initial static shear

iii) <u>*3D image analysis development and capturing strain localization*</u>

To validate the initiation of the shear band at the drop of differential stresses an in-house Single-Stereo camera was employed to evaluate in-field shear stain by 3D DIC for non-contact local shear strain measurement. The results showed that local strains taking place in the localise zone (a shear band) was larger, in the order of two-fold, to that the global average shear strain in the whole specimen) calculated based on the torsional force applied to the top of the specimen, in the order of two-fold. It is found that the rate of shear strain development inside a localised zone can be the major contributor to the strength degradation of the specimen during cyclic and monotonic loading.

iv) <u>*Fujinuma dam-Stability analysis by Newmark-D*</u>

IGI cooperation stability analysis program is modified by incorporating the developed degradation correlation of undrained strength. For the case study, it is assumed that the Fujinuma sand will degrade in a similar manner as Toyoura sand.

Two cases of stability analysis were performed. In the first case, stability analysis was performed with the original Newmark method (without considering the degradation of undrained strength). The computed settlement was 0.15m. In the other case, the Newmark-D method was used and degradation correlation is used to estimate the degraded strength with earthquake time history. The estimated settlement of the crest, in this case, was 2.2m. Such a large settlement provides a better explanation of the collapse of Fujinuma dam.

8.2 Recommendations for future study

i) *Recommendation for Future Experimental investigations*

1) In order to have a complete understanding of degradation and its quantification, different material should be tested and compared with the Toyoura sand. An-isotropic stress conditions should be applied to test with different Ko conditions. Energy approach is used to establish the correlation between the energy induced and the deteriorated strength.

2) Plastic and non- plastic fines showed varying liquefaction strength. It will be essential to investigate its influence on the degradation of undrained strength with clean sand.

3) Different preparation method should be used to check the fabric effect on undrained strength, strain localization.

4) Degradation behavior of unsaturated sand needs to be investigated under different density and stress condition

5) 4 stage test need to be performed, in the first step applying the damage strain , second stage reconsolidating, third stage cyclic loading to achieve desired damage strain followed by the monotonic test

ii) *Recommendation for Future Experimental investigations*

1) Stability analysis of existing earthfall irrigation dams of japan should be done by a stability analysis program to estimate its settlement under different seismic time histories to predict its vulnerabilities for collapse during future earthquakes

2) Incorporating the degradation correlation in the finite element program of IGI (SERID) program. This will give us more realistic results.